Instituto Tecnológico e Nuclear

## 37ièmes Journées des Actinides

# Programme and Abstracts

***24 - 27 March 2007***

**Hotel do Mar**
**Sesimbra**
**PORTUGAL**

*Edited by J.C.Waerenborgh*
*Cover design by Maria Manuela B. Meira Cordeiro*

## *Scope*

These *Journées des Actinides* represent a continuation of a series of annual international conferences, which provide a forum for open and informal discussion of all aspects, fundamental and applied, related to the chemistry and physics of the 5f elements. Typical topics addressed include:

- strongly correlated behaviour, superconductivity, quantum criticality;
- inorganic and organometallic chemistry;
- materials science;
- theory, electronic structure;
- nuclear fuel cycle, environment.

In particular, it aims to emphasize presentations of on-going research projects by young scientists and PhD students, to assess the latest progress in different research programmes, and to stimulate new collaborative projects.

Two special sessions of this conference will be a meeting of Working Group 1, Novel Materials, of the COST Action P16 "Emergent behaviour in correlated matter". These sessions will deal with new systems containing "Actinides and their Brothers", which include non-actinide elements with unusual physical properties like Ce, Yb or Eu.

## *Organizing Committee*

A. P. Gonçalves, Instituto Tecnológico e Nuclear / CFMC-UL

J. C. Waerenborgh, Instituto Tecnológico e Nuclear / CFMC-UL

L. C. J. Pereira, Instituto Tecnológico e Nuclear / CFMC-UL

M. Almeida, Instituto Tecnológico e Nuclear / CFMC-UL

J. A. Paixão, Fac. Ciências e Tecnologia da Univ. Coimbra

M. Godinho, Fac. Ciências da Univ. Lisboa / CFMC-UL

## *International Advisory Committee*

L. Havela (Prague, Czech Republic)

D. Kaczorowski (Wroclaw, Poland)

F. Wastin (Karlsruhe, Germany)

## *Secretariat*

Maria Manuela B. Meira Cordeiro (ITN)

## *Other collaborators (ITN, CFMC-UL)*

Piotr Gaczyński, Susana Sério, Miguel Moura, Marta Dias, Oksana Sologub, Leonid Salamakha.

### *Contacts*

JdA 2007 Secretariat
Instituto Tecnológico e Nuclear, Química
P-2686-953 Sacavém, Portugal
Fax: +351 21 994 6185
E-MAIL: jda07@itn.pt

## ***Support and sponsorship***

***Conference hosted by***

Instituto Tecnológico e Nuclear (ITN)

***With support from***

FCT, Fundação para a Ciência e Tecnologia, Portugal.

ACTINET, European Network for Actinide Sciences.

Actinides User Laboratory, JRC, ITU, Karlsruhe, Germany.

COST (European Cooperation in the field of Scientific and Technical Research) action P16

***Additional sponsorship***

Câmara Municipal de Sesimbra

Região de Turismo da Costa Azul

Caixa Geral de Depósitos

Criolab

# Scientific Programme

## *Saturday, March 24, 2007*

16:00-20:00 **Registration**

19:30-20:00 **Welcome Drink**

20:00-22:00 **Dinner**

## *Sunday, March 25, 2007*

08:30 **WELCOME ADDRESS.**

***Session A – General Aspects.***

08:45 **A1**: **Coexistence of ferromagnetism and the underscreened Kondo effect in heavy fermion uranium compounds**
B. Coqblin, N.B. Perkins and J.R. Iglesias

09:05 **A2**: **Electronic structure and photoemission of Pu and Am compounds**
A. Shick, L. Havela and T. Gouder

09:25 **A3**: **Evidence for a non-Fermi liquid state in $URh_{0.62}Ru_{0.38}Ge$**
W. Miiller, V.H. Tran, R. Wawryk, N. Oeschler and F. Steglich

09:45 **A4**: **Understanding the changing role of 5f electrons through high-pressure studies**
R.G. Haire

10:05 **A5**: **Explaining the magnetic stabilization of Curium: competing spin-orbit and exchange interaction**
K.T.Moore, G. van der Laan, R.G.Haire, M.A.Wall, A.J.Schwartz, P.Söderlind

10:25-10:55 **COFFEE BREAK**

***Session B – Physics and Calculations.***

10:55 **B1**: **From the quadrupolar phases of $UPd_3$ to the magnetism of $PuPd_3$**
K.A. McEwen, H.C. Walker, M.D. Le, E. Colineau and F. Wastin

11:15 **B2**: **Hidden order and low-energy excitations in $NpO_2$**
N. Magnani, P. Santini, S. Carretta, G. Amoretti and R. Caciuffo

11:35 **B3**: **Electronic, structural and magnetic properties of $UH_3$ at ambient and under high pressure from *ab initio* theory**
Wei Luo and R. Ahuja

11:55 **B4**: **Electric field gradients in Ce- and Pu-based 115 compounds**
J. Rusz and P. Oppeneer

12:15-14:00 **LUNCH**

14:00-16:00 ***"Research on rare-earth and actinoid materials" within COST P16***

14:00 **COST1: Magnetic structure of the hydride $CeRuSiH_{1.0}$ deriving from the heavy-fermion ternary silicide CeRuSi**
B. Chevalier, E. Gaudin, S. Tencé, B. Malaman, J. Rodriguez Fernandez, B. Coqblin, G. André

14:20 **COST2: Formation of $YbCu_{5-x}T_x$ and $YbCu_{4.5-x}T_x$ (T=transition metals) solid solutions**
M. Giovannini, R. Pasero, A. Saccone

14:40 **COST3: On the search for quantum criticality in a ferromagnetic system $UNi_{1-x}Co_xSi_2$**
D. Kaczorowski and A. Pikul

15:00 **COST4: Heat capacity of $CeNi_4Si$ compound**
M. Reiffers, M. Timko, M. Mihalik, M. Falkowski, A. Kowalczyk, J. Šebek, E. Šantavá

15:20 **COST5: Formation, Structure and Physical Properties of Novel Compounds $M_2Pd_{14+x}B_{5-y}$, M=Th, Ce, Pr, Nd, Sm, Eu, Gd**
E. Royanian, P. Rogl, E. Bauer, H. Kaldarar, H. Michor, A.P.Gonçalves, G. Giester

15:40 **COST6: Physical Effects Associated with the Spin Dependent Effective Masses of Heavy Quasiparticles: Metamagnetism and Fulde-Ferrell state**
Jozef Spalek, Jan Kaczmarczyk, Maciej Maśka, Marcin Mierzejewski

16:00 **COST7: The low-temperature transport properties of the periodic Anderson model**
V. Zlatić

***Session C –Surface Science.***

16:30 **C1**: **Density functional study of CO adsorption on Pu (100) surface**
Wen-hua Luo, Da-qiao Meng and Gan Li

16:50 **C2**: **Chemical reactivity of plutonium oxide towards oxidising agents: an *in situ* photoemission spectroscopy study**
A. Brevet, P. Berthou, L. Jolly and F. Delaunay

17:10 **C3**: **Inhibition of hydrogen adsorption on uranium surfaces by traces of water vapor**
E. Tiferet, M.H, Mintz, I. Jacob and N. Shamir

17:30 **C4**: **Evidence for differential rates of oxide growth on depleted uranium: implications for $UH_3$ formation**
T.B. Scott, G.C. Allen and J. Glascott

17:50-18:20 **COFFEE BREAK**

***Session D –New Materials.***

18:20 **D1**: **Studies of uranium multilayers: comparisons and perspectives**
R. Springell, S.W. Zochowski, R.C.C. Ward, M.R. Wells, F. Wilhelm, S.D. Brown, L. Bouchenoire, W.G. Stirling and G.H. Lander

18:40 **D2**: **Search for new classes of thermoelectrics: synthesis and properties of three new uranium-heavy atom chalcogenides**
D.M. Wells, D. Bugaris and J.A. Ibers

19:00 **D3**: **Increase of $T_C$ in $UFe_{2+x}$ synthesized by ultrafast cooling**
L. Havela, K. Miliyanchuk, A.P. Gonçalves, J.C. Waerenborgh, L.C.J. Pereira, P. Gaczyński, E.B. Lopes and J. Pešička

19:20 **D4**: **New ternary phases in the U-Fe-Ge system and their magnetic properties**
D. Berthebaud, O. Tougait, M. Potel, A.P. Gonçalves, E.B. Lopes, H. Noël

20:00 **DINNER**

21:30-23:00 **POSTER SESSION**

## *Monday, March 26, 2007*

***Session E – Magnetism.***

08:45 **E1**: **Structure and electronic properties of new U compound $UGa_{1.85}Zr_{0.15}$**
L.Havela, A.V.Andreev, A.P.Gonçalves, J.Šebek, V.Sechovský, Y.F.Popov

09:05 **E2**: **Magnetic, transport and thermal properties of $AnPd_2Sn$ (An = Th, U, Np, Pu) system**
K. Gofryk, D. Kaczorowski, E. Colineau, F. Wastin, R. Jardin, N. Magnani, P. Boulet, J. Rebizant, J-C. Griveau, P. Javorsky and R. Caciuffo

09:25 **E3**: **Magnetic and related properties of $U_4Ir_{13}Si_9$ and $U_4Rh_{13}Si_9$**
A. Pikul and D. Kaczorowski

09:45 **E4**: **Magnetic properties of $NpNiSi_2$**
E. Colineau, F. Wastin, J.P. Sanchez and J. Rebizant

10:05 **E5**: **Towards f-electron single-molecule magnets: Physical properties of a Tm-based "double decker" complex**
N.Magnani, R.Caciuffo, E.Colineau, F.Wastin, G.Amoretti, S.Carretta, P.Santini, A.Baraldi, R.Capelletti, D.T.Adroja, A.Nakamura, M.Watanabe

10:25-10:55 **COFFEE BREAK**

***Session F – Radiochemistry.***

10:55 **F1**: **Application of the chemiluminescence effects and pulse laser spectroscopy methods for U, Pu and Np trace amount detection**
I. Izosimov

11:15 **F2**: **Contribution of the capillarity electrophoresis – inductively coupled plasma mass spectrometry for actinide speciation studies**
J.Aupiais, C.Ambard, S.Topin, N.Baglan, V.Philippini, R.Burgat, S.Faure

11:35 **F3**: **Lanthanides and actinides isotope separation by oscillating extraction**
A.A. Kopyrin, M.A. Afonin and T. Todd

11:55 **F4**: **Actinide targets for the production of radioisotopes by the ISOL method**
T. Stora, R. Catherall, S. Fernandes and J. Lettry

12:15-14:00 **LUNCH**

14:00-15:00 **COST P16 Committee user meeting (session for P16 members)**

15:00-16:00 **USER Lab group meeting**

***Session G – Spectroscopy.***

16:30 **G1**: **Dual nature of 5f electrons in uranium monochalcogenides**
J. Schoenes, K. Litfin, M. Broschwitz and O. Vogt

16:50 **G2**: **Effect of pressure on the resonant multi LO-Phonon Raman scattering and crystal-field excitations in $UO_2$**
T. Livneh and E. Sterer

17:10 **G3**: **Evidence of dynamical spin shielding in Ce from spin-resolved photoelectron spectroscopy**
J.G. Tobin

17:30 **G4**: **Resonant inelastic X-ray scattering spectroscopy of actinide materials at 5d edge surface**
S.M. Butorin

17:50-18:20 **COFFEE BREAK**

***Session H – Fuel.***

18:20 **H1**: **Equilibrium phase relations in the U-Zr-Al ternary system: a prospective study for a metallic U-Zr alloy as nuclear fuel**
O. Tougait, F. Désévédavy, S. Dubois and H. Noël

18:40 **H2**: **Microstructure, sintering and dissolution of $Th_{1-x}U_xO_2$ solid solutions prepared by wet chemistry methods**
N. Hingant, N. Clavier, N. Dacheux, S. Hubert, R. Podor and J. Aupiais

19:00 **H3**: **Resin process potentiality for the elaboration of transmutation targets precursors**
H. Mokhtari, S. Picart, A. Meunier, and R. Thouvenot

19:20 **H4**: **Evaluation of potential hazard of transuranic elements in HLW**
A. Ochkin, A. Merkushkin, S. Stefanovsky and S. Povniy

20:30 **BANQUET**

## *Tuesday, March 27, 2007*

***Session I – Waste and Leaching.***

08:45 **I1**: **Interactions of U(VI) with members of a microbial consortium recovered from a uranium mining waste pile**
T. Reitz, A. Geissler, M.L. Merroun and S. Selenska-Pobell

09:05 **I2**: **Hydrothermal methods for the preparation of actinide compounds**
N. Clavier, N. Dacheux, G. Wallez and M. Quarton

09:25 **I3**: **Temperature programmed decomposition of $Pu(C_2O_4)_2.6H_2O$**
N. Vigier, S. Grandjean and F. Abraham

09:45 **I4**: **XANES/EXAFS of U $L_m$ edge in borosilicate high-ferrous nuclear waste glasses**
S. Stefanovsky, A. Shiryaev, I. Zubavichus and J. Marra

10:05-10:35 **COFFEE BREAK**

***Session J – Structural Chemistry.***

10:35 **J1**: **Periodic density functional study of the uranyl ion interaction with $NiFe_2O_4$**
H. Perron, C. Domain, J. Roques, R. Drot, E. Simoni and H. Catalette

10:55 **J2**: **New three-dimensional lithium uranyl-phosphates and their relations to vanadate analogous**
C. Renard, M. Benseghir, S. Obbade and F. Abraham

11:15 **J3**: **2D and 3D anionic arrangements in alkaline uranyl niobates**
S. Saad, S. Obbade, C. Renard and F. Abraham

11:35 **J4**: **Thermodynamic and structural properties of Protactinium(V) in sulphate medium**
M.V. Di Giandomenico, C. Le Naour, D. Trubert, C. Fillaux, C. Den Auwer, P. Moisy and C. Hennig

11:55 **J5**: **First three-dimensional diamine-containing uranyl-vanadates : hydrothermal synthesis and structure**
M. Rivenet, L. Jouffret and F. Abraham

12:15-**CLOSING SESSION.**

13:00-14:45 **LUNCH**

# POSTERS

**P-1** **Cycling changing of cerium valency in oscillating extraction processes of f-elements**
M. A. Afonin, A.A. Kopyrin, A.A. Fomichev, M.H. Ekzekov

**P-2** **Magnetic properties of $U_2(Fe_{1-x}Ni_x)_{13.6}Si_{3.4}$ single crystals**
A.V. Andreev, E.A. Tereshina, E. Šantavá

**P-3** **Secondary phase formation upon hydrothermal leaching of $UO_{2+x}$ at 70°C and 150°C and interaction with Np(V)**
O.N. Batuk, St.N. Kalmykov, E.V. Zakharova, Yu.A.Teterin

**P-4** **An X-ray diffraction study to determine the composition and thickness of the oxide phases formed during plutonium oxidation**
M. Dawes and P. Morrall

**P-5** **Anomalous increase of ATS scattering at the U $M_4$-edge of UNiGe upon magnetic order**
B. Detlefs, C. Detlefs, K. Prokeš, J. Prchal, A. Kolomiyets

**P-6** **<*kkk*> peaks in 3*k* magnetic structures: incommensurate *k* and behaviour in magnetic field**
B. Detlefs, S.B. Wilkins, P. Javorský, E. Blackburn, G.H. Lander

**P-7** **Peritectic Reactions on the U-Fe-B system**
M.Dias, P.A.Carvalho, O.Sologub, O.Tougait, H.Noel, C.Godart, E.Leroy, A.P.Gonçalves

**P-8** **Volatile Oxides of Some Actinides**
V.P.Domanov

**P-9** **Dissolution of phosphate based ceramics: implication of the neoformed phases**
E. du Fou de Kerdaniel, N. Dacheux, R. Podor, J. Aupiais

**P-10** **Hydrothermal syntheses and structure of $U_2(C_4O_4)_3(OH)_2$, the first $U^{4+}$ squarate hydroxyde**
L. Duvieubourg-Garela, F. Abraham and S. Grandjean

**P-11** **Hydroxyl bridges in uranyl oxalates and squarates**
L. Duvieubourg-Garela, F. Abraham and S. Grandjean

**P-12** **Electrochemical dissolution of uranium monocarbide: first kinetics results**
B. Fourest, A. Maslennikov, V. Sladkov

**P-13 First-principles study of point defects and of helium incorporation in uranium carbide**
M. Freyss, J. Durinck

**P-14 $^{119}$Sn Mössbauer spectroscopy in UPtSn**
P. Gaczyński, A. Grykałowska, B. Nowak and J.C. Waerenborgh

**P-15 Two independent magnetic sublattices in $U_{0.6}Fe_6Sn_6$ compound?**
P. Gaczyński, L.C.J. Pereira, J.C. Waerenborgh

**P-16 On the theory of energy spectra of heavy atoms and ions**
G. Gaigalas, Z. R. Rudzikas

**P-17 FP-LAPW study of the quantum size effects in (001) films of α-uranium**
Li Gan, Tang Tao

**P-18 Models for the initiation of hydride attack sites on uranium**
J. Glascott

**P-19 Magnetic Properties of Perovskites $BaUO_3$, $KUO_3$, Ordered Perovskite $Ba_2CoUO_6$, and $CoU_2O_6$**
Y. Hinatsu, Y. Doi

**P-20 Ligand effect on $ThO_2$ dissolution. Leaching behaviour of $Th_{0.87}Pu_{0.13}O_2$**
Solange Hubert, Guillaume Heisbourg, Nicolas Dacheux, Philippe Moisy

**P-21 Effect of Am doping on the superconductivity of $PuCoGa_5$**
F. Jutier, R. Jardin, E. Colineau, J.-C. Griveau, J. Rebizant, F. Wastin

**P-22 Superconductivity in the new $Y_3Os_8B_6$ boride**
E.B. Lopes, O.L. Sologub, A. Casaca, L. Havela, J. Sebek, E. Santava, Z. Janu, A.P. Gonçalves

**P-23 Plutonium oxide transformation kinetics**
P. Morrall, S. Tull, J. Glascott, P. Roussel

**P-24 New intermetallic compounds in the U-Ru-Si system**
M. Pasturel, O. Tougait, M. Potel, H. Noël, A.V. Zelinskiy

**P-25 Evidence of different stoichiometries for the limiting carbonate complexes of lanthanides(III) by solubility measurements.**
Violaine Philippini, Thomas Vercouter, Pierre Vitorge, Annie Chaussé

**P-26 Functionalized calixarenes-an alternative tool for the remediation of the radioactive contaminated mine waters from Romania**
I.-C. Popescu

**P-27 Raman and infra-red spectroscopy of some inorganic actinide compounds**
C.D.Puxley

**P-28 U-Au-Sb system: phase equilibria at 600°C and crystal structures of compounds**
Leonid Salamakha, Antonio P. Gonçalves, Henri Noël, Thierry Roisnel, Stepan Mudryi, Ivan Scherba, Manuel Almeida

**P-29 New XPS and Band Structure Characteristics of UN**
Małgorzata Samsel-Czekała, Robert Troć, Ewa Talik

**P-30 Magnetic short range order in $DyFe_xAl_{12-x}$ intermetallics**
S. Sério, L. C. J. Pereira, M. Godinho, J. C. Waerenborgh

**P-31 Isothermal section of U-Pt-Sb system at 600 °C (0 - 70 at.% Pt)**
Oksana Sologub, Leonid Salamakha, Antonio P. Gonçalves, Henri Noël, Thierry Roisnel, Manuel Almeida

**P-32 Speciation of uranium(VI) in presence of chloride ions in ionic liquids**
M.-O. Sornein, C. Cannes, C. Le Naour, G. Lagarde, E. Simoni, J.-C. Berthet

**P-33 Thorium partitioning in Murataite-based ceramic produced by inductive melting in cold crucible**
S. Stefanovsky, A. Ptashkin, O. Knyazev, S. Yudintsev, B. Nikonov

**P-34 The $UCu_2T_3Al_7$ alloys in high magnetic fields and their specific heat.**
W. Suski, A.Hackemer, K.Wochowski, A.Gilewski, T.Mydlarz

**P-35 Ferromagnetic properties of single-crystalline $U_2NiSi_3$**
M. Szlawska and D. Kaczorowski

**P-36 Magnetic features and electronic structure of uranium quaternary $U_2ScB_6C_3$**
V. H. Tran, P. Rogl, T. Mori, H. Ripplinger, K.H. Schwarz and W. Miiller

**P-37 Uranium processing in supercritical carbon dioxide**
Y. Weicai, L. Wenhua, Z. Guangfeng

**P-38 Chemical, structural, spectroscopic and electrical studies of three new anhydrous rubidium and cesium uranyl phosphates**
S. Yagoubi, R. Caciuffo, S. Obbade, M. Benseghir, C. Renard, F. Abraham

**P-39 Functional and structural chemistry of uranium(III) amide complexes**
T. Yamamura, D. Li, K. Shirasaki, Y. Yoshida, S. Ohta, I. Satoh, Y. Shiokawa

**P-40 The $A^+$ monovalent cation mobility and crystal structure in $AUV_3O_{11}$**
S. Obbade, C. Renard, F. Abraham

# Oral Presentations

# Abstracts

# A1

## Coexistence of ferromagnetism and the underscreened Kondo effect in heavy fermion uranium compounds.

**B. Coqblin[1], N. B. Perkins [2,3] and J.R. Iglesias[4]**

*1. Laboratoire de Physique des Solides, UMR 8502-CNRS, Université Paris-Sud, 91405-Orsay, France, e-mail : coqblin@lps.u-psud.fr*
*2. Institute für Theoretische Physik, TU Braunschweig, Mendelssohnstrasse 3, 38106 Braunschweig, Germany*
*3. Bogoliubov Laboratory of Theoretical Physics, JINR, Dubna, Russia*
*4. Instituto de Fisica, Universidade Federal do Rio Grande do Sul, 91501-970 Porto Alegre, Brazil*

Many cerium, ytterbium and other anomalous rare-earth (Pr, Sm, Eu, Tm) compounds present a Kondo behaviour. The well known Doniach diagram accounts for the strong competition between the Kondo effect and the magnetic order (essentially, antiferromagnetic) observed in many cerium compounds: the Neel temperature $T_N$ is passing through a maximum versus the Kondo exchange interaction $|J_K|$ (which increases with applied pressure), disappears then at a quantum critical point and yields a strong heavy fermion behaviour above it, in agreement with the phase diagrams of many cerium compounds, such as $CeAl_2$ or $CeRh_2Si_2$ [1].

The situation of actinide systems and, particularly, of uranium compounds is even more complex, because of weaker localisation of the 5f electrons than that of the 4f electrons. Different behaviours have been observed, varying from a mixed valence one or a non magnetic one described for example by spin fluctuations like $UAl_2$ to heavy fermion compounds which order magnetically at low temperatures and even become superconducting like $URu_2Si_2$, $UPd_2Al_3$, $UGe_2$ or URhGe [2].

We discuss here the interesting effect of the coexistence between the Kondo effect and ferromagnetic order which has been observed in some uranium compounds such as UTe [3], $UCu_{0.9}Sb_2$ [4] and $UCo0_{0.5}Sb_2$ [5] which undergo a ferromagnetic ordering at the large Curie temperatures of 102 K, 113 K and 64.5 K, correspondingly, and present a logarithmic decrease of the magnetic resistivity above it. The values close to the free ion values of the uranium magnetic moments deduced from magnetic susceptibility experiments [6] suggest that the 5f electrons are localized. It is interesting to note that these Curie temperatures are much larger than those observed in the rare Kondo and ferromagnetic cerium compounds such as CeAg and $CePt_xSi$ compounds.

In order to describe the physical properties of such ferromagnetic uranium compounds, we have recently developed the Underscreened Kondo lattice (UKL) model. In these compounds the localized spins are not completely screened by the conduction electron spins at temperatures much below the Kondo temperature $T_k$. Thus, we start from the $f^2$ configuration and $S_f$=1 spins to describe the 5f electrons. We consider a Kondo lattice of $S_f$=1 coupled by an intra-site Kondo interaction $J_K$ to the conduction band, interacting among themselves via an inter-site f-f ferromagnetic exchange $J_H$. We use the mean field approximation with four mean field parameters: $\lambda_\sigma = < \Sigma_\alpha c^+_{i\sigma} f_{\alpha i\sigma} >$ (where $\alpha$=1,2 to describe the $f^2$ configuration), the f-magnetization M and the c-magnetization m. The two spin-dependent $\lambda_\sigma$ can give a good description of the Kondo effect in the mean field approximation. The solutions of the self-consistent equations yield a density of states for each spin direction, consisting of a non-hybridized f-band at an energy $E_{0\sigma}$ and a c-f hybridized band with a gap separating two sub-bands around $E_{0\sigma}$.

The detailed results can be found elsewhere [7], while here we present only some of them. Figure 1 shows the plots of the Kondo parameters $\lambda_\sigma$ and of the magnetizations, for $J_K$ =

0.8, $J_H$ = -0.01 (in units of the half conduction band width) and a number of conduction electrons $n_c$ = 0.8. We obtain a strong coexistence between the Kondo effect and the ferromagnetic order at low temperatures below the Curie temperature $T_c$ and a Kondo effect alone between $T_c$ and $T_k$. Figure 2 gives the plots of $T_c$ and $T_k$ versus $J_K$, for $J_H$ = -0.01 and $n_c$ = 0.8. We see that the Kondo temperature $T_k$ starts from zero at a finite $J_K$c value, increases very abruptly above it and finally saturates for high values of $J_K$. The Curie temperature $T_c$ exists for all the $J_K$ values, crosses $T_k$ close to $J_K$c and finally slowly increases versus $J_K$ but remains there always lower than $T_k$. We obtain that the ferromagnetic order exists for all values of the ratio $J_K/J_H$, while the Kondo-ferromagnetism coexistence takes place only for sufficiently large values of the ratio $J_K/J_H$. Figure 2 gives a "ferromagnetic Doniach diagram" for the UKL model, which appears to be significantly different from the Doniach diagram of the regular Kondo lattice model which was described above. In conclusion, the Underscreened Kondo Lattice model accounts for the strong coexistence between ferromagnetism and the Kondo effect observed in some Uranium compounds.

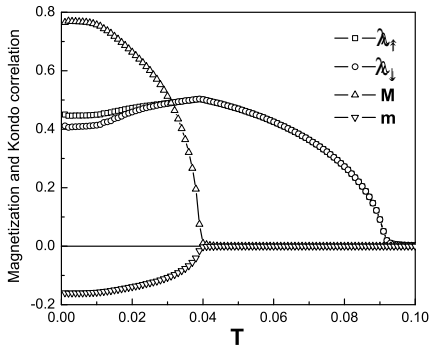


Fig. 1. Plot of M, m and the two parameters $\lambda_\sigma$ for $J_K$ = 0.8, $J_H$ = -0.01 and $n_c$ = 0.8.

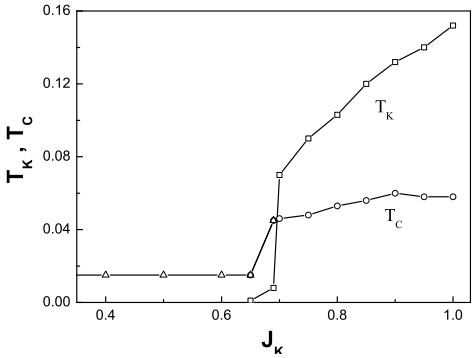


Fig. 2. Plots of $T_c$ and $T_k$ versus $J_K$, for $J_H$ = -0.01 and $n_c$ = 0.8.

## References

[1] B. Coqblin, AIP Conference Proceedings, **846**, pp. 3-93 (2006).
[2] J. Flouquet, Progress in Low Temperature Physics, **15**, pp.139-281 (2006)
[3] J. Schoenes, Journal Less-Common Met. **121**, 87 (1986).
[4] Z. Bukowski, R. Troc, J. Stepien-Damm, C. Sulkowski and V. H. Tran, J. Alloys and Comp., **403**, 65 (2005)
[5] V. H. Tran, R. Troc, Z. Bukowski, D. Badurski and C. Sulkowski, Phys. Rev. B **71**, 094428 (2005)
[6] J. Schoenes, O. Vogt, J. Löhler, F. Hulliger and K. Mattenberger, Phys. Rev. B **53**, 14987 (1996)
[7] N. B. Perkins, J. R. Iglesias, M. D. Nunez-Regueiro and B. Coqblin, cond-mat / 0609199

# A2

## Electronic Structure and Photoemission of Pu and Am compounds

**Alexander Shick[1], Ladislav Havela[2], and Tomas Gouder[3]**

*[1] Institute of Physics, ASCR, Prague, Czech Republic,*
*e-mail: shick@fzu.cz*
*[2]Department of Condensed Matter Physics, Charles University, Prague, Czech Republic*
*[3] European Commission, Joint Research Centre, Institute for Transuranium Elements, Karlsruhe, Germany*

Theoretical description of the situation near the localization threshold in the 5*f* series (i.e around Pu and Am) is a rather complex issue, mainly due to many body effects (electron-electron correlations) playing a prominent role [1]. In the present work, a straightforward and efficient procedure to perform dynamical mean-field (DMFT) calculations of the photoelectron spectra for Pu and Am based materials is described. We start with performing self-consistent *around-mean-field* (AMF)-LSDA+U ground state calculations [2]. Since LSDA+U approximation is generically connected with the DMFT method, the LSDA+U potential is a static approximation to DMFT self-energy Σ(z). Making use of the corresponding LSDA+U eigenvalues and eigenfunctions, we evaluate LSDA+U Green function, and corresponding "bath" Green functions (often called Weiss field in DMFT). Next, we insert the atomic-like self-energy (often called Hubbars I), calculated for the same number of correlated electrons as given by LDA+U, into this "bath", and calculate the new Green function under a condition that $n_f$ is equal to a given number of correlated electrons [3].

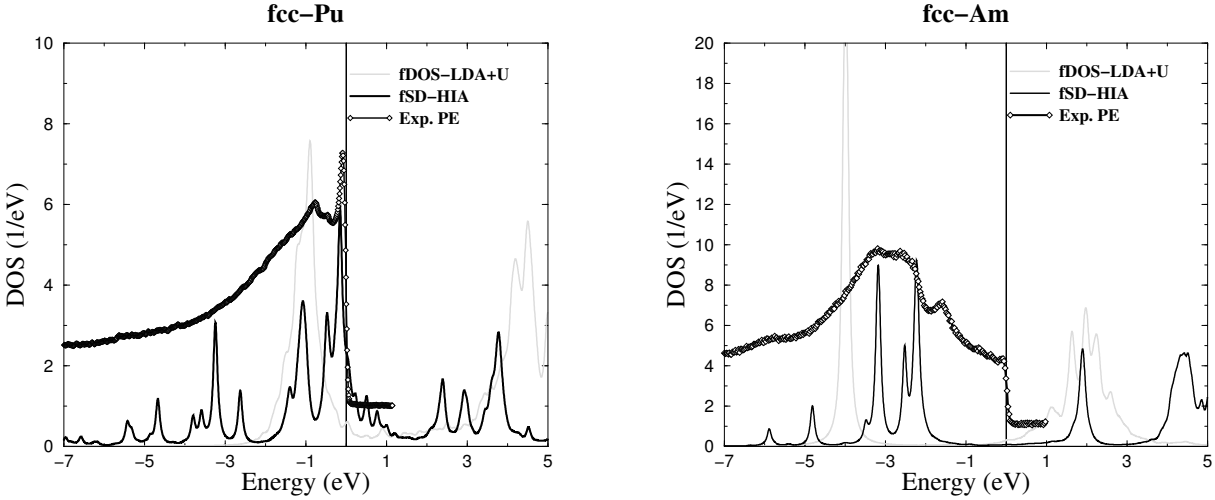


**Fig.1:** *f*-partial density of states (fDOS) from AMF-LDA+U calculations and spectral density (HIA) for δ-Pu and *fcc* Am.

We have applied the theory to access the experimental photoelectron spectra of δ-Pu, Am, PuTe, and AmX (X=N,Sb,Te). The spectral density of *f*-states (fDOS) for δ-Pu is shown in Fig.1 (left). The AMF-LDA+U fDOS manifold at around -1 eV transforms into a set of multiplet transitions with high value of spectral density at $E_F$ . The three narrow features within 1 eV below $E_F$ are consistent with experimental PES for a broad class of Pu compounds. In our calculations, these peaks are directly connected to $f^6 \rightarrow f^5$ multiplet transitions. For *fcc*-Am (see Fig.1 right), the well localised fDOS peak at -4 eV transforms to the multiplet of excited state transitions $f^6 \rightarrow f^5$ below $E_F$, and fDOS manifold around +2 eV to $f^6 \rightarrow f^7$ multiplet transitions. Although there is no doubt that the 5*f* multiplets must dominate the experimental valence-band spectra of Am-based systems, individual lines are not resolved (except for partly resolved features in the spectrum of Am metal), and the position of the 5*f* intensity in the energy spectrum is the main indicator of the agreement with calculations. For

both δ-Pu and Am the calculated spectral density is in a good agreement with photoelectron spectra [4,5].

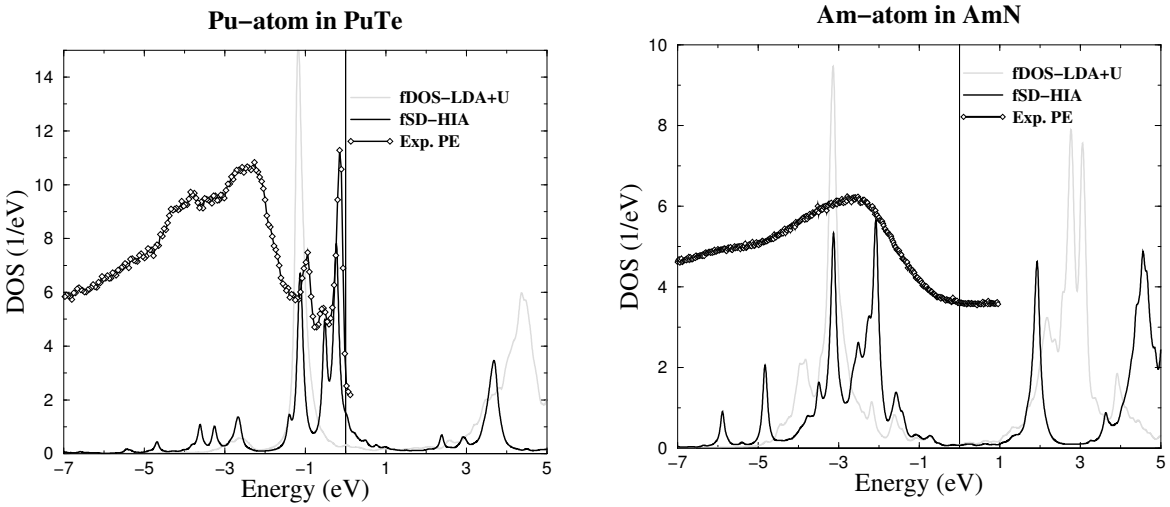


**Fig.2:** The fDOS (AMF-LDA+U) and Spectral Density (HIA) for Pu-atom in PuTe and Am-atom in AmN.

Similarly to δ-Pu, the calculations performed for PuTe (see Fig. 2) reveal the three-peak pattern similar to Pu, in agreement with PES [6]. One should note that the high spectral density at the Fermi level is also explaining the enhanced values of the $\gamma$-coefficient of electronic specific heat, observed in δ-Pu and other Pu systems.

The AMF-LDA+U (with $U$ = 4 eV and $J$ = 0.75 eV ) yields AmN as an indirect gap semiconductor and AmSb as a semi-metal, in agreement with experiment [5]. Again, as in Am, LDA+U fDOS cannot explain experimental PES. In LDA+HIA calculations, the localised fDOS peak transforms to the multiplet of excited-state transitions $f^6 \rightarrow f^5$ (see Fig. 2.), in agreement with PES. In recent LDA+U calculations [7], the Coulomb $U$ has been reduced to unreasonably low value of 2.5 eV in order to place fDOS peaks into the range of experimental PES. There is no reason to do so as PES is related not to the ground state LDA+U fDOS, but to the LDA+HIA spectral density, which is based on multiplet transitions.

To conclude, we show the importance of electron correlations beyond those, which are included in a conventional band theory, for Pu and Am based systems. The calculations explain that atomic-like excitations can be observed even if the 5*f* states are not fully localized as in δ-Pu, and the atomic character fixes the characteristic energies such that similar features are found in spectra of diverse Pu systems.

**Acknowledgement** This work was supported by the Grant Agency of the Academy of Sciences of the Czech Republic under grant No.A100100530, and by the COSP P16 action (project OC144, financed by the Czech Ministry of Education).

## References

[1] S.Y. Savrasov , G. Kotliar, E. Abrahams, *Nature* 410 (2001) 793.
[2] A. Shick, V. Drchal, L. Havela , Europhys. Lett. 69 (2005) 558.
[3] A. Shick, J. Kolorenc, L. Havela, V. Drchal, T. Gouder, Europhys.Lett. 77 (2007) 17003.
[4] L. Havela, F. Wastin, J. Rebizant, T. Gouder, Phys.Rev.B 68 (2003) 085101.
[5] T. Gouder, P.M. Oppeneer, F. Huber, F. Wastin, J. Rebizant, Phys. Rev.B 72 (2005) 115122.
[6] T. Durakiewicz, J.J. Joyce, G.H. Lander, C.G. Olson, M.T. Butterfield et al., Phys.Rev.B 70 (2004) 205103.
[7] D.B. Ghosh, S.K. De, P.M. Oppeneer, M.S.S. Brooks, Phys.Rev.B 72 (2005) 115123.

# A3

## Evidence for a non-Fermi liquid state in $URh_{0.62}Ru_{0.38}Ge$

**W. Miiller[1], V.H. Tran[1], R. Wawryk[1], N. Oeschler[2], F. Steglich[2]**

[1] *W. Trzebiatowski Institute of Low Temperature and Structure Research, Polish Academy of Sciences,*
*PO Box 1410, 50-950 Wroclaw, Poland, e-mail: W.Miiller@int.pan.wroc.pl*
[2] *Max-Planck-Institut für Chemische Physik fester Stoffe, Nöthnitzer Str. 40, 01187 Dresden, Germany*

The physics of strongly correlated electron materials has gained interest during the past years. There are phenomena, such as heavy fermion behaviour, unconventional superconductivity, non-Fermi liquid (NFL), quantum critical points and coexistence of superconductivity and magnetic order, which are still a subject of interest in many scientific laboratories. Investigation of solid solutions formed between URhGe (ferromagnet $T_C$ = 9.5 K [1], superconducting below 0.25 K [2]) and URuGe (paramagnet – spin fluctuator [1]) has revealed an interesting magnetic phase diagram [3,4]. Both the parent compounds crystallize in the orthorhombic TiNiSi type structure (space group Pnma). It was reported that the compositions with x up to 0.25 are ferromagnetic. The Curie temperature initially increases (up to 11 K at x = 0.1), and thereafter $T_C$ decreases and long-range magnetic order vanishes at x = 0.3. The latter composition was reported to be short-range magnetically ordered with strong spin fluctuations [5].

In the present study we have focused our attention on $URh_{0.62}Ru_{0.38}Ge$, which seems to be a point, where magnetic order completely vanishes. Polycrystalline sample was prepared by arc-melting technique and annealed at 800°C for two days. The magnetic properties were studied in the temperature range 1.9 – 400 K and in fields up to 5.5 T. Electrical resistivity was measured over the range of 2 – 300 K, employing a four-probe dc technique. Specific heat measurements were carried out down to 0.3 K and in magnetic fields up to 7 T. Seebeck's coefficient was measured from 2 to 300 K using a differential method. Measurement of Hall effect was performed in temperature range 1.9 - 400 K and in magnetic fields up to 9 T, employing a 5-point ac technique.

The resistivity of $URh_{0.62}Ru_{0.38}Ge$ at high temperature range displays extended maximum at 120 K, characteristic for Kondo-lattice compound. However, for temperatures below 7 K the $\rho$ vs. $T$ dependence follows a power law $\rho(T) \sim T^n$, with $n$ = 1.

The magnetic susceptibility above 100 K fulfils a modified Curie-Weiss law with $\mu_{eff}$ = 1.59 $\mu_B$/f.u. and $\theta_p$ = -55 K. The latter value suggests presence of antiferromagnetic correlations between U atoms. Reciprocal magnetic susceptibility at low magnetic fields and temperatures decreases in a power law manner, $\chi^{-1}(T) \sim T^{-m}$, with $m$ = 1.3 ($\mu_0 H$=0.05 T) and $m$ = 1.65 ($\mu_0 H$=0.01 T).

The specific heat divided by temperature $C_p/T$ exhibits an upturn below 6 K. With decreasing temperature down to 0.3 K the $C_p/T$ ratio does not evidence any signal of either magnetic order or spin-glass freezing. Indeed, the temperature dependence of $C_p$ obeys the relationship $C_p = - a\, T \ln(T/T_0)$ law, with $a$ = 56 (1) mJ/K$^2$mol, and $T_0$ = 54 K. Application of magnetic field reduces a slope of $C_p/T$ (ln($T$)) and recovers Fermi-liquid behaviour for B > 7 T (Fig. 1).

The Seebeck's coefficient, plotted in the inset of Fig. 2, displays a peak at ~ 10 K, and afterwards changes sign to negative values above 26 K. The $S/T$ product vs. temperature (Fig. 2) follows logarithmic dependence $S/T = -a \ln(T) + b$, with $a$ = - 0.49 $\mu$V/K$^2$ and $b$ = 1.56 $\mu$V/K$^2$. Similar temperature dependence of $C_p/T$ and $S/T$ provides clear evidence for NFL features.

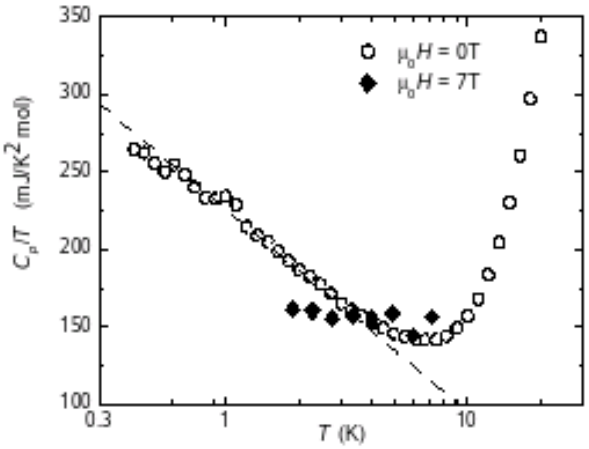


Fig. 1. Temperature dependence of the $C_p/T$ ratio. 0 and 7 T line shows a *lnT* dependence.

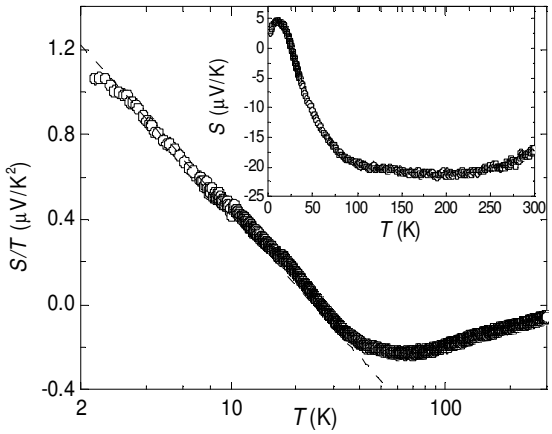


Fig. 2 Temperature dependence of the *S/T*. Dashed at ratio. Dashed line represents a *lnT* dependence. The inset shows the *S(T)* vs *T* curve.

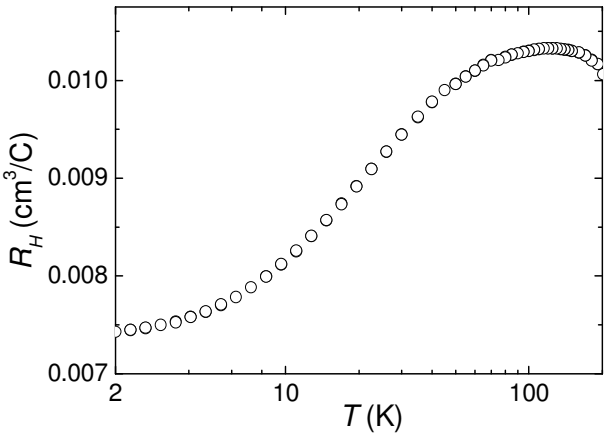


Fig. 3. Temperature dependence of the Hall coefficient $R_H$ at 2-200 temperature range at 9T.

The Hall coefficient $R_H$ exhibits a maximum at ~ 120 K (Fig. 3), typical for the heavy-fermion system. At 2 K $R_H$ levels off at $7.5 \times 10^{-9}$ m$^3$/C, corresponding to 0.18 carriers/f.u. Combining $C_p/T$ = 180 mJ/mol K$^2$ at 2 K with the $R_H$ data one may estimate the electron effective mass to be about $m_{eff} = 360\ m_e$ at 2 K.

In conclusion, the behaviour of the specific heat and magnetic susceptibility of $URh_{0.62}Ru_{0.38}Ge$ is consistent with that predicted in framework of the spin-fluctuation scenario for NFL state ($C_p/T \sim \ln T$ and $\chi^{-1}(T) \sim T^{-4/3}$) [6]. An enhanced electron mass determined by the Hall coefficient, linear temperature dependence of the resistivity and *lnT* dependence observed in the *S/T* ratio certainly support the NFL properties of the studied alloy. Taking into account spin-fluctuation features found in $URh_{0.7}Ru_{0.3}Ge$, the mentioned scenario seems to be plausible.

## References

[1] R. Troć *et al.*, J. Magn. Magn. Mater. **73** (1988) 389.
[2] D. Aoki *et al.,* Nature **413** (2001) 613.
[3] S. Sakarya *et al.*, Physica B **378 - 380** (2006) 970.
[4] W. Miiller *et al.,* Materials Science – Poland, (2007) in press.
[5] V.H. Tran *et al.,* J.Phys.: Cond. Matter (2007) in press.
[6] T. Moriya, Spin Fluctuations in Itinerant Electron Systems (1985, Berlin, Springer)

# A4

## Understanding the Changing Role of 5f Electrons through High-Pressure Studies

**R. G. Haire**

*Oak Ridge National Laboratory, Oak Ridge, TN 37831-6375 USA*

Great strides have been made in experimental and computational high-pressure studies of the actinide in the last six years. Most of these investigations have been concerned with the structural stability of the f-electron metals, although some efforts in this regard have included compounds. The most interesting findings have been with the elemental state of these elements, as the presence and bonding roles of non-actinide atoms in compounds perturbs the involvement of 5f electrons.

The early actinides behave differently than the transplutonium members of the series, the latter often being likened to the lanthanide series of elements. However, this tends to be a misconception that is not fully realized in practice; one reason is the 5f electrons have a much greater spatial extension than their 4f counterparts. The nature of the earlier members of the actinide series are often considered from the standpoint of distortion of the bonding via incorporation of 5f states in their bonding, which brings about significant changes in crystal symmetries. With the transplutonium elements the normal ground-state crystal structures are governed by 6d bonding, similar to that observed with 5d bonding encountered in the lanthanide series. However with significant changes in interatomic distances via pressure, the 5f electrons are more readily perturbed and are found to acquire structural behaviors quite similar to the earlier actinides after incorporating 5f-electron character in their bonding. More recent thoughts have considered the roles of spin polarization and coupling and magnetic interactions in the context of the reduction of crystal symmetries and bonding alterations. Some of these were observed and discussed in the context of the unexpected findings with curium [1], berkelium-curium alloys [2] and correlations of electronic configurations with bonding changes observed under pressure [3].

Presented here is an overview of the pressure behaviors of several actinide materials, some experimental and computational insights into the bonding changes encountered, selected correlations that can be considered in understanding changes occurring in the electronic configurations and bonding, and prospects for future efforts in this arena.

### References

1. S. Heathman, R. G. Haire, T. Le Bihan, A. Lindbaum, M. Idiri, P. Normile, S. Li, R. Ahuja, B. Johansson and G. H. Lander, Science, **309**,110 (2005); and references therein.
2. S. Heathman, R. G. Haire, T. Le Bihan,R. Ahuja, S. Li, W. Luo and B. Johansson, Alloys and Comp., (in press, 2007).
3. R. G. Haire and S. Heathman, Mat. REs, Soc. Symp. Proc., (in press, 2007).

# A5

## Explaining the Magnetic Stabilization of Curium: Competing Spin-Orbit and Exchange Interaction

**K.T. Moore,[1] G. van der Laan,[2] R.G. Haire,[3] M.A. Wall,[1] A.J. Schwartz,[1] P. Söderlind,[1]**

[1]*Lawrence Livermore National Laboratory, Livermore, California 94550, USA.*
[2]*Magnetic Spectroscopy Group, Daresbury Laboratory, Warrington WA4 4AD, UK.*
[3]*Oak Ridge National Laboratory, MS-6375, Oak Ridge, Tennessee 37831, USA.*

Few elements in The Periodic Table have crystal structures stabilized by magnetism. Recently, curium was shown to exhibit magnetic interactions large enough to dictate the crystal structure of its Cm III phase [1], placing it in the ranks of iron and cobalt [2-3] as one of the rare metals with a magnetically-stabilized crystallographic phase. In a diamond-anvil-cell study [1], Cm metal underwent transformations between five different crystal structures when pressurized up to ~100 GPa, Cm I – Cm V. *Ab initio* calculations showed that magnetic correlations play a crucial role in determining the crystal structures observed and that Cm III, which is monoclinic with the space group *C*2/*c*, could only be stabilized with spin polarization of the 5*f* electrons.

Using electron energy-loss spectroscopy (EELS) in a transmission electron microscope (TEM), many-electron atomic spectral calculations and density functional theory we investigate the electronic and magnetic structure of Cm. Via spin-orbit analysis [4-6] of the $N_{4,5}$ edges of Am and Cm metal, we show that the intermediate coupling curve for the 5*f* states, which most actinide metals follow, swings strongly back towards the *LS* coupling limit at Cm. It is this *LS*–inclined intermediate coupling that produces a large spin polarization, in turn causing the magnetic stabilization of Cm. The abrupt and striking change in the behavior of the 5*f* electrons at Cm is caused by the exchange interaction. *jj* coupling prefers all the electrons to be in the $f_{5/2}$ level, which can hold no more than six. The maximal energy gain in *jj* coupling is thus obtained for Am $f^6$ because the $f_{5/2}$ level is completely filled. However, for Cm $f^7$ at least one electron will have to occupy the $f_{7/2}$ level. The $f^7$ configuration has the maximal energy stabilization due to the exchange interaction, with all spins parallel in the half filled shell, and this can only be achieved in *LS* coupling. Thus, the large changes in the electronic and magnetic properties of the actinides at Cm are due to this transition from optimal spin-orbit stabilization for $f^6$ to optimal exchange interaction stabilization for $f^7$. In all cases the spin-orbit and exchange interaction compete with each other, resulting in intermediate coupling, however going from $f^6$ to $f^7$ there is a clear and pronounced shift in the power balance in favor of the exchange interaction.

### References

[1] S. Heathman *et al.*, *Science* **309**, 110 (2005).
[2] O. K. Andersen *et al.*, *Phys. B* **86-88**, 249 (1977).
[3] P. Söderlind *et al.*, *Phys. Rev. B* **50**, 5918 (1994).
[4] G. van der Laan *et al.*, *Phys. Rev. Lett.* **93,** 097401 (2004).
[5] K.T. Moore *et al.*, *Ultramicroscopy* **106**, 261 (2006).
[6] K.T. Moore *et al.*, *Phys. Rev. B* **73**, 033109 (2006).

# B1

## From the quadrupolar phases of $UPd_3$ to the magnetism of $PuPd_3$

**K A McEwen,[1] H C Walker[1], M D Le[1], E Colineau[2], F Wastin[2]**

[1] *Dept. of Physics and Astronomy,University College London, London WC1E 6BT, UK, e-mail: k.mcewen@ucl.ac.uk*
[2] *Institute for Transuranium Elements, Postfach 2340, 76125 Karlsruhe, Germany*

It is now well known that $UPd_3$ displays a sequence of four quadrupolar phase transitions between 8K and 4K. The challenge has been to determine the *order parameters* of these phases, and is complicated by the double hexagonal close packed structure that this fascinating compound exhibits. Over the years, we have carried out a range of macroscopic and microscopic studies in order to elucidate the nature of the quadrupolar phases. Most recently, we have made considerable progress in our understanding of $UPd_3$ following new heat capacity measurements at ITU, and a series of x-ray resonant scattering (XRS) experiments at ESRF.

At the Journées des Actinides meeting in 2006, we presented an interpretation of our results for the first quadrupolar phase of $UPd_3$ below $T_0$ = 7.6K. Our XRS studies in this phases indicated that the order parameter of this phase was $Q_{zx}$, with uranium quadrupole moments on the quasi-cubic sites stacked in an antiferro sequence along the c-axis. Full details are published in [1]. However, this conclusion was at variance with the results of earlier polarised neutron diffraction measurements of $UPd_3$ in applied field that indicated the order parameter was $Q_{xx-yy}$. We shall show how this apparent contradiction can be resolved [2] by an extension of our earlier theoretical analysis of $UPd_3$ [3].

We have recently begun an investigation of $PuPd_3$. This compound exhibits the cubic $AuCu_3$ structure. We will report measurements at ITU of the susceptibility, magnetisation and heat capacity of this compound. These show a phase transition at 24K which we attribute to antiferromagnetic ordering.

### References

[1] H C Walker, K A McEwen, D F McMorrow, S B Wilkins, F Wastin, E Colineau, D Fort, *Phys. Rev. Lett.* **97**, 137203 (2006) and references therein.
[2] K A McEwen, H C Walker, M D Le, D F McMorrow, E Colineau, F Wastin, S B Wilkins, J-G Park, R I Bewley, D Fort, *J. Mag. Mag. Mater.*, Proc International Conference on Magnetism, Kyoto 2006, in press (2007).
[3] K A McEwen, J-G Park, A J Gipson, G A Gehring, *J Phys Condens. Matter* **15** , S1923 (2003)

# B2

## Hidden Order and Low-Energy Excitations in $NpO_2$

**N. Magnani,[1] P. Santini[2], S. Carretta[2], G. Amoretti[2], R. Caciuffo[1]**

[1] *European Commission, Joint Research Centre, Institute for Transuranium Elements, Postfach 2340, D-76125 Karlsruhe, Germany. e-mail: Nicola.Magnani@ec.europa.eu*
[2] *Department of Physics, University of Parma, Viale Usberti 7/A, I-43100 Parma, Italy. e-mail: santini@fis.unipr.it*

The low-temperature properties of $NpO_2$ have recently attracted much attention because its second-order phase transition, occurring at $T_0 \approx 26$ K, has been proposed as the first example of ordering driven by a magnetic multipole (MM) primary order parameter (OP) [1]. No experimental indication of magnetic dipole order has ever been found by neutron diffraction or Mössbauer spectroscopy. Only recently, resonant x-ray [2] and $^{17}$O-NMR [3] measurements demonstrated the occurrence of longitudinal type-I (AF-I) triple-q ordering of $\Gamma_5$ electric quadrupoles, which have been interpreted as secondary OPs induced by a longitudinal type-I triple-q ordering of $\Gamma_5$ magnetic multipoles. In fact, both the saturating susceptibility as $T \rightarrow 0$ and μSR experiments indicate that time-reversal symmetry is broken below $T_0$.

Although the symmetry of the OP has been unveiled, truly direct evidence of the MM primary OP is still lacking and its specific form is unknown. In particular, there are four distinct triplets of $\Gamma_5$ operators which could drive the transition. One of these may be constructed from rank-3 (octupoles), one from rank-5 (triakontadipoles), and two from rank-7 operators. Addressing these topics is however a formidable task as multipolar superexchange is but one of the tiles of the puzzle, which also includes crystal field (CF) and other fundamental interactions. We have recently clarified the problem of the CF in dioxides by taking into account the scaling properties of the CF potential and proposing a common solution which works well over the whole actinide series [4]. Moreover, our specific heat measurements have confirmed the non-degenerate $Np^{4+}$ electronic ground state which is expected for a $\Gamma_5$ OP [5].

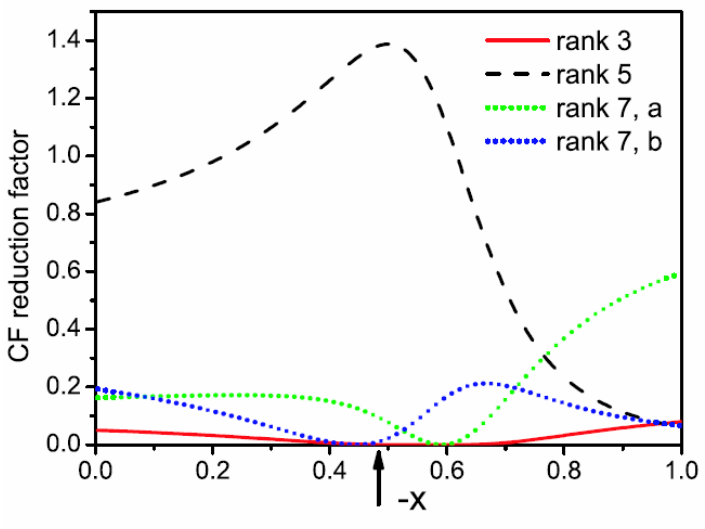


Fig. 1. CF reduction factor (see main text for details) for the $\Gamma_8$ ground quartet as a function of the CF parameter $x$ ($W < 0$). The arrow indicates the most likely value of $x$.

# B2

We have investigated the nature of the hidden order parameter in the ordered phase by calculating the coupled dynamics of spins, $\Gamma_5$ quadrupoles and $\Gamma_5$ triakontadipoles within the random-phase approximation [6]. A key factor in selecting which of these MMs plays a driving role is the CF potential, because this dominant interaction may strongly affect the size of the corresponding multipolar moments. We have estimated this effect for the four possible $\Gamma_5$ MMs by comparing the effective multipolar paramagnetic moment $\mu_{CF}$ associated with the ground $\Gamma_8$-quartet CF wave functions with the corresponding free-ion moment $\mu_0$. Figure 1 shows the calculated reduction factor $\mu_{CF}^2 / \mu_0^2$ as a function of the CF parameter $x$ [7]. The octupolar moment is greatly reduced by the CF and nearly completely quenched for the most likely value $x$ = -0.48, where also the two rank-7 moments are heavily reduced. On the contrary, the rank-5 moment is increased by the CF and peaks at x ≈ -0.5. This shows that the rank-5 MM is by far the most likely driving OP.

We have studied the implications of this finding on the low-energy dynamics in the ordered phase; in particular, we have shown that the powder inelastic neutron scattering (INS) cross section should contain, in addition to the already-observed peak at 6.5 meV [8], a second weaker peak at about 14 meV (Fig. 2). Besides providing direct evidence of MM order, INS could be used to validate the present theoretical results about low-energy excitations.

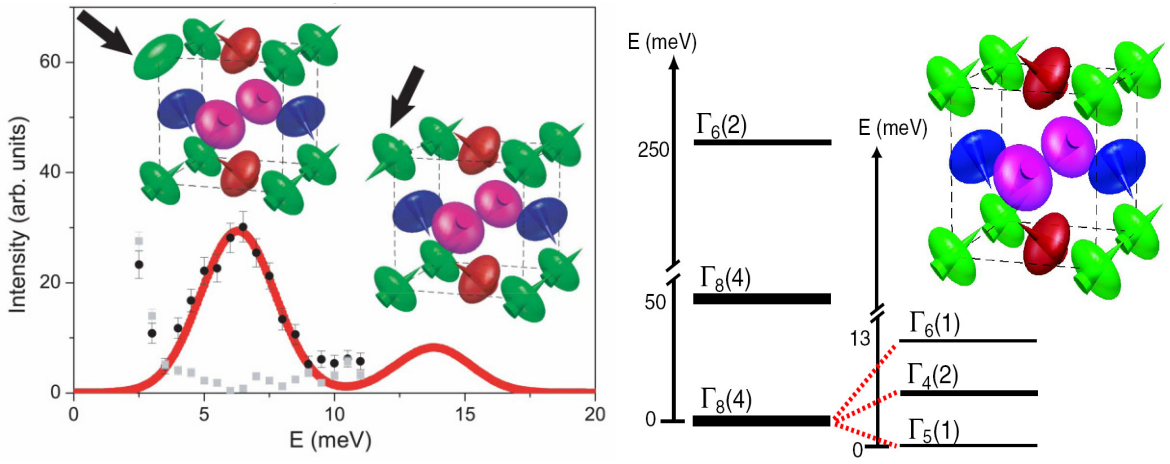


Fig. 2. Left: measured powder INS spectrum [8] for $Q$ = 1.9 Å (black squares: spin flip; gray circles: non-spin flip). Line: Present calculation convoluted with the 3 meV Gaussian resolution function. Right: Calculated cubic CF levels and mean-field splitting of the ground quartet in the ordered phase. Numbers in parentheses are degeneracies. The peak at lower energy in the INS spectrum involves excited states where typically 1 Np ion (indicated by an arrow) has its quadrupole reverted and vanishing $\Gamma_5$ MM moment, corresponding to a transition between the $\Gamma_5$ and the $\Gamma_4$ mean-field states. The peak at thigher energy involves excited states where typically 1 Np ion has its $\Gamma_5$ MM moment reverted, corresponding to a transition between the $\Gamma_5$ and the $\Gamma_6$ mean-field states.

## References


[1] P. Santini and G. Amoretti, *Phys. Rev. Lett.* **85**, 2188 (2000).
[2] J. A. Paixao et al., *Phys. Rev. Lett.* **89**, 187202 (2002).
[3] Y. Tokunaga et al., *Phys. Rev. Lett.* **94**, 137209 (2005).
[4] N. Magnani et al., *Phys. Rev. B* **71**, 054405 (2005).
[5] N. Magnani et al., *Physica B* **359-361**, 1087 (2005).
[6] P. Santini et al., *Phys. Rev. Lett.* **97**, 207203 (2006).
[7] K. R. Lea, M. J. M. Leask and W. P. Wolf, *J. Phys. Chem. Solids* **23**, 1381 (1962).
[8] G. Amoretti et al., *J. Phys. Condens. Matter* **4**, 3459 (1992).

# B3

## Electronic, structural and magnetic properties of $UH_3$ at ambient and under high pressure from *ab initio* theory

**Wei Luo[1] and Rajeev Ahuja[1]**

[1] *Dept. of Physics, Condensed Matter Theory Group, Uppsala University, Box 530 , 751 21 Uppsala, Sweden, e-mail: rajeev@fysik.uu.se*

Uranium is a magnetic mineral for atomic energy. It can be reacted with water to produce Uranium trihydride ($UH_3$) at ambient conditions:

$$U^{3+} + 3H_2O \Leftrightarrow UH_3(beta) + 3H^{\pm} + 1.5O_2(aq).$$

$UH_3$ crystallizes in two different structures, one, called β-$UH_3$ which is stable in cubic phase with space group Pm3n and 6 chemical formula in unit cell; the other one, named α-$UH_3$ is low temperature metastable phase with same space group but 2 chemical formula in the unit cell. β-$UH_3$ is first 5f electron ferromagnet with Curie temperature about $173^0$K [1]. We have performed the total energy calculations to study the electronic, structural and magnetic properties of both phases using *ab initio* methods based on density functional theory (DFT) in conjunction with full potential linear muffin tin orbital method (FPLMTO) and projected augmented plane wave method as implemented in VASP code. At equilibrium volume, both phases show ferromagnetism with spin magnetic moment of 2.40 μB/U for α-$UH_3$ phase and 2.49 μB/U for β-$UH_3$ phase which is contributed mainly by *f* electrons. The calculated bulk modulus using Birch-Murnaghan equation of state is 94 GPa for β-$UH_3$ phase and 99 GPa for α-$UH_3$ phase. Our calculation shows a structural phase transition pressure from β-$UH_3$ to α-$UH_3$ around 10 GPa whereas high-pressure investigation on β-$UH_3$ did not show any structural phase transition up to 29 GPa [2]. The high-pressure phase transition is driven by repulsion between hydrogen atoms.

### References

[1] S. T. Lin and A. R. Kaufmann, *Phys. Rev,* **102,** 640 (1956).
[2] I. Halevy, S. Salhov, S. Zalkind, M. Brill, and I. Yaar, *J. Alloys and Compounds* **370,** 59 (2004).

# B4

## Electric field gradients in Ce- and Pu-based 115 compounds

**Ján Rusz,[1] Peter Oppeneer[1]**

[1] *Department of Physics, Uppsala University, Box 530, S-751 21 Uppsala, Sweden*
*e-mail: jan.rusz@fysik.uu.se*

Electric field gradients (EFG) are very sensitive atom-specific probes of the electronic structure. They sensitively react even to small changes of the charge density surrounding the atom. EFG can be measured in an atom-specific way by nuclear quadrupole resonance experiments in which the quadrupolar frequency $\nu_Q$ is measured, which is proportional to the EFG.

We present an ab initio study of the electric field gradients in Ce*T*$In_5$ and Pu*T*$Ga_5$ compounds (*T* = Co, Rh, Ir) and related alloys, where a small part of the In is replaced by Sn or Cd, thus doping the system by electrons or holes, respectively. Pressure effects are also evaluated.

All these systems crystallize in the tetragonal $HoCoGa_5$ structure. $CeCoIn_5$ and $CeIrIn_5$ are superconductors at low temperature and $CeRhIn_5$ is an antiferromagnet, but under pressure it becomes superconducting [1-4]. The role of Ce *f* electrons is discussed in this context.

We performed calculations within the density functional theory using both the local density approximation and generalized gradient approximation. For the treatment of Ce atom, which contains 4*f* electrons, we employed different models assuming either itinerant or localized *f* electrons. The Pu atom was treated within the around mean-field LDA+U method, which seems to describe well the non-magnetic ground state of the Pu*T*$Ga_5$ compounds [5]. On the base of comparison of our results with known experimental data we discuss the tendency of *f* electrons to localization or itinerancy in the studied compounds and alloys.

For stoichiometric Ce-based compounds we found that the itinerant treatment of *f*-electrons works well for *T* = Co, Ir while $CeRhIn_5$ is better described within the open-core treatment of the 4*f*. This finding is in agreement with the interpretation of previous de Hass – van Alphen measurements of the Fermi surface topology [6-8].

Work on the Pu-115 compounds has been performed in collaboration with A.B. Shick. Discussions with N.J. Curro, O.P. Sushkov and P. Novák are gratefully acknowledged. Financial support from STINT is acknowledged.

### References

[1] C. Petrovic, P.G. Pagliuso, M.F. Hundley, R. Movshovich, J.L. Sarrao, J.D. Thompson, Z. Fisk, P. Monthoux, J. Phys. Condens. Matter 13 (2001) L337.
[2] C. Petrovic, R. Movshovich, M. Jaime, P.G. Pagliuso, M.F. Hundley, J.L. Sarrao, Z. Fisk, J.D. Thompson, Europhys. Lett. 53 (2001) 354.
[3] W. Bao, P.G. Pagliuso, J.L. Sarrao, J.D. Thompson, Z. Fisk, J.W. Lynn, R.W. Erwin, Phys. Rev. B 62 (2000) R14621.
[4] A. Llobet, J. S. Gardner, E. G. Moshopoulou, J.-M. Mignot, M. Nicklas, W. Bao, N. O. Moreno, P. G. Pagliuso, I. N. Goncharenko, J. L. Sarrao, and J. D. Thompson, Phys. Rev. B 69, 024403 (2004).
[5] P.M. Oppeneer, A.B. Shick, J. Rusz, S. Lebègue and O. Eriksson, J. Alloy Compd., in press
[6] D. Hall, E.C. Palm, T.P. Murphy, S.W. Tozer, E. Miller-Ricci, L. Peabody, C. Quay Huei Li, U. Alver, R.G. Goodrich, J.L. Sarrao, P.G. Pagliuso, J.M. Wills, Z. Fisk, Phys. Rev. B 64 (2001) 064506.
[7] H. Shishido, R. Settai, D. Aoki, S. Ikeda, H. Nakawaki, N. Nakamura, T. Iizuka, Y. Inada, K. Sugiyama, T. Takeuchi, K. Kindo, T.C. Kobayasi, Y. Haga, H. Harima, Y. Aoki, T. Namiki, H. Sato, Y. Onuki, J. Phys. Soc. Japan 71 (2002) 162.
[8] R. Settai, H. Shishido, S. Ikeda, Y. Murakawa, M. Nakashima, D. Aoki, Y. Haga, H. Harima, Y. Onuki, J. Phys. Condens. Matter 13 (2001) L627.

# C1

## Density Functional Study of CO Adsorption on Pu (100) Surface

**Wen-hua LUO, Da-qiao MENG, Gan LI**

*China Academy of Engineering Physics, P.O.Box 919-71, 621900, Mianyang, Sichuan, P.R.China*
*e-mail: luowenhua712@yahoo.com.cn*

The adsorption of CO molecular on Pu (100) surface are investigated using the generalized gradient approximation (GGA) of spin-polarized density functional theory (DFT) with RPBE functional. Several possible adsorption configurations considered here (see Table 1), the O-down adsorption is less stable than the C-down adsorption which is found to be strong chemisorption. The stability of adsorption configuration of CO is fourfold tilted > fourfold vertical > twofold vertical > onefold. A CO molecule of the most stable configuration is tilted relative to the surface normal by 56.5°. In this case, the CO bond is elongated to 1.37 Å and the adsorption energy is 31.6 kcal/mol. Mulliken charge distribution analysis indicates that the interaction of Pu with CO mainly takes place in the first layer with the other three layers being only slightly affected. Density of states (DOS) analysis indicates that the interaction between Pu atom and CO molecule results mainly from the contribution of hybridized molecular orbital of CO molecule and hybridized orbital of surface Pu atoms, and adsorptions of CO push the top of 5f band deeper away from the Fermi level, indicating further bonding by the 5f orbitals might be less probable. A similar calculation performed for the C and O atoms indicates that the adsorption at the fourfold site is the most stable among various configurations, with adsorption energies of 164.6 and 170.5 kcal/mol, respectively. Finally, the barriers for dissociation of CO bound in a fourfold site have been calculated to be 6.5 kcal/mol, indicating that the dissociation of a CO molecule can takes place even in the low-temperature regime.

Table 1 The optimized geometrical and energy parameters for CO/Pu (100) system

| configuration | | $\varphi^a$ / ° | $r_{C\text{-}O}$ / Å | $r_{Pu\text{-}C}{}^b$ / Å | $r_{Pu\text{-}O}{}^b$ / Å | $h_{X\text{-}surf}{}^c$ / Å | $E_{abs}$ / eV |
|---|---|---|---|---|---|---|---|
| onefold | O-down | 0 | 1.138 | 4.646 | 3.508 | 3.508 | 0.291 |
| | C- down | 0 | 1.161 | 2.437 | 3.598 | 2.437 | 1.012 |
| twofold vertical | O-down | 0 | 1.137 | 5.557 | 4.483 | 4.173 | 0.288 |
| | C-down | 0 | 1.177 | 2.562 | 3.547 | 1.969 | 1.077 |
| fourfold vertical | O-down | 0 | 1.137 | 5.818 | 4.797 | 4.199 | 0.286 |
| | C-down | 0 | 1.198 | 2.777 | 3.579 | 1.529 | 1.176 |
| fourfold tilted | C-down | 56.47 | 1.372 | 2.383 | 2.321 | 0.776 | 1.371 |
| CO (isolated) | | | 1.136 | | | | |

a: $\varphi$ represents the angle between the C-O bond and the normal vector to the surface.
b: $r$ represents the shortest distance of the C or O atom to the Pu atoms in the first layer.
c: $h$ represents the height of the C or O atom in CO above the surface.

# C2

## Chemical reactivity of plutonium oxide towards oxidising agents: An *in situ* photoemission spectroscopy study

**A. Brevet[1], P. Berthou[1], L. Jolly[1], F. Delaunay[1]**

[1] *CEA Valduc, 21120 Is-sur-Tille, France, e-mail : aude.brevet@cea.fr*

Plutonium differs from transition metals as from other actinides in many physico-chemical properties such as the number of allotropic forms or corrosion through unexpected rapid reactions. Although its electronic structure close to the boundary between itinerancy and localization of the 5f electrons is pointed out, these specific phenomena are not well understood. The focus on plutonium reactivity is thus of fundamental interest to predict plutonium compounds corrosion and to guarantee their safe behaviour during long-term storage.

Whereas plutonium dioxide had always been thought to be the highest stable oxide of plutonium, investigations on plutonium corrosion in atmospheric conditions, particularly with water vapour, have shown the existence of a hyperstoichiometric oxide $PuO_{2+x}$ [1, 2]. X-ray photoelectron spectroscopy (XPS), X-ray Absorption Near-Edge Spectroscopy (XANES) and Extended X-ray Absorption Fine Structure (EXAFS) experiments were achieved to determine the chemical speciation and local structure of this oxide [1, 3-6]. Plutonium valence was initially thought to be Pu(VI), as it was revealed by XPS by a small shoulder at 429.0 eV in the Pu $4f_{7/2}$ transition [1]. But recent EXAFS, XANES or theoretical studies support the assignment of the excess of charge to Pu(V) rather than Pu(VI) [3, 5-8], corroborated by XPS analyses and a contribution observed at 427.2 eV [4], a lower binding energy than previously and thus attributed to a lower oxidation state. The $PuO_{2+x}$ feature in the Pu $4f_{7/2}$ transition of XPS spectra has also not been clearly defined until now so that further investigations are needed.

As reaching back ultra-high vacuum (UHV) after water vapour exposure can need long time without baking, *in situ* XPS analyses on surfaces exposed to water vapour are fastidious. On the other hand, other gaseous compounds such as carbon dioxide and carbon monoxide had already shown oxidising potential towards plutonium [9, 10]. Because of carbon monoxide toxicity, carbon dioxide was first considered to follow plutonium oxidation until hyperstoichiometry by XPS.

Exposures to carbon dioxide were realised *in situ* on a clean surface of plutonium sesquioxide $Pu_2O_3$, grown over metallic plutonium by exposure to $O_2$, to follow its oxidation to $PuO_2$ and to expecting $PuO_{2+x}$. To appreciate reactivity and kinetics of $CO_2$ as an oxidising agent, similar experiments were achieved under $O_2$ exposures. Preliminary analysis of Pu 4f spectra, in correlation with O 1s, C 1s transitions and the valence band, will be discussed.

**References :**

[1] J.L. Stakebake et al., *J. Alloys Compd.* **202**, 251 (1993).
[2] J.M. Haschke et al., *Science* **287,** 285 (2000).
[3] S.D. Conradson et al., *Inorg. Chem.* **42**, 3715 (2003).
[4] J.D. Farr et al., *J. Nucl. Mater.* **328**, 124 (2004).
[5] S.D. Conradson et al., *J. Am. Chem. Soc.* **126**, 13443 (2004).
[6] S.D. Conradson et al., *J. Solid State Chem.* **178**, 521 (2005).
[7] L. Petit et al., *Science* **301**, 498 (2003).
[8] R.A. Penneman et al., *J. Solid State Chem.* **178**, 563 (2005).
[9] D.T. Larson et al., *Inorg. Chem.* **20**, 1945 (1981).
[10] T. Almeida et al., *Surf. Sci.* **287-288**, 141 (1993).

# C3

## Inhibition of hydrogen adsorption on uranium surfaces by traces of water vapor

**E. Tiferet[1], M. H. Mintz[1,2], I. Jacob[1] and N. Shamir[2]**

[1] *Dept. of Nuclear Eng., Ben-Gurion Univ. of the Negev, POB 653, Beer-Sheva 84104, Israel*
[2] *Nuclear Research Centre-Negev, POB 9001, Beer-Sheva 84190, Israel. noah.shamir@gmail.com*

Traces of water vapor (between 1% and 2%) are sufficient to inhibit hydrogen dissociation and adsorption on uranium surfaces (either strained or relieved). Direct Recoil Spectrometry (DRS) was used to monitor the concentrations of adsorbed hydrogen and oxygen on the surface, for exposures of various $H_2O/H_2$ (W/H) partial pressure ratios. Fig. 1 presents the ratio of recoiled hydrogen (H(DR), proportional to surface concentration) to that of recoiled oxygen, O(DR), vs. $H_2$ exposure dose, for various W/H ratios. The experiment was performed on a sample relieved 48 hours at 520 K. Similar (but different) results were obtained on strained and differently relieved samples.

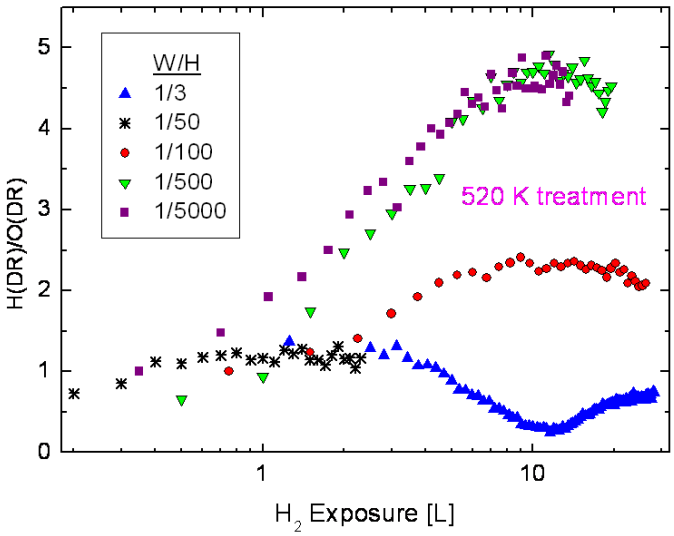


Fig. 1: H(DR)/O(DR) vs. $H_2$ exposure doses, for various W/H ratios, for a given exposure pressure of $H_2$ ($1.5 \times 10^{-8}$ Torr).

It can be seen that for W/H = 1/3 and 1/50, the H/O curves are identical and they are also identical to that obtained for pure water exposures, without hydrogen [1], i.e. total inhibition of $H_2$ co-adsorption is induced by water.

A possible mechanism of the inhibition effect of water on the co-adsorption may involve the comparative capture of $H_2$ dissociation sites by the water dissociation fragments (most likely by the H fragment). Hence, the water dissociation H fragment that easily diffuses on the surface strongly binds to the sites that also form $H_2$ dissociation sites, thus blocks $H_2$ chemisorption. According to such mechanism, the inhibition effect of water should increase with increasing temperature, since the diffusion rate of the H fragment increases, whereas the sticking probability of $H_2$ (physisorption before dissociation) decreases with increasing temperature.

This is evidently obtained as illustrated in Fig. 2, where the above temperature trend is clearly displayed.

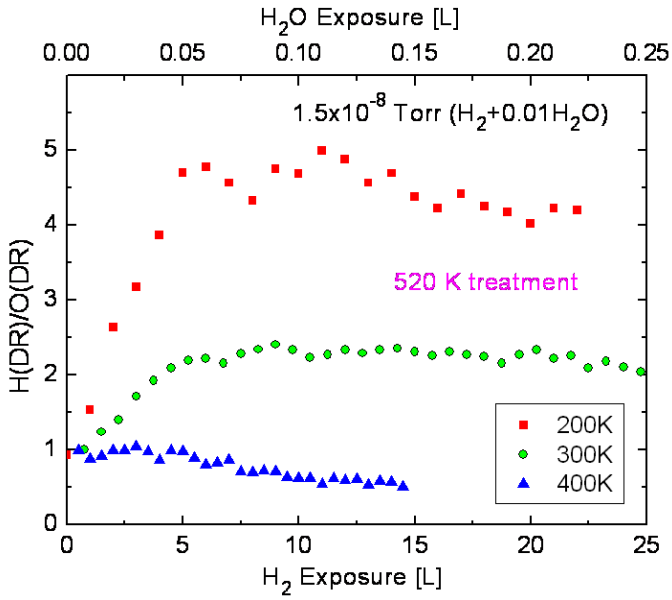


Fig. 2: H(DR)/O(DR) vs. $H_2$ exposure for W/H =1/100 at 3 temperatures.

Replacing water vapor by oxygen (even for much higher relative partial pressures), no inhibition of hydrogen dissociation and adsorption is observed. This proves that the atomic hydrogen, originating from the water dissociation, is the major player in blocking molecular hydrogen dissociation sites.

The above inhibition effect of water is qualitatively independent on the stress characteristics of the uranium surface, i.e. it is obtained either on stressed surfaces or on stress-relieved ones. However, quantitatively, the effect is more pronounced for stress-relieved surfaces due to the attenuation of the number of available $H_2$ dissociation sites, caused by the stress-relief heat treatment.

## References

[1] E. Tiferet, M. H. Mintz, S. Zalkind, I. Jacob and N. Shamir, , *J. All. Comp.*, in press (available on line).

# C4

## Evidence for differential rates of oxide growth on depleted uranium: implications for $UH_3$ formation.

**T. B. Scott,[1] G. C. Allen[1], J. Glascott[2]**

[1] *Interface Analysis Centre, University of Bristol, England, BS2 8BS., e-mail: t.b.scott@bristol.ac.uk*
[2] *AWE, Reading, England, RG7 4PR, e-mail: joe.glascott@awe.co.uk*

The thickness of the oxide layer on uranium is an important control on further corrosion of the metal under a wide range of conditions[1]. To investigate its role in the hydriding process a depleted uranium sample was vacuum annealed at 550ºC for a 72 hour period and was subsequently ion etched at grazing angle to remove regions of the surface oxide layer and reveal the underlying grain structure of the metal. An electron backscatter diffraction (EBSD) system was then used to identify the lattice orientations of the grains observed followed by a further step of ion beam 'cleaning' before the sample was briefly exposed to air under ambient conditions for a 5 minute period to allowed limited re-growth of the surface oxide.
Secondary ion mass spectrometry (SIMS) was used to obtain depth profiles from individual metal grains using signal gating to profile grains simultaneously. The recorded $UO_2^+$ and $UO^+$ ion cluster profiles provided strong evidence that the surface oxide film had different thicknesses over different metal grains and indicated that the initial growth of uranium oxide occurred at differential rates depending on the lattice orientation of the exposed metal grains on which it formed.
Correlation of orientation data with calculated oxide thickness indicated that although the surface oxide coating was considerably less that 50nm the most rapid growth occurred on grain surfaces with the highest atom density. Thus the results suggested that some grains at the metal surface may be unfavourably oriented relative to the sample surface providing zones of limited oxide growth which encourage hydride nucleation. Confirmation of this view was obtained by the reaction of an ion etched uranium surface briefly exposed to air (1 minute) with 500mbar $H_2$ at 250ºC. This resulted in the formation of $UH_3$ precipitates showing preferential growth over some grains at the metal surface relative to others.

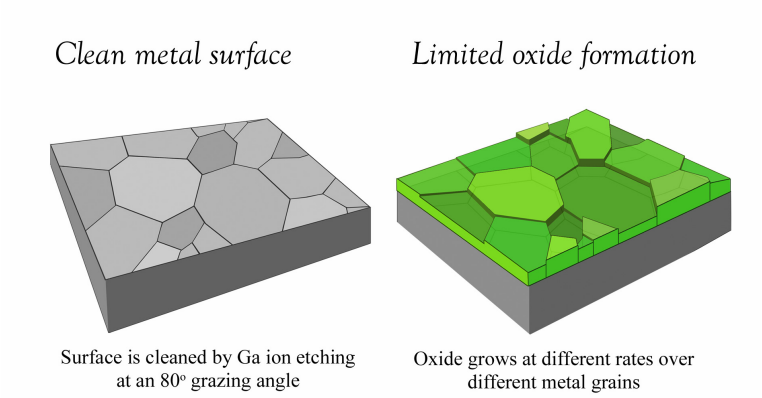


Fig. 1. Differential growth of thin film oxide ($UO_2$) on depleted uranium

### References

[1] L. W. Owen and R. A. Scudamore., *Corros. Sci.* **6**, 461 (1966)
[2] D. Bedere and P. Sans., *J. Less-Common Met.* **91**, 33 (1983)
[3] J. Bloch et al., *J. Less-Common Met.* **103**, 163 (1984)
[4] J. Bloch et al., J. Less-Common Met., **139**, 371 (1988)
[5] M. Brill et al., *J. Alloys Compd.* **231**, 368 (1995)
[6] R. Arkush et al., *J. Alloys Compd.* **244**, 197 (1996)
[7] M. Brill, J. Bloch and M. H. Mintz., *J. Alloys. Compd.* **266**, 180 (1998)

# D1

## Studies of uranium multilayers: comparisons and perspectives

**R. Springell,[1,2] S. W. Zochowski,[1] R. C. C. Ward,[3] M. R. Wells,[3] F. Wilhelm,[2] S. D. Brown,[2,4] L. Bouchenoire,[2,4] S. Langridge,[5] W. G. Stirling,[2] and G. H. Lander.[6]**

*[1]Department of Physics and Astronomy, University College London, London WC1E 6BT, UK*
*[2]European Synchrotron Radiation Facility, BP220, F-38043 Grenoble, France,*
*e-mail:ross.springell @esrf.fr*
*[3]Clarendon Laboratory, University of Oxford, Oxford OX1 3PU, UK*
*[4]Department of Physics, University of Liverpool, Liverpool L69 7ZE, UK*
*[5]ISIS, Rutherford Appleton Laboratory, Chilton, Oxfordshire OX11 0QX, UK*
*[6]European Commission, JRC, Institute for Transuranium Elements, Postfach 2340, Karslruhe, D-76125, Germany*

Following our earlier work on U/Fe multilayers [1,2], we have now extended the programme in a number of new directions. First, we have improved the apparatus at the Clarendon Laboratory, Oxford, so that Nb buffer and capping layers can be grown to enhance growth and prevent oxidation. Second, we have made new U/Fe multilayers and extended the fabrication to U/Co and U/Ni samples. Third, we have made U/Gd samples. The experimental methods consist of X-ray reflectivity (XRR), X-ray diffraction (XRD), magnetization, polarized neutron reflectivity (PNR), and two techniques that are element specific, X-ray circular magnetic dichroism (XMCD) and X-ray resonant magnetic reflectivity (XRMR).

For the U/TM (TM = Fe, Co, and Ni) the multilayer quality is poor. The large misfit between the U and TM atoms and interdiffusion processes cause the interfaces to be amorphous, such that a magnetically "dead" layer is present in the TM layer [2]. XMCD, which is the most sensitive technique for determining any polarization at the U sites, shows that *only* in the case of the U/Fe samples does the U polarize. An approximate profile may be determined from these measurements, which shows a rapidly diminishing U polarization as one moves away from the interface, and a *reversal* of the polarization after about 2 atomic layers of uranium. The maximum polarization is ~ 0.15 $\mu_B$/U atom. The profile is in rough accord with the earlier XRMR measurements [3].

In contrast to the situation of the 3*d* transition elements, all of which have an atomic volume about 50% of that of uranium, gadolinium is 50% *larger* than uranium. The resulting U/Gd multilayers have more sharply defined interfaces and display highly crystalline U and Gd layers, due, either to the respective atomic sizes (uranium is now the smaller of the two elements, so that any lattice strains in this system will be in the opposite sense to those of the U/TM multilayers), or to a reduction in the chemical interdiffusion. X-ray diffraction spectra indicate a preferred *c*-axis growth of hcp Gd and an hcp uranium phase with a *c*-axis of 5.62Å, which is only 2.5% different from the Gd bulk value of 5.78Å. Hexagonal-close-packed U, which does not exist in the bulk form, has previously been reported in thin U films [4], and the *c*-axis parameter given is close to that found in our study. However, a consideration of the atomic sizes indicates an extremely unlikely in-plane lattice match between the U and Gd, since this would involve an increase in the atomic volume of uranium of close to 50%. The likely situation is then, not the formation of a U/Gd superlattice, but layers of U and Gd that are highly crystalline, oriented along the same axis, but not aligned within the plane.

Particularly striking is that the contrasting behaviour of the reflectivity spectra of multilayers grown with thick Gd or thick U layers respectively, shown in figure 1. The former samples

display considerable roughness, which we attribute to a column-like growth of the Gd, resulting in a large step-like electron density profile. Samples with thick U layers however, have incredibly smooth interfaces, evidenced by the large number of Bragg peaks seen over a relatively small Q-range, when compared to those with thick Gd.

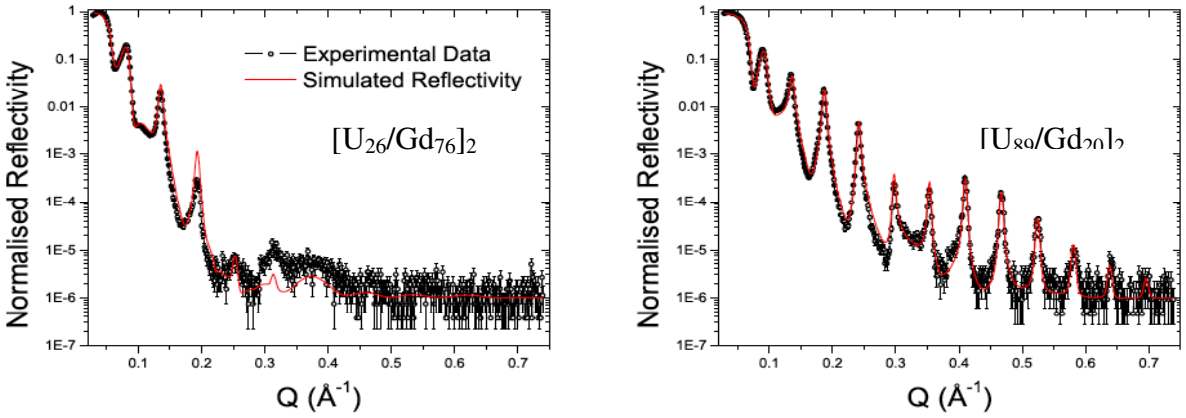


Figure 1 - Reflectivity taken on two U/Gd multilayers; left $[U_{26}/Gd_{76}]_{20}$ and right $[U_{89}/Gd_{20}]_{20}$. The data are the black points, and the continuous red curve is a fitted simulation. In the thick Gd sample (left) the intensity falls off very quickly indicating considerable roughness at the interfaces, whereas in the thick U sample (right) many Bragg peaks (13) from the bilayer repeat can be observed, indicating excellent interface quality. Data taken with laboratory source X-rays, Cu Kα radiation, λ=1.54Å.

XMCD at the U $M_{4,5}$ edges shows a small signal, smaller than in U/Fe, but different from that found in a U-Gd alloy grown as a thin film. Magnetisation and PNR show that the moment of Gd is much reduced from the bulk value, attaining only about ~ 60% of the bulk, but there is no dead layer. It is not clear of the origin of this reduction in the Gd moment, but the formation of small magnetic domains at the interface, because of the strain effects, and the consequent large coercive field may be one possibility. Such a large reduction of the Gd moments has been observed also in Gd/Mo multilayers [5].

Further measurements are in progress; this talk will cover also some proposed extensions of our programme.

**References**

[1] A. Beesley et al., *J. Phys. Condens. Matter* **16**, 8491 (2004)
[2] A. Beesley et al., *J. Phys. Condens. Matter* **16**, 8507 (2004)
[3] S. D. Brown et al., *J. Appl. Phys.* **93**, 6519 (2003)
[4] L. Berbil-Bautista et al., *Phys. Rev. B* **70**, 113401 (2004)
[5] J. V. Harkins and P. E. Donovan, *J. Phys. Condens. Matter* **8**, 685 (1996)

# D2

## Search for New Classes of Thermoelectrics: Syntheses and Properties of Three New Uranium-Heavy Atom Chalcogenides[1]

**Daniel M. Wells, Daniel Bugaris, James A. Ibers**

*Department of Chemistry, Northwestern University, 2145 Sheridan Rd., Evanston, IL USA*
*ibers@chem.northwestern.edu*

In our search for new actinide thermoelectrics we have concentrated on the syntheses of compounds where potentially the phonon contributions to their thermal conductivities are minimized. Thus we seek materials with the following characteristics: (a) being composed of heavy elements; (b) containing a large number of atoms in a high symmetry unit cell; (c) being complex, preferably with some disorder; (d) having small electronegativity differences among the elements present.

We will present the syntheses of three new uranium compounds that possess some of these characteristics. $UTa_2S_6OCl_6$ has been synthesized from the reaction of $UCl_4$ and $TaS_{2-x}O_x$. The compound crystallizes as orange needles and rectangular plates with two formula units in space group *P*-1. Its structure is shown in Fig. 1. $[Ta_4(Se_2)_8][UI_6]$ has been prepared from the reaction of U, Ta, Se, and $I_2$. The black material crystallizes as bipyramids with four formula units in the tetragonal space group $P4_2/n$. Its structure is shown in Fig. 2. In keeping with the above discussion, this compound is a particularly attractive candidate as a possible thermoelectric. It contains many heavy atoms in a highly symmetric unit cell; the $[UI_6]^{2-}$ anion shows considerable vibration; the $[Ta_4(Se_2)_8]^{2+}$ cation is actually an infinite chain that could be conductive. $Cs_2UHg_2Se_5$ has been synthesized from the reaction of U, HgSe, Se, $Cs_2Se_3$, and CsI. The compound crystallizes as black needles with two formula units in space group $P2/n$. Its structure is shown in Fig. 3.

Attempts to modify these syntheses to incorporate Te, rather than S or Se, will be described. Up-to-date physical measurements on these compounds will be reported.

[1]Supported by the U. S. Department of Energy BES Grant ER 15522.

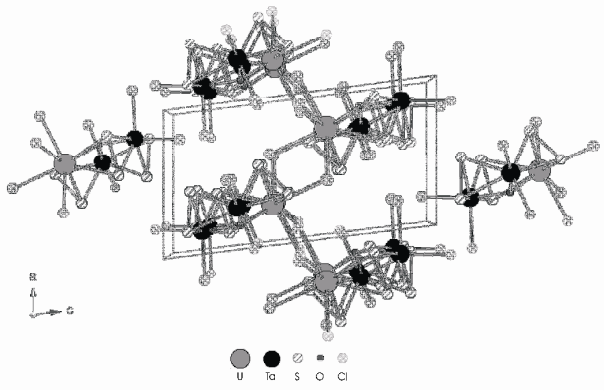


Fig. 1. The structure of $UTa_2S_6OCl_6$

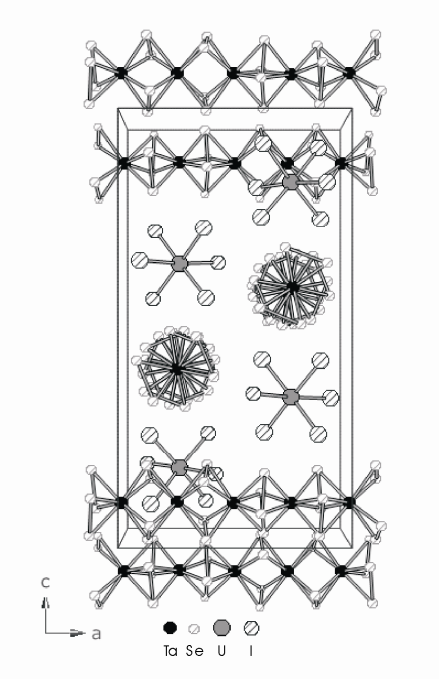


Fig. 2. The structure of $[Ta_4(Se_2)_8][UI_6]$

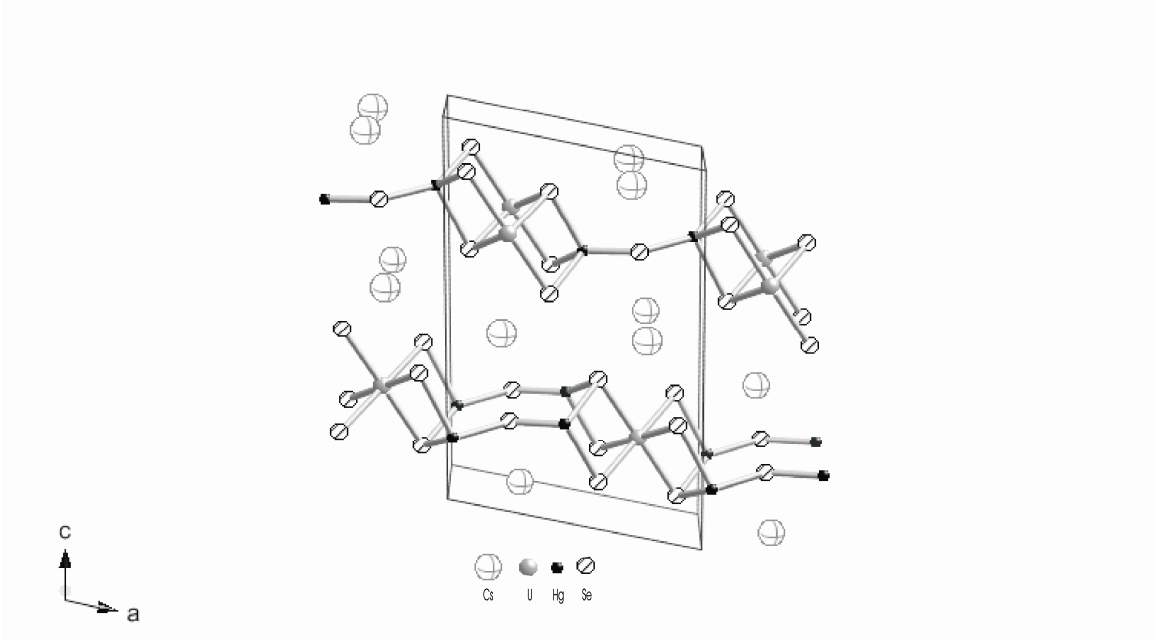


Fig. 3. The structure of $Cs_2UHg_2Se_5$

# D3

## Increase of $T_C$ in $UFe_{2+x}$ synthesized by ultrafast cooling

**L. Havela[1], K. Miliyanchuk[1], A.P. Gonçalves[2], J.C. Waerenborgh[2], L.C.J. Pereira[2], P. Gaczyński[2], E.B. Lopes[2], J. Pešička[1]**

[1] *Faculty of Mathematics and Physics, Charles University, Ke Karlovu 5, 12116, Prague, Czech Republic; havela@mag.mff.cuni.cz*
[2] *Dep. Química/CFMC-UL, Instituto Tecnológico e Nuclear, P-2686-953 Sacavém, Portugal*

We found that $UFe_2$ has a slightly modified magnetic behaviour when prepared by splat cooling than in the bulk form [1]. As the Curie temperature $T_C$ is known to decrease for a reduced Fe concentration [2], a slight increase of $T_C$ could be attributed to an excess of Fe. Such excess cannot be incorporated into the bulk Laves phase [2], but such a possibility was suggested after studies of ball-milled $UFe_2$ [3]. Therefore we tested how much Fe can be embedded into the Laves phase using splat cooling on the nominal stoichiometries $UFe_{2+x}$, $x$ = 0 - 4, and what is the microstructure and properties of rapidly cooled splats. Our results demonstrate that the cubic Laves phase structure can accommodate excessive Fe up to the stoichiometry $UFe_{2.3}$. Although further increasing Fe concentration in the melt reduces the melting point to the eutectic concentration $UFe_6$, which could make the fast cooling more efficient (it indeed manifests in smaller grains, see Fig.1), all Fe over the stoichiometry $UFe_{2.3}$ segregates in the form of α-Fe. Scanning electron micrographs on Fig.1 show that unlike splat-cooled $UFe_2$ with grains in the range 1-10 μm [1], the off stoichiometric materials consist of grains well below 1 μm, approaching the range of nanocrystallinity. The lattice parameter $a$ of the Laves phase structure decreases, which is opposite than in Fe-deficient samples, which were synthesized by arc melting and water quenching from 1000 °C in the concentration range $UFe_{1.7}$-$UFe_2$ [2].

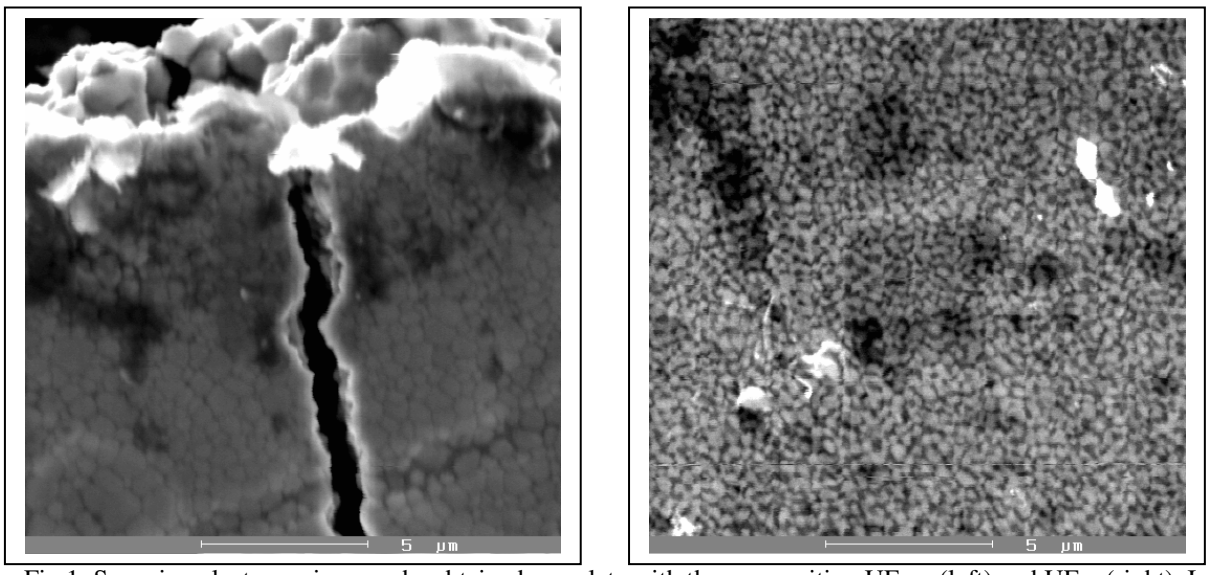


Fig.1: Scanning electron micrographs obtained on splats with the composition $UFe_{2.3}$ (left) and $UFe_4$ (right). In the right panel, the light material is the U phase (corresponding to about $UFe_{2.3}$, dark one pure Fe. Notice the scale at the bottom.

Magnetization measurements indicate that $T_C$ increases from 164 K for $UFe_2$ splat to ≈ 220 K in $UFe_{2.3}$. In agreement with the structure data, $T_C$ does not grow over this limit; instead a ferromagnetic "impurity" signal of α–Fe superimposes in increasing amount for higher Fe concentration. The comparison of the spontaneous moment $\mu_s$ = 1.90 $\mu_B$/f.u in $UFe_{2.3}$ with 1.00 $\mu_B$/f.u. in $UFe_2$ suggests that the moments of Fe occupying the U sublattice

can be much higher than the Fe moments in $UFe_2$, determined as 0.60 $\mu_B$ by neutron diffraction (assuming that the compensation of spin and orbital moments of U persists) [4] even if we consider that also the magnetization of the Fe sublattice may increase. $^{57}$Fe Mössbauer spectroscopy results indicate that the magnetic hyperfine field $B_{hf}$ on Fe nuclei in the Fe sublattice increases by about 30% in $UFe_{2.3}$ comparing to $UFe_2$. In addition, another Fe signal appears (with isomer shift by about 0.1 mm/s higher) and with more than doubled $B_{hf}$, which is attributed to Fe placed into "wrong" position in the U sublattice. Supposing then that the Fe moments would increase to 0.70 $\mu_B$ for the Fe sublattice (following the increasing $B_{hf}$) the antistructure Fe atoms should contribute by ≈1.7 $\mu_B$ each to the total magnetization.

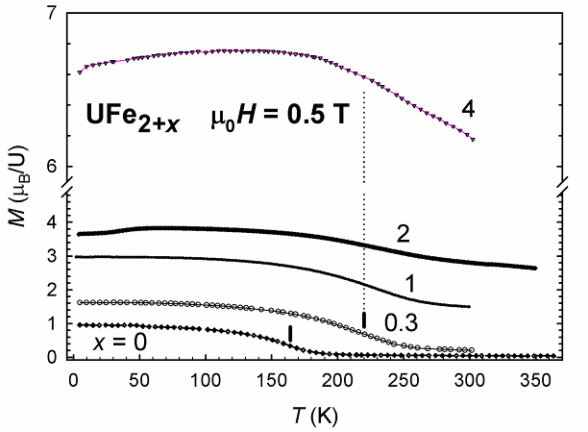


Fig.2: temperature dependence of magnetization in $\mu_o H$ = 0.5 T (ZFC mode) for $UFe_{2+x}$ splats. Vertical bars and the dashed line indicate the respective $T_C$ values.

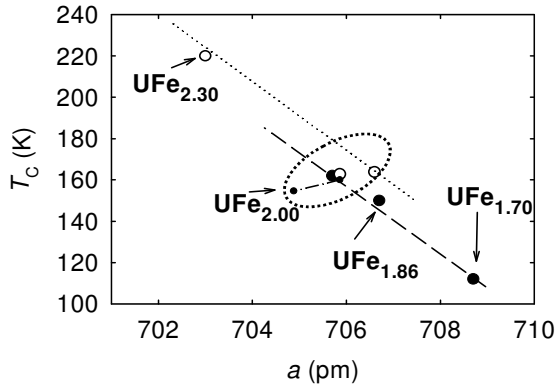


Fig.3: Relation of $T_C$ and the lattice parameter $a$ for various $UFe_x$ systems. Full symbols mark values on bulk $UFe_{2-y}$ samples [2], empty symbols are our data on bulk $UFe_2$ and splats. The dash-dotted line shows the pressure dependence of $T_C$ for bulk $UFe_2$ [5] using the experimental bulk modulus value $B_0$ = 239 GPa.

The variations of $a$ seen in Fig.3 illustrate the fact the Fe concentration tuning affects the structure similarly both for Fe excess and deficiency and also the $T_C$ values scale accordingly. The small increase of $T_C$ between $UFe_2$ bulk and splat (the latter having slightly larger $a$) can be a purely volume effect, as suggested by the reduction of $T_C$ due to lattice compression in a high-pressure experiment [5]. But the dominant $T_C$ variations are due to varying Fe concentration, underlining the prominence of 3*d* magnetism in $UFe_2$.

**Acknowledgements**

This work was supported by the Program GRICES/ASCR 2007, by the Grant Agency of the Czech Republic under the grant No. 202/07/0418, and by the Grant Agency of the Academy of Sciences of the Czech Republic under the grant No. A100100530.

**References**

[1] L. Havela, A.P. Gonçalves, K. Miliyanchuk, L.C.J. Pereira, J. Pešička, E.B. Lopes, Proc. 35ièmes Jornées des Actinides, Baden 2005, F-23.
[2] A.T. Aldred, J.Magn.Magn.Mater. 10 (1979) 42.
[3] M. Timko, A. Szlafarek, A. Zentko, J. Kovac, J.Magn.Magn.Mater. 196-197 (1999) 655.
[4] B. Lebech, M. Wulff, G.H. Lander, J. Rebizant, J.C. Spirlet, A. Delapalme, J.Phys.:Cond.Matter. 1 (1989) 10229
[5] P.H. Frings, J.J.M. Franse, P.E. Brommer, J.Phys.C: Solid State Phys. 18 (1985) 1955

# D4

## New ternary phases in the U-Fe-Ge system and their magnetic properties

**D. Berthebaud[1], O. Tougait[1], M. Potel[1], A.P. Gonçalves[2] , E.B. Lopes[2], H. Noël[1]**

[1] *Laboratoire de Chimie du Solide et de matériaux, Université de RennesI, U.M.R C.N.R.S. 6226, Avenue du Général Leclerc, F-35042 Rennes Cedex, France*
[2] *Dept. de Química, Instituto Tecnológico e Nuclear/CFMC-UL, P-2686-953 Sacavém, Portugal*

A comprehensive investigation of the ternary systems combining iron, germanium and an f-element having a particular electronic configuration (Ce and U) has been initiated. Our experimental studies comprise the assessment of isothermal section at 900°C of the ternary phase diagrams, the structural characterization of the new compounds, and the investigation of their magnetic and transport properties.

At the beginning of our study, numerous investigations dealing with the crystal-chemistry and physical properties of ternary uranium iron germanides were available in the literature. Four ternary compounds were known, with the following characteristics:

- UFeGe (a=6.828 Å, b=4.259 Å, c=7.286 Å, Pnam, TiNiSi-type) shows a structural transition corresponding to a monoclinic distorsion below 500K (a=6.986 Å, b=4.308 Å, c=6.992 Å, β=93.71°, P121/m1, UFeGe-type).Spin fluctuation behavior has been observed for this compound [1].
- $U_2Fe_{15}Ge_2$ (a= 8.423 Å, c= 8.356 Å, $P6_3/mmc$,$Th_2Ni_{17}$-type), ferromagnetic ordering has been observed with curie temperature as high as 505K [2] .
- $UFe_2Ge_2$(a= 4.004 Å, c= 9.985 Å, I4/mmm, $CeAl_2Ge_2$-type) [3] has been reported as a Pauli paramagnet [4].
- $UFe_6Ge_6$ (a= 5.1268(4) Å, c= 4.0507(5) Å, P6/mmm, $YCo_6Ge_6$-type) [5] exhibits two magnetic transitions with ferromagnetic ordering below Tc=322K and antiferromagnetic ordering below $T_N$=230K.

New phases have been characterized and their crystal structures were determined from X-ray diffraction data:

- $UFe_{1-x}Ge_2$ (a= 4.0965(5)Å, b= 15.844(5) Å, c= 4.059(5) Å, Cmcm, $CeNiSi_2$-type)
- $U_3Fe_4Ge_4$ (a= 13.685(5) Å, b= 6.640(5) Å, c= 4.086 (5) Å, Immm, $Gd_3Cu_4Ge_4$-type)
- $U_9Fe_7Ge_{24}$ (a= 12.379(1) Å, b= 12.379(1) Å, c= 18.288(1) Å, I4/mmm, $U_9Fe_7Ge_{24}$-new structure type)
- $U_{68}Fe_{8-x}Ge_{66}$ (a= 10.875(5) Å, c= 25.250(5) Å, I4/mmm, $U_{68}Fe_8Ge_{66}$-new structure type)

$U_3Fe_4Ge_4$ and $U_{68}Fe_{8-x}Ge_{66}$ show ferromagnetic ordering below 20 K and 30 K respectively.

Other magnetic and transport measurements are in progress.

### References

[1] F. Canepa *et al., J. Alloys Compd.*, **234** (1996) 225-230
[2] T. Berlureau et al., *Mater. Lett*. ***9(1)*** (1989) 21.
[3] R. Marazza et al., *J. Less Com. Met*., **53** (1977) 193-197.
[4] A. Szytula et al., *J. Phys. Chem. Sol.*, **49( 9)** (1988), 1113-1118.
[5] A.P. Gonçalves et al., *J. Alloys Compd.* **204** (1994), 59-64

# E1

## Structure and electronic properties of new U compound $UGa_{1.85}Zr_{0.15}$

**L. Havela[1], A.V. Andreev[2], A.P. Gonçalves[3], J. Šebek[2], V. Sechovský[1], Y.F. Popov[4]**

[1] *Dept. Condensed Matter Physics, Charles University, Ke Karlovu 5, 12116, Prague, Czech Republic*
[2] *Institute of Physics, Academy of Sciences, Na Slovance 2, 18221, Prague, Czech Republic*
*e-mail: andreev@mag.mff.cuni.cz*
[3] *Dep. Química, Instituto Tecnológico e Nuclear, P-2686-953 Sacavém, Portugal*
[4] *Faculty of Physics, Moscow State University, 119992, Moscow, Russia*

$UGa_2$ and $UZr_2$ crystallize in a hexagonal crystal structure of the $AlB_2$ type, space group *P6/mmm*. $UGa_2$ is a highly anisotropic 5*f*-electron ferromagnet ($\mu_U$ = 2.7 $\mu_B$, $T_C$ =125 K), whereas $UZr_2$ is a weak Pauli paramagnet with presumably broad 5*f* band [1]. The chance to study effects of variable 5*f* localization in the solid solution $UGa_{2-x}Zr_x$ looked very intriguing. However, the occupation of crystallographic positions is different in both compounds, and the solubility is actually negligible. Inspecting possible intermediate phases, a new compound was found at $x$ = 0.15. X-ray powder diffraction analysis showed that its symmetry is evidently lower than hexagonal. Here we report on the crystal structure of $UGa_{1.85}Zr_{0.15}$ (determined by XRD on single crystal). Its basic electronic properties were studied on a polycrystal.

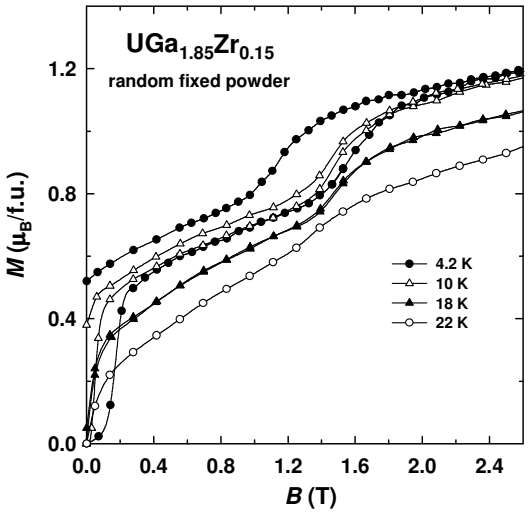


Fig. 1. Magnetization curves measured on fixed random powders at various temperatures.

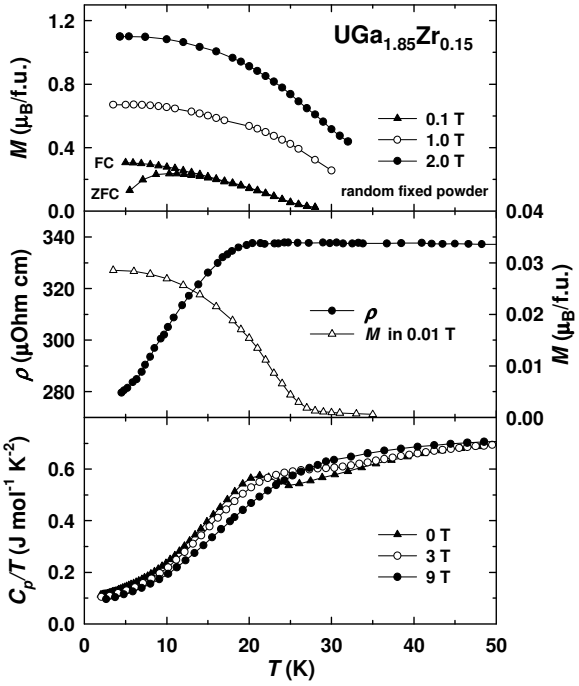


Fig. 2. Temperature dependence of magnetization $M$ measured on fixed random powders, of electrical resistivity $\rho$ and of specific heat $C_p(T)/T$.

The crystal structure determined using a single crystal (approx. 0.02x0.02x0.03 $mm^3$) is orthorhombic (space group *Cmcm*) with the lattice parameters $a$ = 9.307(1) Å, $b$ = 7.495(1) Å, $c$ = 9.374(1) Å. U atoms occupy entirely the 8*e* sites and share the 4*c* sites with Zr. Ga atoms occupy 3 positions, one of them is shared with Zr. The structure corresponds to the $Pu_3Pd_5$ structure type identified in the vicinity of $UGa_2$ already [2]. The shortest inter-uranium distance 3.753 Å is larger than the Hill limit. The low-temperature magnetization curve measured on fixed random powder (Fig. 1) exhibits spontaneous moment of 0.55 $\mu_B$ and metamagnetic transition (MT) at 1.5 T with ≈ 0.5 $\mu_B$ magnetization increment. Both the MT and the magnetization process of ferromagnetic component exhibit a large hysteresis, rapidly decreasing with increasing $T$. The Curie temperature $T_C$ = 20.5 K was determined from the

Arrott plot. The thermomagnetic hysteresis seen in low (0.1 T) field (Fig. 2) correlates with the field hysteresis (Fig.1). Specific heat and electrical resistivity exhibit clear ferromagnetic-type anomalies in vicinity of $T_C$. It has enhanced $\gamma$ coefficient of 110 mJ/mol K$^2$ (considerably larger than 5 mJ/mol K$^2$ in $UGa_2$). This indicates a narrow 5*f* band at $E_F$.

The longitudinal ($\lambda_{\parallel}$) and transverse ($\lambda_{\perp}$) magneto-striction (MS) has been measured in pulsed fields up to 20 T. A comparison of magnetization and MS curves at 4.2 K (Fig. 3) shows that the domain-wall movement in the ferromagnetic component is not accompanied by MS. It means that the domains have only 180° walls evidencing a uniaxial type of magnetic anisotropy. Both $\lambda_{\parallel}$ and $\lambda_{\perp}$ exhibit hysteresis loops in fields below 3 T which correspond well to the MT. Shift of the curves towards higher fields and much wider hysteresis as compared with steady fields (Fig 1) reflects a large magnetic viscosity, which is typical for U compounds. From the experimental $\lambda(B)$ curves, the isotropic ($\lambda_i$) and anisotropic ($\lambda_a$) parts of MS were determined from standard relations for polycrystals: $\lambda_i = (\lambda_{\parallel} + 2\lambda_{\perp})/3$; $\lambda_a = 2\ (\lambda_{\parallel} - \lambda_{\perp})/3$. The isotropic component $\lambda_i$ characterizes change of the volume, $\Delta V/V = 3\ \lambda_i$. Volume effect at the MT reaches $0.8*10^{-4}$. This $\Delta V/V$ value is similar to that of other U intermetallics where the MS at the MT was studied ($<2*10^{-4}$, UCoAl, UNiAl, UNiGa). Negative anisotropic MS (i.e., the sample shrinks in direction of magnetic moment and expands in perpendicular direction) is also typical for U intermetallics, however, the magnitude of observed effect is rather small due to uniaxial anisotropy. In $UGa_2$ with multiaxial (easy-plane) magnetic anisotropy, the anisotropy constant $\lambda^{\gamma,2}$, describing the orthorhombic distortion, is $-4*10^{-3}$. In $UGa_{1.85}Zr_{0.15}$, $\lambda_a$ reaches $-0.25*10^{-3}$ in 20 T and has no trend to saturation. If we assume the saturation value of $\lambda_i$ to be of the same order as in $UGa_2$, we can estimate the anisotropy field in $UGa_{1.85}Zr_{0.15}$ as more than 100 T.

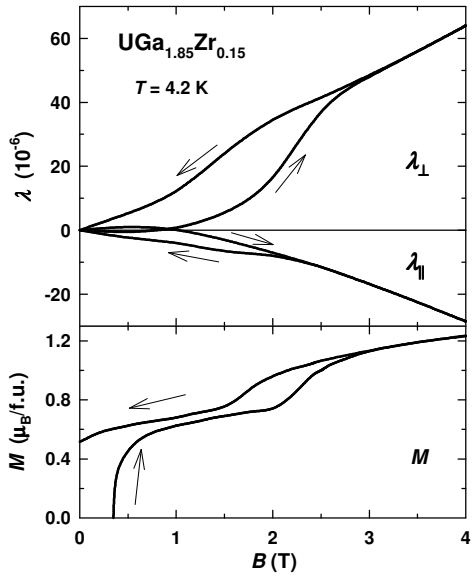


Fig. 3. Field dependence of the longitudinal ($\lambda_{\parallel}$) and transverse ($\lambda_{\perp}$) magnetostriction and magnetization *M* measured in pulsed fields at $T = 4.2$ K.

For a high uniaxial anisotropy case, the spontaneous magnetic moment obtained on randomly oriented polycrystal is equal to 50% of the value measured along an easy magnetization axis. The same can be applied for the magnetization increment at MT in the case of low transition field, as in $UGa_{1.85}Zr_{0.15}$. Therefore, the magnetic moment may reach rather high value 2.2 $\mu_B$ above the transition. The observed magnetization curve at 4.2 K can be explained for example by +++- arrangement of moments 2.2 $\mu_B$/U and field-induced transition into ferromagnetic state. Other explanations can be based on a transition from non-collinear to a collinear ferromagnetic structure, on breaking of ferrimagnetic coupling of the two non-equivalent U sites, or on a band metamagnetism, i.e. enlarging the local moment size under the influence of field. The last model seems to be supported by the suppression of $\gamma$ in high fields ($\gamma = 90$ mJ/mol K$^2$ in $B = 9$ T).

## References

[1] V. Sechovsky and L. Havela, In: Handbook of Ferromagnetic Materials, v. 4, Eds. E.P. Wohlfarth and K.H.J. Buschow (North Holland, Amsterdam, 1988), p. 309-491, and references therein.
[2] A.P. Gonçalves and L. Havela, J. Alloys Comp. 394 (2005) L1.

# E2

## Magnetic, transport and thermal properties of $An$Pd$_2$Sn ($An$ = Th, U, Np, Pu) system

**K. Gofryk[1], D. Kaczorowski[2], E. Colineau[1], F. Wastin[1], R. Jardin[1], N. Magnani[1], P. Boulet[1], J. Rebizant[1], J-C. Griveau[1], P. Javorsky[1] and R. Caciuffo[1]**

[1] *European Commission, Joint Research Centre, Institute for Transuranium Elements, Postfach 2340, 76125 Karlsruhe, Germany*
[2] *Institute of Low Temperature and Structure Research, Polish Academy of Sciences, P. O. Box 1410, 50-950 Wrocław, Poland*

In recent years uranium–based compounds with the composition U$T_2M$, where $T$ is a $d$–electron transition metal and $M$ stands for a $p$-electron element, have attracted much attention owing to large variety of their intriguing physical behaviour driven by hybridisation of 5$f$–electronic states with $s,p,d$–states of neighbouring atoms [1-3]. Previous studies on the stannide UPd$_2$Sn revealed that this compound is a non-superconducting non-magnetic heavy fermion system [4,5]. Recently, we briefly reported on the properties of the Np-based counterpart NpPd$_2$Sn [6]. This compound orders antiferromagnetically at $T_N$ = 15 K, and its electrical resistivity and specific heat reveal features of a heavy–fermion ground state. Here we report for the first time on the synthesis, structural and physical characterization of another member of the $An$Pd$_2$Sn family, namely PuPd$_2$Sn. Moreover, with the aim of discussing the new data in the broader context of the physical behaviour observed across the $An$Pd$_2$Sn series, some properties of ThPd$_2$Sn and UPd$_2$Sn have been reinvestigated on newly prepared samples and the results are also presented in this contribution.

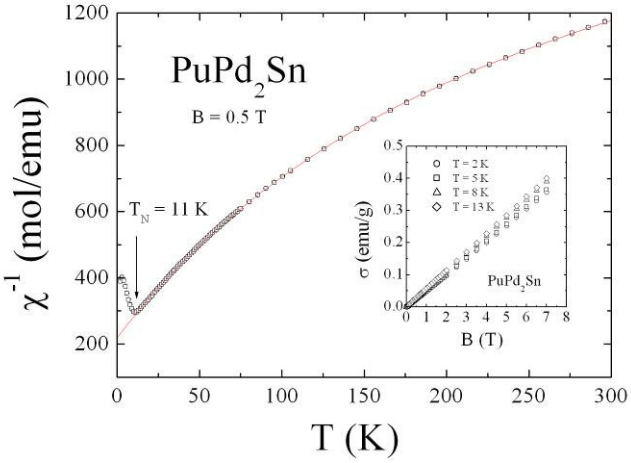


Fig.1. Inverse magnetic susceptibility vs. temperature for PuPd$_2$Sn. The solid line is a modified Curie-Weiss fit. Inset: magnetization vs. magnetic field strength measured at a few temperatures below and above $T_N$.

Polycrystalline samples of ThPd$_2$Sn, UPd$_2$Sn, NpPd$_2$Sn and PuPd$_2$Sn were prepared by arc-melting stoichiometric amounts of the constituents under argon atmosphere. The as-cast buttons were checked by X–ray powder diffraction and shown to be single phases with orthorhombic unit cells. The structure refinements yielded for all the compounds the space group *Pnma*, and the lattice parameters as follows: $a$ = 10.2259(3) Å, $b$ = 4.5767(1) Å, $c$ = 7.0676(2) Å for ThPd$_2$Sn, $a$ = 9.9563(4) Å, $b$ = 4.6009(2) Å, $c$ = 6.8745(3) Å for UPd$_2$Sn, $a$ = 10.031(3) Å, $b$ = 4.544(1) Å, $c$ = 6.974(2) Å for NpPd$_2$Sn and $a$ = 10.0525(9) Å, $b$ = 4.5022(4) Å, $c$ = 7.0652(6) Å for PuPd$_2$Sn.

Magnetic measurements were performed in the temperature range 2–300 K and in magnetic fields up to 7 T using a Quantum Design SQUID magnetometer. These studies confirmed the paramagnetic character of UPd$_2$Sn and revealed in PuPd$_2$Sn an antifferomagnetic ordering below $T_N$ = 11 K (see Fig. 1). In the paramagnetic region, the magnetic susceptibility of the Pu-based compound follows a modified Curie–Weiss law with the effective magnetic moment $\mu_{eff}$ of 0.97 $\mu_B$, the paramagnetic Curie temperature $\theta_p$ = -30 K and the temperature independent term $\chi_0$ = 4.8 x 10$^{-4}$ emu/mol. The experimental value of $\mu_{eff}$

is larger than the free $Pu^{3+}$ ion value expected for Russell-Saunders coupling (0.84 $\mu_B$) but it is quite close to that anticipated for intermediate coupling (1.01 $\mu_B$). Interestingly, the absolute value of the paramagnetic Curie temperature is much larger than $T_N$ as usually found in systems with strong Kondo interactions. As seen in the inset to Fig. 1, the magnetization measured in the ordered state is proportional to the strength of the applied magnetic field with no hint of any metamagnetic–like transition up to 7 T.

Heat capacity studies were performed on each of the *An*$Pd_2Sn$ samples in the temperature range 2–300 K and in applied magnetic fields up to 9 T using a Quantum Design PPMS platform. As shown in Fig. 2, the specific heat of $PuPd_2Sn$ achieves near room temperature a value of about 100 J/(mole K) that corresponds to the Dulong–Petit limit. The magnetic phase transition at $T_N$ = 11 K manifests itself as a λ–like anomaly in $C_p(T)$. In an applied magnetic field this peak gradually weakens and shifts to lower temperatures. The $C_p/T$ ratio extrapolated from the region just above $T_N$ is as large as 570 mJ/(mole $K^2$), while the Sommerfeld coefficient derived from the ordered state is about 180 mJ/(mole $K^2$) (see the inset to Fig. 2). The latter value may be compared with the $\gamma$ values derived for $UPd_2Sn$ and $NpPd_2Sn$, which are 130 mJ/(mole $K^2$) [4] and 400 mJ/(mole $K^2$) [6], respectively. Using the specific heat data of $ThPd_2Sn$ the crystal field (CF) splitting of the $Pu^{3+}$ multiplet in $PuPd_2Sn$ is estimated to be of the order of 150 K with a doublet being the CF ground state. Similar analysis performed for $NpPd_2Sn$ resulted in a total CF splitting of the $Np^{3+}$ multiplet of about 280 K. Also in this case, the CF ground state is a doublet.

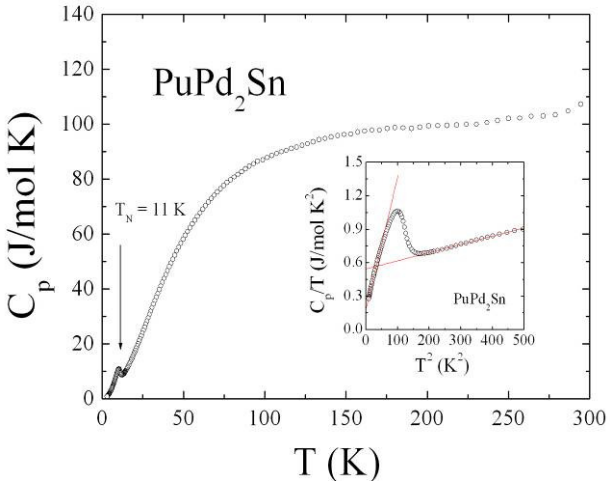


Fig.2. Specific heat vs. temperature for $PuPd_2Sn$. Inset: low-temperature data in the form $C_p/T$ vs. $T^2$. The solid lines are the extrapolations mentioned in the text.

The hitherto obtained results for $NpPd_2Sn$ and $PuPd_2Sn$ suggest that both compounds may be classified as moderately enhanced heavy fermion systems, alike their U-based counterpart. Further experiments (thermoelectric power and Hall effect measurements, Mössbauer spectroscopy) are presently underway to verify this hypothesis.

This work was made possible thanks to the support of the European Community-Access to Research Infrastructures action in financing the access to the Actinide User Laboratory at the ITU-Karlsruhe under the contract N°RITA-CT-2006-026176-"Actuslab-2".

## References

[1] C. L. Seaman et al., *Phys. Rev. B* **53**, 2651 (1996).
[2] T. Takabatake et al., *J. Phys. Soc. Japan* **58**, 1918 (1998).
[3] K. Gofryk et al., *Solid State Commun.* **133**, 625 (2005).
[4] C. Rossel et al., *Solid State Commun.* **60**, 563 (1986).
[5] I. Maksimov et al., *Physica B* **312-313**, 283 (2002).
[6] D. Kaczorowski et al., *Physica B* **359-361**, 1102 (2005).

.

# E3

## Magnetic and related properties of $U_4Ir_{13}Si_9$ and $U_4Rh_{13}Si_9$

**A. Pikul and D. Kaczorowski**

*Institute of Low Temperature and Structure Research, Polish Academy of Sciences, P Nr 1410, 50–950 Wrocław 2, Poland, e-mail: A.Pikul@int.pan.wroc.pl*

The ternary intermetallic compound $U_4Ir_{13}Si_9$, which crystallizes in an orthorhombic unit cell of the $Er_4Ir_{13}Si_9$-type (space group *Pnmn*), was briefly reported in the literature to exhibit at low temperatures complex magnetic behaviour with distinct anomalies in the magnetic susceptibility, related to magnetic phase transitions that occur at 18 and 6.4 K [1]. Recently we performed a complementary study on the magnetic properties of this material by means of magnetization, heat capacity, electrical resistivity and thermoelectric power measurements. Furthermore, a similar set of experiments was carried out for an isostructural phase $U_4Rh_{13}Si_9$, whose physical properties have not been reported before.

Polycrystalline samples of $U_4Ir_{13}Si_9$ and $U_4Rh_{13}Si_9$ were prepared by arc-melting the stoichiometric amounts of the constituents under purified-argon atmosphere and subsequent annealing in evacuated silica tubes at 900°C for two weeks. Quality of the products was checked by x-ray powder diffraction. The x-ray patterns were indexed within orthorhombic symmetry with the lattice parameters: $a = 18.921(1)$ Å, $b = 10.954(1)$ Å, and $c = 3.900(1)$ Å for $U_4Ir_{13}Si_9$, and $a = 18.913(1)$ Å, $b = 10.956(1)$ Å, and $c = 3.862(1)$ Å for $U_4Rh_{13}Si_9$, being in good agreement with the data reported in the literature [1]. No traces of any secondary phases were found on the diffractograms.

Magnetic measurements were performed in the temperature range 1.8–400 K and in magnetic fields up to 5 T using a Quantum Design MPMS SQUID magnetometer. The electrical resistivity was measured from 4.2 K up to room temperature and in magnetic fields up to 8 T employing a conventional four-point dc technique. Thermoelectric power measurements were done in the interval 6–200 K using a differential method with copper as a reference material. The heat capacity was measured in the temperature range 1.9–200 K using a Quantum Design PPMS platform.

Fig. 1 presents the low-temperature dependencies of the magnetization in $U_4Ir_{13}Si_9$ and $U_4Rh_{13}Si_9$. For both compounds the $\sigma$ ($T$) curve exhibits an antiferromagnetic-like maximum located at $T_N = 18$ K and $T_N = 30$ K for $U_4Ir_{13}Si_9$ and $U_4Rh_{13}Si_9$, respectively, followed at lower temperatures by some other anomalies of complex shape. The overall character of $\sigma$ ($T$) observed for the Ir-containing phase is similar to that reported in Ref. 1. In the ordered state the magnetization of both ternaries is proportional to the strength of applied magnetic field, and independent of the magnetic history of the measured sample. These findings indicate antiferromagnetic character of the magnetic ordering in the two materials. The complexity of the observed behaviour may be ascribed to the unique crystal structure of the compounds studied that boasts as many as three different crystallographic sites for the uranium atoms.

In the paramagnetic region the inverse magnetic susceptibilities of $U_4Ir_{13}Si_9$ and $U_4Rh_{13}Si_9$ are strongly curvilinear functions of temperature, which may be approximated by a modified Curie–Weiss law with the parameters: $\mu_{eff} = 2.17\ \mu_B$, $\theta_p = -24$ K and $\chi_0 = 7.1 \times 10^{-3}$ emu/mol for $U_4Ir_{13}Si_9$ and $\mu_{eff} = 2.20\ \mu_B$, $\theta_p = -38$ K and $\chi_0 = 8 \times 10^{-4}$ emu/mol for $U_4Rh_{13}Si_9$. The results obtained for the Ir-containing compound are in reasonable accordance with the data given in Ref. 1. The reduced values of the effective magnetic moment may indicate some partial delocalization of the uranium 5*f* electrons. The paramagnetic Curie temperatures are consistent with the respective values of $T_N$. In turn, the quite large temperature independent terms most likely arise due to Pauli contributions of *d* electrons of Ir and Rh.

The low-temperature specific heat data, shown in Fig. 2, corroborate the magnetic ordering in $U_4Ir_{13}Si_9$ and $U_4Rh_{13}Si_9$ setting in at $T_N = 18$ and 30 K, respectively. Moreover, the $C/T$ vs. $T$ curves confirm the complex magnetic behaviour of both compounds in the ordered state. Worth to note is enhanced magnitude of the $C/T$ ratio at low temperatures, which extrapolated to zero Kelvin yields $\gamma = 150$ and 200 mJ/(mol$_U$ K$^2$) for the Ir- and Rh-containing silicide, respectively. These values clearly indicate strong electronic correlations in both ternaries.

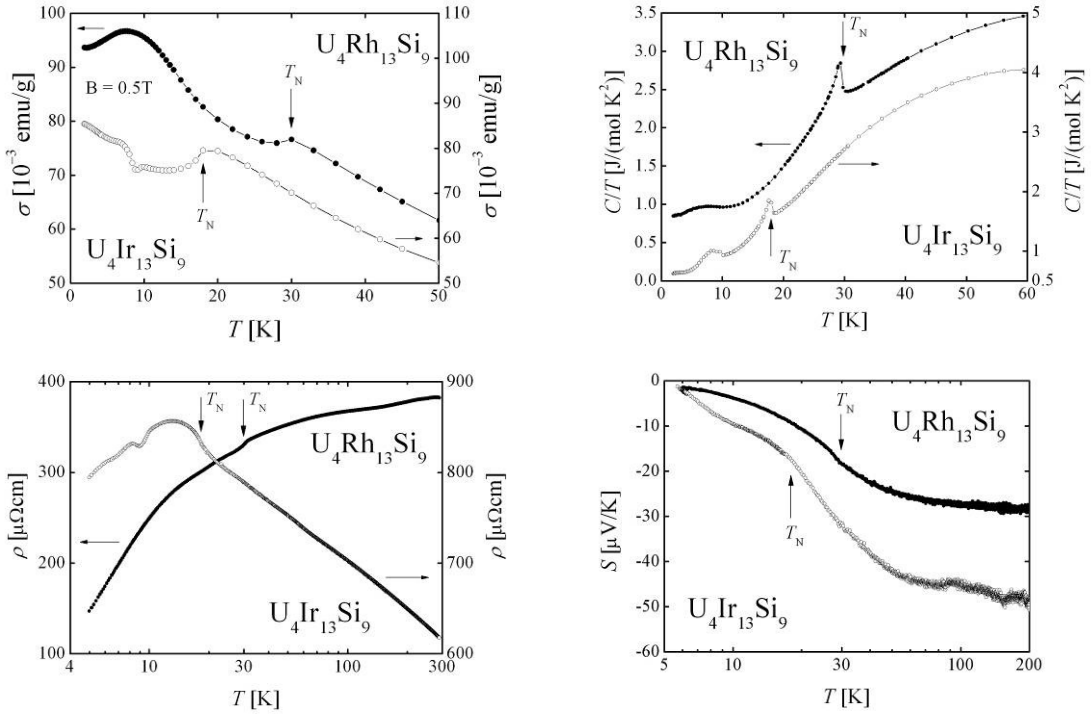


Despite rather similar magnetic behaviour, the character of electrical conduction in $U_4Ir_{13}Si_9$ and $U_4Rh_{13}Si_9$ is notably different (see Fig. 3). In the paramagnetic region the resistivity of the former compound shows a Kondo-like negative temperature coefficient, whereas that of the later one changes with temperature in a manner typical for spin fluctuators. For $U_4Ir_{13}Si_9$ a broad bump in $\rho(T)$ is seen below $T_N$, characteristic of antiferromagnets with large magnetic unit cells, while in the case of $U_4Rh_{13}Si_9$ just a kink in $\rho(T)$ is observed. This dissimilarity may indicate the formation of different magnetic structures in the two compounds but it may also arise because of strong anisotropy in the scattering of charge carriers. Alike $\sigma(T)$ and $C(T)$, the $\rho(T)$ curves exhibit distinct anomalies in the ordered state at the same temperatures, hence proving intrinsic nature of these features, which probably manifest some changes in the arrangement of the uranium magnetic moments in the three different magnetic sublattices.

As displayed in Fig. 4, the thermoelectric power of $U_4Ir_{13}Si_9$ and $U_4Rh_{13}Si_9$ exhibits similar temperature dependence. The Seebeck coefficient is negative in the entire temperature range and $S(T)$ shows kinks at the magnetic phase transitions. Worthwhile noting is large magnitude of the thermopower at high $T$ that reaches about –50 and –30 μV/K for the Ir- and Rh-containing phase, respectively, thus being of the order typical for heavy fermion systems.

[1] A. Verniere et al., *Journal Alloys Compd.* **218**, 197 (1995).

# E4

## Magnetic properties of $NpNiSi_2$

**E. Colineau,[1] F. Wastin[1], J.P. Sanchez[1,2] and J. Rebizant[1]**

[1] *European Commission, Joint Research Centre, Institute for Transuranium Elements, Postfach 2340, D-76125 Karlsruhe, Germany, e-mail: eric.colineau@ec.europa.eu*
[2] *CEA, Département de Recherche Fondamentale sur la Matière Condensée, 38054 Grenoble cedex 9, France, e-mail: jean-pierre.sanchez@cea.fr*

The study of isostructural families provides valuable information that allows identifying trends and key parameters that clarify general mechanisms driving the physical properties of intermetallic compounds. During the last decade, extensive studies have been performed in particular on the ternary series AnTX [1], $AnT_2X_2$ [1] and $An_2T_2X$ [2] compounds (where An is an actinide, T a transition metal and X belongs to column IV). On the contrary, very few data exist on the $AnTX_2$ system that crystallizes in the orthorhombic Cmcm (n°63) structure. Whereas $UFeSi_2$ is a weakly temperature dependent paramagnet and $UCoSi_2$ a spin fluctuation system, $UNiSi_2$ is a ferromagnetically ordered ($T_C$ = 95 K) Kondo lattice with rather well-localized 5f-electrons [3]. The 1.2 $\mu_B$ U-moments are directed along the shorter (c) –axis [4]. The specific heat Sommerfeld coefficient amounts to $\gamma = 21$ mJ $mol^{-1}$ $K^{-2}$ [5].
In order to extend these investigations to trans-Uranium systems, we have undertaken the study of $NpNiSi_2$ and present here the first results on this system, obtained by magnetization, electrical resistivity, specific heat and $^{237}$Np Mössbauer spectroscopy.

$NpNiSi_2$ orders ferromagnetically (F) at $T_C$ = 51.5 K, as evidenced by magnetization (Figure 1a), that also reveals a strong anisotropy between the **b-** and **c-** (easy) axis, along which a saturation moment of 1.07 $\mu_B$ is observed.

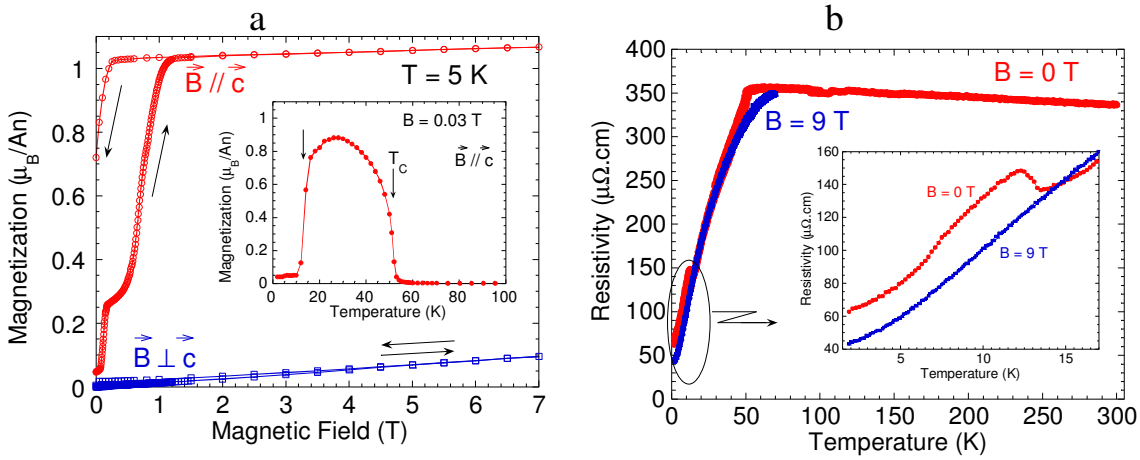


Fig. 1a. Magnetization of $NpNiSi_2$ at T = 5K for **B//c** and **B⊥c**. The insert shows the temperature dependence with a magnetic field of 0.03T applied along the c-axis (easy axis).
Fig. 1b : Electrical resistivity of $NpNiSi_2$. The insert shows the low-temperature part.

A second anomaly is observed around 13 K (Figure 1) and could correspond either to domain effects or to the onset of antiferromagnetic (AF) ordering. Further, note the 2-steps increase of M(H) at T = 5 K that indicates the occurrence of an intermediate domain or F/AF phase. The electrical resistivity (Figure 1b) confirms the onset of magnetic order at 51.5 K and also the presence of a second anomaly around 13 K, that vanishes when magnetic fields (> 0.3 T) are applied. This, together with the magnetization data would suggest the existence of a low-

temperature antiferromagnetic phase, easily destroyed (to induced ferromagnetism) with the application of an external magnetic field.
The specific heat (Figure 2a) exhibits a clear lambda-type transition at $T_C$ = 51.5 K, in good agreement with the other techniques. However, no anomaly is observed at lower temperature, which would then rule out the hypothetic ferro-to-antiferromagnetic transition suggested by magnetization and resistivity measurements. The Sommerfeld coefficient amounts to 145 mJ $mol^{-1}$ $K^{-2}$, which classifies $NpNiSi_2$ as a moderate heavy fermion system contrarily to its U-homologue.
Finally, the $^{237}$Np Mössbauer spectra also confirm the onset of magnetic ordering below 52 K and allow to infer the local magnetic moment carried by the neptunium atoms $\mu_{Np}$ = 1.39 $\mu_B$. The value of the isomer shift ($\delta_{IS}$ = 6.1 mm/s vs $NpAl_2$) suggests a $Np^{3+}$ charge state, i.e. a $5f^4$ electronic configuration.

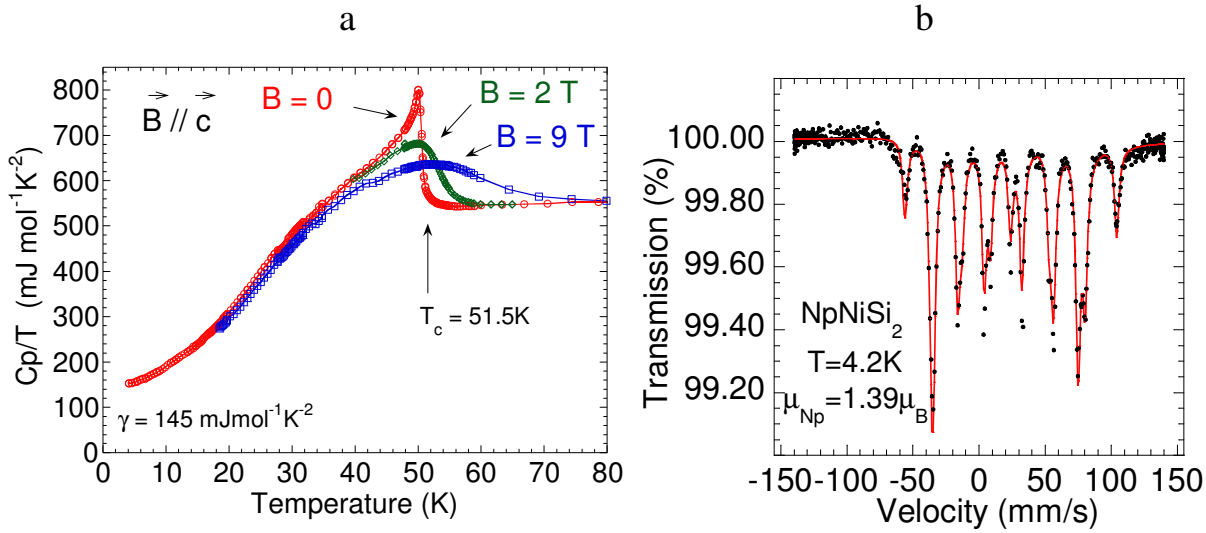


Fig. 2a. Specific heat of $NpNiSi_2$ for different magnetic fields applied along the c-axis.
Fig. 2b : $^{237}$Np Mössbauer spectrum of $NpNiSi_2$ recorded at T = 4.2 K

The logarithmic decrease of ρ(T) in the paramagnetic region is typical of a Kondo lattice. This, together with crystal field effects could explain the reduction of the Np magnetic moments (compared to the $Np^{3+}$ free ion) and suggest a rather localized 5f electron system, similarly to the uranium homologue $UNiSi_2$ [3].

**Acknowledgements**
The high purity Np metals required for the fabrication of the compound were made available through a loan agreement between Lawrence Livermore National Laboratory and ITU, in the frame of a collaboration involving LLNL, Los Alamos National Laboratory and the US Department of Energy.

**References**
[1] V. Sechovsky and L. Havela, in : Ferromagnetic Materials, Vol.4, Eds E.P. Wohlfarth and K.H.J. Buschow, Elsevier, p. 415-468 (1988). and references therein.
[2] M.N. Peron et al., J. Alloys Comp. **201**, 203 (1993).
[3] D. Kaczorowski, Solid State Comm. **99**, 949 (1996).
[4] A. Das et al., Solid State Comm. 114, 87 (2000).
[5] T. Taniguchi et al., J. Magn. Magn. Mater. **177-181**, 55 (1998).

# E5

## Towards *f*-electron single-molecule magnets: Physical properties of a Tm-based "double decker" complex

**N. Magnani,[1] R. Caciuffo[1], E. Colineau[1], F. Wastin[1], G. Amoretti[2], S. Carretta[2], P. Santini[2], A. Baraldi[2], R. Capelletti[2], D.T Adroja[3], A. Nakamura[4], M. Watanabe[5]**

[1] *European Commission, JRC, Institute for Transuranium Elements, Postfach 2340, D-76125 Karlsruhe, Germany. e-mail: Nicola.Magnani@ec.europa.eu*
[2] *Department of Physics, University of Parma, Italy*
[3] *ISIS Spallation Source, Rutherford Appleton Laboratory, Chilton, Oxford, United Kingdom*
[4] *Advanced Science Research Center, Japan Atomic Energy Agency, Tokai, Japan*
[5] *Nuclear Science and Engineering Directorate, Japan Atomic Energy Agency, Tokai, Japan*

One of the best examples of noninteracting quantum objects embedded in a solid state environment is provided by magnetic molecules. In particular, much interest has been attracted by molecules containing transition-metal ions whose spins are so strongly exchange coupled that at low temperature each molecule behaves like a single-domain particle with fixed total spin S. Indeed, these systems are appealing both for fundamental physics and for envisaged applications. From a fundamental point of view, these zerodimensional magnetic units can be considered model systems to investigate quantum phenomena like quantum tunneling of the magnetization. Moreover, being mesoscopic objects, these molecules also offer the possibility to study the transition between the quantum and classical regimes. As far as potential applications are concerned, properly engineered magnetic molecules could be used to realize high-density information storage devices and to implement quantum computation algorithms.

Single-molecule magnets (SMMs) are a particular class of magnetic molecules which exhibit magnetization hysteresis at low temperatures, *i.e.* whose physical properties resemble those of a macroscopic magnet. Typical examples of SMMs are transition-metal complexes such as $Mn_{12}$ [1] and $Fe_8$ [2], which have strong intramolecular exchange interactions (producing a high-spin ground state) and very weak magnetic interaction between molecules.

It has been suggested that SMMs with better performance (higher anisotropy and blocking temperatures) might be produced if rare-earth or actinide elements are used. The first complex of this kind to be reported [3] was a lanthanide-based double-decker phtalocyanine compound $[Pc_2Ln^{III}]^-$ (Fig. 1). Evidence for quantum tunneling of the magnetization in the complexes with Ln = Tb, Dy was recently presented [4]; however, precise information on the ligand field and 4*f* energy spectra (which is of crucial importance for studying and understanding the magnetic properties of these molecules) are still lacking [5].

The present work deals with experimental and theoretical results on the $[Pc_2Tm^{III}]^-$ complex.

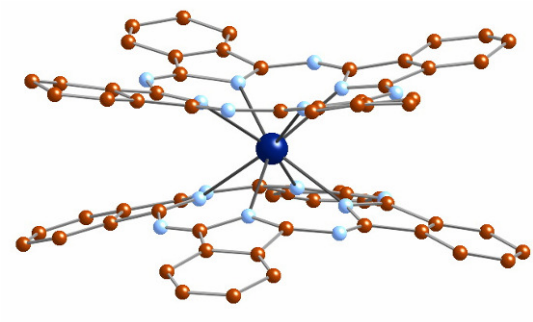

Fig. 1. Structure of the $[Pc_2Ln^{III}]^-$ complex. Large atom: Ln. Small light atoms: N. Small dark atoms: C.

# E5

Optical spectroscopy measurements have been performed on a Bomem DA8 Fourier-transform spectrometer operating in the 500 – 24000 $cm^{-1}$ range, with an apodized resolution as fine as 0.02 $cm^{-1}$, using samples prepared in Tokai. Narrow peaks attributable to electronic excitations of the $Tm^{3+}$ ions have been detected only in the energy region corresponding to the $^3H_6 \rightarrow {}^3H_5$ transition. These spectra display two structures, each composed by a peak and a shoulder, separated by a gap value of 15.2 $cm^{-1}$ (Fig. 2). In addition, each of the two structures unveils the presence of a smaller energy gap (corresponding to the separation between each peak and its shoulder).

INS measurements were performed on the HET spectrometer at the ISIS Spallation Source. By comparing spectra at different momentum transfer Q, a clear magnetic signal around 1.8 meV was revealed, superimposed to the elastic peak tail. No other magnetic peak was detected up to about 90 meV. Despite the fact that a lower resolution is obtainable, the presence of an excited level of $Tm^{3+}$ at 1.8 meV (≈ 15 $cm^{-1}$) within the ground $^3H_6$ multiplet is consistent with the gap in the optical measurements.

Specific heat measurements as a function of temperature and magnetic field have been performed on the new 14-Tesla Physical Properties Measurements System (PPMS-14T) at the ITU. Temperatures down to 330mK were achieved using the $^3$He insert.

The experimental results have been analyzed by a ligand-field model which accounts for the nominal $C_4$ local symmetry of the rare-earth sites, instead of the approximate $D_{4d}$ point symmetry considered in the literature. This allowed us to establish the correct structure of the lowest-lying energy levels and to extract precise values of the ligand-field parameters. Using these parameters as a starting point, the magnetic properties can be calculated for all the rare-earth series.

The perspectives regarding an extension of the work to 5*f*-based complexes are discussed.

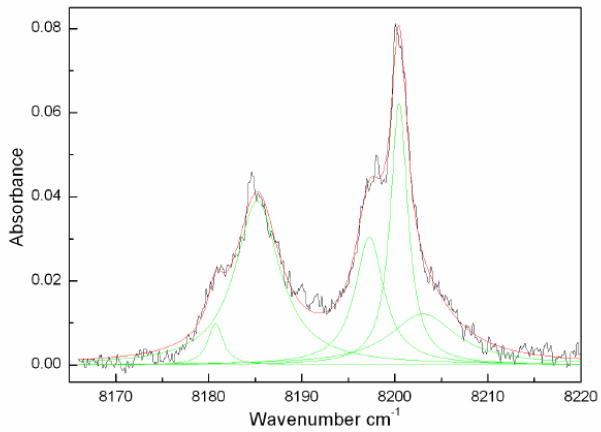


Figure 2. Optical absorption spectra at T = 15 K, in the energy region corresponding to the $^3H_6 \rightarrow {}^3H_5$ transition

## References


[1] R. Sessoli et al., *Nature* **365**, 141 (1993).
[2] D. Gatteschi et al., *Science* **265**, 1054 (1994).
[3] N. Ishikawa et al., *J. Am. Chem. Soc.* **125**, 8694 (2003).
[4] N. Ishikawa et al., *Angew. Chem. Int. Ed.* **44**, 2931 (2005).
[5] N. Ishikawa et al., *Inrog. Chem.* **42**, 2440 (2003).

# F1

## Application of the Chemiluminescence Effects and Pulse Laser Spectroscopy Methods for U, Pu and Np Trace Amount Detection

**Igor Izosimov**

*Khlopin Radium Institute, 194021 St.Petersburg, Russia, e-mail: izig@mail.ru*

Selective and sensitive direct actinide elements trace amounts detection in the different samples presents today major importance for ecology, radwaste handling and control, rehabilitation of contaminated areas and risk assessment. In recent years in the element and isotope analyses of environmental samples the laser radiation is used more and more widely. The laser radiation can be tuned smoothly in the wide range of wavelength, has a high energy resolution and high power in comparison with usual light sources. These qualities of the laser radiation open new possibilities in determination of element and isotope composition of the environmental samples.

However the practical use of the laser spectroscopy methods in the analysis of different samples encounters one essential difficulty, namely it is necessary to get the investigated element from the sample to a zone of interaction with laser radiation. That is why the most attractive from practical point of view is to use the solutions of investigated samples. But in this case, as a rule, one cannot determine the isotopic composition of a sample.

The time-resolved technique (Time Resolved Laser Induced Fluorescence (TRLIF) method) allows to separate useful long-lived fluorescence from short-lived fluorescence impurity and from scattered light, that enables to increase considerably the sensitivity of a method in the application to long-lived fluorescence of lanthanides and actinides in solutions.

Now the following actinides: $UO_2^{2+}$,$Cm^{3+}$, $Am^{3+}$,$Cf^{3+}$, $Es^{3+}$, *and* $Bk^{3+}$and some complexes of above-indicated actinides valence forms can be detected by TRLIF method. The most progress is achieved in $UO_2^{2+}$,$Cm^{3+}$*and* $Am^{3+}$ TRLIF detection.

It is very attractive to apply the Time Resolved Laser Induced Fluorescence (TRLIF) method for actinides trace amount detection in solutions because of its high sensitivity. But many actinides and their complexes (including Pu and Np) do not give the direct luminescence in solutions. For the detection of non-luminescent actinides and molecules containing actinides in solutions it is very perspective to use chemiluminescence methods in combination with time resolution method and chemiluminescence multi-step excitation [1]. The chemiluminescence registration gives high sensitivity of actinides detection and multi-step chemiluminescence excitation gives high selectivity of actinides detection.

The Limits Of Detection (LOD) for spectrometers using the registration of chemiluminescence are in the range from $10^{-6}$ mol/1 to $10^{-13}$ mol/l depending on the type of solutions and type of detectable molecule [2,3]. Chemiluminescence is widely used as a base for detection methods in many fields, such as flow injection analysis, chromatography, biology, medicine, etc. [2]. We have observed and study the chemiluminescence effects in solutions containing U, Pu and Np. It's open possibility for chemiluminescence application in *Nuclear Chemistry.* The sensitivity of the chemiluminescence methods is higher than sensitivity of other methods (LIPAS for example) which are used for non-luminescent actinides and molecules detection now. The combinations of the chemiluminescence effects with high sensitivity and high selectivity laser spectroscopy methods make it possible to carry out an effective detection both of luminescent and *non-luminescent* actinides and molecules containing actinides (especially U, Pu and Np) in different solutions.

The selective excitation of actinide gives rise a chemical reaction between molecule or complex containing excited actinide and chemiluminescence agent added into solution. As a

result of the reaction the light is emitted (chemiluminescence) and registered by a secondary emission photocell.

In this report the different multi-step schemes of chemiluminescence excitation and it's applications for selectivity increasing are discussed. It is shown that chemiluminescence induced by excited actinides complexes has delay time about several microseconds relative to excited laser pulse (fig.1), so the time resolved methods for chemiluminescence registration may be effectively applied for sensitivity increasing.

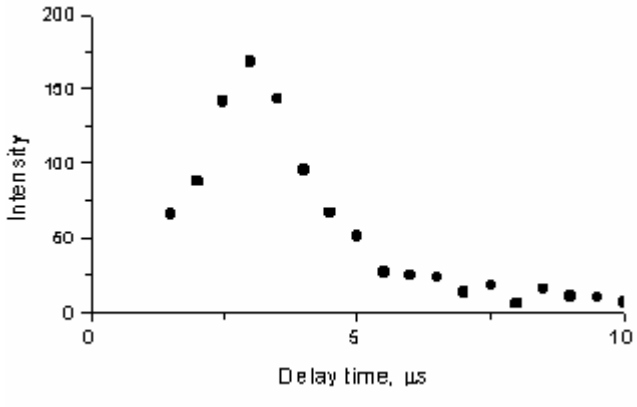


Fig.1.Kinetic curve of luminol chemiluminescence induced by excited plutonyl complexes
Plutonyl complexes were excited by pulsed laser radiation.

## References

[1] I.N. Izosimov et al. "Pu, Np and U Valence States and the Determination of There Molecular Form by Chemiluminescence and Pulsed Laser Spectroscopy". In: Proc. International Conference Actinides 2005. Manchester, UK. 2005, p.779.

[2] C.Dodeigne, L.Thunus, R.Lejeune. "Chemiluminescence as a Diagnostic Tool". *Talanta* **51(3)**, 415 (2000).

[3] T.Schlederer, Fritz P.G. "Method of detecting substances by chemiluminescence".United States Patent 5,736,320. 1998.

# F2

## Contribution of the capillary electrophoresis – inductively coupled plasma mass spectrometry for actinide speciation studies

**Aupiais Jean[1], Ambard Chrystel[1], Topin Sylvain[1], Baglan Nicolas[1], Philippini Violaine[2], Burgat Romain[3], Faure Stéphane[3]**

[1] *CEA – Département Analyse & Surveillance de l'Environnement, Service Radioanalyse Chimie Environnement, Bruyères-le-Châtel 91680, France, e-mail: jean.aupiais@cea.fr*
[2] *CEA – Département de Physico-Chimie, Service d'Etudes du Comportement des Radionucléides, Gif-sur-Yvette 91191, France, e-mail:violaine.philippini@cea.fr*
[3] *CEA – Département de Traitement des Matériaux Nucléaires, Service Analyses Déchets, Is-sur-Tille 21120, France, e-mail:stephane.faure@cea.fr*

The understanding of actinide behaviour in the biosphere (soil, air and water) depends on their chemical form (speciation). Due to the various oxidation states (III, IV, V and VI), the chemical properties of An in the environment may be deeply different when focusing on migration, complexation, biosorption, bioaccumulation etc. Therefore, the detection of these species at trace or ultra-trace level is one of the major challenges for the analyst. Recently, a new hyphenated technique the CE – ICPMS has reached technological reliability and allows now performing actinide speciation studies. We propose here, through a few examples, to show the capability of CE-ICPMS to detect inorganic and organic actinide species, to determine their stability constants, or to solve some questions about the limiting complex or the nature of the complex.

**Determination of stability constants $UO_2^{2+}/SO_4^{2-}$ & $NpO_2^{+}/CO_3^{2-}$**

The average electrophoretic mobility of *n* species involving one cation and one ligand is defined by the following relations; for $UO_2^{2+}$ $\mu_{U(VI)}^{app} = \mu_{UO_2^{2+}}\Phi_{UO_2^{2+}} + \mu_{UO_2SO_4}\Phi_{UO_2SO_4}$ and for $NpO_2^{+}$ $\mu_{Np}^{app} = \mu_{NpO_2^{+}}\Phi_{NpO_2^{+}} + \mu_{NpO_2(CO_3)^{-}}\Phi_{NpO_2(CO_3)^{-}}$, where $\mu_i$ are the intrinsic electrophoretic mobility of the specie *i* and $\Phi_i$ its molar fraction ($\sum \Phi_i = 1$). The determination of the stability constant is then possible and leads to experimental values in good agreement with the recommended data: $\log\beta^0 = 3.19\pm0.09$ (OECD $3.15\pm0.02$) and $\log\beta^0 = 5.1\pm0.1$ (OECD. $4.96\pm0.02$).

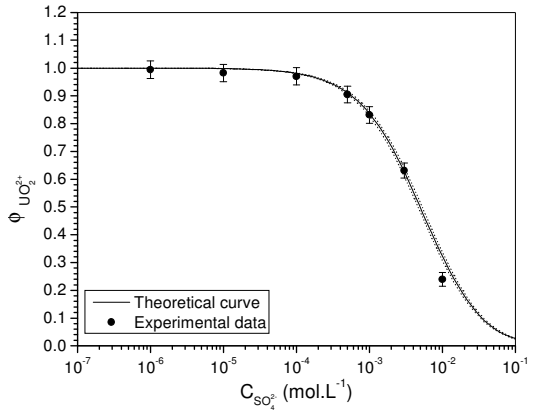


Fig 1.a: variation of the molar fraction of free uranyl ($10^{-6}$ M) vs the sulfate concentration. Conditions of separation buffer β-alanin/ $HClO_4$; pH 3,55, I = 0.11 M.

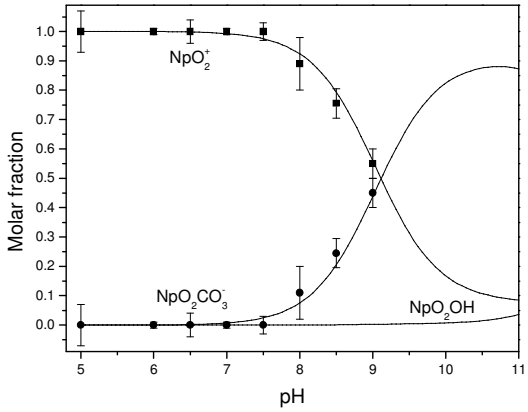


Fig 1.b: variation of the molar fraction of free neptunyl ($10^{-8}$ M) vs pH. Condition of separation buffers MES, EPPS and AMPSO, $[CO_3^{2-}] = 2\times10^{-4}$ M, I = 50 mM

**Qualitative detection of $Ln(CO_3)_i^{3-2i}$ (i=3,4) at high ionic strength (I = 3 M)**

This study has been initiated to identify whether 1 or 2 groups of limiting complexes $Ln(CO_3)_3^{3-}$ and $Ln(CO_3)_4^{5-}$ were existed. By extension, it could be possible to settle about the existence of limiting complexes for Cm and Am with 3 or 4 ligands. It is expected for light R.E. a limiting complex with 4 carbonates and 3 for the heavy R.E. Indeed, the light R.E. present smaller ionic radii (corresponding to higher μ - see box in Fig.2). As a consequence, light R.E. complexes should be faster than the heavier ones. It can be seen in Fig.2 an opposite behaviour. This could be interpreted as the stabilization of highly charged complexes by sodium cations present in the solution. This is the first indirect evidence, in situ, of the stabilization by ion pairing.

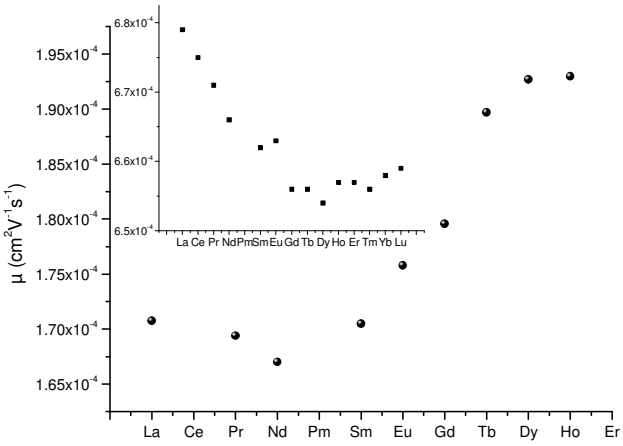


Fig. 2: variation of $\mu_{complex}(Ln)$. Condition of separation $Na_2CO_3$ 1 M, pH = 11, 57 cm×20 μm, V = - 15 kV, $I$ = 3 M – box: $\mu^0(Ln^{3+})$

**Speciation of $Pu^{4+}$, $Pu^{3+}$ and $PuO_2^+$ by aminocarboxylic acids NTA & DTPA at 2 ionic strengths (I = 50 mM & I = 1 M)**

Some amino carboxylic acids are potentially present in the environment. Due to their selectivity for actinides, they can be a potential vector for the migration. The figures below show the capability to detect and to quantify oxidation states as well as to confirm without ambiguity the nature of the species. The electrophoretic mobility determined under very different conditions (Fig 3.a and 3.c) for the complex $Pu(IV)DTPA^-$ give the same value after ionic strength correction.

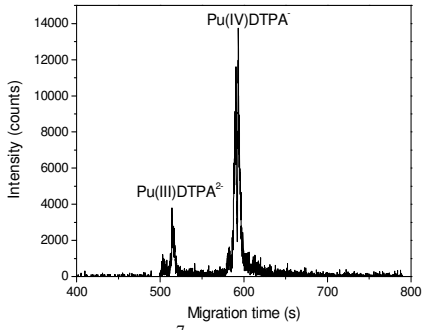


Fig. 3.a: [Pu] = $1.8\times10^{-7}$ M. Condition for separation : MES = 50 mM, DTPA = 0.1 mM, CTAB = 0.5 mM, pH = 6.1, 100 cm×75 μm, V = - 25 kV, $I$ = 50mM.

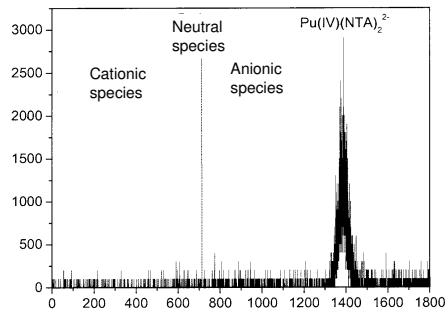


Fig. 3.b: [Pu] = $2.3\times10^{-7}$ M. Condition for separation : MES = 50 mM, NTA = 0.1 mM, pH = 6.1, 100 cm×75 μm, V = + 25 kV, $I$ = 50mM.

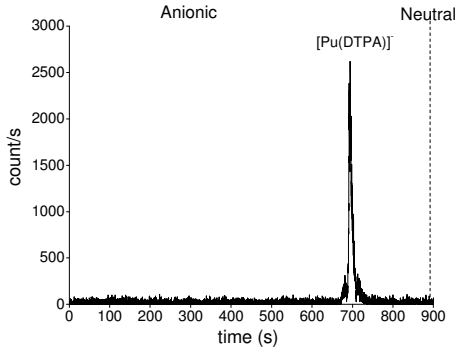


Fig 3.c: [Pu] = $1\times10^{-7}$ M. Condition for separation : $NH_4NO_3$ 1 M, MES = 50 mM, DTPA =0.04 mM, TTAB = 2 mM, pH = 5.2, 80 cm×20 μm, V = - 15 kV, $I$ = 1 M.

# F3

## Lanthanides and actinides isotope separation by oscillating extraction

**A.A. Kopyrin [a], M.A. Afonin [a], T. Todd [b]**

*[a] Saint-Petersburg Institute of Technology, 26 Moskovsky av., 190013, Saint-Petersburg, Russia, afonin1@lti-gti.ru*
*[b] Idaho National Laboratory, Idaho Falls, Idaho 83415, USA*

A new separation extraction method was created based on an oscillatory extraction/stripping process in two extractors coupled by a bulk liquid membrane. The experimental setup to investigate the kinetics of non-stationary processes was built at the Saint Petersburg State Institute of Technology, in the Rare Earth Department. This setup could be used to separate macro-concentration of similar elements or isotopes as well.

The setup consisting of two extractors coupled by liquid membrane (tributyl phosphate in hydrocarbon) is described elsewhere [1].

To compare the separation of Nd isotopes under thermal oscillation and at constant temperature, experiments were performed with the same initial conditions except temporal-temperature profiles in one extractor. Two experiments (with and without the influence of temperature, inducing non-steady state extraction in system) consisting of two extractors coupled by liquid membrane were performed to compare the isotopic effects under constant temperature of both extractors and under oscillatory temperature in one.

The samples for mass spec measurement in the experiment with constant temperature were taken after 250 min from the start of the experiment. It was found that light Nd isotopes (143-146) are concentrated in the second (stripping) extractor while heavy Nd isotopes (148,150) are concentrated in first extractor. The enrichment of heavy isotopes (148, 150) of 0.5% was observed. During the experiment, the organic phase was contacted with both aqueous phases about 50 times. The average enrichment factor per contact was equal to 1.01.

The samples for mass spec measurement in the experiment with oscillating temperature were taken after 350 min from the start of the experiment. It was found that light Nd isotopes (143-146) were concentrated in second extractor (stripping) while heavy Nd isotopes (148,150) were concentrated in first extractor. The enrichment of heavy isotopes (148, 150) of 1.2 % was observed. During the experiment, the organic phase was contacted with both aqueous phases about 76 times. The average enrichment factor per contact was equal to 1.016.

The enrichment of heavy Nd isotopes (148, 150) in the extraction part, as compared with the stripping part, of the three-phase extraction system in non-equilibrium and non- stationary conditions at oscillating temperature was observed to be 0.9-1.2 %, which is two times better than at constant temperature. The possible explanation of the results could be based on the difference of isotope properties in the kinetics of extraction, where there are differences in the average concentrations of the isotopes in the organic phase. Therefore different isotopes concentrations appear in the different extractors.

To compare the separation of Pr and Nd under thermal oscillation and at constant temperature the experiments were performed with the same initial conditions except temporal-temperature profiles in one extractor. Two experiments (with and without influence of temperature inducing non-steady state extraction in system) consisting of two extractors coupled by liquid membrane were performed to compare the metal separation coefficients under constant temperature of both extractors and under oscillatory temperature in one.

Using temperature oscillation, the separation factor for Nd and Pr was increased 1.6 times in comparison with the extraction at constant temperature and reached the value 2.8.

The possibility of actinide separation using oscillatory extraction in a three phase extraction system is discussed.

**Acknowledgements.** This work was supported by the U.S. Department of Energy, Office of Basic Energy Sciences, under grant RUC2-20011-ST-04 administered by the Civilian Research and Development Foundation.

**References**

[1] Afonin M.A. et all *Czech. J. Phys*. 56 (2006), D445

# Actinide targets for the production of radioisotopes by the ISOL method

**T. Stora, R. Catherall, S. Fernandes, J. Lettry**

[1] *AB-ATB-IF (ISOLDE), CERN, CH-1211 Geneva 23, Switzerland,*
*e-mail: Thierry.Stora@cern.ch*

The Isotope Separation On-Line (ISOL) method produces radioactive nuclides in thick high-temperature targets via spallation, fission or fragmentation nuclear reactions induced by high energy proton beams. The delay between the genesis of radioisotopes and their availability as Radioactive Ion-Beam (RIB) is governed by diffusion and effusion processes within the target and the ion source. These mechanisms have to be optimized to minimize this delay and its resulting decay losses, and maintained for prolonged irradiation periods. At CERN-ISOLDE, a pulsed 1.4GeV, 2kW average power, proton beam from the PSBooster is used to produce more than 800 radioactive isotopes of 70 different chemical elements and attracts a wide community of physicists in nuclear and atomic physics, solid state physics, astrophysics and life sciences. The EURISOL-DS European project is the design study of the next generation European ISOL radioactive ion beam facility that shall be based on a high energy protons driver beam of 5 MW average power hopefully resulting in 3 orders of magnitude increase in radioactive ion beam intensities to access new short-lived isotopes. In particular rare neutron rich isotopes are produced by fission reactions with actinide targets, such as uranium or thorium carbides. The development of new uranium targets, compatible with the increased beam intensity foreseen within EURISOL, is actively undertaken. Actual target production standards, and the technical and scientific challenges ahead will be presented.

# G1

## Dual nature of 5f electrons in uranium monochalcogenides

**J. Schoenes[1], K. Litfin[2], M. Broschwitz[1], O. Vogt[3]**

[1] *Institut für Physik der Kondensierten Materie, Technische Universität Braunschweig, Mendelssohnstrasse 3, 38106 Braunschweig, Germany, e-mail: j.schoenes@tu-bs.de*
[2]*Institute for Transuranium Elements, European Commission, J.R.C., Postfach 2340, 76125 Karlsruhe, Germany*
*3Laboratorium für Festkörperphysik, ETH Zürich, 8093 Zürich, Switzerland*

The question of whether the 5f electrons are localized or itinerant has been the key question in actinide solid state research for several decades. Yet, in 1996 some of us [1] reported magnetic susceptibility and electrical transport measurements on a series of pseudo-binary $U_xLa_{1-x}S$ compounds and concluded that "whether or" should be replaced in this case by "as well as", thus introducing the idea of a dual nature of 5f electrons in a material. This idea has received support from the theoretical side [2] and some further experiments [3,4]. In the present contribution we discuss the state of the art of the dual nature of 5f electrons in UX (X = S, Se, Te) and $U_xLa_{1-x}S$.

The borderline behavior of 5f electrons in uranium monochalcogenides is beautifully documented by the temperature dependence of the electrical resistivity [5,6]. While the resistivity of US increases linearly above $T_C$, the resistivity of UTe displays a Kondo-like decrease. This coexistence of ferromagnetic order and Kondo-behavior has only been explained very recently in an underscreened Kondo-lattice theory [7].

An alternative way to increase the U-U separation in uranium monochalcogenides is the substitution of uranium by lanthanum. In the case of $U_xLa_{1-x}S$ one observes single-ion Kondo behavior for $0.08 \leq x \leq 0.3$, coexistence of magnetic order and Kondo-behavior for $0.4 \leq x \leq 0.6$ and ferromagnetic order without Kondo-behavior for $0.8 \leq x \leq 1.0$ [1]. The analysis of the susceptibility data in terms of carrier concentration and effective mass [1] indicates that for $x \leq 0.3$ one out of three 5f electron per added uranium hybridizes with the 6d electrons and the other two 5f electrons are in a localized state. For $0.3 \leq x \leq 0.6$ all additional 5f electrons occupy the localized state. The total screening of 5f electrons decreases and magnetic order sets in. For $0.7 \leq x \leq 1.0$ the additional 5f electrons go again partially in the hybridized conduction band. At x = 1.0 one 5f and one 6d electron occupy the conduction band. Optical and magneto-optical Kerr effect measurements show distinct behavior in the three different regimes [4,8].

The most direct way to decrease the U-U separation is the application of hydrostatic pressure. We have performed optical reflectivity experiments up to 40 GPa in an diamond anvil pressure cell on UX and $U_xLa_{1-x}S$ compounds with x = 0, 0.4, 0.8 and 1.0 [9]. In the following we will show that again the behavior differs markedly in the three regimes supporting the dual nature of the 5f state in this class of materials.

The reflectivity spectra through the diamond have been fitted with one Drude term and up to four Lorentz oscillators. Fig. 1 shows, as an example, the pressure dependence of one of the fitting parameters, namely the plasma energy of the free carriers. For LaS one finds a small decrease with pressure in the NaCl-type structure, followed by a jump at the phase transition into the CsCl-type structure near 25 GPa. The sign of this jump is unexpected at first sight, since the dc conductivity increases. Yet, the second parameter of the Drude fit, which is the damping, reconciles the two results, since it decreases by a factor 4-5 at the transition. In the fcc phase of $U_{0.4}La_{0.6}S$ the plasma energy decreases continuously, while the damping remains nearly constant. This indicates that in this regime, in which additional 5f electrons enter into the localized state, pressure has a similar effect and decreases the free carrier concentration.

This contrasts with the samples $U_{0.8}L_{0.2}S$ and US. Here the plasma energy increases with pressure as does the damping, indicating that the free carrier concentration increases with pressure. Actually, the same trend is observed comparing USe and US at ambient pressure. Further fit parameters, like the oscillator strength of the Lorentz oscillators, will be shown to corroborate the above conclusions.

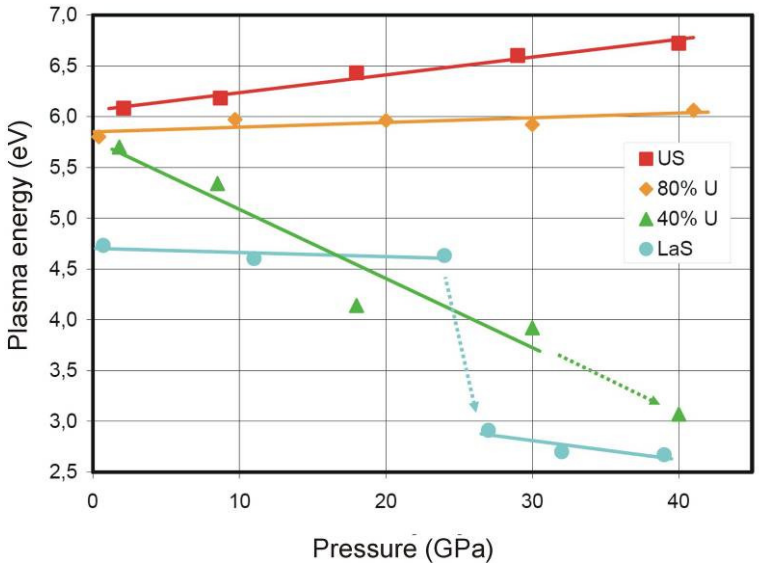


Fig. 1. Pressure dependence of the plasma energy of $U_xLa_{1-x}S$

## References

[1] J. Schoenes et al. *Phys. Rev. B* **53**, 14987 (1996).
[2] G. Zwicknagl et al. *Phys. Rev. B* **65**, 081103 (2002).
[3] M. Broschwitz et al. *Phys. Rev. B* **69**, 184408 (2004).
[4] J. Schoenes et al. *Physica B* **359-361**, 1141 (2005).
[5] J. Schoenes et al. *Phys. Rev. B* **30**, 6578 (1984).
[6] J. Schoenes, *J. Less-Common Met.* 121, 87 (1986).
[7] N.B. Perkins, B. Coqblin et al, Preprint and JdA 2007.
[8] M. Broschwitz et al. *Phys. Rev. B* **66**, 054425 (2002).
[9] K. Litfin, Dissertation Technical University Braunschweig (2006)

# G2

## Effect of pressure on the resonant multi LO- phonon Raman scattering and crystal- field excitations in $UO_2$

**Tsachi Livneh and Eran Sterer**

*Dept. of Physics, Nuclear Research Center Negev, P.O. Box 9001, Beer- Sheva, 84190, Israel*
*e-mail: T.Livneh@NRCN.org.il*

The strong interactions between electrons and longitudinal optical (LO) phonons, which are known to play an important role in $UO_2$ [1], are manifested in Raman scattering measurements. We investigated the Raman scattering in $UO_2$ under pressures of up to 29 GPa with excitation energy range of 1.16-2.41 eV [2]. At ambient pressure up to six order multi-LO-phonon bands were detected, with a resonant profile, which follows the $UO_2$ absorption (threshold of ~2.0 eV). These bands are likely attributed to "forbidden" Fröhlich LO(Γ) scattering [2]. The 1150 $cm^{-1}$ band has been reassigned to the 2LO band rather than to the $\Gamma_5$-$\Gamma_3$ crystal field electronic transition [3].

Resonant coupling has been found between $^3H'_4 \rightarrow {}^3F'_2$ intermultiplet crystal field (CF) excitations ($\gamma_1$-$\gamma_4$ ranges from 4130 to 4580 $cm^{-1}$) and n·LO phonons (n=1-4, $\omega_{LO}\approx 578$ $cm^{-1}$) [4]. Figure 1a compares the electronic-phononic Raman spectra in $UO_2$ (solid line) with the room temperature absorption spectrum of $UO_2$ [3] (dashed line).

Figure 1b displays the very good agreement between the positions of the CF+n·LO Raman bands and yet unassigned bands from a previously measured optimized forth derivative optical absorption spectrum [5]. It points at the significant contribution of LO phonon-assisted CF electronic transitions in the absorption spectrum. For both types of excitations (n·LO and $E_{CF}$+n·LO) the increase in pressure is accompanied by a red shift in the onset of resonance. The pressure dependence of CF-n·LO coupled modes frequencies is practically the sum of the pressure dependences of their constituents (for example $\partial\omega_{\gamma 1}/\partial P = -4.8 \pm 0.4$ and $\partial\omega_{LO}/\partial P = 1.45 \pm 0.04\,cm^{-1}$/GPa).

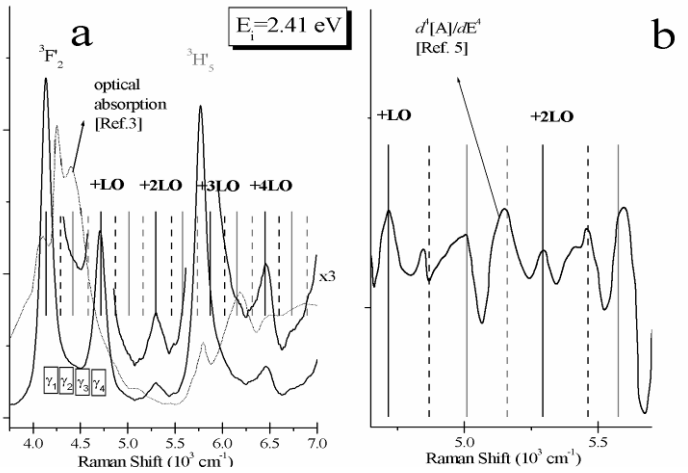


### References

[1] J.M. Cassado, J.M. Harding, G.J. Hyland, *J. Phys: Condens. Matter* **6** 4685 (1994)
[2] T. Livneh and E. Sterer, *Phys. Rev. B* **73**, 085118 (2006)
[3] J. Schoenes, *J. Chem. Soc. Faraday Trans. II*, **83**, 1205 (1987)
[4] T. Livneh, *Phys. Rev. B* , submitted.
[5] T. R. Griffiths and H.V. St. A. Hubbard, *J. Nucl. Mater.* **185** 243 (1991).

# G3

## Observation of Dynamical Spin Shielding in Ce: Why It Matters for Pu Electronic Structure

**J.G. Tobin[1], S.W. Yu[1], T. Komesu[2], B.W. Chung[1], S.A. Morton[1,2] and G.D. Waddill[2]**

[1] *Lawrence Livermore National Laboratory, Livermore, CA, USA*
*Email Presenting author: Tobin1@LLNL.Gov*
[2] *University of Missouri- Rolla, Rolla, MO,USA*

Using Fano Effect measurements [1-3] upon polycrystalline Ce, we have observed a phase reversal between the spectral structure at the Fermi Edge and the other 4f derived feature near a binding energy of 2 eV. The Fano Effect is the observation of spin polarized photoelectron emission from NONMAGNETIC materials, under chirally selective excitation, such as circularly polarized photons. Within various models, the peak at the Fermi Energy ($f^1$ peak, quasiparticle peak, Kondo peak) is predicted to be the manifestation of the electrons which shield the otherwise unpaired spin associated with the peak at 2 eV ( $f^0$ peak or Lower Hubbard Band). Utilizing high-energy photoelectron spectroscopy, on and off resonance, the bulk nature and f-character of both features have been confirmed. Thus, observation of phase reversal between the $f^0$ and $f^1$ peak is a direct experimental proof of spin shielding in Ce, confirming the original picture of Gunnarsson and Shoenhammer, albeit with a slight modification. (See Fig. 1.)

The results for Ce will discussed in light of our recent work on Pu [4-8]. The Pu results demonstrated the importance of spin-orbit splitting in the Pu 5f states, but left open the questions of electron correlation and magnetic cancellation. [4]

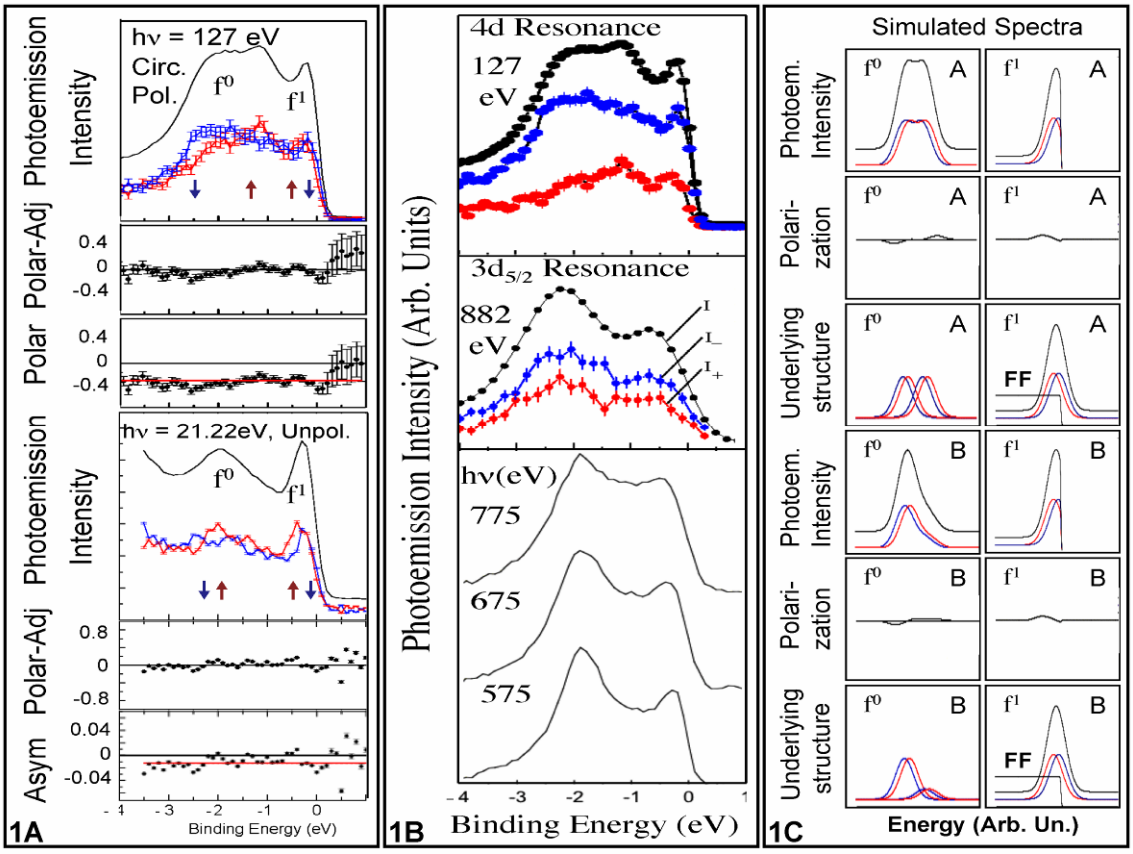


Figure 1

Figure 1 Caption
(Figure 1A) Spin-resolved (blue and red) and spin-integrated spectra (black) of polycrystalline Ce are shown here, along with corresponding polarizations and asymmetry data. Error bars for the spin-resolved spectra are included. Blue (red) corresponds to spin down (up).
(Figure 1B) Top panel: Spin-resolved and spin-integrated spectra of polycrystalline Ce at the 4d to 4f resonance. Middle panel: Spin-resolved and spin-integrated spectra of polycrystalline Ce at the $3d_{5/2}$ resonance. Bottom panel: Spin-integrated spectra of polycrystalline Ce. Color conventions follow those of Figure 1A. The energy bandwidth was 0.32 eV at 575 eV, 0.43 eV at 675 eV and 0.56 eV at 775 eV. Thus the resolving power ($E/\Delta E$) in each case was near 1500.
(Figure 1C) Spectral simulations for Case A and B. Color conventions follow those of Figure 1A. FF stands for Fermi Function.

## Acknowledgements
This work was performed under the auspices of the U.S. DOE by University of California Lawrence Livermore National Laboratory under contract W-7405-Eng-48. Work by LLNL and UMR personnel was funded in part by the Office of Basic Energy Science at DOE. The APS, the ALS and the Beamline 4 Facilities have been built and operated under funding from the Office of Basic Energy Science at DOE.

## References
1. J.G. Tobin, S.W. Yu, T. Komesu, B.W. Chung, S.A. Morton and G.D. Waddill, EuroPhys. Lett. **77**, 17004 (2007) and references therein.
2. S.W. Yu, T. Komesu, B.W. Chung, G.D. Waddill, S.A. Morton, and J.G. Tobin, Phys. Rev. B **73**, 075116 (2006) and references therein.
3. J.G. Tobin, S.A. Morton, B.W. Chung, S.W. Yu and G.D. Waddill, Physica B, **378-380**, 378 (2006) and references therein.
4. J.G. Tobin, J. Alloys Compd. (2006), doi:10.1016/j.jallcom.2006.10.107.
5. J.G. Tobin, K.T. Moore, B.W. Chung, M.A. Wall, A.J. Schwartz, G. van der Laan, and A.L. Kutepov, Phys. Rev. B **72**, 085109 (2005).
6. G. van der Laan, K.T. Moore, J.G. Tobin, B.W. Chung, M.A. Wall, and A.J. Schwartz, Phys. Rev. Lett. **93**, 097401 (2004).
7. J.G. Tobin, B.W. Chung, R. K. Schulze, J. Terry, J. D. Farr, D. K. Shuh, K. Heinzelman, E. Rotenberg, G.D. Waddill, and G. Van der Laan, Phys. Rev. B **68**, 155109 (2003).
8. K.T. Moore, M.A. Wall, A.J. Schwartz, B.W. Chung, D.K. Shuh, R.K. Schulze, and J.G. Tobin, "Phys. Rev. Lett. **90**, 196404 (2003).

# G4

## Resonant Inelastic X-ray Scattering Spectroscopy of Actinide Materials at 5d Edge

**Sergei M. Butorin**

*Department of Physics, Uppsala University, Sweden, e-mail: sergei.butorin@fysik.uu.se*

RIXS measurements at the actinide 5d threshold provide an opportunity to study in detail elementary excitations in actinide compounds due to higher resolution of such experiments in comparison with those at the actinide 3d and 4d thresholds. It has turned out that the technique is very sensitive to the valency and the chemical state of actinide in contrast to x-ray absorption spectroscopy having a drawback of the substantial smearing of spectral structures due to large core-hole lifetime broadening. In this situation, the virtually unlimited resolution (defined by the response function of the instrument) of the RIXS technique and its ability to enhance transitions to low-lying excited states are especially useful. RIXS spectroscopy provides good signatures in terms of new distinct transitions, representing electronic excitations within the 5f shell and having a characteristic profile. This helps to distinguish between actinide species with different oxidation states, especially in case when one of species has much lower concentration than another. Experimental data for systems of light actinides, such as U, Np, and Pu, will be presented and discussed along with the results of model calculations.

# H1

## Equilibrium Phase relations in the U-Zr-Al ternary system: a prospective study for a metallic U-Zr alloy as nuclear fuel.

**O. Tougait,[1] F. Désévédavy[1], S. Dubois[2] and H. Noël[1]**

[1] *Université de Rennes1, Sciences chimiques de Rennes, UMR-CNRS 6226, Campus de Beaulieu, 263 Av. du Général Leclerc, 35042 Rennes Cedex, France, e-mail: tougait@univ-rennes1.fr*
[2] *CEA Cadarache, DEN/DEC/SESC, 13108 Saint Paul Lez Durance Cedex, France, e-mail:*

The Reduced Enrichment Research and Test Reactor (RERTR) international program has initiated a tremendous effort to develop new dispersion fuels. Till the mid 1980's research and test reactors used High-Enriched Uranium (HEU) fuels in the form of U-Al alloys with U enriched at a level of 93% $^{235}U$. Concerns about proliferation of HEU for non-peaceful purposes led to the development of Low-Enriched Uranium (LEU) fuels, such as $U_3Si_2$ comprising less that 20 % $^{235}U$. However, for high performance reactors, new nuclear fuels with loading up to 15 g U/ $cm^3$ are highly desirable to maintain or increase the fission rates. Moreover, to readily convert HEU to LEU reactors, the easiest way is to use standard process and current fuel geometry. Fuels are typical Al-matrix composites that are cladded in Al alloy by roll bonding method to make thin plate-type assemblies. Al is used to evacuate the heat produced by fission reactions, its loading is about 50 vol %. Uranium metal itself has a density of about 19 g. $cm^{-3}$. It possesses three allotropic forms: alpha ($\alpha$) (orthorhombic) stable up to 668 °C, beta ($\beta$) (tetragonal) stable from 668 °C to 775 °C and gamma ($\gamma$) (body-centered cubic) from 775 °C to melting point of 1132°C. This high temperature $\gamma$-phase is the most stable under irradiation [1]. Unfortunately, the transformation $\gamma \rightarrow \alpha$ can not be suppressed by quenching the high-temperature $\gamma$ form, but this can be achieved by chemical alloying.

U-Mo alloys, containing 7 wt. % Mo (U-7Mo) can retain the high temperature $\gamma$-phase, they appeared therefore as the most promising candidates (high uranium density, reprocessing). First examinations of post-irradiated U-7Mo dispersion fuel deplorably show a dramatic swelling of the plate, mainly due to the formation of a U-Mo-Al interaction layer and its poor fission gas retention [2]. Comprehensive studies in the U-Mo-Al system [3, 4], including assessment of the ternary phase diagram, diffusion experiments, micro-characterization (using $\mu$-DRX and $\mu$-SAX) of irradiated as well as non-irradiated samples have proved that the strong chemical reactions between the U-Mo fuel material and the Al-matrix result in the formation of two ternary compounds, $UMo_{2-x}Al_{20+x}$ and $U_6Mo_{4+x}Al_{43-x}$.

To quell the swelling of the fuel-plate, alternative $\gamma$-stabilizer elements for U-alloying should be considered. Zirconium shows a complete solubility in $\gamma$-uranium and has a lower neutron absorption cross section than molybdenum. Evaluation of U-Zr alloys as potential candidate for dispersion fuel was carried out in the form of assessment of two isothermal sections at 800°C and 400°C of the U-Zr-Al system.

In the literature, reports about the U-Zr-Al ternary system are scarce. They are due to G. Petow and co-workers only [5-7]. The experimental work was restricted to the Al rich part of the ternary diagram, limited by $UAl_2$ – $ZrAl_2$ –Al. No ternary compound was claimed, only extension of the binaries $UAl_2$ and $UAl_3$ in the ternary system, with solubility up to 23 at. % Zr and 17 at. % Zr respectively were announced for equilibrium at 600°C.

A total of 66 samples were synthesized, the polycrystalline samples (each weighing ~0.4g) have been prepared by melting the elemental components in an arc furnace. The samples, placed in alumina crucibles, were introduced and sealed in evacuated quartz tubes under residual atmosphere of argon. The reaction tubes were annealed at 800°C for 15 days or at

400°C for 60 days and then quenched to room temperature. Each sample was analyzed by powder X-ray diffraction and its microstructure was studied on polished surfaces using a Jeol JSM 6400 scanning electron microscope (SEM). Finally, the chemical compositions were evaluated by Energy Dispersive x-ray Spectroscopy (EDS). Binary compounds with point composition, such as $UAl_3$, $UAl_2$, $ZrAl_2$ and $Zr_2Al$ were used as external standards to obtain quantitative data.

The isothermal section at 400°C of the U-Zr-Al ternary system is shown in Fig. 1. In the Al-rich part of the diagram, three ternary extensions of the binaries $UAl_2$, $ZrAl_2$ and $UAl_3$ are established, their limits of solubility are assess to 21 at. % Zr, 2 at. % U and 15 at. % Zr respectively, in agreement with the previous observations [4-6]. All the other binary phases were found to have negligible extension into the ternary system. In the U and Zr corners, two large solubility domains, based on α-phase and γ-phase respectively are observed. The whole ternary phase diagram does not comprise any ternary compound.

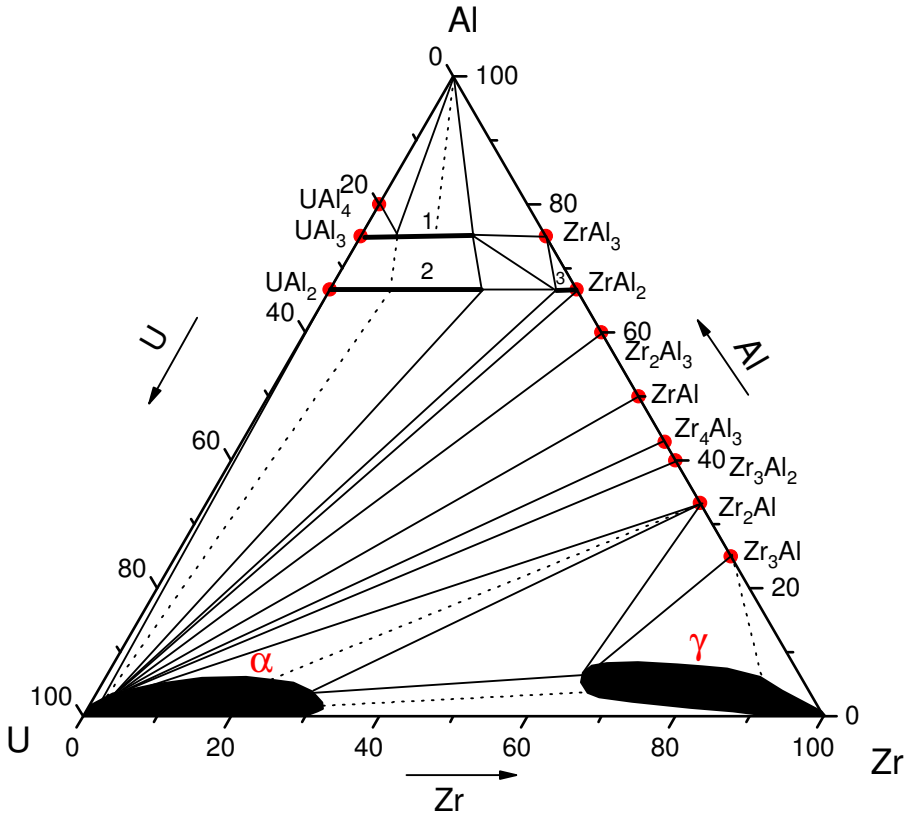


Fig. 1. isothermal section at 400°C of the U-Zr-Al ternary system

## References

[1] J.L. Snelgrove, G.L. Hofman, C.L. Trybus, T.C. Wiencek, Development of Very-High Density Fuel by the RERTR Program, Procedings of the International Meeting on RERTR, Seoul South Korea, 1996.

[2] A. Leenaers, S. Van den Berghe, E. Koonen, C. Jarousse, F. Huet, M. Trotabas, M. Boyard, S. Guillot, L. Sannen, M. Verwerft, J. Nucl. Mater., 335, (2004) 39-47

[3] S. Dubois, F. Mazaudier, J.P. Piron, P. Martin, J.C. Dumas, F. Huet, H. Noël, O. Tougait, C. Jarousse, P. Lemoine. Proceedings of the 9th International Topical Meeting on Research Reactor Fuel Management, Budapest, Hongrie, 2005.

[4] H. Noël, O. Tougait, S. Dubois, to be published

[5] G. Petzow, S. Steeb, I. Ellinghaus, J. Nucl. Mater., 4 (1661) 316-321.

[6] G. Petzow, H.E. Exner, A.K. Chakraborty, J. Nucl. Mater., 25 (1668) 1-15

[7] H.E. Exner, G. Petzow, Metall, 23 (1969) 220-225.

# H2

## Microstructure, sintering and dissolution of $Th_{1-x}U_xO_2$ solid solutions prepared by wet chemistry methods

**N. Hingant[1], N. Clavier[2], N. Dacheux[1], S. Hubert[1], R. Podor[3], J. Aupiais[3]**

[1] *Groupe de Radiochimie, IPNO, Bât. 100, Univ. Paris-Sud-11, 91406 Orsay, France*
*hingantn@ipno.in2p3.fr*
[2] *ICSM, UMR 5257, 30207 Bagnols/Cèze, France*
[3] *LCSM, Université H. Poincaré – Nancy I, BP 239, 54506 Vandœuvre lès Nancy, France*
[4] *CEA/DAM/DIF/DASE/SRCE, BP12, 91680 Bruyères le Châtel, France*

In the field of the fourth nuclear reactors generation, several fuel families, usually stable at high temperature, such as oxides, carbides or nitrides are actually extensively studied. These samples are more often obtained through dry chemistry methods from powdered mixtures. However, several processes based on wet chemistry methods, such as precipitation or hydrothermal processes should appear of great interest in the aim to control some physico-chemical properties like sintering capability, chemical durability or resistance to radiation damage. For this reason, $Th_{1-x}U_xO_2$ solid solutions, were first prepared as modelling solids for $Th_{1-x}Pu_xO_2$ , $Th_{1-x}Np_xO_2$ or $U_{1-x}Pu_xO_2$ compounds in order to establish the effect of the improvement of homogeneity and initial reactivity either on the sintering and the chemical durability of the samples.

The influence of the morphology of $Th_{1-x}U_xO_2$ solid solutions on their chemical durability during leaching tests was first examined through the precipitation of $Th_{1-x}U_x(C_2O_4)_2{\cdot}2H_2O$, as crystallized low-temperature precursors. Two chemical routes, both starting from a mixture of cations in acidic solution and oxalic acid were considered. The first one, based on that previously reported in the literature [1], consists in a direct precipitation in an open vessel at $T$ = 50°C under ultrasonic agitation. In the second one, the mixture is placed in a PTFE closed container set in autoclave then heated at $T$ = 180-210°C for few days in order to reach hydrothermal conditions. The solids prepared from both methods were then extensively characterized using various techniques such as XRD, SEM, EPMA… (Fig.1).

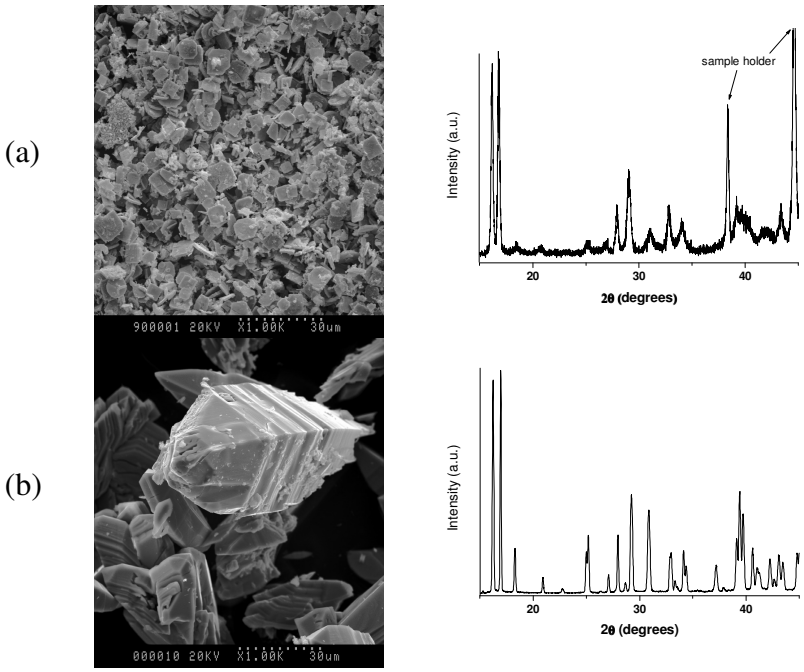


Figure 1. SEM micrography and associated XRD diagram of $Th_{0.5}U_{0.5}(C_2O_4)_2{\cdot}2H_2O$ prepared *via* direct precipitation (a) or using hydrothermal conditions (b).

SEM micrographies allow to evidence great variations in the powder morphology depending on the method of preparation. Indeed, the average grain size is significantly enhanced when using hydrothermal conditions, with the presence of small crystals of about 50 µm in length, while the associated specific surface area is found to $S_{SA}$ = 0.5-2 $m^2.g^{-1}$. The better crystallization state of these samples was also confirmed through XRD analyses since the FWHM of the XRD lines is significantly narrower when using hydrothermal conditions. Finally, the chemical composition of the samples was checked using EPMA: whatever the sample considered, both elementary weight percentages and mole ratios were found consistent with the calculated values.

$Th_{1-x}U_x(C_2O_4)_2{\cdot}2H_2O$ samples were then calcined ($T$ = 400°C) in order to eliminate volatile compounds (CO, $CO_2$) and to improve the reactivity of the powders. Indeed, the specific surface area $S_{SA}$ of dioxides coming from hydrothermal syntheses reaches 40 $m^2.g^{-1}$ instead of 16 $m^2.g^{-1}$ when using direct precipitation. The associated mechanism of transformation leading from $Th_{1-x}U_x(C_2O_4)_2 \cdot 2H_2O$ to $Th_{1-x}U_xO_2$ during the heat treatment was elucidated through TGA/DTA experiments. Finally, the powders were shaped by uniaxial pressing then fired at high temperature (1300-1400°C) to prepare densified samples. SEM micrographies of the resulting pellets (Fig. 2) revealed that the morphology of the initial precursor is conserved in the sintered samples. This was correlated to an important open porosity ; the closed one being estimated to about 3%.

(a) 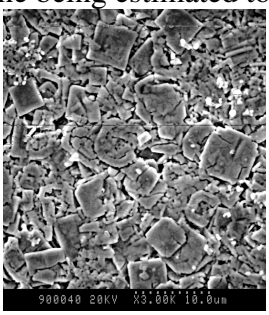 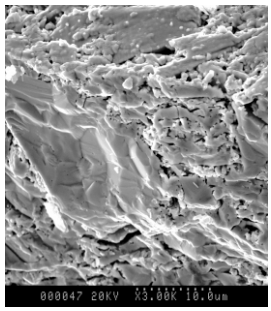 (b)

Figure 2. SEM micrograph of densified samples of $Th_{0.5}U_{0.5}O_2$ prepared from direct precipitation (a) or from hydrothermal conditions (b).

Afterwards, leaching tests were undertaken in dynamic conditions (i.e. high renewal of the leachate) in order to determine the normalized dissolution rates of the sintered pellets. Aliquots of the leachate were then taken off at regular times and the elementary concentrations were determined using ICP-AES. Normalized leaching rates calculated from the uranium amount released in solution varied from $2.10^{-4}$ $g.m^{-2}.day^{-1}$ ($x$ = 0.5) to 1.5 $10^{-3}$ $g.m^{-2}.day^{-1}$ ($x$ = 0.75) in $10^{-1}$M $HNO_3$ at room temperature. These values appeared in good agreement with those reported in the literature for $Th_{0.5}U_{0.5}O_2$ and $Th_{0.25}U_{0.75}O_2$ [2-3]. Moreover, the dissolution appeared to be congruent for all the sample studied. In order to link the morphology, thus the method of preparation, and the chemical durability, further leaching tests are now undertaken on samples precipitated in hydrothermal conditions.

## References

[1] E. Oktay, A. Yayli, *J. Nucl. Mater.* **77**, 288 (2001).

[2] G. Heisbourg, S. Hubert, N. Dacheux and J. Ritt, *J. Nucl. Mat.* **147**, 321 (2003).

[3] G. Heisbourg, PhD-Thesis, IPNO-T-03.09, Université Paris-Sud-11 (2003).

# H3

## IResin process potentiality for the elaboration of transmutation targets precursors

**Hamid Mokhtari[1], Sébastien Picart[1], Annabelle Meunier[1], René Thouvenot[2]**

[1] *CEA Valrhô Marcoule, DRCP/SCPS/LCA, BP 17171, 30207 Bagnols/Cèze, France*
[2] *UMR CNRS 7071, Université Pierre et Marie Curie, 4, Place Jussieu, 75252 Paris cedex 05, France*

In the scope of the elaboration of nuclear fuels precursors for transmutation, the resin process stands for a simple solution. Indeed, it is based on the loading of carboxylic resins with actinide cations and its further thermal treatment leading to homogeneous oxides or carbides type materials [1]. Moreover, it produces millimetric kernels which are easy to be handled in shielded cell and which could play a part in the making of "Sphere-Pac" fuels [2].
The challenge is to monitor the loading of the cationic exchange resin to its highest level and with the right specificity as regards the actinides. Owing to the low dissociation degree of the carboxylic resins, the pH of the solution as well as the redox states of the actinides must be optimized in order to favour the ionic exchange and avoid the hydrolysis of the metallic cations.
Hereafter, one has to find out the right parameters of the thermal treatment (atmosphere, gas stream, heating rate), to reach the right metal to carbon ratio after combustion. It should be close to zero if one wants to stop at the oxide; it can vary between 3 or 6 if one wants to pursue on a carboreduction in order to get to the carbide.

The first studies attempt to understand the neodymium(III) and uranium(VI) behavior towards their fixation on carboxylic resins.
The experiments show a fast kinetic (2 up to 3 hours) and a loading rate around 30% and 45% in weight, respectively for the neodymium and uranium elements which implies that the resin exchange capacity is quantitatively exploited. A good homogeneity of the cations within the sphere is also observed.
As shown in the figure 1, the thermal treatments of the loaded resins present a drastic decrease of the sphere diameter,. After the carbonization step, $Nd_2O_3$, $U_3O_8$ and $UO_2$ are identified by X-Ray diffraction. As far as the carbon-cation ratio is concerned, it tends to 6 which is in adequation with the requirements to elaborate carbide [1].

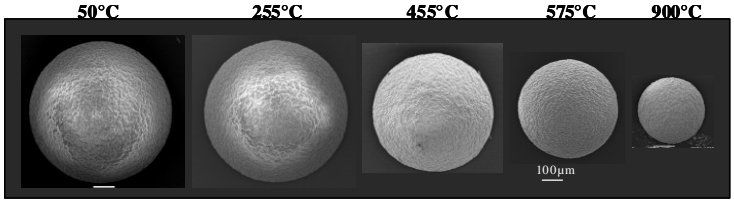


Fig. 1. Morphology of the neodymium loaded resins during the thermal treatment under air atmosphere

### References

[1] G. W. Weber et al., *Nuclear Technology* **35**, 217 (1977).
[2] K. L. Peddicord et al., *Progress in Nuclear Energy* **18**, 265 (1986).

# H4

## Evaluation of Potential Hazard of Transuranic Elements in HLW

**Alexander Ochkin,[1] Alexei Merkushkin[1], Sergey Stefanovsky[2], Sergey Povniy[3]**

[1] *D.Mendeleev University of Chemical Technology, Miusskaya sq.9, Moscow 125047 Russia, ochkin@rctu.ru*
[2] *SIA Radon, 7th Rostovskii lane 2/14, Moscow 119121 Russia, profstef@mtu-net.ru*
[3] *FSUE "PA Mayak" Ermolaev st. 18, Ozyorsk 456780 Russia*

Operation of commercial nuclear reactors generates significant amount of transuranic (TRU) elements: Np, Pu, Am, Cm. The first two of them are recovered at spent fuel radiochemical reprocessing whereas americium and curium are high level waste (HLW) constituents. For example, residual plutonium content in HLW is only about 0.025% of total plutonium in spent fuel [1]. Due to long half-life periods and high radiation hazard these actinides cannot be incorporated in glassy matrices. Therefore there are only two possible ways: 1) recovery of actinides from HLW and their transmutation in fast neutron reactors and 2) incorporation in matrices stable for about 100,000 years.

To evaluate potential hazard of these actinides the product of activity *A* into dose factor ε (H = A×ε) was proposed [2]. The results of calculation of the potential hazard for the most important radionuclides taking into account their daughter products for spent fuel with burn-up of 34 MW×day/kg [3] are given in Table 1. Only the radionuclides whose contribution into the total potential hazard of the actinides is more than 1% are taken into consideration.

Table 1. Potential hazard from some TRU radionuclides in HLW referred to 1 metric tonne of spent fuel with burn-up of 34 MW×day/kg.

| Radio-nuclide | $A \cdot 10^{-11}$ Bq/t U [3] | Dose factor ε, Sv/Bq | $A \cdot \varepsilon \cdot 10^{-3}$, Zv / % of total after storage for years | | | | |
|---|---|---|---|---|---|---|---|
| | | | 0 | $10^3$ | $10^4$ | $5 \cdot 10^4$ | $10^5$ |
| $^{239}$Pu | 0.031* | $2.5 \cdot 10^{-7}$ | 0.77/0.006 | 0.75/0.051 | 0.578/1.01 | 0.183/1.56 | 0.044/0.54 |
| $^{241}$Am | 335 | $2.0 \cdot 10^{-7}$ | 6760/52.7 | 1360/92.8 | 0.824/1.44 | 1.43/12.2 | 2.12/45.8 |
| $^{242m}$Am | 2.2 | $1.9 \cdot 10^{-7}$ | 42.6/0.332 | 1.29/0.088 | 0.0026/0.045 | 0.105/0.89 | 0.158/3.40 |
| $^{243}$Am | 3.6 | $2.0 \cdot 10^{-7}$ | 72.2/0.56 | 68.2/4.65 | 42.5/74.0 | 9.74/82.8 | 2.25/48.5 |
| $^{244}$Cm | 4.9 | $1.2 \cdot 10^{-7}$ | 5840/45.5 | 30.3/2.06 | 11.7/20.4 | 0.173/1.47 | 0.003/0.06 |
| $^{245}$Cm | 0.065 | $2.1 \cdot 10^{-7}$ | 1.37/0.011 | 2.28/0.155 | 1.23/2.15 | 0.051/2.15 | 0.008/0.18 |
| $\sum A \cdot \varepsilon \cdot 10^{-3}$, Sv | - | - | 12870 | 14670 | 57.42 | 11.76 | 4.636 |

The results of calculation depend on storage time of spent fuel before radiochemical reprocessing because decay of $^{241}$Pu to $^{241}$Am and $^{244}$Cm to $^{244}$Pu changes isotopical composition of HLW. For example, mass of $^{241}$Am increases from 41 to 266 g for 5 years of storage due to $^{241}$Pu decay. It is seen that the highest potential hazard is due to two americium isotopes together with their daughter products.

For recent years there is a tendency to increase the burn-up level of the fuel for PWR type reactors to reduce operational expenses. However it is not taken into consideration that content of americium and curium isotopes increases faster than burn-up level grows. To evaluate potential hazard due to TRU isotopes generated at radiochemical processing of HLW some data recalculated to 1 g of radionuclides listed in Table 1are presented in Table 2.

Table 2. Potential hazard due to some radionuclides listed in Table 1 recalculated to 1 g.

| Radio-nuclide | $T_{1/2}$, years | Activity, Bq/g | Dose factor ε, Sv/Bq | $A \cdot \varepsilon \cdot 10^{-3}$, Sv, after storage for years | | | | |
|---|---|---|---|---|---|---|---|---|
| | | | | 0 | $10^3$ | $10^4$ | $5 \cdot 10^4$ | $10^5$ |
| $^{239}$Pu | 24110 | $2.38 \cdot 10^9$ | $2.5 \cdot 10^{-7}$ | 0.575 | 0.560 | 0.431 | 0.137 | 0.033 |
| $^{241}$Am | 432,2 | $1.26 \cdot 10^{11}$ | $2.0 \cdot 10^{-7}$ | 25.4 | 5.11 | 0,0031 | 0,0054 | 0,0080 |
| $^{242m}$Am | 152 | $3.59 \cdot 10^{11}$ | $1.9 \cdot 10^{-7}$ | 68.3 | 2.07 | 0.0042 | 0.168 | 0.253 |
| $^{243}$Am | 7370 | $7.38 \cdot 10^9$ | $2.0 \cdot 10^{-7}$ | 1.47 | 1.39 | 0.867 | 0.199 | 0.046 |
| $^{244}$Cm | 18,1 | $2.99 \cdot 10^{12}$ | $1.2 \cdot 10^{-7}$ | 358 | 1.86 | 0.718 | 0.0106 | 0.00018 |
| $^{245}$Cm | 8500 | $6.35 \cdot 10^9$ | $2.1 \cdot 10^{-7}$ | 1.33 | 2.21 | 1.19 | 0.050 | 0.008 |

Then, summarized potential hazard of actinides remained in HLW may be calculated as a sum of all the products given in Table 2 into mass of corresponding radionuclides. At that, variation of these values with time may be run down.

## References

[1] Yu.V.Glagolenko et al., *Radiat. Safety Journ.* (Russ.) **3**, 2 (1997).
[2] N.S. Babaev et al., *Atomic Energy (Russ.)* **98**, 123 (2005).
[3] A.G. Zelenkov et al., *Atomic Energy (Russ.)* **51**, 53 (1981).

# I1

## Interactions of U(VI) with members of a microbial consortium recovered from a uranium mining waste pile

**Thomas Reitz[1], Andrea Geissler[1], Mohamed L. Merroun[1], Sonja Selenska-Pobell[1]**

[1] *Forschungszentrum Dresden-Rossendorf, Institute of Radiochemistry, P.O. Box 510119, 01314 Dresden, Germany (e-mail: thomas.reitz@fzd.de)*

Treatments of a soil sample from a uranium mining waste pile with uranyl nitrate led to a shifting in the crenarchaeal populations from subgroup 1.1a to 1.1b. Efforts to culture members of these *Crenarchaeota* resulted in an enrichment of a mixed microbial consortium consisting of representatives of 1.1b *Crenarchaeota* and *Firmicutes*.
In this study interactions of U(VI) with a pure culture of *Paenibacillus* sp. JG35+U4-B1 isolated from the mentioned consortium were studied by using a combination of wet chemistry and microscopic methods. Preliminary analyses on U sorption showed that the *Paenibacillus* strain studied accumulated up to 85 mg U/g dry biomass from a solution with an initial uranium concentration of 120 mg U/l. Live/Dead cell staining indicated that less than 10% of the U-treated cells were viable. Transmission electron microscope (TEM) analyses showed that the cells of the isolated strain accumulated uranium intracellularly as needle-like fibrils (Fig. 1A), and also at the cell surface (Fig. 2A). Energy dispersive X-ray (EDX) analysis of these U accumulates demonstrated the presence of U and P peaks (Figs. 1B and 2B) indicating that in both cases the phosphate groups are, probably, the main functional binding sites for U(VI).

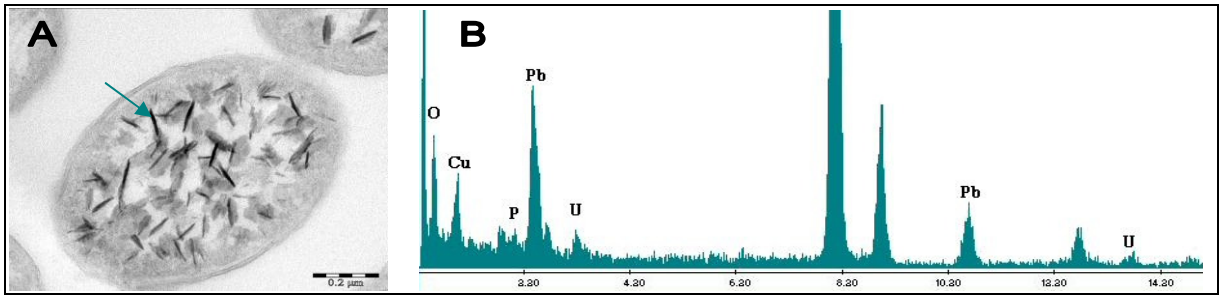


Fig. 1. Transmission electron micrograph of intracellular uranium accumulates of *Paenibacillus* sp. JG35+U4-B1 (A) and energy-dispersive X-ray spectrum (B) of the point marked with the arrowhead

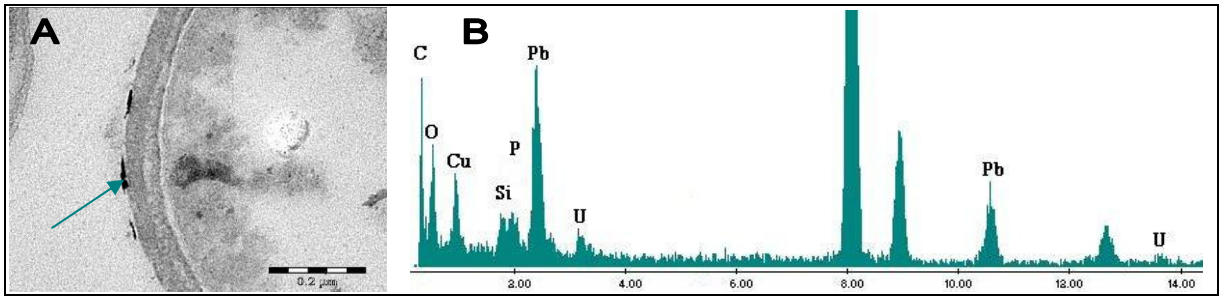


Fig. 2. Transmission electron micrograph of uranium accumulates on the cell surface of *Paenibacillus* sp. JG35+U4-B1 (A)and energy-dispersive X-ray spectrum (B) of the point marked with the arrowhead

Efforts to culture other strains from the mentioned consortium and especially of the yet to be cultured 1.1b-*Crenarchaeota* are in progress in our laboratory. Because our results indicated that these archaeal populations are strongly induced by the addition of U(VI) the study of these organisms is of importance for understanding the natural behavior of U in soils and also for remediation of contaminated sites.

# I2

## Hydrothermal methods for the preparation of actinide compounds

**Nicolas Clavier[1], Nicolas Dacheux[2], Gilles Wallez[3], Michel Quarton[3]**

[1] *ICSM, UMR 5257, 30207 Bagnols sur Cèze, France*
*clavier@ipno.in2p3.fr*
[2] *Groupe de Radiochimie, IPNO – Bât. 100, Univ. Paris-Sud, 91400 Orsay, France*
*3 Université Pierre et Marie Curie-Paris 6, CNRS UMR 7574, 4 place Jussieu, 75005 Paris, France*

In the framework of the 1991 french law dedicated to the management of radwaste, several phosphate-based ceramics have been proposed as host matrices for the specific immobilization of radionuclides [1]. All present several interesting properties such as high weight loadings in actinides, good sintering capability, strong resistance to aqueous corrosion and to radiation damage. In this context, the recent use of original methods of preparation, like precipitation in hydrothermal conditions, allowed to prepare new low-temperature single phase precursors of these high-temperature compounds. The use of such original phases leads to the preparation of actinide phosphates usually unreachable with conventional methods and provides some improvements in the physico-chemical properties of the final samples.

In a first study, three phosphate-based systems, which can be defined through the $M/PO_4$ mole ratio, were examined (tab. 1): $An(OH)PO_4$ (An = Th, U), $M_2(PO_4)_2(HPO_4) \cdot H_2O$ (MPHPH; M = Ce, Th, U, Np, Pu) and $LnPO_4 \cdot n\ H_2O$ (Ln = La - Dy).

Tab. 1. Relationships between precursors and high temperature phases in phosphate-based systems

| $M/PO_4$ | Precursor | System - SG | $T_{form.}$ (°C) | HT phase | System - SG | $T_{transf.}$ (°C) |
|---|---|---|---|---|---|---|
| **1** | $LnPO_4 \cdot n\ H_2O$ | Hex. - *$P3_121$*<br>Mon. - *$P2_1/n$*<br>Tet. - *$I4_1/amd$* | 70 - 190 | $LnPO_4$ | Mon. - *$P2_1/n$*<br>Tet. - *$I4_1/amd$* | 200 - 900 |
| | $An(OH)PO_4$ | Ort. - *Cmca* | 220 | $Th_2O(PO_4)_2$<br>$U_2O(PO_4)_2$ | Ort. - *Cmca* | 500<br>1350 |
| **2/3** | MPHPH | Ort. - *Cmcm* | 90 - 160 | TAnPHP<br>α-TAnPD<br>β-TAnPD | Ort. - *Cmcm*<br>Ort. - *Cmcm*<br>Ort. - *Pcam* | 170<br>200<br>950 |

For $An^{IV}/PO_4 = 1$, the initial precipitation of $Th(OH)PO_4$, then its condensation between 450°C and 500°C, appears as the only way known up to know to prepare the $Th_2O(PO_4)_2$ compound [2]. A similar transformation mechanism was evidenced for the uranium compound, but the difference in the temperature of stability of both Th and U compounds seems to be responsible of the failure in attempts to prepare $Th_{2-x}U_xO(PO_4)_2$ solid solutions at high temperature.

For $Ln^{III}/PO_4 = 1$ systems, three different $LnPO_4 \cdot nH_2O$ structures were precipitated, depending on the ionic radius and the temperature considered. At 150°C, they are monazite (monoclinic system, $n = 0$) for lanthanum and cerium, rhabdophane (hexagonal system, $n = ½$) from neodymium to dysprosium, and xenotime (tetragonal system, $0 < n < 3$) from holmium to lutetium [3]. In this system, rhabdophane-type compounds can be also used as crystallized low-temperature precursors of monazites since this structure first dehydrates when heating between 200°C and 400°C then turns into monazite between 700°C and 900°C. This method of preparation allowed to improve the densification of the sintered pellets

obtained after heating at high temperature, as a consequence of the higher reactivity of the initial powder.

Phosphates of tetravalent cations precipitated with $M^{IV}/PO_4 = 2/3$ ($M^{IV}$ = Th, U, Ce) were identified to the phosphate-hydrogenphosphate hydrates family $M^{IV}_2(PO_4)_2(HPO_4) \cdot H_2O$. The formation of $Th_{2-x/2}An_{x/2}(PO_4)_2(HPO_4) \cdot H_2O$ solid solutions was also evidenced with uranium ($x \leq 4$), neptunium ($x \leq 2$) and plutonium ($x < 4$). The transformation mechanism leading from Thorium Phosphate-Hydrogenphosphate Hydrate (TPHPH) to Thorium Phosphate-Diphosphate (β-TPD) was then elucidated : TPHPH first dehydrates between 170°C and 200°C leading to anhydrous $Th_2(PO_4)_2(HPO_4)$ (TPHP). In a second step (200-270°C), the condensation of $HPO_4$ groups into $P_2O_7$ entities leads to the formation of a low-temperature form of thorium phosphate-diphosphate, called α-TPD. α-TPD was found to be stable up to 950°C, then turned into the well-known β-TPD above this temperature [4]. From dilatometry experiments performed on β-TUPD solid solutions, even though the temperature of densification appears unchanged (1250°C), the complete sintering ($d_{exp.}/d_{calc.}$ = 99%) occurs faster when starting from TUPHPH solid solutions (after only 5 to 10 hours of heating). Moreover, in these operating conditions, the homogeneity of the pellets (fig. 1) is also significantly improved when using the precursor [5].

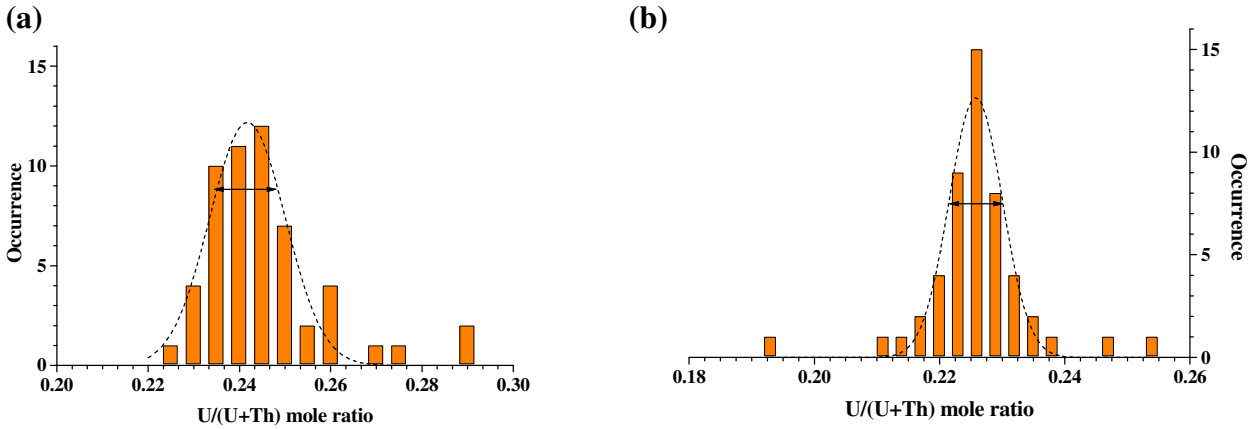


Fig. 1. Distribution of the U/(U+Th) mole ratio in β-TUPD sintered sample prepared by direct evaporation (a) and through the initial precipitation of TUPHPH (b).

Due to the good results obtained on phosphate-based compounds, the precipitation of low-temperature crystallized precursors was also applied to other systems such as actinide oxalates and silicates. On the one hand, oxalates were studied as precursors of actinide dioxides nuclear fuels [6] and could provide some great improvements in the homogeneity of the final solids. On the other hand, An(IV) silicates, and particularly coffinite ($USiO_4$), which is unreachable through conventional ways of preparation, could appear of particular interest due to the significant role they could play in the long-term behaviour of spent fuel.

## References

[1] X. Deschanels, CEA Technical Report, DTCD/2004/5 (2004).
[2] N. Dacheux, N. Clavier, G. Wallez, M. Quarton, *Sol. St. Sci.* **submitted** (2007).
[3] O. Terra, N. Clavier, N. Dacheux, R. Podor, *New J. Chem.* **27**, 957 (2003).
[4] N. Dacheux, N. Clavier, G. Wallez, V. Brandel, J. Emery, M. Quarton, M. Genet, *Mat. Res. Bull.* **40**, 2225 (2005).
[5] N. Clavier, N. Dacheux, G. Wallez, M. Quarton, *J. Nucl. Mat.* **352**, 209 (2006).
[6] B. Arab-Chapelet, S. Grandjean, G. Nowogrocki, F. Abraham, *J. All. Comp.* **in press** (2007).

.

# I3

## Temperature programmed decomposition of $Pu(C_2O_4)_2.6H_2O$

**N. Vigier[1,2], S. Grandjean[1], F. Abraham[2]**

[1] *CEA Valrhô Marcoule, DRCP/SCPS/LCA, Bât 399, BP 17171, 30207 Bagnols-sur-Cèze, France, e-mail: stephane.grandjean@cea.fr*
[2] *UCCS – Equipe Chimie du Solide, UMR CNRS 8181, ENSCL-USTL, B.P. 108, 59652 Villeneuve d'Ascq Cedex, France, e-mail: Francis.Abraham@ensc-lille.fr*

The conversion of actinide nitrates into actinide oxides as final treatment of solutions containing actinides is a method of choice in the nuclear industry. Considering the recycling of some actinides in a new fuel, this operation requires the development of chemical methods for preparing these compounds as high purity and reactive materials. On this purpose, actinide oxalates thermal decomposition has been extensively studied because these compounds decompose into oxide at low temperature. Regarding the current fuel cycle, the oxalic conversion of plutonium into oxide at the end of the PUREX process is one of the most important steps. However, the structure of some intermediates during the thermal decomposition of Pu(IV) oxalate into oxide is still speculative and the reaction detailed mechanisms are quite misunderstood and divergent from a study to another [1-7].
As a result, this work deals with a detailed structural investigation on the main solid intermediates, using thermal analysis (ATG-DSC) (figure 1), micro chromatography evolved gas analysis (EGA-GC) (figure 2), X-ray diffraction (XRD) (figure 3), UV/Visible spectroscopy (UV-VIS) (figure 4) and infrared spectroscopy (IR) (figure 5), to investigate the reaction mechanism in the thermal decomposition of the Pu(IV) oxalate $Pu(C_2O_4)_2.6H_2O$ into oxide under air or argon. Distinct reaction paths were established depending on the atmosphere used and the identity of some intermediates was assessed comparatively to previous studies and uncertainties about the Pu(III) intermediates formed were clarified. Under air, the transitory reduction of Pu(IV) into Pu(III) is for the first time established directly by UV-VIS analysis of the solid intermediates and XRD investigations confirm the identity of the crystallized intermediate compounds, i.e. the hexa- and di-hydrated oxalate structures and the final oxide.

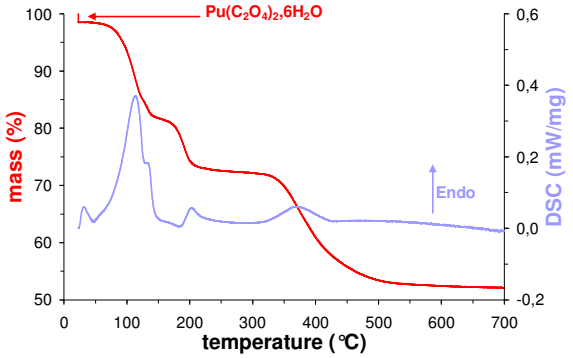


Fig. 1. TG-DSC plot starting from a $Pu^{IV}(C_2O_4)_2.6H_2O$ sample under argon atmosphere

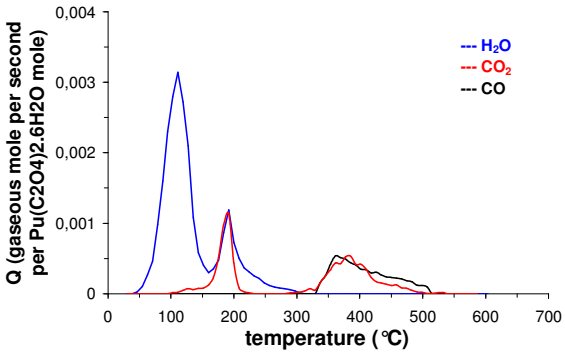


Fig. 2. EGA-GC plot starting from a $Pu^{IV}(C_2O_4)_2.6H_2O$ sample under argon atmosphere

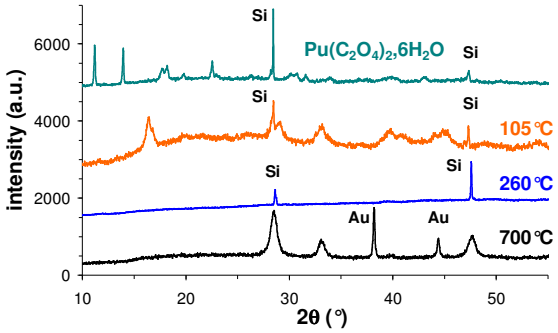


Fig. 3. XRD patterns of $Pu^{IV}(C_2O_4)_2.6H_2O$ and its intermediate products of decomposition, isolated at the specified temperatures, under argon atmosphere

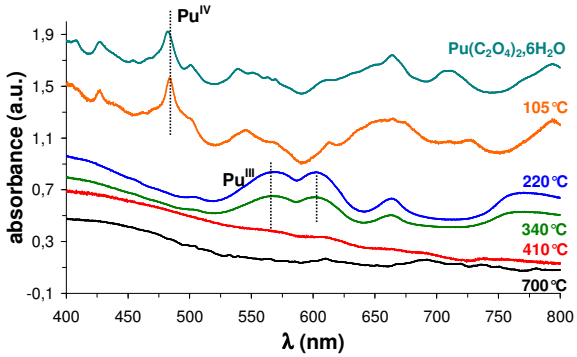


Fig. 4. UV-VIS spectra of $Pu^{IV}(C_2O_4)_2.6H_2O$ and its intermediate products of decomposition, isolated at the specified temperatures, under argon atmosphere

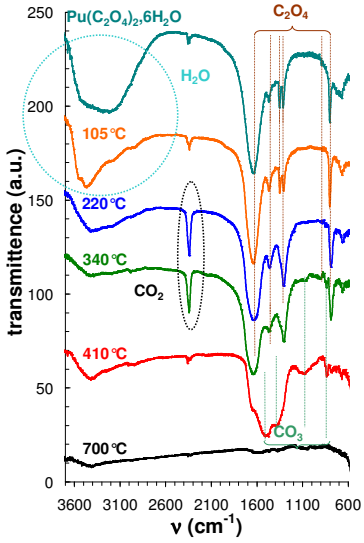


Fig. 5. IR spectra of $Pu^{IV}(C_2O_4)_2.6H_2O$ and its intermediate products of decomposition, isolated at the specified temperatures, under argon atmosphere

## References

[1] M.N. Myers, *U.S.A.E.C.*, document HW 45128 (1956).
[2] G.S. Rao et al., *J. Inorg. Nucl. Chem.* **25**, 1293-1295 (1963).
[3] I.L. Jenkins et al., *J. Inorg. Nucl. Chem.* **26**, 131-137 (1964).
[4] A. Glasner, *J. Inorg. Nucl. Chem.* **26**, 1475-1476 (1964).
[5] D.A. Nissen, *J. Therm. Anal.* **18**, 99-109 (1980).
[6] R.D. Kozlova et al., *Radiokhimiya* **26**, (3) 311-316 (1984).
[7] A.I. Karelin et al., *J. Radioanal. Nucl. Chem.* **143**, (1) 241-252 (1990).

# I4

## XANES/EXAFS of U $L_{III}$ Edge in Borosilicate High-Ferrous Nuclear Waste Glasses

**Sergey Stefanovsky,[1] Andrey Shiryaev[2], Ian Zubavichus[3], James Marra[4]**

[1] *SIA Radon, 7th Rostovskii lane 2/14, Moscow 119121 Russia, profstef@mtu-net.ru*
[2] *Institute of Crystallography RAS, Leninskii av. 59, Moscow, Russia*
[3] *RRC Kurchatov Institute, Kurchatov sq. 1, Moscow, Russia*
[4] *Savannah River National Laboratory, Building 773-42A, Aiken, SC USA*

Borosilicate glass is used as a matrix for immobilization of Savannah River Plant waste at the Defense Waste Processing Facility (DWPF) [1]. The waste contains major iron, aluminum, sodium and uranium (~12 wt.%) and minor strontium, corrosion products (Cr, Mn, Co, Ni, Zr) and process contaminants (Si, P, S, F, Cl, etc.). Uranium in borosilicate glass is normally present in a hexavalent form [2,3] but occurrence of transition elements (Fe, Mn) may affect uranium valence state. In this case up to ~23 % of total uranium may exist in a tetravalent form [4]. In the present work we used X-ray absorption spectroscopy o study the effect of waste loading and uranium content on valence state and coordination of uranium in high-ferrous borosilicate glassy products.

Glasses were produced from mixtures of waste surrogate and commercially available Frit 320 (in wt.%: 8 $Li_2O$, 8 $B_2O_3$, 12 $Na_2O$, 72 $SiO_2$) at waste loading of 45, 50, 55, 60 and 65 wt.% (corresponded to 5.29, 5.87, 6.46, 7.05 and 7.64 wt.% uranium oxides recalculated to $U_3O_8$) in alumina crucibles in a resistive furnace at temperatures of 1150, 1200, 1250, 1300 and 1350 $^0$C, respectively). The melts were solidified in turned-off furnace.

The X-ray absorption spectra of the U $L_{III}$ edge of glasses were obtained at "Structural Materials Science" beamline at synchrotron source at Russian Research Centre "Kurchatov Institute". The spectra were acquired at the first and at the third harmonics (sample chamber was evacuated in the latter case) of the bending magnet using a Si(111) double crystal monochromator. The measurements were performed in fluorescence mode. The glass samples were measured at room temperature either as dispersed powder or as pellets made from powder mixed with sugar. Powders of chemically pure uranium oxides $UO_3$ and $UO_2$ were used as standards and measured in identical conditions. In order to assess both oxidation state and local atomic environment of uranium, measurements of Near-Edge (XANES) and of Extended region (EXAFS) were performed. Experimental EXAFS spectra were fitted in R-space using a IFEFFIT package and crystal structures of variable uranium oxides and silicates.

XANES spectra of all the samples studied are given on Figure 1. Shape and position of U $L_{III}$ edges are similar for all the glasses. About 90% of total uranium in the samples is present in hexavalent form and this value does not depend on waste loading and uranium oxide content in the materials. Actually these materials are glass-crystalline and composed of a U-bearing matrix glass depleted with iron and a spinel structure phase strongly enriched with iron. In our previous work [4] using XPS we found about 80% of total uranium in hexavalent form in the glass with 45% waste loading (5.29 wt.% $U_3O_8$).

Normalized EXAFS spectra (region with visible oscillations) are plotted on Fig. 2. In line with the XANES results, the samples are rather similar. Fitting of EXAFS spectra using IFEFFIT shows general similarity of uranium environment in all studied samples. In all samples the first coordination sphere is split (Figure 3). The effective coordination number for the nearest neighbors is close to 2 (varies between 1.8 and 2.1) and they are situated at 1.8 ±

0.05 Å. A second subset of neighboring oxygen atoms is at 2.2 ± 0.05 Å with effective coordination number between 3.4 and 4. This structure resembles somewhat distorted uranyl-ion. The value of $\sigma^2$, i.e. proxy of the Debye-Waller factor, was between 0.005 and 0.007. The most logical interpretation of our experiments is that the samples contain some quasi-continuum distribution of U-O nearest neighbor distances. Such behavior is logical keeping in mind structure of homogeneous glass.

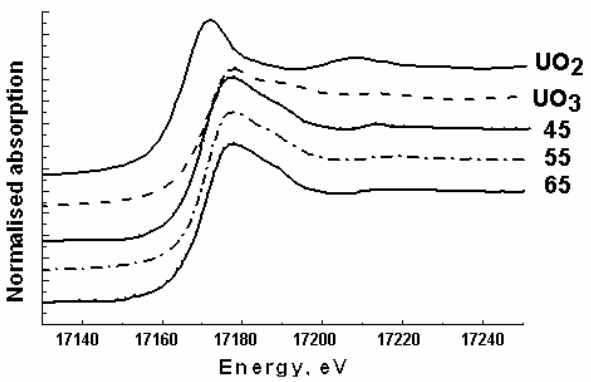


Figure 1. XANES spectra of U $L_{III}$ edge in glasses with 45, 55 and 65 wt.% waste loading and uranium oxides.

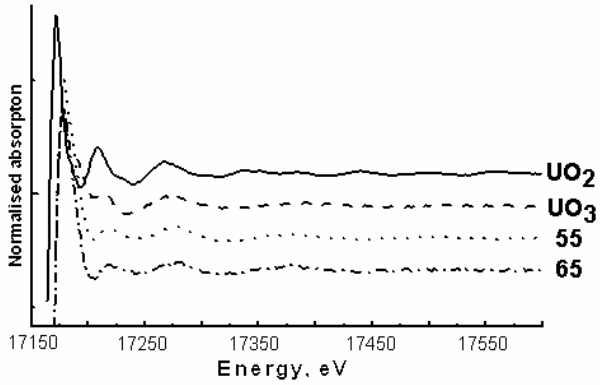


Figure 2. Part of U EXAFS spectra of glasses with 55 and 65 wt.% waste loading and uranium oxides.

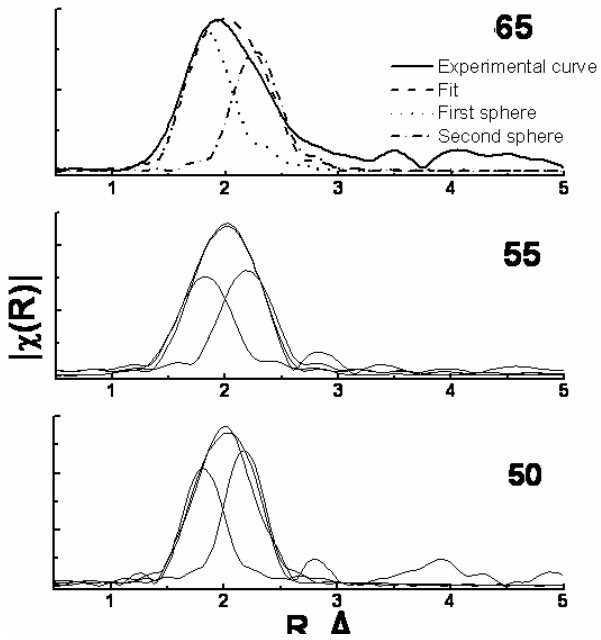


Figure 3. Magnitude of Fourier transform for several glass samples. Experimental data and fit results are shown.

Existence of the clearly defined second coordination sphere of the uranium ion would indicate formation of separate U-rich phase. Fourier transforms of our experimental spectra show indications for existence of weak peak between 3 and 4 Å. However, its shape and position are poorly defined. Such behavior exhibits no well-defined coordination sphere in the vitreous phase. Processing of the real parts of the Fourier transforms with variable **k**-weights (where **k** is a photoelectron wavenumber) suggests that this peak most likely represents oxygen ions surrounding the distorted uranyl ion.

It can be concluded that uranium in amount of up to ~8-9 wt.% being predominantly hexavalent is quite uniformly distributed in the vitreous phase of the high-ferrous glass-ceramics. No formation of U-bearing phases was found even at 65 wt.% waste loading.

The work was supported by US DOE (Contract "Application of the Cold Crucible Induction Heated Melter to DOE Wastes").

## References

[1] S.L. Marra et al., *Proc. Waste Management '99 Conf.*, Tucson, AZ, 1999. CD-ROM.
[2] B.W. Veal et al., *Handbook on the Physics and Chemistry of the Actinides* 1987, pp. 271-309.
[3] A.S. Aloy et al. *Mat. Res. Soc. Symp. Proc.* **824**, 345 (2004).
[4] S.V. Stefanovsky et al. *Proc. 36$^{iemes}$ Journées des Actinides*, Oxford, UK, 2006. CD-ROM. ID P-38.

# J1

## Periodic density functional study of the uranyl ion interaction with $NiFe_2O_4$

**H. Perron[1, 2], C. Domain[1], J. Roques[2], R. Drot[2], E. Simoni[2], and H. Catalette[1]**

[1] *EDF-R&D, Département Matériaux et Mécanique des Composants, Les Renardières, Ecuelles, F-77818 Moret-sur-Loing Cedex, France.*

[2] *Université Paris XI, Institut de Physique Nucléaire, Bâtiment 100, 91406 Orsay Cedex, France.*

Among the oxides of nuclear interest, iron-based spinel-type compounds are present as corrosion products in the nuclear power plants primary circuit. In aqueous phase, they can be found as colloids that could be activated after having passed near the core of the reactor or interact with ions from the solution. It is thus of first importance to determine their physical and chemical properties in order to minimize the dosimetry. Unfortunately, due to the extreme temperature and pressure conditions (up to 350°C and 160 bars) experiments are difficult to set up. Therefore, the use of atomic scale modelling can thus provide support to this lack of experimental data.

All calculations were performed using the Vienna *ab initio* Simulation Package [1], VASP, in periodic density functional theory (DFT) within the generalised gradient approximation (GGA) as defined by Perdew and Wang [2]. Atoms were described with pseudopotentials developed on plane wave basis sets generated with the projector augmented wave (PAW) method [3].

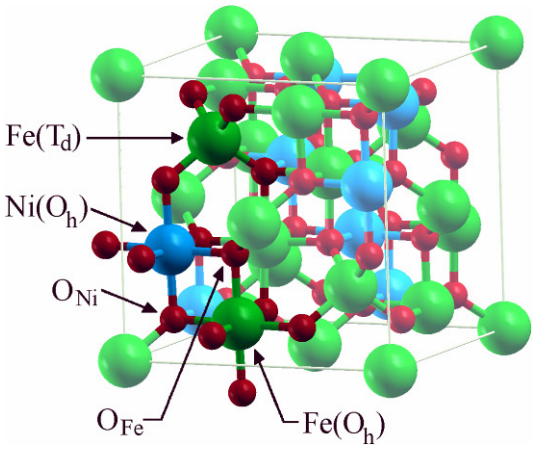


In a first step, the bulk of nickel ferrite $NiFe_2O_4$ has been studied in terms of structural and electronic properties. The optimized lattice parameter, the calculated bulk modulus as well as the local and total magnetic moment were found to be in good agreement with experimental data [4,5]. The inverse spinel structure was characterized as more stable than the normal one. The local spin order on metallic species and the resulting magnetic moment is also consistent with experimental data.

Then, the $NiFe_2O_4$ (220) face, which is one of the most stable, has been modelled in order to first investigate the interaction with the solvent (water molecules). These results revealed the importance of hydrogen bonds on the surface. In addition, it showed that water can eventually dissociate with proton transfer on oxygen surface species.

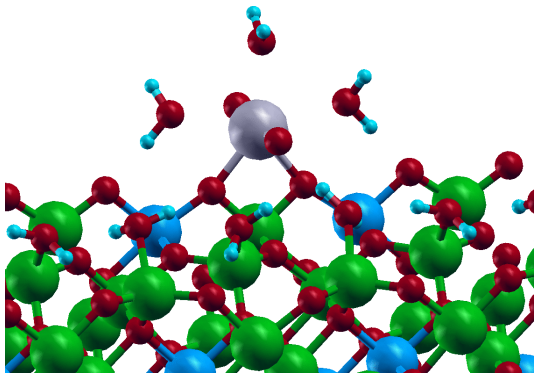

Finally, the uranyl ion sorption has been studied at different protonation rates. The first results showed that the relative stabilities of the different surface complexes are strongly dependent on the saturation of the surface. Among these different structures, some are unstable on a saturated surface while they were characterized as the most stable ones for lower protonation rates.

### References

[1] G. Kresse, J. Furthmüller, Phys. Rev. B 54 (1996) 11169.
[2] J. P. Perdew, Y. Wang, Phys. Rev. B 45 (1992) 13244.
[3] P. E. Blöchl, Phys. Rev. B 50 (1994) 17953.
[4] A. G. Bhosale, B. K. Chougule, Mater. Chem. Phys. 97 (2006) 273.
[5] S. H. Lee, S. J. Yoon, G. J. Lee, *et al.*, Mater. Chem. Phys. 61 (1999) 147.

# J2

## New three-dimensional lithium uranyl-phosphates and their relations to vanadate analogous.

**C. Renard, M. Benseghir, S. Obbade, F. Abraham**

*UCCS, UMR CNRS 8181, ENSCL,*
*Université des Sciences et Technologies de Lille, BP 90108, 59652 Villeneuve d'Ascq Cedex, France*
*catherine.renard@ensc-lille.fr*

The uranyl phosphates represent an important part of the uranium minerals and display many analogies with arseniates. Mostly they are hydrated and adopt layered networks built from corner shared $AO_4$ (A = P or As) tetrahedra and uranyl polyhedra (square, pentagonal and/or hexagonal bipyramids), the cations and water molecules occupy the interlayer space. Alkali uranyl phosphates typically adopt autunite-type structures, containing only octahedral uranyl. Locock and Burns [1,2] have recently reported new three dimensional structures in which uranium-phosphate (or arseniate) sheets are connected through pentagonal bipyramids to create large tunnels occupied by $A^+$ (A = Cs, Rb or K) and water molecules.

The vanadate behavior in the uranyl compounds is quite different even when vanadium is tetrahedrally coordinated. Lately, Obbade et al. [3,4] have described a new monovalent cation uranyl vanadate family with three dimensional structures The uranyl-vanadate frameworks release non crossing channels occupied by the monovalent cation, $Li^+$ or $Na^+$. These vanadates are built from uranyl-vanadate layers with autunite anion sheet topology common to many phosphates but never met in layered vanadates.

We report in this presentation the synthesis and study of three new lithium uranyl phosphates: $Li(UO_2)_4(PO_4)_3$, $Li_2(UO_2)_3(PO_4)_2O$ and $Li_3(UO_2)_7(PO_4)_5O$. The powders were synthesized via solid state reaction and single crystals were obtained by fusion of the stoechiometric powder. The crystal structures were refined from single crystal X-ray diffraction data. The uranium atoms occupy square and pentagonal bipyramids. The uranium square pyramids and orthophosphate units are connected by corners to form $^2_\infty[(UO_2)(PO_4)_2]^{4-}$ called simple sheets (Fig.1a) and/or $^2_\infty[(UO_2)_2(PO_4)_3]^{5-}$ called double sheets (Fig.1b) with autunite-type anion topology. The uranyl pentagonal bipyramids share two opposite edges to form $^1_\infty[UO_5]^{4-}$ infinite chains (Fig. 1c) linking the sheets. The lithium cations are located in non crossing tunnels between the chains. The various stacking sequences of the simple and double layers generate three different structures: simple layer stacking in $Li_2(UO_2)_3(PO_4)_2O$, double layer stacking in $Li(UO_2)_4(PO_4)_3$ and intergrowth of mixed simple and double sheets stacking in $Li_3(UO_2)_7(PO_4)_5O$ (Fig. 1d). These compounds are isostructural to the vanadate counterparts. However, the phosphate tetrahedra, smaller than the vanadate ones, deform the layers and change the symmetry and/or the periodicity.

The electrical conductivity of $Li(UO_2)_4(PO_4)_3$ and $Li_2(UO_2)_3(PO_4)_2O$ was measured using impedance spectroscopy method. The rather low conductivity of the lithium cations is explained by the crystal structure and the $Li^+$ position in the tunnels. These results corroborate those on the analogous three-dimensional alkali uranyl vanadate.

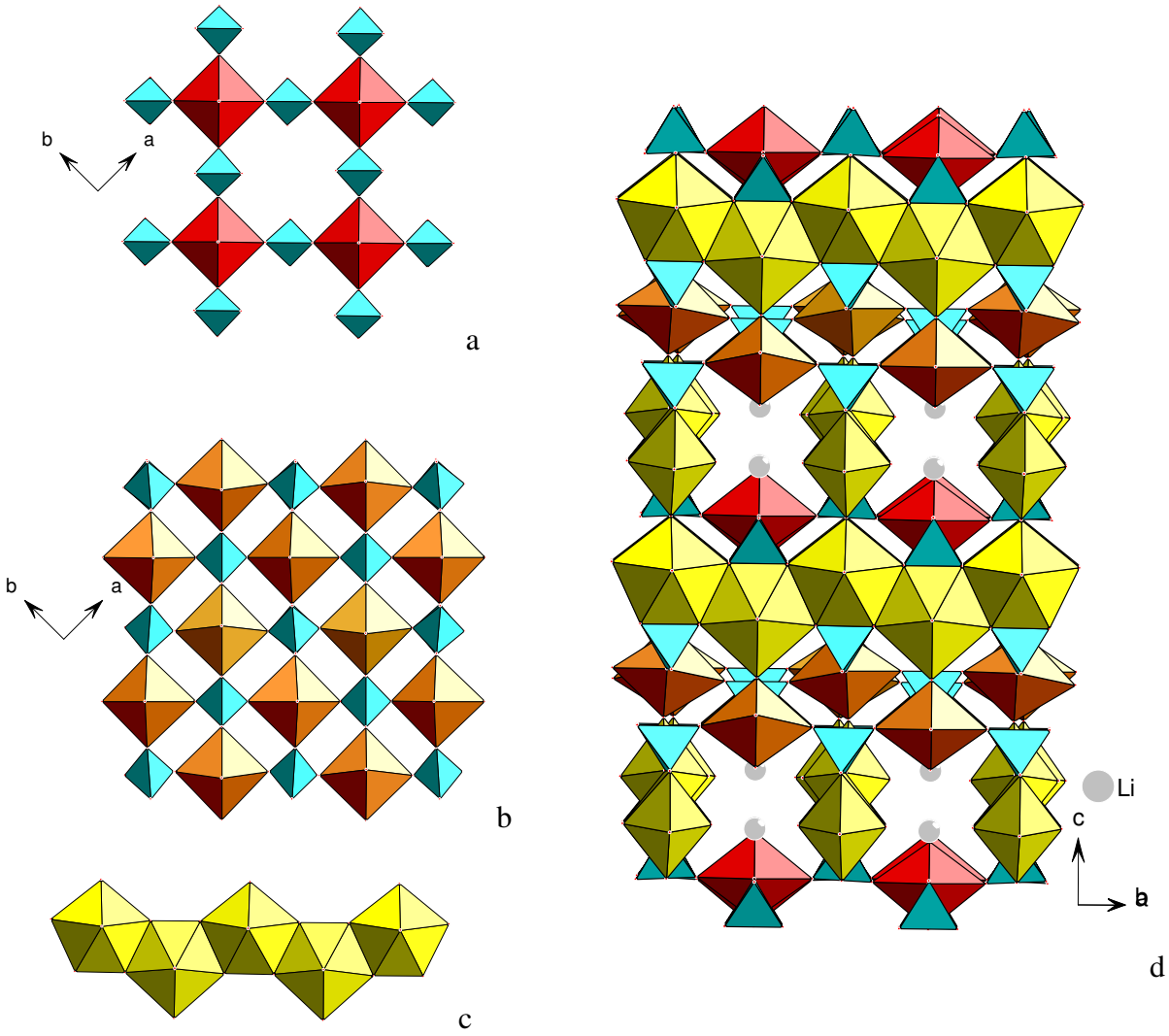


**Fig. 1** : Simple (a) and double (b) layers, chains (c) and their association (d) to form $Li_3(UO_2)_7(PO_4)_5O$.

## References

[1] A.J. Locock, P.C. Burns, *J. Solid State Chem.* **167**, 226 (2002).
[2] A.J. Locock, P.C. Burns, *J. Solid State Chem.* **175**, 372 (2003)
[3] S. Obbade, C. Dion, M. Rivenet, M. Saadi and F. Abraham, *J. Solid State Chem.* **177**, 2058 (2004).
[4] S**.** Obbade**,** L. Duvieubourg, C. Dion and F. Abraham, *J. Solid State Chem.* (2006) in press.

# J3

## 2 D and 3D Anionic Arrangements in Alkaline Uranyl Niobates.

**S. Saad, S. Obbade, C. Renard, F. Abraham**

*Unité de Catalyse et de Chimie du Solide - UMR CNRS 8181*
*ENSCL – Bât. C7 – BP 90108 - 59652 Villeneuve d'Ascq Cedex - France*

The chemistry of actinides has attracted a great deal of interest these last two decades with the assessment of nuclear waste disposal and improvement of reprocessing. In this connection, a large variety of new compounds resulting from the association of uranyl ion and various inorganic oxoanions (vanadate, tungstate, molybdate, niobate, phosphate...) have been prepared and characterized. In this regard, a number of alkaline metal uranyl oxoanion compounds have been recently prepared and display a rich structural chemistry. The structural diversity of these compounds is related to :1) the various coordination polyhedra of uranium U(VI) (hexagonal bipyramid, pentagonal bipyramid and distorted octahedron), 2) that of the transition metal oxyanion (tetrahedron, square pyramid, trigonal bipyramid or octahedron) and 3) the huge possibilities of linkages between these polyhedra. Thus, the inorganic architectures formed in alkaline metal uranyl oxoanion compounds are governed in part by the uranyl and oxoanion geometries, but also by the alkaline cation which plays a key role on both connectivity and dimensionality of the obtained crystal structures. For example, $AUMO_6$ compounds have been characterized both for $M$ = V and Nb and adopt layered structures. In $AUVO_6$, $A$ = Na, K, Cs, Ag, the $^{2}_{\infty}[(UO_2)_2V_2O_8]^{2-}$ layers are built from $UO_7$ pentagonal bipyramids linked by $V_2O_8^{6-}$ units formed by two inverse $VO_5$ square pyramids sharing an edge. In $AUNbO_6$, $A$ = K, Rb, the $^{2}_{\infty}[(UO_2)NbO_4]^{-}$ layers are built from edge-sharing of two types of chains formed from edge-shared $UO_5$ pentagonal bipyramids and corner-shared $NbO_5$ triangular bipyramids, respectively. Astonishingly $CsUNbO_6$ adopts a structure derived from the carnotite as the $AUVO_6$ compounds. Surprisingly with Tl a tunneled structure was obtained for the compound $TlU_2Nb_2O_{11.5}$. With phosphate and arsenate oxoanions, only hydrated inorganic compounds with general stoichiometry $A[(UO_2)_2M_2O_8](H_2O)_m$ (A = monovalent cations, M = P or As and m = 3, 4, 5) have been obtained and characterized by bidimensional autinite-type sheets formed of uranyl square bipyramids shared by equatorial vertices to orthophosphate tetrahedra. The interlayer region contains water groups and monovalent cations.

To explain the role of the alkaline metal and oxoanion we decided a systematic reinvestigation of the A - U - Nb - O systems. Thus, different new alkaline uranyl niobates $A_xUNbO_{6-x/2}$ (A = alkaline metal and x =0 - 0.5) and $Cs_9U_8Nb_5O_{41}$ has been synthesized by high temperature solid-state reaction, using a mixture of $U_3O_8$, $Cs_2CO_3$ and $Nb_2O_5$. Tthe crystal structures were solved by direct methods using single crystal X-ray diffraction data.

The crystal structure of $LiUNbO_6$ is characterized by $^{2}_{\infty}[UNbO_6]^{-}$ layers of uranophane sheet anion topology parallel to the (1 0 0) plane. These layers are formed by the association by edge-sharing of $^{1}_{\infty}[UO_5]^{4-}$ chains of edge-shared $UO_7$ pentagonal bipyramids and $^{1}_{\infty}[NbO_4]^{3-}$ chains of corner-shared $NbO_5$ square pyramids alternating along the [0 1 0] direction. The $Li^+$ ions are located between two consecutive layers and hold them together; the $Li^+$ ions and two layers constitute a neutral "sandwich" $\{(UNbO_6)^{-} - (Li)_2^{2+} - (UNbO_6)^{-}\}$. In this unusual structure the neutral sandwiches are stacked one above another with no formal chemical bonds between the neutral sandwiches, figure 1.

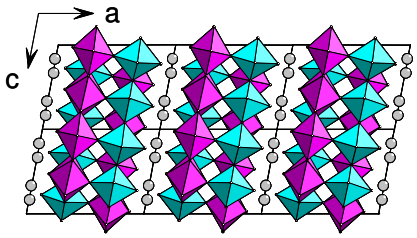


**Fig. 1 :**.Crystal structure of the $LiUNbO_6$

The homeotypic compounds $AUNbO_6$ (A = Na, K), and $A_{0.5}UNbO_{5.75}$ (A = Rb, Cs) have open-framework structures built from the association by edge-sharing in two directions of parallel $^{1}_{\infty}[UO_5]^{4-}$ chains of edge-shared $UO_7$ pentagonal bipyramids and $^{1}_{\infty}[Nb_2O_8]^{6-}$ ribbons of two edge-shared $NbO_6$ octahedra further linked by corners, figure 2. In Na, K and Rb compounds, the mono-dimensional large tunnels created in the [0 0 1] direction by this arrangement can be considered as the association by rectangular faces of two columns of triangular face-shared trigonal prisms of uranyl oxygen atoms. In $AUNbO_6$ (A = Na, K), all the trigonal prisms are occupied by the alkaline metal, in $Rb_{0.5}UnbO_{5.75}$, they are half-occupied. In $A_{0.5}UNbO_{5.75}$, the polyhedral arrangement is more symmetric and the tunnels created in the [0 1 0] direction are built of face-sharing cubes of uranyl oxygens totally occupied by the Cs atoms. This last compound well illustrates the structure-directing effect of the conterion.

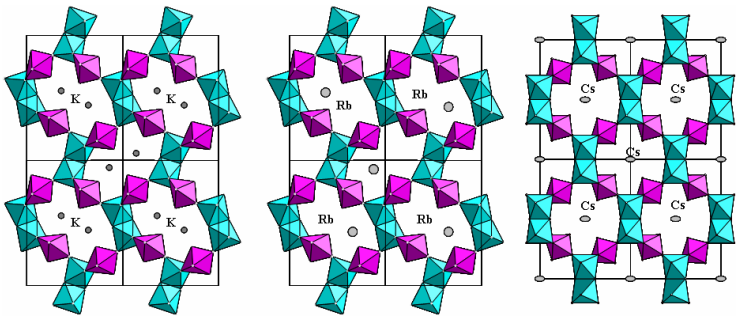


**Fig.2**. Crystal structures of $KUNbO_6$. $A_{0.5}UnbO_{5.75}$ (A = Rb, Cs).

The crystal structure of $Cs_9U_8Nb_5O_{41}$, is formed by $UO_7$ pentagonal bipyramids and $NbO_5$ square pyramids, sharing edges and corners to build infinite layers $[(UO_2)_8O_4(NbO_5)(Nb_2O_8)_2]^{9-}$. The alkaline cations $Cs^+$ are localized in the interlayer spaces, figure 3.

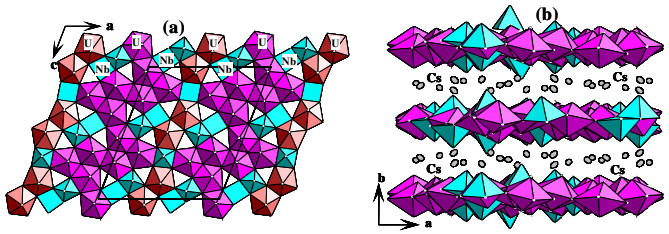


**Fig. 3:** (a) Infinite sheet $^{2}_{\infty}[(UO_2)_8O_4(NbO_5)(Nb_2O_8)_2]^{9-}$ in $Cs_9U_8Nb_5O_{41}$
(b) Projection of the $Cs_9U_8Nb_5O_{41}$ crystal structure along the [110] direction

To evidence the alkaline cations mobility in these structures, ionic conductivity measurements were carried out. The observed linear evolution of $log\sigma$ with reverse temperature shows that the ionic conductivity obeys to the Arrhenius law over the studied temperature range.

# J4

## Thermodynamic and structural properties of Protactinium(V) in sulphate medium

**Maria Vita Di Giandomenico,[1] Claire Le Naour[1], Didier Trubert[1], Clara Fillaux[2], Christophe Den Auwer[2], Philippe Moisy[2], Christoph Hennig[3]**

[1] *Centre National de la Recherche Scientifique/IN2P3/Paris XI, Institut de Physique Nucléaire, 91406 Orsay Cedex. e-mail: digiando@ipno.in2p3.fr*
[2] *Commisariat à l'Energie Atomique/Valrhô, DEN/DRCP/SCPS, 30207 Bagnols sur Ceze Cedex*
[3] *Rossendorf Beam Line/ESRF, Forschungszentrum Rossendorf, 38043 Grenoble*

Protactinium is experiencing a renewal of interest in the frame of long-term energy production. Modelling the behaviour of this element in the geosphere requires thermodynamic and structural data relevant to environmental conditions. Because of its tendency to polymerisation, hydrolysis and sorption on all solid supports [1], the equilibria constants of monomers species were determined at tracer scale (ca. $10^{-12}$ M) with $^{233}$Pa. The complexation constants of Pa(V) and sulphate ions were calculated starting from a systematic study of the apparent distribution coefficient D in the system TTA/Toluene/$H_2O$/$SO_4^{2-}$/$H^+$/$Na^+$/$ClO_4^-$ and as a function of ionic strength ($\mu$), temperature ($\theta$), free sulphate, protons and chelatant concentration.

First of all, the interaction between free species $H^+$, $SO_4^{2-}$, $Na^+$ leads to the formation of $HSO_4^-$ and $NaSO_4^-$, for which concentrations depend upon the related thermodynamic constants. For this purpose a computer code was developed in order to determine all free species concentration. This iterative code takes into account the influence of temperature and ionic strength (SIT modelling) on thermodynamic constants [2,3].

The direct measure of Pa(V) in the organic and aqueous phase by $\gamma$-spectrometry had conducted to estimate the apparent distribution coefficient D as function of free sulphate ions. The experiments, done changing different parameters, show a strong dependence of D with: temperature, TTA and protons concentration. Complexation constants have been determined after a mathematical treatment of D [4]. The extrapolation of these constants at zero ionic strength has been realized by SIT modelling at different temperatures. Besides, enthalpy and entropy values were calculated.

Parallely, the structural study of Pa(V) was obtained with $^{231}$Pa. XANES and EXAFS spectra show unambiguously the absence of the trans dioxo bond that characterizes the other early actinide elements like U and Np. In concentrated sulphuric acid (13M), Pa(V) is proved to exhibit a single oxo bond. In 0.5M and 0.05M HF medium, the results indicate the absence of any oxo bond: Pa(V) exists in the form of a pure fluoro-complex [5].

### References

[1] R. Guillaumont et al., *Actinides Rev.* **1**, 135 (1968)
[2] O. Söhnel et al., Densities of Aqueous Solutions of Inorganic Substances. *Elsevier*: Amsterdam, Netherlands, **335**, (1985).
[3] B. Allard et al., Modelling in Aquatic Chemistry. *OECD*: Paris, France **724** (1997).
[4] J. Rydberg. *Ark Kemi*, **8**, 101-112 (1955).
[5] C. Le Naour et al., *Inorg. Chem.*. **44**, 9542-9546, (2005).

# J5

## First three-dimensional diamine-containing uranyl-vanadates : hydrothermal synthesis and structure

**Murielle Rivenet, Laurent Jouffret, Francis Abraham**

*Unité de Catalyse et de Chimie du Solide, Equipe Chimie du Solide, UCCS UMR CNRS 8181, USTL, ENSC-B.P. 90108, 59652 Villeneuve d'Ascq Cedex, France,*
*e-mail: murielle.rivenet@ensc-lille.fr*

Owing to the potential applications of open-framework uranium-bearing materials in the fields of radioactive waste management, uranium geochemistry, ion-exchange and catalysis, research on this type of materials has dramatically increased these last years. The more often, organic agents are used so as to exert influence over structural features. Amines have historically been used in various uranium-based systems including molybdate [1], phosphate [2], phosphite [3], selenate [4], selenite [5], arsenate [6] sulphate [7] and fluoride [8] but the amine-uranyl-vanadate systems remained unexplored so far.

Our series of reactions was conducted using Teflon-lined 23mL digestion bombs. The solutions were prepared by mixing inorganic reagents ($UO_2(NO_3)_2.6H_2O$ and $V_2O_5$) with amines in aqueous acid (HCl). The digestion bombs were heated to 180°C for a time varying from 24h to 30 days depending upon the samples. Crystalline powders were collected after cooling to ambient temperature, filtration and washing with deionized water. The obtained compounds belong to two groups depending upon their bi- or three-dimensional structure.

- Bi-dimensional (2D) uranyl-vanadates were obtained using either linear diamines (1,2-ethylenediamine, 1,3-diaminopropane) or cyclic diamines (piperazine , 1-methylpiperazine and 1,4-diazabicyclo[2,2,2]octane). These new materials were described in a recent paper [9].
- Three-dimensional (3D) compounds were obtained by using linear diamines with a carbon chain length varying from three to six carbons (1,3-diaminopropane, 1,4-diaminobutane, 1,5-diaminopentane, 1,6-diaminohexane). Their crystal structures are herein described for the first time.

As can be seen in table 1, the obtained compounds all exhibit similar orthorhombic parameters close to 15.5, 14.1 and 13.6 Å for a, b and c, respectively. Using single-crystal X-ray diffraction data, the crystal structures of the obtained compounds were solved in the non-centrosymmetric space group Cmc21. All the compounds are isotypic and contain the same $[(UO_2)_2(VO_4)_2]^{2-}$ layers built from $(UO_5)_\infty$ zig-zag chains of edge shared $UO_7$ pentagonal bipyramids running down the b-axis further connected by $VO_4$ tetrahedra (figure 2).

| Number of carbons in the amine | | 3 | 4 | 5 | 6 |
|---|---|---|---|---|---|
| Space group | | Orthorhombic $Cmc2_1$ | | | |
| Cell parameters (Å) | a | 15,408(2) | 15,654(1) | 15,722(4) | 15,775(9) |
| | b | 14,152(2) | 14,194(8) | 14,130(7) | 14,208(5) |
| | c | 13,651(2) | 13,677(9) | 13,582(2) | 13,677(8) |
| Cell volume ($Å^3$) | | 2976,8(4) | 3038,9(6) | 3016,5(3) | 3065,9(8) |

Table 1. Cell parameters of the three-dimensional amine-containing uranyl-vanadates compounds

Going along the chain of edge-sharing, the apices of adjacent tetrahedra alternate *up* (U) and *down* (D) with the sequence UUDDUU as defined by Burns [10]. The layers are connected to each other by means of $UO_7$ pillars (figure 3). The structural connectivity is quite similar to that of pentahydrated uranyl orthovanadate $(UO_2)_3(VO_4)_2.5(H_2O)$ [11] except that half of the $UO_7$ pillars are replaced by the linear amines. The $UO_2^{2+} \leftrightarrow (diamine)^{2+}$ substitution was confirmed by carrying experiments in complementary systems. It leaves large voids within the structure leading to crossed channels running down b and c axes. In each compound, amines were found in the channels. Depending upon their chain length, the amines lie at varying angles in between the $UO_7$ pillars. Further experiments of $(diamine)^{2+}$ exchange by $NH_4^+$ are under study and will be discussed.

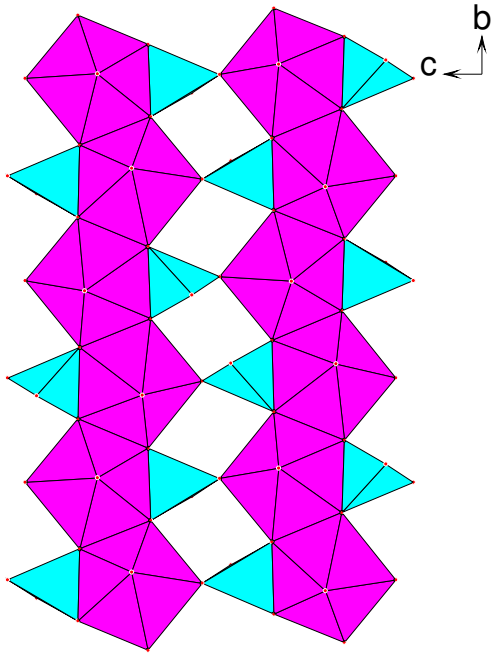


Figure 2. The uranophane type uranyl vanadate sheet in the three-dimensional amine-containing uranyl-vanadates.

(fig 3a)

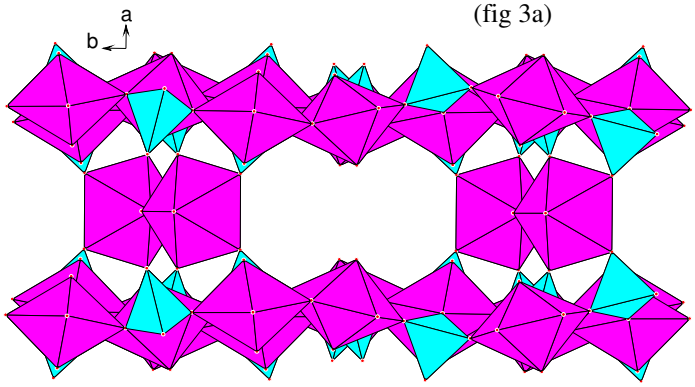


(fig 3b)

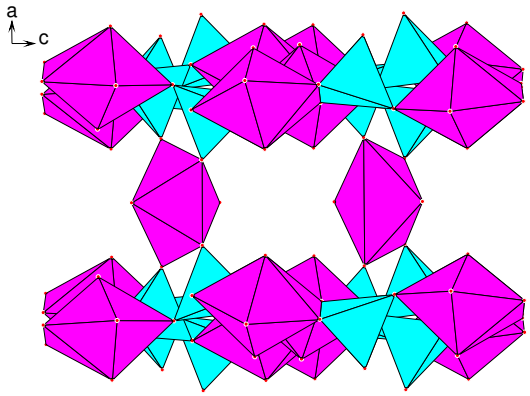


Figure 3. Channels in the three-dimensional amine-containing uranyl-vanadates compounds

## References

[1] S.V. Krivovichev, T. Armbruster, D.Y. Chernyshov, P.C. Burns, E.V.Nazarchuk, W. Depmeier, *Microporous Mesoporous Mater.* **78** 225 (2005).
[2] M.B. Doran, C.L. Stuart, A.J. Norquist, D. O'Hare, *Chem. Mater.* **16** 565 (2004).
[3] M. Doran, S.M. Walker, D. O'Hare, *Chem. Commun.* (2001) 1988.
[4] S.V. Krivovichev, V. Kahlenberg, I.G. Tananaev, R. Kaindl, E. Mersdorf, B.F. Myasoedov, *J. Am. Chem. Soc*. **127** 1072 (2005).
[5] P.M. Almond, T.E. Albrecht-Schmitt, *Inorg. Chem.* **42** 5693 (2003).
[6] A.J. Locock, P.C. Burns, *J. Solid State Chem.* **177** 2675 (2004).
[7] A.J. Norquist, M.B. Doran, D. O'Hare, *Inorg. Chem.* **44** 3837 (2005).
[8] M.B. Doran, B.E. Cockbain, A.J. Norquist, D. O'Hare, *Dalton Trans.* (2004) 3810.
[9] M. Rivenet, N. Vigier, P. Roussel, F. Abraham, *J.Solid State Chem.* **180,** 722 (2006)
[10] A.J. Locock, P.C. Burns, *J. Solid State Chem.* **176** 18 (2003).
[11] M. Saadi, C. Dion, F. Abraham, *J. Solid State Chem.* **150**, 72 (2000).

# COST1

## Magnetic structure of the hydride $CeRuSiH_{1.0}$ deriving from the heavy-fermion ternary silicide CeRuSi

**B. Chevalier,[1] E. Gaudin[1], S. Tencé[1, 5], B. Malaman[2], J. Rodriguez Fernandez[3], B. Coqblin[4], G. André[5]**

*[1] Institut de Chimie de la Matière Condensée de Bordeaux (ICMCB), CNRS [UPR 9048], Université Bordeaux 1, 87 Avenue du Dr. A. Schweitzer, 33608 Pessac, France, e-mail: chevalie@icmcb-bordeaux.cnrs.fr*
*[2] Laboratoire de Chimie du Solide Minéral, associé au CNRS [UMR 7555], Université Henri Poincaré-Nancy1, BP 239, 54506 Vandoeuvre les Nancy Cedex, France.*
*[3] CITIMAC, Facultad de Ciencias, Universidad de Cantabria, 39005 Santander, Spain.*
*[4] Laboratoire de Physique des Solides, Université Paris-Sud, UMR 8502 CNRS, 91405 Orsay, France.*
*[5] LLB, CEA-Saclay, 91191 Gif-Sur-Yvette Cedex, France*

The ternary silicide CeRuSi which crystallizes in the tetragonal CeFeSi-type structure is considered as a non-magnetic heavy-fermion system [1]. Its investigation by specific heat $C_p$ measurements reveals a shallow maximum at 0.5 K ($C_p/T$ = 220 mJ/mol $K^2$) associated with the formation of a coherent heavy-fermion ground state. The analysis of these last measurements suggests a Kondo temperature around 25 K.
The crystal structure of CeRuSi can be described by a stacking along the *c*-axis of two layers formed by $[Ce_4Ru_4]$ antiprisms and separated by one layer of $[Ce_4]$ pseudo-tetrahedral units [2]. The $[Ce_4Ru_4]$ antiprisms surrounding the Si-atom are also observed in the crystal structure of the ternary silicide $CeRu_2Si_2$ considered as a moderate heavy-fermion compound ($\gamma$ = 385 mJ/mol $K^2$) [3, 4]. Moreover the $[Ce_4]$ pseudo-tetrahedral units are interesting for hydrogen insertion. Recently, we have reported that the ternary compounds CeCoSi and CeCoGe, which are isomorphous to CeRuSi, absorb hydrogen [5, 6]. The resulting hydrides crystallize as the parent compounds in the tetragonal CeFeSi-type structure where H-atoms are inserted in the $[Ce_4]$ tetrahedral interstices. The hydrogenation induces an increase of the unit cell volume and also a pronounced anisotropic expansion of the unit cell: the *a*-parameter decreases whereas the *c*-parameter increases.
Hydrogen insertion in CeCoSi and CeCoGe leads to the destruction of their antiferromagnetic properties. For instance, CeCoSi shows a Néel temperature of 8.8(2) K whereas $CeCoSiH_{1.0}$ presents a spin fluctuation behaviour below $T_{sf}$ = 130(5) K [5]. In order to explain this transition antiferromagnetism $\rightarrow$ spin fluctuation, the electronic and magnetic structures of CeCoSi and $CeCoSiH_{1.0}$ were self-consistently calculated within the local spin density functional (LSDF) theory. Analysis of the electronic structures and of the chemical bonding properties leads to suggest that the chemical effect of hydrogen prevails over the cell expansion effect which enhances the magnetization in a different way. The demagnetisation of cerium at low temperature in $CeCoSiH_{1.0}$ could be associated to the strong Ce-H interaction, which is bonding throughout the conduction band [5, 6]. In other words, the hydrogenation of the ternary compounds adopting the tetragonal CeFeSi-type structure allows to study the influence on their physical properties of the competition between the increase of the unit cell volume linked to the H-insertion and the occurrence of the Ce-H chemical bonding.
In this view it is interesting to investigate the hydrogenation of a compound as CeRuSi having a unit cell volume higher than that of CeCoSi or CeCoGe. We report here on the investigation of the new hydride $CeRuSiH_{1.0}$ by x-ray diffraction on single-crystal, magnetization, electrical resistivity, thermoelectric power and specific heat measurements and neutron powder diffraction. We show that this hydride is an antiferromagnet presenting a complex magnetic

phase diagram. We discuss these physical properties in relation to those previously reported on the heavy-fermion $CeRu_2Si_2$ where a long-range order can be induced by the replacement of Ce by La or Si by Ge [7, 8].

Combining the results of our study, we can draw a tentative magnetic phase diagram of $CeRuSiH_{1.0}$ (Fig. 1). Four magnetic phases are distinguished in the ordered state below $T_{N1}$ = 7.5(2) K, where this hydride orders antiferromagnetically. The phases (I) and (II) correspond to an antiferromagnetic arrangement; the second occurring at $T_{N2}$ = 3.1(2) K in the magnetically ordered region. The phase (III) which appears between the two critical fields $H_{C1}$ and $H_{C2}$, shows a ferrimagnetic character. Finally, the phase (IV) existing for $H > H_{C2}$ exhibits a higher magnetization (ferromagnetic ?). The magnetic phase diagram of $CeRuSiH_{1.0}$ shows some similarities with that of $(Ce_{0.8}La_{0.2})Ru_2Si_2$ [7]. In this case also, a long-range magnetic order is induced in the heavy-fermion $CeRu_2Si_2$ by slightly expanding its lattice through the substitution of a few percent of cerium by lanthanum. This compound exhibits two antiferromagnetic transitions at 5.6(2) and 1.8(2) K which are strongly influenced by the applied field.

The neutron diffraction reveals that $CeRuSiH_{1.0}$ develops: (i) between $T_{N1}$ and $T_{N2}$ an incommensurate structure with a wave vector $\mathbf{k} = (k_x\ k_x\ 1/2)$ (sine-wave modulation of the Ce-magnetic moments aligned along the *c*-axis, $k_x$ increases with decreasing temperature as illustrated in Fig. 2); (ii) below $T_{N2}$ a square-modulated phase $\mathbf{k} = (k_x \cong 1/3\ k_x\ 1/2)$ showing the presence of the third-order harmonics (the structure is nearly commensurate and $k_x$ is independent of the temperature).

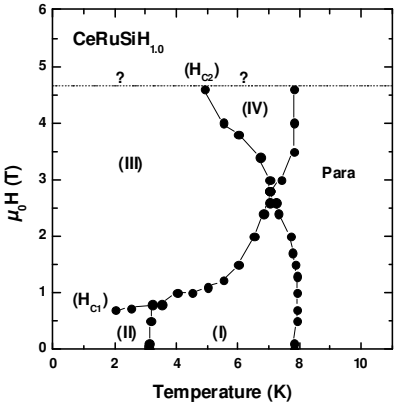


Fig. 1 Field-temperature phase diagram of hydride $CeRuSiH_{1.0}$.

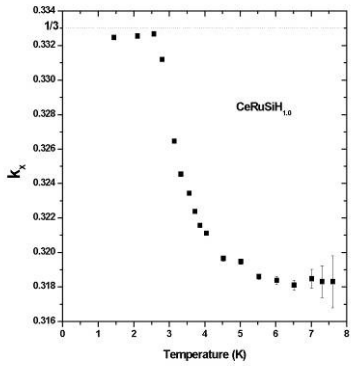


Fig. 2 Temperature dependence of the $k_x$ vector relative to the magnetic structure of $CeRuSiH_{1.0}$.

## References

[1] L. Rebelsky et al., *J. Appl. Phys.* **63**, 3405 (1988).
[2] R. Welter et al., *J. Alloys Comp.* **202**, 165 (1993).
[3] J. D. Thompson et al., *Solid State Comm.* **56**, 169 (1985).
[4] M. J. Besnus et al., *Solid State Comm.* **55**, 779 (1985).
[5] B. Chevalier et al., *Phys. Rev. B* **70**, 174408 (2004).
[6] B. Chevalier et al., *J. Phys. : Condens. Mater* **18**, 6045 (2006).
[7] J.-M. Mignot et al., *Physica B* **171**, 357 (1991).
[8] J.-M. Mignot et al., *Solid State Comm.* **77**, 317 (1991).

# Formation of $YbCu_{5-x}T_x$ and $YbCu_{4.5-x}T_x$ (T=transition metals) solid solutions

**M. Giovannini, R. Pasero, A. Saccone**

*Department of Chemistry, University of Genova, Via Dodecaneso 31, I-16146 Genova, Italy*
*e-mail: giovam@chimica.unige.it*

Several aspects make Yb compounds attractive for research studies, such as valence fluctuations and other low-temperature anomalies. Recently a strong emphasis was given to the investigation of $YbCu_{5-x}M_x$ (M=Au, Ag, In, Ga, Al) solid solutions, where the substitution of Cu by M offers the possibility to study the evolution of interesting features such as valence changes, Kondo effect and non Fermi liquid (NFL) behaviour [1,2,3]. In these solid solutions replacement of Cu by Au, Ag or In stabilize the cubic $AuBe_5$-type structure (existing in the case of $YbCu_5$ only above 1.5 GPa), whereas Ga and Al induce the formation of the hexagonal $CaCu_5$-type structure.
From an experimental reinvestigation of the Cu-rich region (70 at%<Cu<100 at%) of the binary Yb-Cu phase diagram using x-ray diffraction, differential thermal analysis and electron probe microanalysis [4], we have confirmed that the $YbCu_5$ compound does not form at ambient pressure. Instead, starting from the Cu side, the Cu-richest compound results to be $YbCu_{6.5}$ (derived-structure of the $CaCu_5$ type); the other Cu-rich compounds forming in this range are $YbCu_{4.5}$ and $YbCu_{3.5}$, both superstructures of the cubic $AuBe_5$. Furthermore, we have seen that, whereas $YbCu_{6.5}$ and $YbCu_{3.5}$ form peritectically at about 850°C, $YbCu_{4.5}$ melts congruently at higher temperatures. Moreover, from an experimental investigation on the formation of solubility for the above-mentioned binary compounds into the ternary field of Yb-Cu-T systems (T=transition elements), we found that $YbCu_{4.5}$ is the only compound forming solid solution. The crystal structure of $YbCu_{4.5}$ was studied by Černý and co-workers and it consists of a very complicated superstructure of 7448 atoms per unit cell derived by the cubic $AuBe_5$-type structure via the introduction of planar defects [5]. Owing to the large unit cell and the presence of inherent disorder in the structure, this compound belongs to the group of the complex metallic alloys (CMA) which are attracting considerable attention due to the fact that they show distinctive differences with respect to the behaviour of normal metallic alloys.
We discuss our results concerning the existence of $YbCu_{4.5-x}T_x$ (T=transition metals) solid solutions, and the competition in compound formation between these superstructures derived by the cubic $AuBe_5$-type and the parent cubic $YbCu_{5-x}T_x$.

## References

[1] J.H. He et al., *Journal of the Physical Society of Japan* **66**, 2481 (1997).
[2] E. Bauer et al., *Phys Rev. B* **56**, 711 (1997).
[3] M. Giovannini et al., *J. Phys.:Condens. Matter* **17**, S877 (2005) and references therein.
[4] M. Giovannini et al., in preparation.
[5] R. Černý et al., *J. Phys.: Condens. Matter* **8**, 4485 (1996).

# On the search for quantum criticality in a ferromagnetic system $UNi_{1-x}Co_xSi_2$

**D. Kaczorowski and A. Pikul**

*Institute of Low Temperature and Structure Research, Polish Academy of Sciences, P. O. Box 1410, 50–950 Wrocław, Poland, e-mail: D.Kaczorowski@int.pan.wroc.pl*

Since a few years the unusual physical behaviours of *f*-electron systems being at the verge of magnetic ordering, where quantum fluctuations compete with thermal ones, have been at the very centre of condensed matter physics [1]. Most of the hitherto performed experimental studies on the quantum criticality were devoted to phases with antiferromagnetic correlations, for which theoretically predicted non-Fermi liquid properties have been established [1,2]. Ferromagnetic quantum critical points are much less known both from the theoretical and experimental point of views [2,3], and hence it is tempting to investigate systems in which ferromagnetism can be tuned down to absolute zero temperature by external parameters, like pressure, magnetic field or/and composition.

The ternary uranium silicides $UTSi_2$ (T = Fe, Co, Ni), crystallizing in the orthorhombic $CeNiSi_2$-type crystal structure, were reported to span a variety of magnetic properties driven by the hybridization between the U 5*f* and T 3*d* electronic states. Whereas $UNiSi_2$ is a ferromagnetically ordered ($T_C$ = 95 K) Kondo lattice with rather well localised 5*f* electrons [4-6], $UCoSi_2$ behaves as a spin fluctuation system [4], and $UCoSi_2$ shows features of a weakly temperature dependent Pauli paramagnet [4]. The previous findings motivated us to undertake a detailed study of the solid solution $UNi_{1-x}Co_xSi_2$ ($0 < x < 1$), with the main focus on the alloys being close to a ferromagnetic instability, expected to occur for a certain Co-content $x_c$. Our first attempt was to check for a possible non-Fermi liquid character of the dc magnetic susceptibility, electrical resistivity and heat capacity of the specimens having nearly critical composition.

As expected, with substituting Co for Ni the ferromagnetism in the $UNi_{1-x}Co_xSi_2$ system gradually weakens. Figure 1 presents the evolution of the Curie temperature with the Co-content (similar change was found for the saturation and remanent magnetization). Apparently, the ferromagnetic order persists up to nearly pure $UCoSi_2$ being suppressed only very near $x = 1$.

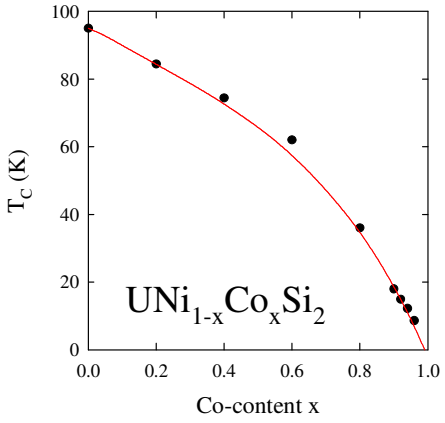


The main results obtained for two characteristic compositions, i.e. $UNi_{0.4}Co_{0.6}Si_2$ and $UNi_{0.02}Co_{0.98}Si_2$, are presented in Figure 2. The former alloy shows features typical for a strongly anisotropic ferromagnet with pronounced domain effects. In the paramagnetic region, the electrical resistivity is dominated by Kondo interactions, as found also for $UNiSi_2$ [4]. For the latter alloy no long-range magnetic ordering occurs above 1.72 K. Instead, some spin-glass characteristics can be recognized below 10 K. Upon applying magnetic field these spin-freezing features entirely disappear (not shown). The resistivity of this alloy varies with the temperature in a manner characteristic of spin fluctuations.

At present, resistivity and specific heat measurements of $UNi_{0.02}Co_{0.98}Si_2$ as well as of a few samples with $x < 0.98$ are being carried out at temperatures below 2 K in order to establish the ground state properties of the $UNi_{1-x}Co_xSi_2$ system at the very verge of the magnetic instability. These results will be reported at the conference.

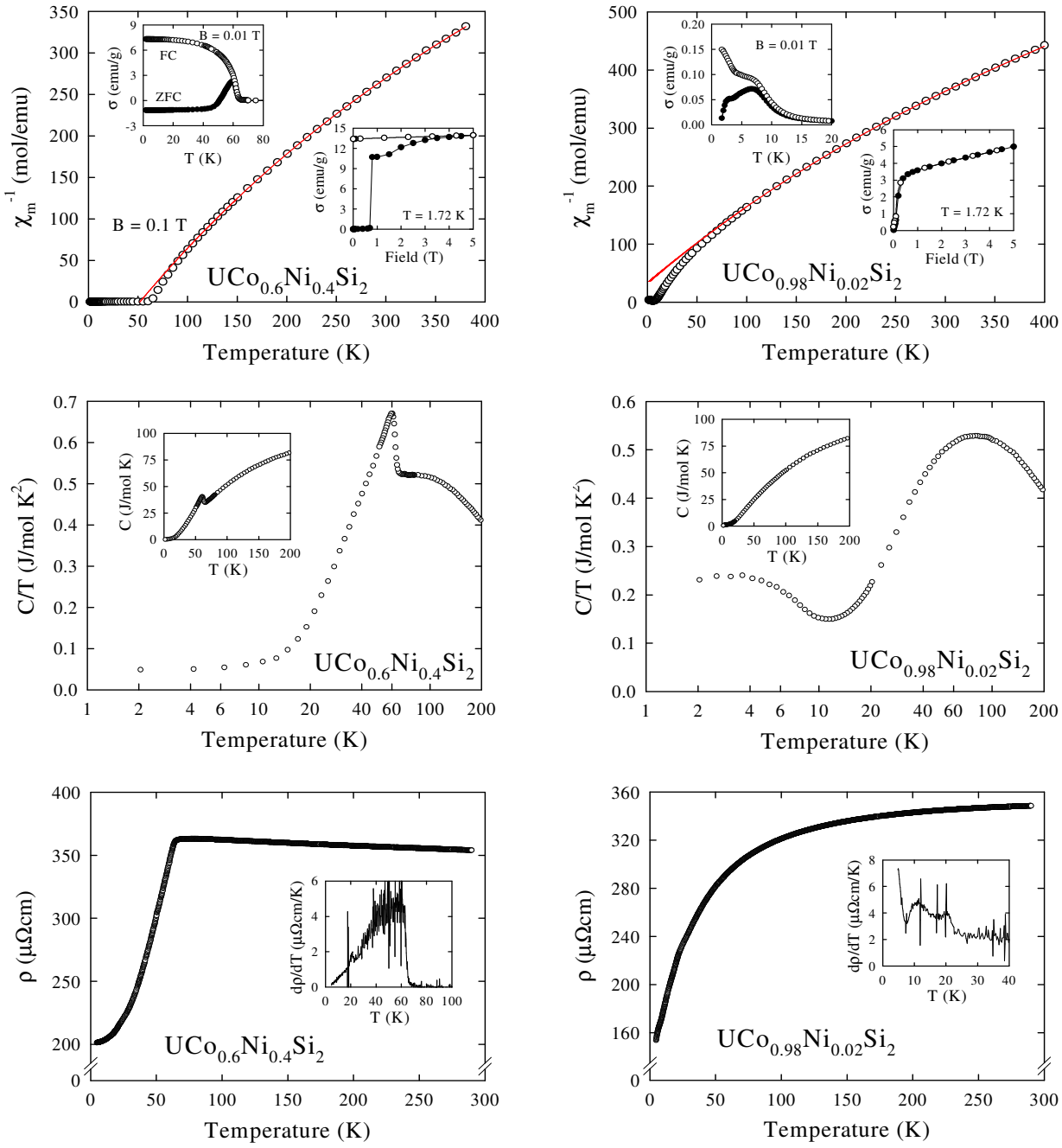


Figure 2

## References

[1] P. Coleman, and A. Schofield, *Nature* **433**, 225 (2005).
[2] G. R. Stewart, *Rev. Mod. Phys.* **73**, 797 (2001).
[3] T. R. Kirkpatrick, and D. Belitz, *Phys. Rev. B* **67**, 024419 (2003).
[4] D. Kaczorowski, *Solid State Commun.* **99**, 949 (1996).
[5] T. Taniguchi, H. Morimoto, Y. Miyako, and S. Ramakrishnan, *J. Magn. Magn. Mater.* **177-181**, 55 (1998).
[6] A. Das, S. K. Paranjpe, P. Raj, A. Satyamoorthy, K. Shashikala, and S. K. Malik, *Solid State Commun.* **114**, 87 (2000).

# COST4

## Heat capacity of $CeNi_4Si$ compound

**M. Reiffers,[1] M. Timko[1], M. Mihalik[1], M. Falkowski[2], A. Kowalczyk[2], J. Šebek[3], E. Šantavá[3]**

[1] *Institute of Experimental Physics, Slovak Academy of Sciences, Watsonova 38, Kosice, Slovakia, e-mail: reiffers@saske.sk*
[2] *Institute of Molecular Physics, Polish Academy of Sciences, Smoluchowskiego 17, 60-179 Poznań, Poland*
[3] *Institute of Physics, Academy of Sciences of the Czech Republic, Na Slovance 2, 182 21 Praha 8, Czech Republic*

Cerium based ternary compounds demonstrate different phenomena depending on the valence of the Ce ion. It is believed that the hybridization between the conducting electrons and the 4f Ce electrons should be responsible for the valence state of Ce. Depending on the strength of the f-ligand hybridization one observes in these compounds phenomena such as magnetic ordering, heavy fermion behavior, Kondo effect, valence fluctuations and superconductivity. Concerning the hybridization effects and mixed-valence behavior in the Ce-based compounds and alloys some information can be extracted from the analysis of the Ce(3*d*) states of the X-ray photoemission spectra. The appearance of the $3d^9 4f^0$ configuration is related to the modification of the valence state, whereas the $3d^9 4f^2$ satellite is a measure of the hybridization strength $\Delta$. Value of the hybridization parameter $\Delta \approx 85$ meV for $CeNi_4B$ [1] is decreasing with reduction of Ce-Ce distance along c-axis reaching value $\Delta \approx 37$ meV and $\Delta \approx 36$ meV for $CeNi_4Al$ [2] and $CeNi_4Si$ [3], respectively.

Recently, the detailed analysis of the heat capacity data of the intermetallic compounds $RNi_4Al$ (R = Ce; Pr; Nd, and Dy), prepared by arc melting in the tri-arc furnace, was presented in [4]. In contrary to $CeNi_4Al$ compound prepared by the induction melting [1], no Schottky term and no magnetic entropy were found in this compound [4]. We present the heat capacity measurements of $CeNi_4Si$ and we discussed them with results of magnetic susceptibility and X-ray photoemission spectroscopy (XPS) measurements presented in [3].

The $CeNi_4Si$ compound was prepared by the induction melting of stoichiometric amounts of the constituent elements in a water-cooled boat, under argon atmosphere. The crystal structure was determined by the X-ray powder diffraction technique, using Cu-$K_\alpha$ radiation. $RNi_4Si$ compounds crystallize in the hexagonal $CaCu_5$-type of structure, the space group *P6/mmm*. The lattice parameters are $a = 4.795$ Å and $c = 4.663$ Å for $CeNi_4Si$. Heat capacity measurements were performed by a PPMS commercial device (Quantum Design) in the temperature range 2 – 300 K by the relaxation method using the two- $\tau$ model.

The detailed analysis of heat capacity data can be performed by a comparative method. In the first step heat capacity data of a nonmagnetic isostructural analogue has to be fully described by the electronic part $C_e$ and phonon contribution $C_p$ and in the next step the determined $C_p$ contribution together with $C_e$ of explored compound has to be subtracted from heat capacity data of this compound to obtain magnetic contribution of specific heat. One good candidate for non-magnetic analogue of $CeNi_4Si$ was $LaNi_4Al$. The heat capacity data of $CeNi_4Si$ coincide quite well with those of $CeNi_4Al$ and $LaNi_4Al$ indicating that in the case of $CeNi_4Si$ the comparative method cannot be used. The analysis of calculated phonon contribution of $LaNi_4Al$ presented in [4] does not fit very well for $CeNi_4Si$ and that is why we had to estimate phonon contribution directly on $CeNi_4Si$. The electronic part of the specific heat is expressed as $C_e = \gamma T$ and the low temperature lattice contribution as $C_p = \beta T^3$. Plotting the low-temperature heat capacity data in the form of $C/T$ vs $T^2$ dependence, we obtained the

value of the electronic specific heat $\gamma$ = 22 mJ/molK$^2$ for $CeNi_4Si$ (see Fig.1.). The obtained value of the electronic coefficient corresponds with $\gamma$ = 29 mJ/molK$^2$ which was obtained on $CeNi_4Al$ [2]. Subtraction of $\gamma T$ from the specific heat data then yields the phonon part.

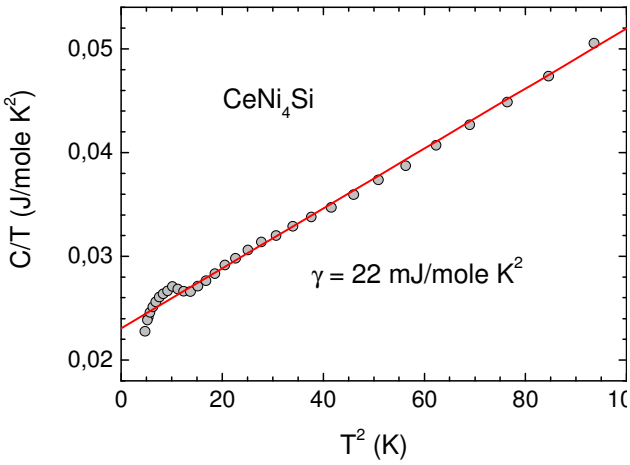


Fig. 1. $C/T$ vs $T^2$ dependence of heat capacity of $CeNi_4Si$.

As a result of the calculated phonon part subtraction, there is no significant magnetic contribution to heat capacity of $CeNi_4Si$ indicating that tetravalent cerium with zero magnetic moment dominates in this compound. Heat capacity results support recent susceptibility and XPES results [3] suggesting presence of tetravalent cerium in the $CeNi_4Si$ compound.

The magnetic susceptibility data of a bulk $CeNi_4Si$ sample measured at a field 1T were analyzed in the paper [3]. The susceptibility were well described by the Curie-Weiss law $\chi(T) = \chi_0 + C/(T - \theta_p)$. The fit to the data in the temperature range 2-300K yields paramagnetic temperature Curie $\theta$ = -2 K and an effective magnetic moment $\mu_{eff}$ = 0.52 $\mu_B$/f.u. The derived magnetic effective moment is much lower in comparison with free $Ce^{3+}$ ions value, which is equal to 2.54 $\mu_B$. Since the magnetic moment of tetravalent cerium is zero, so then the observed reduction of magnetic moment can be explained in a natural way by fractional occupation of $4f^0$ ($Ce^{4+}$) and $4f^1$ ($Ce^{3+}$) configurations. The field dependences of magnetization presented in [3] revealed possible presence of ferromagnetic impurity at $T$ = 1.7 K but additional measurements at $T$ = 10 K and measurements of $M(T)$ in whole temperature range in magnetic fields $\mu_0 H$ = 0.3 T and 0.05 T confirmed that the sample is free from any ferromagnetic parasitic phase at high temperatures.

This work has been supported partly by the COST – ECOM P16; Science and Technology Assistance Agency – the contract No. APVT–51–031704; VEGA 2/4050/04; VEGA 6065, the contract No. I/2/2003 of the Slovak Academy of Sciences for the Centers of Excellence.

## References

[1] T. Toliński et al., *J. Phys.: Condens. Matter* **15**, 1397 (2003).
[2] T. Toliński et al., *Phys. Rev.* **B 70**, 064413 (2004).
[3] A. Kowalczyk et al., *Solid State Commun.* **139,** 5 (2006)
[4] P. Svoboda et al., *Physica* **B 378–380**, 1107 (2006).

# COST5

## Formation, Structure and Physical Properties of Novel Compounds $M_2Pd_{14+x}B_{5-y}$, M=Th, Ce, Pr, Nd, Sm, Eu, Gd

**E. Royanian[1,2], P. Rogl[1], E. Bauer[2], H. Kaldarar[2]**
**H. Michor[2], A. P. Gonçalves[3], G. Giester[4]**

[1] *Institute of Physical Chemistry, University of Vienna, A-1090 Wien, Austria*
*e-mail: peter.franz.rogl@univie.ac.at*
[2] *Institute of Solid State Physics, Vienna University of Technology, A-1040 Wien, Austria*
[3] *Dept. Química ITN / CFMC-UL, E. N. 10, P-2686-953 Sacavém, Portugal,*
[4] *Institute of Mineralogy and Crystallography, University of Vienna, A-1090 Wien, Austria*

**Introduction:** The recent discovery of $CePt_3Si$ ($CePt_3B$ type) as the first heavy fermion superconductor without a center of symmetry [1] has triggered widespread research activities to search for a novel superconducting state in related ternary or quaternary alloy systems [2]. To gain more insight into general physical properties of such compounds, our studies were extended to rare earth palladium boride systems in search for novel materials with similar property characteristics and/or a possibly high Seebeck effect due to strong electron correlations. Novel and hitherto unknown compounds were found to exist near the composition $REPd_7B_{2.5}$ for all light rare earth elements from La to Gd. The investigation was furthermore extended to include the actinoid elements Th and U. The present paper aims at a detailed investigation and evaluation of these compounds in order to characterize their crystal structure, thermodynamic, electric and magnetic behavior and elucidate ground states and phase transitions appearing in this series.

**Experimental:** Alloys with nominal composition $M_2Pd_{14+x}B_{5-y}$, M=Th, U, La, Ce, Pr, Nd, Sm, Eu, Gd, with a weight of 1 gram each were prepared by argon arc-melting on a water-cooled copper hearth in Ti-gettered argon from elemental ingots with minimal purity of 99.9 mass%. All alloys were sealed in quartz tubes and annealed at T = 900°C for 240 h before quenching in cold water. X-ray powder diffraction data from as-cast and annealed alloys were collected employing a Guinier-Huber image plate system with Cu-$K_{\alpha 1}$ ($8<2\Theta<100°$). Single crystals were mechanically isolated from the crushed as-cast alloy $Nd_2Pd_{14}B_5$. The structure of $Nd_2Pd_{14+x}B_{5-y}$ was solved by direct methods and refined with the aid of the SHELXL-97 and SHELXS-97 program. Measurements of the various physical properties were carried out with a series of standard techniques [3].

**Crystal structure of $Nd_2Pd_{14.9}B_{4.9}$:** Direct methods for space group type $I4_1/amd$ revealed 1 Nd- and 4 Pd-sites. Two boron sites were located from a difference Fourier synthesis in close relation to the structure type of $Y_2Pd_{14}B_5$ [4], however, leaving high residual densities which were compensated by introducing an additional Pd-atom Pd5. The Pd5 as well as the B2 site, however, are only partially occupied (about 50% each), a complicated defect structure arises in which either the Pd5 or the B2 site per unit cell is half filled. The final structure (R-value = 0.020) arrives at a chemical formula $Nd_2Pd_{14.9}B_{4.9}$ and is closely related to the $Sc_4Ni_{29}Si_{10}$-type [5]. As one of the typical structural units for metal rich borides, B1-atoms are found in deformed Archimedian antiprisms capped on one side by an additional Pd-atom and B2-atoms are in a coordination unit formed by two trigonal prisms face-connected on a common quadratic base and formed by seven palladium atoms. Interatomic distances agree well with the metallic radii of pure elements.

**Isotypic compounds $M_2Pd_{14}B_5$, M=Th, Ce, Pr, Nd, Sm, Eu, Gd:** Rietveld analyses of the X-ray intensities, systematic extinctions, and size of unit cells suggest isotypism with the structure of $Nd_2Pd_{14.9}B_{4.9}$ in all cases of the light rare earth elements Ce, Pr, Nd, Sm, Eu, Gd. The graph volume vs. rare earths, indicates a 3+ ground state for both Ce and Sm, but a valence state closer to divalent Eu. Whilst no indications were found for formation of

isostructural $U_2Pd_{14}B_5$, X-ray intensities and unit cell dimensions of the thorium analog compare well with the $Nd_2Pd_{14.9}B_{4.9}$ type.

**Physical properties**: Ternary $M_2Pd_{14}B_5$ have been investigated with respect to physical properties by means of temperature dependent resistivity and heat capacity measurements.

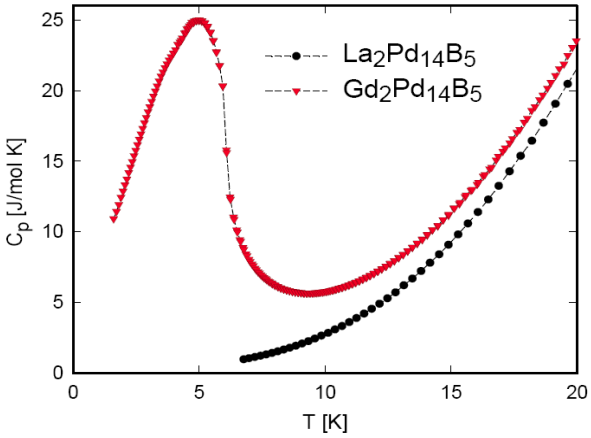


Fig. 1: Temperature dependent specific heat Cp of $Gd_2Pd_{14}B_5$. The heat capacity of $La_2Pd_{14}B_5$ defines the nonmagnetic background.

Studies at low temperatures indicate clear long-range magnetic order in $Gd_2Pd_{14}B_5$ below 6 K (compare Fig. 1). Heat capacity measurements suggest that the compounds based on Ce, Nd and Sm order magnetically below 2 K, while both Pr and Eu seem not to exhibit a magnetically ordered state. The total angular momentum j = 4 of the Pr ion in the context of crystalline electric field effects of the tetragonal crystal structure of $Pr_2Pd_{14}B_5$ can create a non-magnetic ground state due to singlet formation or due to the presence of a non-magnetic doublet. The absence of long range magnetic order in the Eu based compound would be a result of a valency of the Eu ion which significantly deviates from the 2+ state. Note that Eu in the 2+ state would behave like Gd and as a consequence, ordering should occur around that value deduced for the isomorphous $Gd_2Pd_{14}B_5$. The intermediate electronic configuration of the Eu ion in $Eu_2Pd_{14}B_5$ results in a significantly enhanced electronic contribution to the specific heat, attaining about 0.8 J/molK$^2$ for T $\rightarrow$ 0. A hump-like structure in the heat capacity of $Pr_2Pd_{14}B_5$ around 4 K may refer to a low-lying CEF level above the nonmagnetic ground state. The electrical resistivity, ρ, of $M_2Pd_{14}B_5$, in general, is characterized by small RRR values originated by defects inherent to the present crystal structure. Low temperature ρ(T) data of the compounds based on Ce, Nd, Sm, Eu and Gd exhibit a minimum in the vicinity of 20 K followed by an increase towards lower temperatures. Although a nonmagnetic origin like variable range hopping is conceivable due to statistical disorder of the crystal structure, a magnetic source is more likely, since magnetic fields of the order of several Tesla completely suppress the anomalies indicated above.

Work supported by the Austrian FWF, P18054 and performed within COST Action P16. P.R. is grateful for a STM within WG1 of COST P16.

## References

[1] E. Bauer, G. Hilscher, H. Michor, C. Paul, E.W. Scheidt, A. Grybanov, Yu. Seropegin, H. Noel, M. Sigrist, P. Rogl; *Phy. Rev. Lett.,* **92**, 027003,1-4 (2004

[2] E. Bauer, G. Hilscher, H. Kaldarar, H. Michor, E.W. Scheidt, P. Rogl, A. Gribanov, Yu.Seropegin, J. Magn. Magn. Mater. (2007) in press

[3] E. Bauer, St. Berger, Ch. Paul, M. Della Mea, G. Hilscher, H. Michor, M. Reissner, W. Steiner, A. Grytsiv, P. Rogl, W. Scheidt, *Phys. Rev. B* **66**, 214421 (2002)

[4] P. Salamakha, A.P. Goncalves, O. Sologub, M. Almeida, *J. Alloys Comp.* **360,** 61-68 (2003)

[5] Yu.B. Kuz'ma, O.M. Dub, V.A. Bruskov, N. Chaban, L.V. Zavalii, *Kristallografiya* **33**, 841-844 (1988).

# Physical Effects Associated with the Spin Dependent Effective Masses of Heavy Quasiparticles: Metamagnetism and Fulde-Ferrell state

**Jozef Spalek,[1] Jan Kaczmarczyk,[1] Maciej Maśka,[2] and Marcin Mierzejewski[2]**

[1] *Marian Smoluchowski Institute of Physics, Jagiellonian University, Reymonta 4, PL-30-059 Krakow, Poland, e-mail: ufspalek@if.uj.edu.pl*
[2] *Institute of Physics, Silesian University, Uniwersytecka 4, PL-40-007 Katowice, Poland*

Spin-dependent masses for correlated and almost localized systems have been proposed some time ago [1]. They have been detected experimentally for the heavy-fermion systems quite recently [2]. In our contribution we demonstrate that in the applied magnetic field this may lead to the metamagnetic behavior with a simultaneous localization of f electrons. A nontrivial dependence of the linear specific heat associated with this transition is demonstrated. Additionally, we have considered also the stability of the Fulde-Ferrell-Larkin-Ovchinnikov (FFLO) superconducting state for both the extended s-wave and d-wave solutions. With the increasing field the transition from the BCS state to the FFLO state is discontinuous, whereas the transition from FFLO state to the normal state is continuous. The physical differences with what is observed for $CeCoIn_5$ are analyzed.

Work performed under the auspices of COST P-16 Network. Also, the Grant from Polish Ministry of Science and Higher Education is acknowledged.

## References

[1] For a brief review see: J. Spalek, *Physica B* **378-380**, 654 (2006).
[2] A. McCollam et al., *Phys. Rev. Lett.* **94**, 186401 (2005); R. Daou et al., *Phys. Rev. Lett.* **96**, 026401 (2006).

# COST7

## The low-temperature transport properties of the periodic Anderson model

**V. Zlatić**[1]

[1] *Institute of Physics, Bijenicka c. 46, 10001 Zagreb, Croatia, e-mail: zlatic@ifs.hr*

The low-temperature properties of heavy fermions (HF) and valence fluctuators (VF) with 4*f* or 5*f* ions are continuing to attract considerable attention. Several recent papers [1,2] report on a correlation between the low-T Seebeck coefficient $\alpha$ and specific heat coefficient $\gamma=C_V/T$ and show that the low-T ratio $q=\alpha/\gamma T$ in most systems is about the same, although $\gamma$ and $\alpha/T$ vary by orders of magnitude. A similar 'quasi-universal' behavior is exhibited by the low-T Kadowaki-Woods (KW) ratio [3], $\rho/(\gamma T)^2$, where $\rho$ is the electrical resistance. These results suggest a 'universal law' for the low-T power factor $P=\alpha^2\sigma$ and bring to the fore the validity of the Wiedemann-Franz (WF) law and the renormalization of the thermoelectric 'figure-of-merit' $ZT = \alpha^2\sigma T / \kappa$ , where $\kappa$ is the thermal and $\sigma$ the electrical conductivity. The 'universality' of the KW and the *q*-ratio has been addressed recently by several authors [4-6] who treated the *N*-fold degenerate periodic Anderson model (PAM) by different approximations. Here, we discuss the results obtained by the dynamical mean field theory (DMFT) and establish the Fermi liquid (FL) laws for the systems described by the PAM. We show that the KW ratio and *P(T)* have an explicit *N*-dependence, while the *q*-ratio and *ZT* do not. We also show that there is a temperature window in which the electron correlation leads to a large deviation from the WF law and give rise to $ZT > 1$. For details and further discussion see references [6,7].

The FL laws of the periodic Anderson model describe a coherent transport of charge and heat in a stoichiometric compound and are completely analogous to the phase-shift expressions of Kondo alloys. The FL behavior is universal when plotted on the reduced scale $T/T_K$, where $T_K$ is defined by the maximum of the Kondo resonance which we obtain from the DMFT. The parameter dependence of transport coefficients is described by $T_K$ which depends exponentially on *N* and the effective coupling *g*. The Kondo scale of an asymmetric Anderson model with constant particle number, $n=n_f+n_c$, is uniquely related to the *f*-electron number $n_f$.

The FL laws explain the near-universal behavior of the KW and the *q*-ratio of many HF and VF systems. We find $\lim_{T\to 0} [|e| \alpha / \gamma T] = 2/n_c$, where $n_c$ is the number of *c*-electrons which depends on pressure or doping. This shows that the *q*-ratio can deviate somewhat from the universal value and agrees with recent chemical pressure data [2,8]. The KW ratio is given by $\lim_{T\to 0} [\rho/ (\gamma T)^2] \approx A/Nn_c^2$ and its *N*-dependence was recently emphasized by Kontani [6]. Here, we point out the $n_c^2$ dependence which affects systems with low carrier concentration or systems close to the MI transition. In addition to the KW ratio and the *q*-ratio, the power factor *P(T)* and the Lorenz ratio $L(T)=\kappa/ \sigma T$ are also constant in the FL regime.

The dependence of transport coefficients on $n_c$ and *N* is particularly important for pressure or doping experiments. A pressure-induced charge transfer between hybridized *f*- and *c*-states modifies the effective coupling *g* and the effective degeneracy *N*, which affects the low-T properties (pressure can change the transport coefficients by orders of magnitude). Our results show that an increase of *N* and $n_c$ reduces the slope of $\rho(T)$ and extends the coherent FL regime to higher temperatures. This agrees with the pressure data on 4*f*-intermetallics in which an increase of pressure induces a continuous change from the HF to VF behavior [9].

The rapid rise of $\rho(T)$ with temperatures destroys eventually the coherent propagation of hybridized quasiparticles and we explain the properties of stoichiometric compounds above the coherent FL regime by an effective single impurity Anderson model in which the *c*-electrons scatter incoherently on 4*f*-ions. Such a 'poor man's' approach reduces the lattice problem of charge and heat transport to an impurity model with Kondo scale $T_K$ and $n=n_f+n_c$ electrons. For a *N*-fold degenerate *f*-state or an *f*-state with the CF splitting [6], we find by NCA that $\alpha(T)$ and $P(T)$ have a maximum and $L(T)$ has a shallow minimum located around $T_K$. The overall description of the lattice problem can be obtained by interpolating between the FL solution valid for $T<T_K$ and the 'poor man's' solution valid for $T>T_K$.

A further remarkable consequence of the FL laws is an enhancement of the low-T 'figure-of-merit' due to the deviations of $L(T)$ from the FW law. Neglecting phonons, which is a rather severe approximation, we find $ZT=\alpha^2/L$ in the FL regime. Since $\alpha^2$ increases and $L$ decreases with T, there is a T-range in which the Kondo effect enhances $ZT$. Note, tuning the HF or VF systems by doping might lead to $ZT>1$ at temperatures at which the WF law is invalidated by correlations. Even though the functional form of $ZT$ is not correct for $T \geq T_K/3$, the FL result captures the essential features: an increase of $\alpha^2$ and a decrease of $L$ lead to $ZT>1$. The 'poor man's' calculation [6] and recent DMFT+NRG results for the spin-1/2 PAM [10] indicate a maximum of $ZT$ around $T_K$. The enhancement of $ZT$ is due to the renormalization of both $\alpha$ and $\kappa$ and $ZT>1$ is not restricted to $\alpha > 150\ \mu V/K$. The condition $\alpha=150\ \mu V/K$ is derived using the WF law and does not hold for correlated systems described by the periodic Anderson model. We expect an optimal situation regarding $ZT$ for heavy fermions with small $T_K$ (large CF splitting) and systems close to the MI transition. In valence fluctuators with large $N$ and, hence, large $T_K$, the WF law holds up to rather high T and $ZT$ is small despite large $\alpha$.

From the above discussion it is clear that pressure and chemical pressure experiments on the 4*f* and 5*f* systems described by the PAM can provide a stringent test for validity of the FL laws and the universal transport properties. It would be interesting to study the pressure-induced deviations from the universal value of the *q*-ratio and the KW ratio, using $P(T)$ or $L(T)$ as the consistency checks. These later quantities are defined solely in terms of transport coefficients and should be well suited for pressure experiments. We hope, our results will facilitate the search for new correlated thermoelectric with a useful low-temperature $ZT$.

**References**

[1] K. Behnia, D. Jaccard and J. Flouquet, J. Phys, C: Condensed Matt. **16**, 5187, (2004).
[2] J. Sakurai and Y. Isikawa, J. Phys. Soc. Japan **74**, 1926 (2005).
[3] K. Kadowaki and S. B. Woods, Solid State Commun. **71**, 1149 (1987).
[4] K. Miyake and H. Kohno, J. Phys. Soc. Japan **74**, 254 (2005).
[5] H. Kontani, J. Phys. Soc. Japan **73**, 515 (2004).
[6] V. Zlatić and R. Monnier, Phys. Rev. B 71, 165109 (2005); Zlatic et al., cond-mat/0512288
[7] V. Zlatić, R. Monnier and J. Freericks, cond-mat/
[8] Z. Hossain et al. Phys. Rev. B 69, 014422 (2004).
[9] H. Wilhelm et al., Phys.Rev. B**66**, 064428 (2002); H. Wilhelm et al., J.Phys.: Cond. Mat.**17**, S823 (2005).
[10] C. Genzebach et al., Phys. Rev. B {\bf 74}, 195119 (2006).

# Poster Presentations

# Abstracts

# P1

## Cycling changing of cerium valency in oscillating extraction processes of f-elements

**M. A. Afonin, A.A. Kopyrin, A.A. Fomichev, M.H. Ekzekov**

*Saint-Petersburg Institute of Technology, 26 Moskovsky av., 190013, Saint-Petersburg, Russia, kopyrin@lti-gti.ru*

Realization of the process in non-stationary conditions using phenomena of oscillating extraction allows using the differences in kinetics of ion complexation and extraction, their transport through the boundary area in both directions to separate elements [1,2]. To achieve high elements separation factors using oscillating extraction it is possible to use cycling changing of cerium valency in oscillatory Belousov-Zhabotinsky (BZ) reaction.
The oscillatory BZ reaction in extraction system gives advanced increasing of effective separation coefficients of chemically similar elements in comparison with classical methods. The experimental setup (fig.1.) for investigation of kinetics of non-stationary processes was created. The case of two extractors, coupled by bulk liquid membrane was investigated. The software for automation of the setup devices calibration, controlling of the process during the experiment and for experiment results processing is developed.

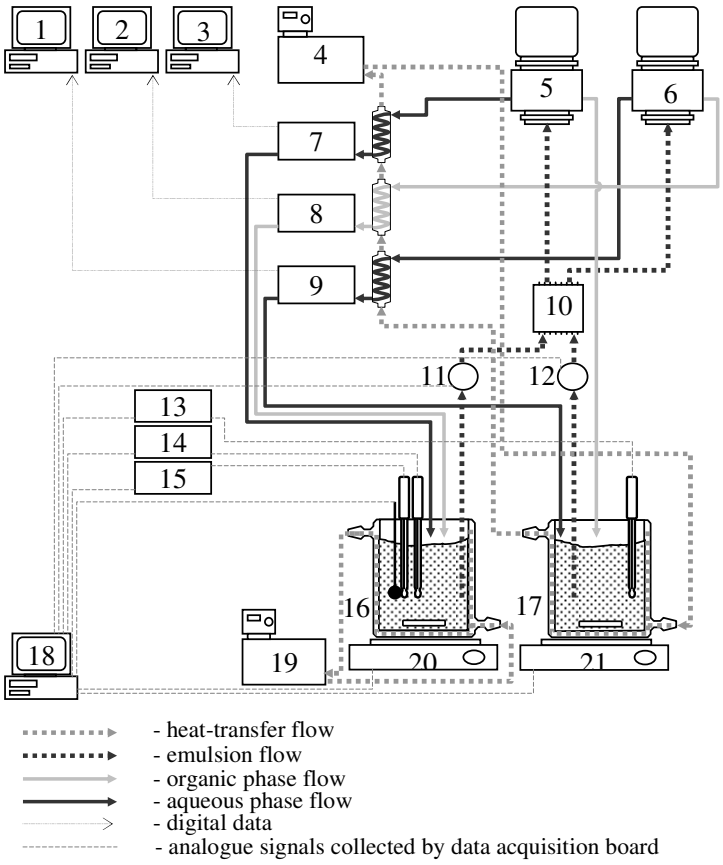


Fig. 1. Experimental setup: 1-3, 18 computers; 4, 19 – thermostats; 5, 6 – centrifugal separators EC-33 NIKIMT; 7, 8, 9 – spectrophotometers SF-2000 OKB Spectrum; 10 – peristaltic pump; 11, 12 – turbidimeters; 13 –pH-meter; 14, 15 - potentiometers; 16, 17 – extractors; 20, 21 – magnetic stirrers.

Flow sheet of the experimental setup for investigation of non-stationary extraction systems (fig. 1.) is following: the emulsion is pumped from thermostatic extractors 16, 17 to

centrifugal separators 5, 6 through the turbidimeters 11, 12 by peristaltic pump 10. After separation from the separator 5 organic phase flows to the extractor 17 and from the separator 6 organic phase flows to spectrophotometer 8 for analysis and it flows to the extractor 16. Passing through both aqueous phases organic phase forms bulk liquid membrane. After spectrophotometers 7, 9 aqueous phases come back to their corresponding extractors. Data acquisition of pH, red/ox potential of aqua phase, temperature and emulsion turbidity performs with frequency above 1 Hz using DAQ board in computer 18 and specially designed software. Diode-array spectrophotometers get spectra every 6-15 seconds. By deconvolution of each spectrum, using especially designed software we can get concentration of several elements.

Mathematical model of the non-stationary membrane extraction is developed. As the basis of mathematical model of non-equilibrium extraction of Nd and Pr the skeletal mechanism of Field-Kõrös-Noyes (FKN) used, known as Oregonator. The autocatalytic one-electron oxidation of $Ce^{3+}$ producing by $BrO_3^-$ is a core of this mechanism [3].
Investigation of models' properties is carried out. It is shown that the model is able to reproduce most of oscillating conditions described in literature for chemical oscillators based on BZ reaction. The relations between characteristic oscillations' properties and some system parameters' values are determined. The algorithms of effective modeling of some spread experimental oscillating conditions are proposed.

The values of activation energy for direct and reverse reactions of extraction and stripping reactions of Pr and Nd were calculated from experimental temporal dependencies of metal concentration and temperature by solving reverse kinetics problem using proposed mathematical model.

Using oscillatory BZ reaction as a factor deflecting the system from the stationary state effective separation coefficient of pare Pr/Nd exceeded 3±0,2.

**Acknowledgements**
This work was supported by the U.S. Department of Energy, Office of Basic Energy Sciences, under grant RC0-20000-SC14 and RUC2-20011-ST-04 administered by the Civilian Research and Development Foundation.

**References**
[1] M. A. Afonin et al, *Journal of Alloys and Compounds*, Vol. 374 (2004), **426-430**.
[2] A. A. Kopyrin et al, *Radiochemistry*, Vol. 47, No. 4, 2005, **387-391**. Translated from Radiokhimiya.
[3] A. A. Kopyrin et al, *Czech. J. Phys*. 56 (2006), **D435**

# P2

## Magnetic properties of $U_2(Fe_{1-x}Ni_x)_{13.6}Si_{3.4}$ single crystals

**A.V. Andreev[1], E.A. Tereshina[1,2], E. Šantavá[1]**

[1] *Institute of Physics, Academy of Sciences, Na Slovance 2, 18221, Prague, Czech Republic*
*e-mail: andreev@mag.mff.cuni.cz*
[2] *Dept. Condensed Matter Physics, Charles University, Ke Karlovu 5, 12116, Prague, Czech Republic*

Uranium forms intermetallic compounds with 3d metals (Fe and Co) in the hexagonal $Th_2Ni_{17}$ structure only when 3d metal is partly substituted by third element, e.g, Si. A homogeneity range of $U_2T_{17-y}Si_y$ is $3.3 \le y \le 4.5$ for T = Fe [1] and $1 \le y \le 3.4$ for T = Co [2]. Therefore, there is only the narrow Si-content zone at $y \sim 3.4$ where the continuous $U_2(Fe_{1-x}Co_x)_{17-y}Si_y$ solid solutions can be formed. The results of magnetization study of $U_2(Fe_{1-x}Co_x)_{13.6}Si_{3.4}$ single crystals were reported in Ref. [3]. All compounds are ferromagnetic, the spontaneous magnetic moment $M_s$ decreases monotonously with increasing Co content while the Curie temperature $T_C$ has a non-monotonous concentration dependence (resulting of known competitive trends in $R_m(Fe_{1-x}Co_x)_n$ systems). The absolute values of the anisotropy constants $K_1$ and $K_2$ for $x$ up to ~0.8 are high enough to suggest noticeable U contribution to the anisotropy, i.e., a magnetic state of U. At $x = 0.9$, $K_1$ and $K_2$ approach values which can be provided by 3d-metal sublattice without U contribution and U is expected to be non-magnetic above $x = 0.9$. It is of interest to check the observed features of magnetism of $U_2(T,Si)_{17}$ in compound with T = Ni. It was found that Ni does not form such compounds but a limited solubility is possible for the system $U_2(Fe_{1-x}Ni_x)_{13.6}Si_{3.4}$.

In the present work we studied width of the homogeneity range in this system, grew the single crystals and measured the magnetization along the principal axes as a function of the field and temperature. The single crystals were grown by the Czochralski method from stoichiometric mixtures of the pure elements (99.9% U and Fe, 99.99 % Ni and 99.999% Si) in a tetra-arc furnace.

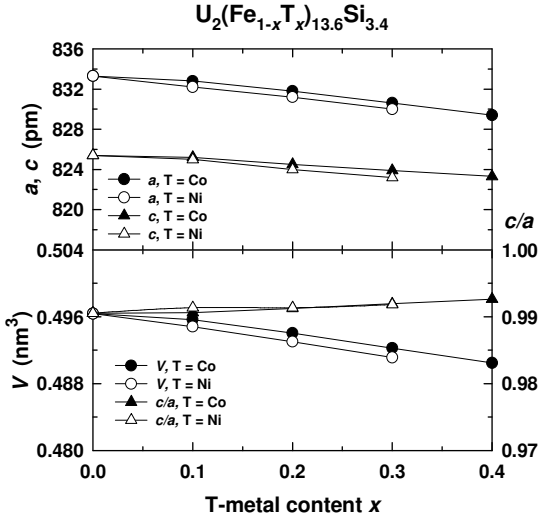


Fig. 1. The concentration dependencies of the lattice parameters $a$ and $c$, the unit-cell volume $V$ and ratio $c/a$ for $U_2(Fe_{1-x}T_x)_{13.6}Si_{3.4}$ solid solutions, T = Co, Ni.

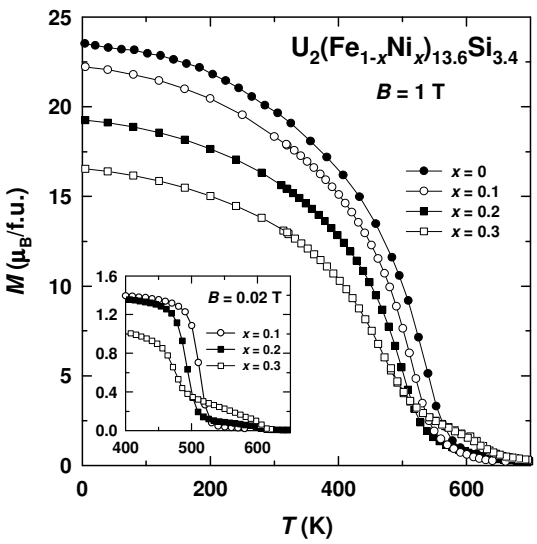


Fig. 2. The temperature dependencies of magnetization measured along the $a$ axis of $U_2(Fe_{1-x}Ni_x)_{13.6}Si_{3.4}$ crystals in 1 T and 0.02 T (inset) fields.

The X-ray powder diffraction analysis showed that the alloy with $x = 0.4$ is multiphase with the tetragonal $ThMn_{12}$ structure of the main phase. In alloys with $x \le 0.3$, the hexagonal crystal structure of the $Th_2Ni_{17}$ type was approved. The thermomagnetic analysis indicated

traces ($x$ = 0.2) and about 10-15% ($x$ = 0.3) of the $ThMn_{12}$-type impurity phase (Fig. 2). Thus we assumed that solubility limit of Ni in $U_2(Fe_{1-x}Ni_x)_{13.6}Si_{3.4}$ is about $x$ = 0.3. Within this homogeneity range, a slight decrease of the lattice parameters is very similar to that of $U_2(Fe_{1-x}Co_x)_{13.6}Si_{3.4}$ (Fig. 1). As seen from the temperature scans of the magnetic moment, both $M_s$ and $T_C$ decrease monotonously with increasing Ni content. It is because Ni has low contributions to the magnetic moment and the exchange interactions in the $R_2T_{17}$ compounds. Their concentration dependences are compared with that of analogous Co solutions in Fig. 3.

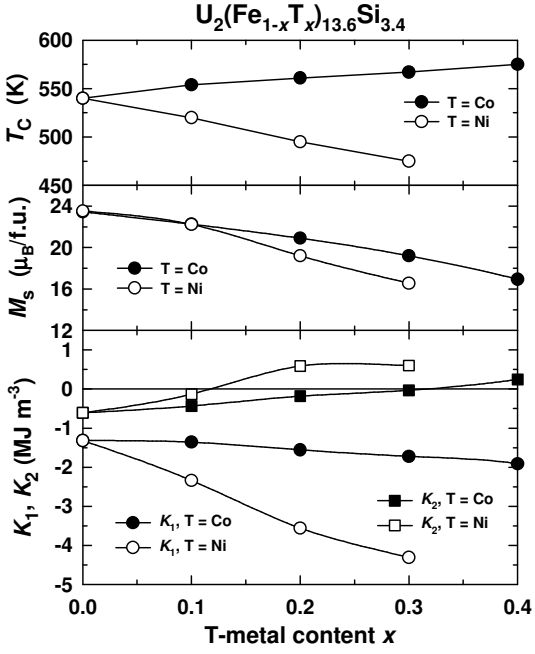


Fig. 3. The concentration dependences of $T_C$, $M_s$, $K_1$ and $K_2$ in $U_2(Fe_{1-x}T_x)_{13.6}Si_{3.4}$, T = Co, Ni.

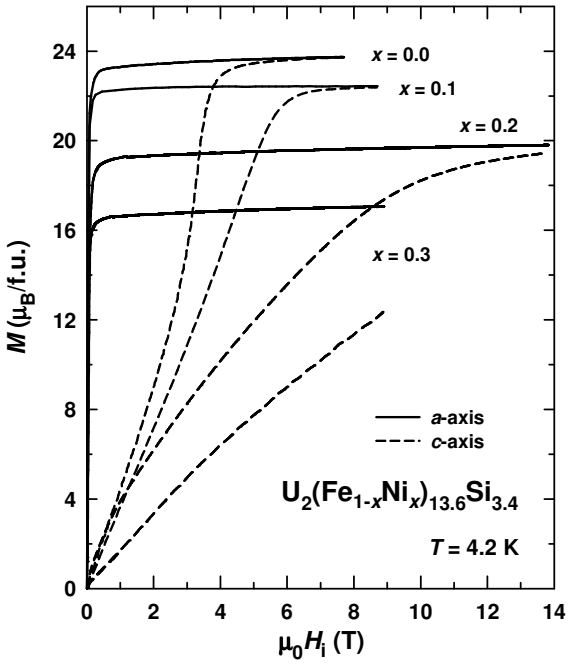


Fig. 4. The magnetization curves at 4.2 K along the principal axes for $U_2(Fe_{1-x}Ni_x)_{13.6}Si_{3.4}$ single crystals.

The magnetization curves presented in Fig. 4 show the easy-plane magnetic anisotropy for $x \leq 0.3$. A small anisotropy within the basal plane observed at $x$ = 0 [3] becomes negligible at higher $x$, similar to the Co system. The field-induced transition at $x$ = 0 described by a large negative $K_2$ disappears at $x$ = 0.1 where the $c$-axis curve is practically linear and a negative curvature (described by positive $K_2$) develops at $x \geq 0.2$. Similar but slower evolution of the magnetic anisotropy was observed in $U_2(Fe_{1-x}Co_x)_{13.6}Si_{3.4}$ where $K_2$ changes its sign at $x$ = 0.3 (Fig. 3). The absolute value of $K_1$ increases with increasing $x$ in both Co and Ni systems. The large anisotropy constants observed at $x$ = 0.2 and 0.3 cannot be provided by 3d-metal sublattice and therefore indicate a magnetic state of uranium.

This work is a part of the research project AVOZ10100520 and has been supported by grants GACR 202/06/0185 and GAAV IAA100100530.

## References

[1] T. Berlureau, P. Gravereau, B. Chevalier, J. Etourneau, J. Solid State Chem. 104 (1993) 328.
[2] A.V. Andreev, E.A. Tereshina, E. Šantavá, K. Koyama, Y. Homma, I. Satoh, T. Yamamura, Y. Shiokawa, K. Watanabe, J. Alloys Comp. (2007), in press (doi:10.1016/j.jallcom.2006.10.096).
[3] A.V. Andreev, Y. Homma, T. Komatsubara, Y. Shiokawa, I. Satoh, J. Alloys. Comp. 422 (2006) 6.

# P3

## Secondary phase formation upon hydrothermal leaching of $UO_{2+x}$ at 70°C and 150°C and interaction with Np(V)

**O.N. Batuk[1], St.N. Kalmykov[1], E.V. Zakharova[2], Yu.A.Teterin[3]**

*[1] Lomonosov Moscow State University, address: radiochemistry division, chemistry department, MSU, Leninskie Gory, Moscow, 119992, Russia, e-mail: batuk@radio.chem.msu.ru*
*2 Frumkin Institute of Physical Chemistry and Electrochemistry, Moscow, Russia*
*3 Research centre "Kurchatovskiy institute", Moscow, Russia*

The understanding of processes and mechanisms of radionuclide leaching from spent nuclear fuel (SNF) upon its storage in geological conditions is important for performance assessment (PA) of such repositories. Neptunium-237 is the radionuclide of prior importance for PA since its long half-life ($2.14\times10^6$ years) and potentially high mobility in oxidizing conditions. On the other hand the behavior of $UO_{2+x}$ (that is the main component of SNF) in hydrothermal conditions and its interaction with Np(V) is an important and less studied issue.

*Conditions of hydrothermal experiments.* Behavior of industry produced $UO_{2+x}$ sample upon hydrothermal conditions at 70°C and 150°C was studied in oxidizing conditions. The initial sample was characterized by scanning electron microscopy (SEM), X-ray diffraction (XRD) and photoelectron spectroscopy (XPS). Oxygen coefficient for bulk sample was determined by polarography. Hydrothermal leaching of the sample was performed in teflon vessels placed into steel autoclaves. Simulated ground water was used as background solution, which consisted of Na, K and Ca carbonates and chlorides. $^{237}Np(V)$ was added to make the total concentration of $1\times10^{-6}$ M. The experiment was conducted during 6 months and samples of solid phases were taken periodically and analyzed by XRD, SEM-EDX and XPS to determine changes in bulk phase and on the surface. Concentrations of uranium and neptunium in solution were determined by alpha spectroscopy after micro- and ultrafiltration. Changes in main element composition were analyzed by ICP-MS. The partitioning of Np on the solids was studied by sequential extraction technique using sequential treatment by deionized water, 0.5 M acetic acid and 3 M nitric acid.

*Results and discussion.* The initial $UO_{2+x}$ sample had a bulk composition of $UO_{2.075}$ with stoichiometry on the surface close to $U_4O_9$. Cubic structure of $UO_{2+x}$ is maintained until $U_3O_7$ ($UO_{2.33}$). The lattice parameter was determined by XRD as 5.4638±0.0007 Å.

According to the XRD different leaching behavior of $UO_{2+x}$ samples at 70°C and 150°C was established. For sample leached at 70°C decrease of lattice parameter was observed (Table 1) that correspond to bulk oxidation, however the solid sample kept cubic structure. The presence of the secondary phases was not detected by XRD for this sample. For sample leached at 150°C the decrease of lattice parameter was smaller than for sample leached at 70°C. However the intense secondary phase formation was established. According to XRD the formation of shoepite ($UO_2(OH)_2$), Na and K uranium oxides, compreignacite ($Na_2[(UO_2)_3O_2(OH)_3]_2(H_2O)_7$) and $(Ca,Na,K)U_2O_7\cdot2H_2O$. According to SEM-EDX (Fig. 1) needle-like uranium phase formation was indicated that is possibly shoepite. However in case of sample leached at 70°C few needle-like crystals were established compared with sample leached at 150°C.

Table 1. Lattice parameters of $UO_{2+x}$ samples leached at 70°C and 150°C

| Sampling interval after beginning of experiment | lattice parameter, Å | |
|---|---|---|
| | 70°C | 150°C |
| 1 week | 5.460(3) | 5.4604(8) |
| 1 month | 5.442(2) | 5.4621(7) |
| 1.5 months | 5.432(4) | 5.4640(4) |
| 2.5 months | - | 5.4641(5) |
| 4 months | 5.430(3) | 5.4363(6) |
| 6 months | 5.432(2) | 5.431(1) |

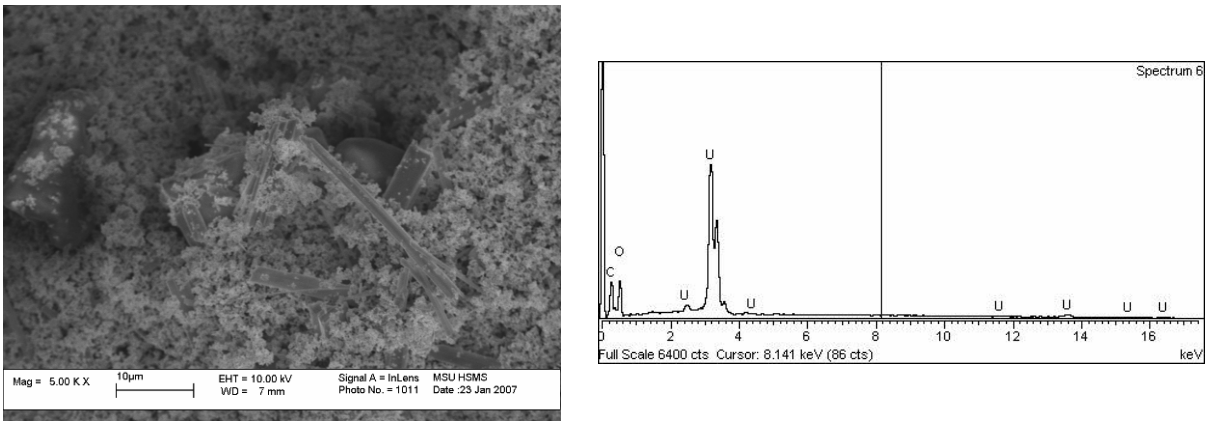


Fig. 1. SEM image of $UO_{2+x}$ sample leached at 150°C and EDX spectrum of needle-like crystal region (possibly shoepite).

After less than one week of neptunium interaction with $UO_{2+x}$ in simulated groundwater solution at hydrothermal conditions quantitative sorption of neptunium was observed at both temperatures. According to the sequential extraction only about 1% of Np was washed by deionized water that corresponds to the physically adsorbed species. The washing of samples by 0.5 M of acetic acid enabled to remove neptunium species sorbed by surface complexation mechanism. Earlier it was demonstrated that sorption of Np onto $UO_{2+x}$ under ambient conditions follows the surface complexation mechanism of Np(IV) and Np(V) at low pH and neutral pH interval correspondingly [1]. In this case only about 1% of neptunium was washed by 0.5 M acetic acid solution. Almost quantitative Np recovery was established by complete dissolution of the solids by 3 M nitric acid. The possible mechanism of Np sequestration could be explained either by formation of insoluble $NpO_2$ or its incorporation to U(VI) secondary phases. Earlier Burns et al. [2] established the incorporation of Np(V) to Na-compregnacite and uranophane while meta-shoepite did not incorporate Np.

We acknowledge to ISTC for financial support (project 2694).

**References:**

[1] O.N. Batuk et al., *J.Nucl.Matt.*, in press.
[2] P.C. Burns et al., *Radiochim.Acta* **92**, 151-159 (2004).

# P4

## An X-ray diffraction study to determine the composition and thickness of the oxide phases formed during plutonium oxidation

**Marina Dawes[1] and Peter Morrall[1]**

[1] *AWE, Aldermaston, Reading, Berkshire RG7 4PR, UK*
*marina.dawes@awe.co.uk*

Plutonium has a highly electropositive nature, and therefore has a perpetual corrosion layer on its surface. This oxide overlayer is multiphase and the quantity of each component oxide present is dependent on the reaction conditions.
Much work has been done on the study of plutonium oxidation as a function of oxygen pressure and temperature, but the majority has been by gravimetric analysis, i.e. by measuring weight gain of the sample, or pressure-volume-temperature, i.e. by measuring the amount of gas consumed. However, such studies only quantify the evolution of a general oxide. They are not able to determine which oxide phases are formed on the metal surface, nor their thickness.
This study presents initial results on the first quantification of the individual phases in the plutonium oxide overlayer during *in situ* oxidation. The quantification of each oxide layer is achieved using X-ray diffraction (XRD) and the application of a purpose-built mathematical model to deduce the thickness information.

# P5

## Anomalous increase of ATS scattering at the U $M_4$-edge of UNiGe upon magnetic order

**B. Detlefs[1,2], C. Detlefs[2], K. Prokeš[3], J. Prchal[4], A. Kolomiyets[1]**

*[1]European Commission, Joint Research Center, Institute for Transuranium Elements, Postfach 2340, 76125 Karlsruhe, Germany, e-mail: blanka.detlefs@esrf.fr*
*[2]European Synchrotron Radiation Facility, BP 220, 38043 Grenoble, France*
*[3]Hahn-Meitner-Institut, Glienicker Str. 100, D-14109 Berlin, Germany*
*[4]Charles University in Prague, Faculty of Mathematics and Physics, Dept. of Condensed Matter Physics, Ke Karlovu 5, 121 16 Prague 2, Czech Republic*

Anisotropic tensor susceptibility (ATS) or Templeton scattering may lift glide plane or screw axis extinction rules when the incident photon energy is tuned to an absorption edge. Generally this effect is attributed to a distortion of the charge distribution of the scattering atom by its neighbors in the crystal lattice, i.e. a local electric quadrupole moment. More recently, such quadrupoles (and the corresponding x-ray resonant scattering signals) induced by long-range magnetic order or formed directly were also observed, leading to renewed interest in orbital and quadrupolar ordering phenomena.

Several experimental and theoretical studies, however, indicate that scattering tensors of quadrupolar symmetry may also exist without a distortion of the local charge density, i.e. in the absence of an electric quadrupole moment on the scattering site.

Here we present an experimental study of resonant X-ray scattering (RXS) at the U $M_4$ edge of UNiGe. UNiGe was chosen because it crystallizes in the non-symmorphic space group *Pnma*, i.e. that it contains glide planes and screw axes that lead to the systematic extinction of certain Bragg reflections (*H K L*). The glide plane and screw axis extinction rules may be lifted when the scattering amplitude has a tensorial character. This may be the case for resonant X-ray scattering [1-3]. The effect is known as anisotropic susceptibility (ATS) or Templeton scattering. Templeton scattering may arise from irreducible representations that are totally symmetric under the local point group (in the case of UNiGe, these are U atoms positioned at 4*c* Wyckoff sites with $C_{1h}$ symmetry) but not under the global point group ($D_{2h}$ symmetry in *Pnma*). We show that in UNiGe the ATS scattering can occur at Bragg reflections with $H + L \neq 2n$.

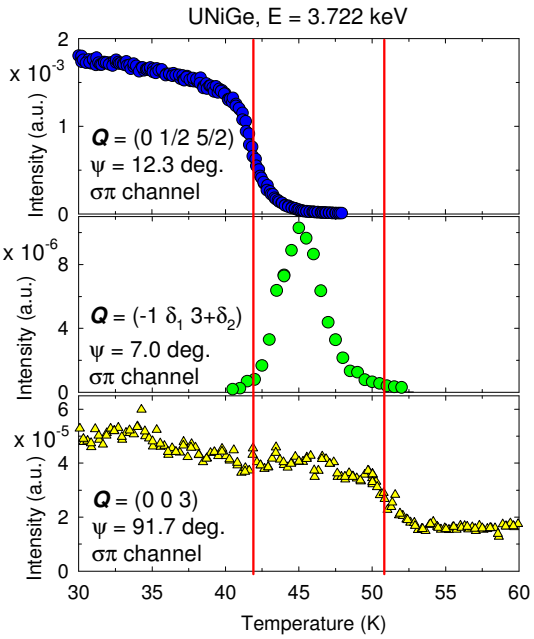


Fig. 1. RXS signal in UNiGe at U $M_4$-edge at three different scattering vectors. The first two correspond to magnetic dipole signal, the lower panel shows the ATS reflection Q = (0 0 3). Different azimuthal angle Ψ was chosen in order to maximize the signal.

The experiment was performed on the ID20 beamline at the ESRF Grenoble, France with the sample mounted in a displex closed-cycle cryostat with base temperature 10 K. The energy of the photon beam with incident σ polarization was tuned to the U $M_4$-edge

(3.728 keV) and polarization analysis of the scattered beam using Au(111) crystal was employed together with an azimuthal scan technique.

We found a significant increase in the (*H K L*) = (0 0 3) ATS reflection as the system orders magnetically below $T_N$ = 51 K (see Fig. 1), even though this reflection does not correspond to a second order harmonic of the magnetic wave vector where an induced quadrupolar moment would appear. The polarization and azimuthal dependence of the signal above and below $T_N$ are identical, indicating that only the amplitude changes but not its symmetry. We interpret this surprising behavior as a manifestation of the mechanism described by Lovesey et al. [4], where excited intermediate states with core holes polarized parallel or antiparallel to the local magnetic moment lead to two resonances at slightly different energies and opposite amplitudes. The resulting signal is confirmed to have quadrupolar symmetry (see Fig. 2). From the absence of any change of the signal at $T_M$ ~ 41.5 K we conclude that it relies on the presence of a local magnetic moment only, not its wavevector (nor its harmonic).

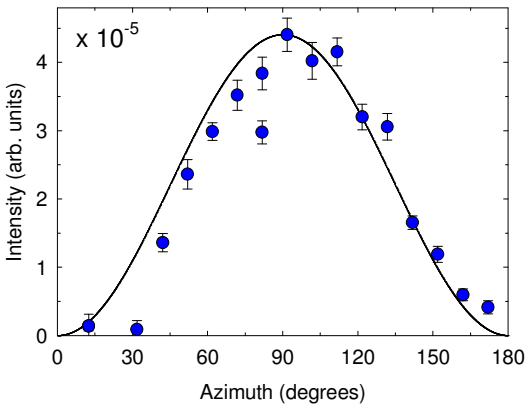


Fig. 2. RXS signal in UNiGe at ***Q*** = (0 0 3), U *M*4-edge, σπ polarization channel, *T* = 10 K.

B. D. acknowledges the European Commission for support given in the frame of the program 'Training and Mobility of Researchers'.

## References

[1] D. H. Templeton and L. K. Templeton, Acta Crystallogr. A 41, 133 (1985).
[2] V. E. Dmitrienko, Acta Crystallogr. A 40, 89 (1984).
[3] P. Carra and B. T. Thole, Rev. Mod. Phys. 66, 1509 (1994).
[4] S.W. Lovesey, E. Balcar, C. Detlefs, G. van der Laan, D.S. Silvia and U. Staub, J. Phys.: Condens. Matt. 15, 4511 (2003).

# P6

## <*kkk*> peaks in 3*k* magnetic structures: incommensurate *k* and behaviour in magnetic field

**B. Detlefs[1,2], S.B. Wilkins[1,2,3], P. Javorský[1,4], E. Blackburn[1,5], G.H. Lander[1]**

[1]*European Commission, Joint Research Center, Institute for Transuranium Elements, Postfach 2340, 76125 Karlsruhe, Germany, e-mail: blanka.detlefs@esrf.fr*
[2]*European Synchrotron Radiation Facility, BP 220, 38043 Grenoble, France*
[3]*Brookhaven National Laboratory, Physics Department, Bldg 510B, Upton, NY, 11973-5000, USA*
[4]*Charles University in Prague, Faculty of Mathematics and Physics, Dept. of Condensed Matter Physics, Ke Karlovu 5, 121 16 Prague 2, Czech Republic*
[5]*Dept. of Physics, Univ. of California, San Diego, USA*

Recently, new diffraction peaks of type <kkk> were observed in $UAs_{0.8}Se_{0.2}$ by resonant x-ray scattering (RXS) [1] and subsequently confirmed by neutron diffraction [2]. These extra reflections, albeit very weak ((less than $10^{-4}$ of the main Bragg peaks arising from magnetic order), are apparently associated uniquely with the 3*k* magnetic configuration and are indeed of magnetic dipole origin. The possibility of observation of these peaks in RXS experiment stems from the large resonant enhancement that occurs when the incident photon energy is tuned to the $M_4$ edge of uranium. The consistency between the results of two different experimental methods suggests little possibility of experimental artifacts, such as surface effects if observed only with RXS technique. The new reflections are associated with the phase coherence of the three different propagation directions that make up the 3*k* configuration and can be explained as raising from a 4th order term in the free-energy expansion that is proportional to $M_{kx}M_{ky}M_{kz}M_{kc}$, where the individual components of the magnetization propagating along the three perpendicular axes are $M_{kx}$ etc, and the term $\boldsymbol{k}_c = \boldsymbol{k}_x + \boldsymbol{k}_y + \boldsymbol{k}_z$ represents the *coherent* part of the different magnetisation distributions [3].

Here we bring further experimental evidence about these unusual diffraction peaks in two different systems $USb_{0.9}Te_{0.1}$ and $UAs_{0.8}Se_{0.2}$.

Although significant efforts were made in Refs. 1 and 2 to eliminate multiple scattering and higher-order diffraction effects, one way to ensure that such effects are further minimised is to examine a material in which the magnetic ordering is *incommensurate*. USb, a well-known (cubic) 3*k* antiferromagnet with $k = 1$, moves towards incommensurate *k* with a small doping of Te [4]. In our experiment, we show that in $USb_{0.9}Te_{0.1}$, $k = 0.596(2)$ r.l.u. just below $T_N$, as reported [4], but below about 160 K the material exhibits frustration with magnetic scattering distributed over a wide range of modulation vectors around $k \sim 0.667$ r.l.u. In addition to this extension of the modulation along the longitudinal direction [0 0 L], the scattering in the transverse direction is broad in *q* as well, showing the short-range ordering of the magnetic correlations. On cooling into the ordered state, no sign of any *external* structural distortion (i.e. a distortion from cubic to tetragonal) was observed. This is consistent with the fact that all the antiferromagnet configurations in the

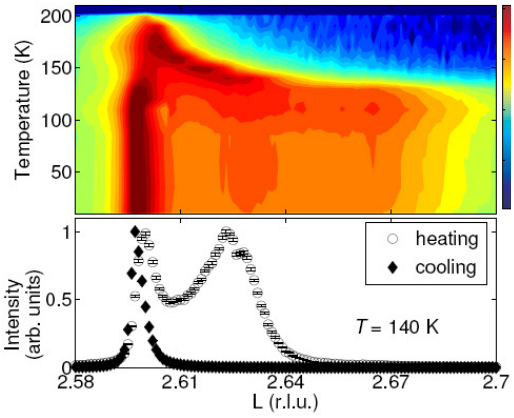


Fig. 1. Magnetic intensity from the sample of $USb_{0.9}Te_{0.1}$ as a function of scattering vector (00L) and temperature. The sample was first cooled to 10 K and then data collected as the sample was heated (upper panel). Lower panel shows data at $T = 140$ K on both heating and on cooling. Scale in the upper panel is logarithmic and linear in the lower one.

USb-UTe solid solutions are 3*k* in nature [4].

An azimuthal scan of the $\boldsymbol{Q}$ = (-*k k* 2+*k*) confirms that this reflection arises from the [-111] dipole component, showing the 3*k* nature of the configuration. Also the same level of intensity (as compared to the standard <*k*00> magnetic reflections) is consistent with data from $UAs_{0.8}Se_{0.2}$ [1]. This is very important confirmation as the observation of very weak reflections at highly symmetric lattice points must always be regarded with caution as complicated effects from higher-order components in the incident photon or neutron beam or multiple scattering may always produce weak reflections at these special positions. In the case of $USb_{0.9}Te_{0.1}$ with an incommensurate *k*, these special positions do not overlap.

We used the method of application of an external perturbation (magnetic field) to confirm the 3*k* nature of the $T^* < T < T_N$ phase in the previously studied commensurate system $UAs_{0.8}Se_{0.2}$. In Refs. 1 and 2 it was shown that the <*kkk*> reflections disappear (on cooling) below $T^* \sim 50$ K and it was suggested that $T^*$ corresponds to a transition between the high-temperature 3*k* to the lower temperature 2*k* state. Bulk measurements of specific heat and magnetisation showed anomalies also at this temperature [1]. With high-resolution photons we show that below $T^*$ there is an external lattice distortion to at least a tetragonal symmetry (and may be lower) and this results in a splitting of the (008) charge reflection. These results are consistent with the idea that the material transforms on cooling from the high-temperature 3*k* state to the low-temperature 2*k* state, which has lower than cubic symmetry.

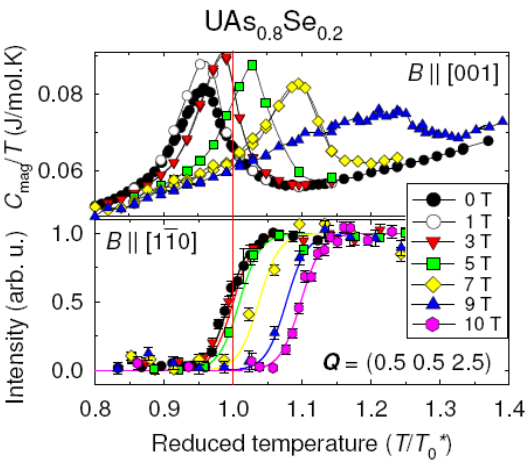


Fig. 2. Specific heat (upper part) on sample I divided by T and with the phonon contribution subtracted and (lower part) intensity of the (0.5 0.5 2.5) reflection in sample II of UAs0.8Se0.2 as a function of temperature normalized to T* at B=0.

We also show that the change in the intensity of the <*kkk*> reflection as a function of applied field follows (approximately) the temperature of the phase transition, allowing us to identify it as the one between 2*k* ($T < T^*$) and 3*k* ($T^* < T < T_N$) states. As the field is increased, the 2*k* state is stabilized at the expense of the 3*k* modulations. The rise of $T^*$ is much greater for $B \parallel$ [001] (specific heat data) than for $B \parallel$ [1-10] (RXS data). Such a behaviour can be expected from the comparison with data on UAs and $UAs_{0.75}Se_{0.25}$ showing similar field effects.

Both these experiments stress the need for a quantitative theory to explain also the intensities of the <*kkk*> reflections.

B. D. acknowledges the European Commission for support given in the frame of the program 'Training and Mobility of Researchers'.

## References

[1] N. Bernhoeft, J. A. Paixão, C. Detlefs, S. B. Wilkins, P. Javorsky, E. Blackburn, and G. H. Lander, Phys. Rev. B **69** 174415 (2004)

[2] E. Blackburn, N. Bernhoeft, G. J. McIntyre, S. B. Wilkins, P. Boulet, J. Olivier, A. Podlesnyak, F. Juranyi, P. Javorsky, G. H. Lander, K. Mattenberger, and O. Vogt, Phil. Mag. **86** 2553 (2006)

[3] C. Detlefs et al., unpublished

[4] P. Burlet, S. Quezel, J. Rossat-Mignod, O. Vogt, and G. H. Lander, Physica B **102** 271 (1980)

# P7

## Peritectic Reactions on the U-Fe-B system

**M.Dias[1] , P.A. Carvalho[2], O.Sologub[1], O.Tougait[3], H.Noel[3], C.Godart[4], E.Leroy[4], A.P Gonçalves[1]**

*[1]Departamento de Química, Instituto Tecnológivo e Nuclear, Sacavém, Portugal*
*marta.dias@itn.pt*
*[2]Departamento de Engenharia de Materiais, Instituto Superior Técnico, Lisboa, Portugal*
*[3]Sciences Chimiques de Rennes, Laboratoire de Chimie du Solide et Matériaux, UMR CNRS 6226, Université de Rennes 1, Rennes, France*
*[4]Chimie Mettalurgique des Terres Rares,ICMPR-CNRS UMR7182, Thiais, France*

In this work we present the cascade of peritectic reactions on the U-Fe-B ternary system. Our results are based in the analysis of X-ray powder diffraction and scanning electron microscope, complemented with energy dispersive x-ray spectroscopy.
The results of a systematic investigation of the U-Fe-B isothermal section at 950ºC show the existence of two new compounds, $UFe_4B$ (structure closely related with the $CeCo_4B$-type, and a small hexagonal cell a=4,932(1) Å and c=7,037(2) Å) and $U_2Fe_{21}B_6$ ($Cr_{23}C_6$- type structure, a=10,766 (4) Å) [1], in addition to the previously reported $UFeB_4$ and $UFe_3B_2$ [2].
All these ternary compounds melt incongruently and form by peritectic reactions. In order to obtain single phase materials it is necessary to achieve a deeper characterization of these reactions.
These peritetics reactions are clearly evidenced in the microstructure of samples such $U_2$:Fe:$B_{10}$, U:$Fe_3$:$B_3$ and $U_2$: $Fe_8$: $B_3$.
.

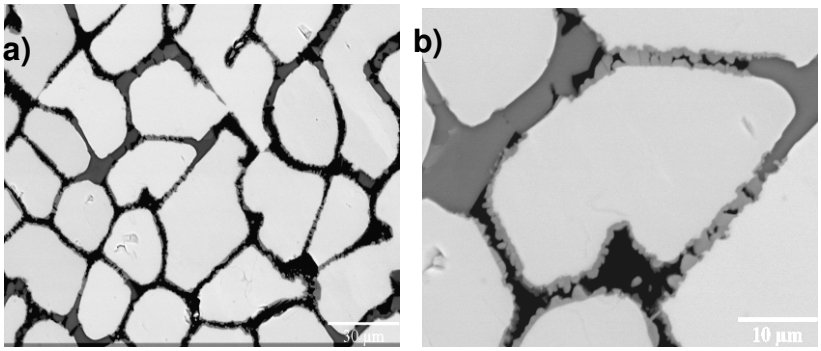

**Figure 3-** Low magnification BSE image presenting the typical microstructure of $U_2$:Fe:$B_{10}$, b) Magnified detail of a)

### References

[1] M.Dias, P.A. Carvalho, O.Sologub, O.Tougait, H.Noel, C.Godart, E.Leroy, A.P Gonçalves, *Intermetallics*, **15** (2006) 413.
[2] I.P. Valovka, Yu.B. Kuzma, Inorg.Mater. **14** (1978) 356.

### Acknowledgments

M.Dias thanks FCT the PhD SFRH/BD/21539/2005 fellowship. This work was partially supported by the exchange Program GRICES/EGIDE 2007-2008 and FCT/POCTI, Portugal, under nr. QUI/46066/2002

# P8

## Volatile Oxides of Some Actinides

**V.P.Domanov**

*Joint Institute for Nuclear Research, Dubna, Moscow reg., 141980, Russia, domanov@nrmail.jinr.ru*

It was known earlier that actinides oxides were not volatile. We managed to find conditions of transformation of some actinides into volatile oxides. A short review of the results on this topic is presented.

A distinctive property of the performed thermochromatographic (TC) experiments was the use of tracer quantities of the studied actinide in a chemically active form, for example, hydrides. The other features of these experiments were described earlier [1-3]: they were carried out using open quartz TC columns (i.d.=3 mm); oxygen served as a reagent and helium was a carrier gas; the flow rate of the gas mixture $\nu$=20 $cm^3.min^{-1}$, an initial sample contained a studied actinide was heated in the gas stream at 700-750°C; the starting temperature of the thermogradient (TG) section was 640±10°C and the final temperature was −165°C (cooling with liquid nitrogen); the temperature gradient $\alpha$ = −18°C; the duration of each experiment $\tau$ was 30 min.

In these conditions, actinides formed volatile oxides which were transported in the gas stream and adsorbed at certain temperatures. After completing every experiment the TG section was cut into equal portions and their inner surface was treated with a suitable solvent. The $\alpha$-sources were prepared from the obtained solutions and measured using an $\alpha$-spectrometer consisted of a silicon surface barrier detector and corresponding electronic units.

It was found that uranium formed volatile dioxide and trioxide that were adsorbed at 450±25°C and 250±25°C. The values of adsorption $-\Delta H_a^0$ enthalpy for $UO_2$ and $UO_3$ on quartz were calculated. They were equal to 172±6 $kJ.mol^{-1}$ and 126±6 $kJ.mol^{-1}$ correspondently.

Two plutonium radioisotopes $^{238}Pu$ and $^{239}Pu$ were used in similar experiments. Contrary to the previous results, plutonium formed three oxides. The centers of their deposition zones were registered at 450±30C°, 250±30C° and at negative temperature −105±25C°. It was shown that $PuO_2$ was adsorbed in the first zone, $PuO_3$ was deposited in the second zone and the last one was formed through adsorption of very volatile octovalent plutonium in the form of $PuO_4$. The calculated values of $-\Delta H_a^0$ for isolated plutonium oxides on quartz were equal to: 175±7 $kJ.mol^{-1}$ ($PuO_2$), 122±7 $kJ.mol^{-1}$ ($PuO_3$) and 47±8 $kJ.mol^{-1}$ ($PuO_4$).

The mass spectrometric measurements performed by Ronchi et al. [4] confirmed the occurrence of $UO_2$, $UO_3$, $PuO_2$ and $PuO_3$ in the gas phase.

Analogous experiments with traces quantities of $^{237}Np$ showed that neptunium was also to produce volatile oxides [5]. They formed two TC peaks located at 400-450°C and 220-270°C. It was managed to show that the first peak was formed by $NpO_2$ deposition and the second peak was formed by $NpO_3$ adsorption. Based on experimental data, the values of $-\Delta H_a^0$ $NpO_2$ on quartz was equal to 167±6 $kJ.mol^{-1}$ and $-\Delta H_a^0$ $NpO_3$ = 124±6 $kJ.mol^{-1}$.

One could readily see that the volatilities of dioxides formed by uranium, neptunium and plutonium were in close agreement. The values of $-\Delta H_a^0$ for trioxides of these actinides were also similar.

The recent experiments with tracers of $^{243}Am$ showed that formation of two volatile oxygen-bearing compounds is characteristic for americium [6]. They were adsorbed at 500±25°C and 330±25°C. Similar distribution of $\alpha$-along the TC column was obtained in the experiments with uranium and neptunium. Based on this, it was assumed that the first peak was formed through $AmO_2$ deposition and the second was connected with $AmO_3$ adsorption. The values

of $-\Delta H_a^0$ for the supposed oxides on quartz were calculated. They were equal to 180±7 kJ.mol$^{-1}$ ($AmO_2$) and 144±7 kJ.mol$^{-1}$($AmO_3$). The calculated values are higher than those for U, Np and Pu oxides. These differences do not contradict the known concept. Noting the similarity of physical and chemical properties of U, Np and Pu, in a certain valence state, Haissinsky [7] explained that "these properties change gradually with increasing atomic number, i.e. with decreasing atomic radius".
An experimental approach to the TC isolation of curium in the form of volatile oxides $CmO_2$ and $CmO_3$ is discussed.

## References

[1] V.P. Domanov, G.V. Buklanov, Yu.V. Lobanov. In: Abstract Book of the7th Inter.Conf. on Chemistry and Migration Behavior of Actinides and Fission Products in Geosphere, Lake Tahoe, C.E.A. Palmer (Ed.), 164 (1999).
[2] V.P. Domanov et al., Radiokhimiya, **44**, 106 (2002) (in Russian).
[3] V.P. Domanov et al., J. Nucl. Sci. Technol., **Suppl. 3**, 579-584 (Nov., 2002).
[4] C. Ronchi et al., J. Nucl. Mater. **280**, 111 (2000).
[5] V.P. Domanov. In: Recent Advances of Actinide Science. The Proceedings of the 8th Actinide Conference. Manchester, UK, 4-8 VII 2005, RSC publish., R. Alvarez et al. (Ed.), 275 (2006).
[6] V.P. Domanov. In: Application of Radiotraicers in Chemical, Environmental and Biological Sciences. Extend. Abstracts of the Inter. Conf. "ARCEBS 06", Jan. 23-27, 2006, Kolkata, India. S. Lahiri (Ed.), v.**2**, 58 (2006).
[7] M. Haissinsky, J.-P. Adloff. Radiochemical Survey of the Elements, Elsevier Publish. Comp., Amsterdam/London/New York, 164 (1965).

# P9

## Dissolution of phosphate based ceramics: implication of the neoformed phases

**E. du Fou de Kerdaniel,[1] N. Dacheux[1], R. Podor[2], J. Aupiais[3]**

[1] *Groupe de Radiochimie, Institut de Physique Nucléaire d'Orsay, Bât 100, Univ. Paris-Sud – 11, 91406 Orsay, France*
*dufoudek@ipno.in2p3.fr*
[2] *LCSM, Université H. Poincaré – Nancy I, BP 239, 54506 Vandœuvre lès Nancy, France*
*3 CEA/DAM/DIF/DASE/SRCE, BP12, 91680 Bruyères le Châtel, France*

In the field of the specific immobilization of radionuclides coming from the reprocessing of nuclear wastes and / or dismantled nuclear weapons, several phosphate matrices were studied. Potential candidates as Thorium Phosphate Diphosphate and associated solid solutions (β-$TAn^{IV}PD$, $Th_{4-x}An_x^{IV}(PO_4)_4P_2O_7$), monazite/brabantite solid solutions ($Ln^{III}_{1-2x}Ca_xAn_x^{IV}PO_4$) and britholites ($Ca_9Nd_{1-x}An_x^{IV}(PO_4)_{5-x}(SiO_4)_{1+x}F_2$) appeared as promising materials for the specific immobilization of tri- and tetravalent actinides. The optimization of the synthesis of such materials was realized and it was then necessary to test their chemical durability through several dissolution experiments.

The preparation of monazite/brabantite solid solutions and britholites samples was realized using a dry synthesis route, by grinding mechanically the powdered mixture then firing at high temperature ($T$ = 800-1400°C). The obtained powders were then characterized, shaped through uniaxial pressing then finally heated at high temperature ($T$ = 1300-1400°C) [1] leading to well densified samples. Afterwards the samples were put in contact with several acidic media at different pH and temperatures, in static and dynamic conditions. Aliquots were taken off at regular times and the concentrations of the elements present in solution were then measured using ICP-MS and ICP-AES in order to determine the associated normalized dissolution rates. Correlatively, the neoformed phases that precipitated at the surface of the solid were extensively characterized through various techniques including grazing XRD, EPMA, SEM and µ-Raman.

For all the samples, the dissolution appeared to be congruent during the first hours / days (depending on the solid) and rapidly became uncongruent in static conditions due to the precipitation, as instance, of thorium and lanthanides as neoformed phases. This problem was partly avoided by making dissolution tests with high renewal of the solution (called dynamic conditions). The normalized dissolution rates determined ranged from $10^{-5}$ g.m$^{-2}$.day$^{-1}$ ($10^{-4}$M $HNO_3$, $T$ = 90°C ) to $10^{-3}$ g.m$^{-2}$.day$^{-1}$ ($10^{-1}$M $HNO_3$, $T$ = 90°C ) for monazite / brabantite solid solutions and from $10^{-4}$ g.m$^{-2}$.day$^{-1}$ ($10^{-3}$ M $HNO_3$, $T$ = 25°C) to 5 g.m$^{-2}$.day$^{-1}$ ($10^{-1}$ M $HNO_3$, $T$ = 90°C) for britholites (Fig 1.) These values appeared to be in very good agreement with those found in the literature for natural samples [2 - 3].

The neoformed phases precipitated at the surface of britholites were clearly evidenced and fully characterized through several physico-chemical techniques. However, due to their very high chemical durability thus to the low quantities of neoformed phases, it was not possible to entirely characterize them in details during the dissolution of monazite / brabantite solid solution.

Grazing XRD, SEM and µ-Raman analyses suggested the formation of rhabdophane-type compounds during the dissolution of britholites (Fig 2). The (Nd + Ca +Th + U) / (P + F) moles ratios calculated for this phase was found to be close to 1 which allowed to propose the general formula $Nd_{1-2x}Ca_xTh_{x-y}U_y(PO_4,F) \cdot ½\ H_2O$. Another neoformed phase was identified to amorphous hydrated silica, $SiO_2 \cdot n\ H_2O$ (mainly evidenced by EPMA and µ-Raman experiments).

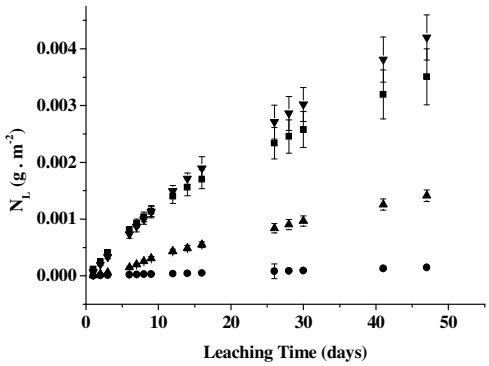


**Figure 1.** Evolution of the normalized leaching $N_L$(P) (■), $N_L$(Ca) (▼), $N_L$(Th) (●) and $N_L$(U) (▲) obtained during the dissolution of (Th , U) – britholites in dynamic conditions ($10^{-1}$ M $HNO_3$, $T$ = 90°C).

SEM and XRD experiments revealed the presence of two phases precipitated at the surface of leached monazite / brabantite samples. These were identified to Thorium Phosphate HydrogenPhosphate Hydrate (TPHPH), on the one hand, and rhabdophane-like compound of general formula $La_{1-2x}Ca_xTh_{x-y}U_yPO_4 \cdot ½\ H_2O$, on the other hand. Some complementary characterizations are now under progress.

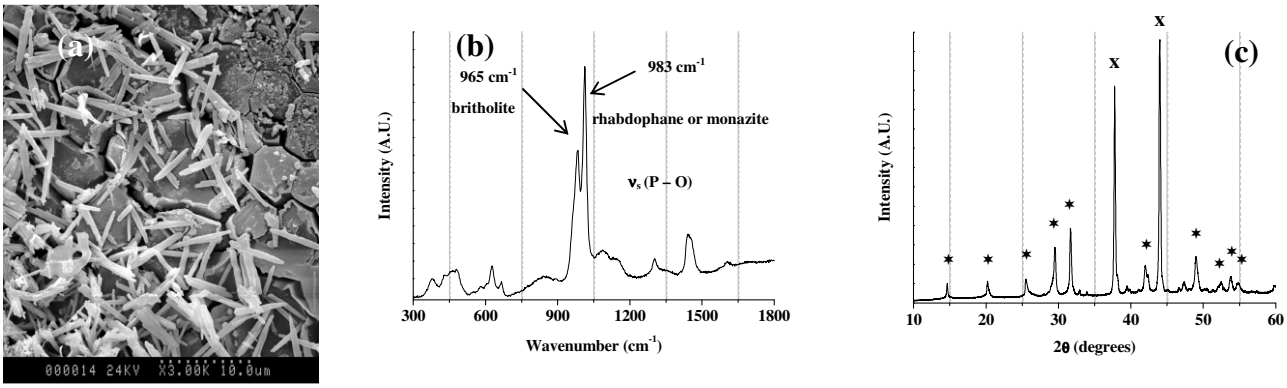


**Figure 2.** SEM micrograph (a), µ-Raman spectrum (b) and grazing XRD diagram (c) ($Nd_{1-2x}Ca_xTh_{x-y}U_y(PO_4,F) \cdot ½\ H_2O$ (★) and sample holder (x)) of Th – britholite leached in static conditions ($10^{-1}$ M $HNO_3$, $T$ = 90°C)

In order to check the thermodynamical stability of the neoformed phases observed during the dissolution, over-saturation experiments were also realized. The cations were mixed in acidic solutions (nitrate or chloride) and complexed with a phosphating reagent (5M $H_3PO_4$) in PTFE closed containers which were placed on a sand bath at $T$ = 150°C. By this way, $Ln_{1-2x}Ca_xTh_xPO_4 \cdot ½\ H_2O$ (Ln = La, Ce, Pr, Nd) – rhabdophane samples were prepared for $x \leq 0.2$. Their evolution was followed by XRD, SEM, EPMA and µ-Raman. It appeared that the segregation occurred after few hours to several months of precipitation time depending on the thorium weight loading; thorium being precipitated as TPHPH and lanthanides as $LnPO_4 \cdot ½\ H_2O$ - rhabdophane. Due to their very low solubility constants, both phases exhibit some properties of interest for the retention of radionuclides.

## References

[1] O. Terra, N. Dacheux, F. Audubert, R. Podor, *J. Nucl. Mater.*, 352, **224** (2006).
[2] C. Chaïrat**,** E. H. Oelkers, J. Schott and J. E. Lartigue, *J. Nucl. Mat.*, 354, **14** (2006).
[3] E.H. Oelkers, F. Poitrasson, Chem. Geol.**,** 191, **73** (2002)

# P10

## Hydrothermal syntheses and structure of $U_2(C_4O_4)_3(OH)_2$, the first $U^{4+}$ squarate hydroxyde

**L. Duvieubourg-Garela[1], F. Abraham[1], S. Grandjean[2].**

*1- UCCS -Equipe Chimie du Solide , UMR CNRS 8181, ENSCL-USTL, B.P. 90108, 59652 Villeneuve d'Ascq Cedex, France*
*2- Laboratoire de Chimie des Actinides, CEA VALRHO/DRCP/SCPS, Bât 399 BP 17171, 30208 Bagnols sur Ceze Cedex, France*

Among actinides, uranium, the heaviest natural element, is the most studied since depleted uranium is easy to manipulate with, it is produced industrially for nuclear industry, and it is an important constituent of nuclear waste. Uranium (IV) is easily oxidized to U(VI), so uranyl chemistry is extensively studied. However, in some nuclear industry processes involving precipitation by organic acids, tetravalent uranium is used preferentially to hexavalent uranium. In this case, hydrazinium nitrate ($N_2H_5^+$, $NO_3^-$) is added to the solution to stabilize tetravalent uranium. The precipitation of U(IV) by oxalic acid has been largely studied. In our group we are studying the precipitation of U(IV) by other organic acids, the first goal of this study is to determine all the compounds suitable to be formed. Using mild hydrothermal reaction between a solution of U(IV) added with squaric acid, single crystals of the first $U^{4+}$ squarate hydroxyde $U_2(C_4O_4)_3(OH)_2$ have been isolated. The crystal structure of this new compound built from original dimeric units of $U^{4+}$ polyhedra is described in this presentation.

The crystal structure has been determined from single crystal X-ray data collected at 298 K with a Bruker SMART CCD 1K diffractometer and refined by full-matrix least-squares methods to agreement indices R = 0.0279 and wR = 0.0827 calculated for 1227 unique observed reflections ($I > \sigma(I)$). The symmetry is orthorhombic, space group Pbcn with a = 9.029(2), b = 10.253(2), c = 17.497(4) Å. The $U^{4+}$ atom is nine-coordinated by oxygen atoms that belong to six squarate ligands and to two hydroxide ions with U – O distances in the range 2.256 – 2.415 Å (Fig. 1). Two $UO_8$ polyhedra related by an inversion center share their OH – OH edge to form a dimeric unit $U_2O_{14}$. The U – U distance within the dimmer is 3.869(1) Å. The four oxygen atoms of each squarate ion coordinate four different U atoms leading to a three dimensional arrangement of $U_2O_{14}$ dimers and squarate molecules (Fig. 2). Whereas dimeric units of uranium-centered oxygen polyhedra have already been described in $U^{6+}$ inorganic and organic compounds, $U_2(C_4O_4)_3(OH)_2$ is the first example of dimerization of $U^{4+}$ oxygen polyhedra.

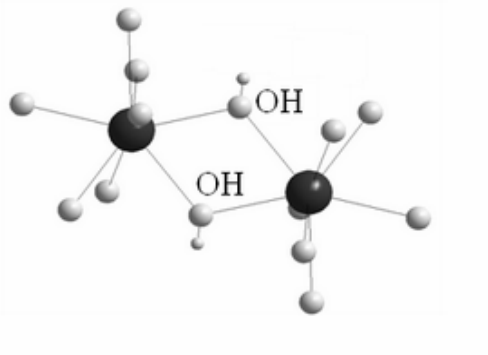


Fig.1 The dimeric unit $U_2O_{14}$ in $U_2(C_2O_4)_3(OH)_2$

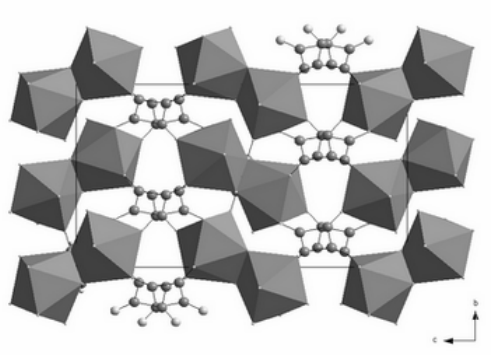

Fig.2 The three dimensional arrangement of $U_2O_{14}$ units connected through squarate ions

# P11

## Hydroxyl bridges in uranyl oxalates and squarates

**L. Duvieubourg-Garela[1], F. Abraham[1] and S. Grandjean[2].**

*1- UCCS -Equipe Chimie du Solide , UMR CNRS 8181, ENSCL-USTL, B.P. 90108, 59652 Villeneuve d'Ascq Cedex, France*
*2- Laboratoire de Chimie des Actinides, CEA VALRHO/DRCP/SCPS, Bât 399 BP 17171, 30208 Bagnols sur Ceze Cedex, France*

Uranyl structural chemistry is the object these last years of a considerable development. Many new inorganic uranyl compounds have been described [1], in particular in our research group several uranyl vanadates with 2D or 3D arrangements of uranyl and vanadates polyhedra have been characterized [2]. Complexes of uranyl ion with organic ligands such as carboxylates, and particularly oxalate, are also very important in nuclear fuel technology and waste management as, for example, the migration of hexavalent uranium as organic complexes. Many studies are also carried out to design new uranyl organic frameworks with interesting properties. Using mild hydrothermal conditions several uranyl oxalates and squarates containing hydroxide anions have been recently isolated [3-6]. In all these compounds, the uranyl coordination is completed in the equatorial plane by five oxygen atoms (that belong to oxalate or squarate ligands, hydroxide ions or water molecules) to form a pentagonal bipyramidal (pbp) environment. The hydroxide anions act as bidentate ligands and are shared between uranyl coordination polyhedra to form various polymeric units called hereafter structural polyhedral building units SPBU. The SPBU are further connected through the organic anion to one- or two-dimensional arrangements.

The goal of this presentation is to review these uranyl oxalate and squarate hydroxides using the SPBU description. Up today three oxalate hydroxides have been reported, the two forms, α (**1**) and β (**2**), of the compound $[(UO_2)_2(C_2O_4)(OH)_2(H_2O)_2]$ where the two water oxygens pertain to the coordination polyhedra of U, and the compound $[(UO_2)_2(C_2O_4)(OH)_2(H_2O)_2].H_2O$ (**3**) with a supplementary non-coordinated water molecule [3]. Three compounds $A[(UO_2)_2(C_2O_4)_2(OH)(H_2O)_2]$ (**4**) with $A = NH_4^+$ [7], $Na^+$ [4], $K^+$ [5] have also been described. Recently we reported the synthesis and the crystal structure of one uranyl squarate hydroxide $[(UO_2)_2(C_4O_4)(OH)_2(H_2O)_2]$ (**5**) and a mixed oxalate squarate complex $K[(UO_2)_2(C_2O_4)(C_4O_4)(OH)].H_2O$ (**6**) [6].

For $UO_2/OH = 2$ (compounds **4** and **6**), the equatorial plane of the $UO_7$ pentagonal bipyramid contains only one hydroxyl oxygen atom which is shared between two pbp to form dimeric SPBU, the other oxygen atoms of the equatorial plane belong to organic ligands that connect the SPBU to built two dimensional networks. For $UO_2/OH = 1$ (compounds **1**, **2**, **3** and **5**), the equatorial plane of the $UO_7$ pentagonal bipyramid contains two hydroxyl oxygen atoms that are in *cis* (compound **1** and **3**) or in *trans* positions (compound **2** and **5**) allowing, in this last configuration, the formation of linear chains of *trans* corner-shared polyhedra; these chains SPBU are further connected by oxalate (**2**) or squarate (**5**) anions to form 2D networks. For the *cis* configuration of OH groups, two types of SPBU are formed, dimeric units of edge-shared pbp in (**1**) and tetrameric units of corner-shared bpb in (**3**). These SPBU are further connected through oxalate anions to form 1D and 2D arrangements in (**1**) and (**3**), respectively.

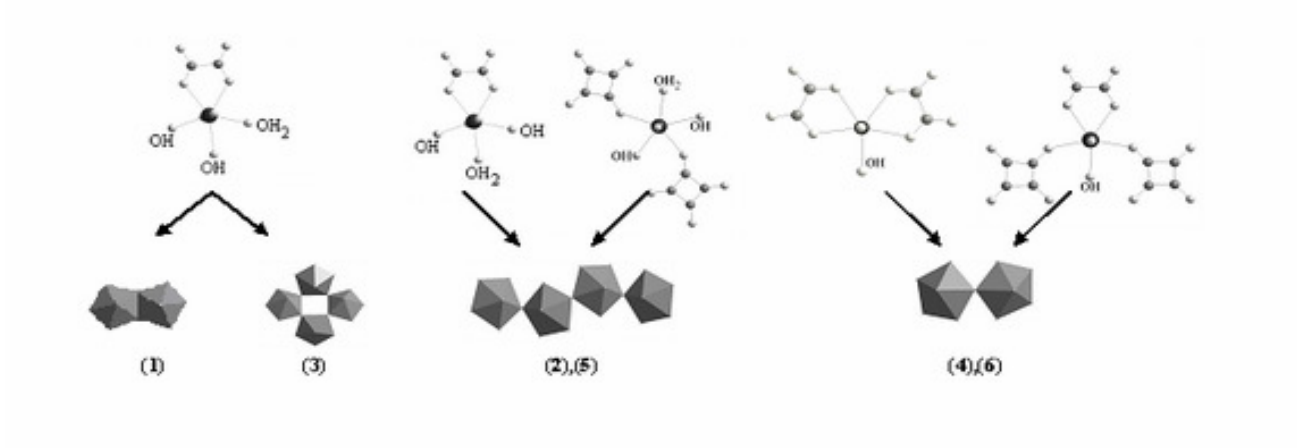


Fig. The various environments of uranium and the SPBU in uranyl oxalate and squarate hydroxides

Other SPBU of uranyl polyhedra with bidentate hydroxyl ions as sharing atoms can be imagined and the use of other dicarboxylates as connecting agents should lead to many new 1D or 2D arrangements, the use of tri- or tetra-carxoxylates should offer a fertile ground to search for new three dimensional frameworks built from these uranyl SPBU.

[1] P.C. Burns, The Canadian Mineralogist, Vol.43, 2005, 1839-1894

[2] F. Abraham and S. Obbade, "Structural Chemistry of uranium vanadates: from 2D to 3D networks" in "Structural Chemistry of Inorganic Actinide Compounds" Ed. S. V. Krivivitchev, P. C. Burns, I. G. Tananaev, Elsevier 279-313 (2007)

[3] L. Duvieubourg, G. Nowogrocki, F. Abraham, S. Grandjean, Journal of Solid State Chemistry 178 (2005) 3437–3444

[4] P. Thuéry, Polyhedron 26 (2007) 101-106

[5] P.A.Giesting, P.C.Burns, N.Porter, Mater.Res.Soc.Symp.Proc.Vol.893 2006

[6] L. Duvieubourg Garela, F. Abraham, S. Grandjean, Polyhedron, submitted (2007)

[7] M.Yu.Artem'eva, .Yu. N. Mikhailov, Yu.E.Gorbunova, L.B. Serezhkina, V.N. Serezhkin, Russian Journal of Inorganic Chemistry, Vol.28, n°9, 2003, 1337-1339

# P12

## Electrochemical dissolution of uranium monocarbide: first kinetics results

**B. Fourest,[1] A. Maslennikov[2], V. Sladkov[1]**

[1] *Institute of Nuclear Physics, Radiochemistry Group, University Paris-Sud, F-91406 Orsay Cedex, France, e-mail: fourest@ipno.in2p3.fr*
[2] *A. N. FRUMKIN Institute of Physical Chemistry and Electrochemistry, RAS, Moscow, Russia, e-mail:maslennikov@ipc.rssi.ru*

Uranium-based carbides (UC and mixed carbides (U,Pu)C) have been selected as potential fuels for reactors of Generation IV. The procedure which could be used for the carbide fuels reprocessing is expected to differ from the traditional PUREX process. In the simplified flowsheet for the carbide fuels, the dissolution step should play a determining role. Electrochemical techniques have already been applied either in order to accelerate the dissolution process of carbide fuels [1] or to destroy the organic species which have been found to be accumulated in the dissolution solutions [2]. In order to understand and improve the mechanisms involved in such applications, the knowledge of the fundamental properties of UC towards oxidation is essential. A preliminary study on the electrochemical processes occurring at a UC electrode, both in acidic and basic media, has recently been published [3]. The present work was aimed to estimate, through controlled potential electrolyses, the contribution of the electrochemical reactions pointed out by voltammetry to the efficiency of the UC dissolution.

The experiments were carried out with a three electrode system comprising a UC working semi-spherical electrode, an $Hg/Hg_2Cl_2$ reference electrode and a Pt wire counter electrode. The UC microspheres were prepared by arc melting. The absence of $UC_2$ and excess carbon in the matter of the working electrode was proved by XRD data. U(VI) determination in the electrolytes was performed either by a fluorescence technique, in 0.5 $MH_3PO_4$, or by a capillary electrophoresis (CE) procedure developed for this purpose.

According to [1], the voltamograms (or "Multistep Potential Sweep Coulometry" MPSC curves) obtained at a UC electrode in acid solutions can be decomposed in different (passive, pseudopassive and transpassive) regions (see the insert of Fig. 1). The electrolyses in 1M $HNO_3$ and, for comparison, in 1M $HClO_4$, were thus carried out at 0.5, 1.0 and 1.3 V/SCE,

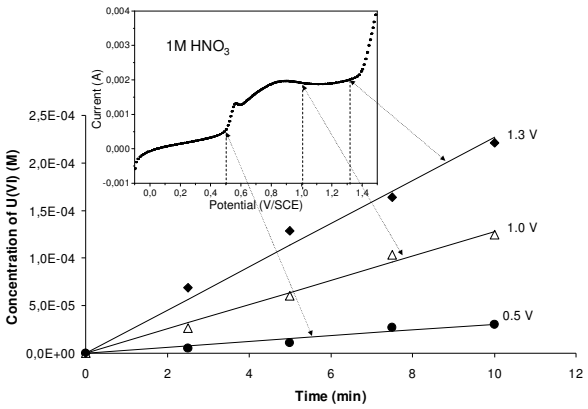


Fig. 1: Variations of U(VI) dissolved during controlled potential electrolyses at a UC electrode (S ~ 0.1 $cm^2$ , factor of dilution :10) in 1M $HNO_3$ (V=20 ml). Insert: voltammogram obtained at 5 mV/s with the same electrode and electrolyte.

corresponding to the lower and upper boundaries of the pseudopassive region and to its middle (Fig. 1). In all runs, the concentration of dissolved U(VI) increased linearly with the time of electrolysis, at least for the first ten minutes after potential application (see Fig. 1). The related kinetics constants were measured to increase from 46±3 mg $cm^{-2}$ $h^{-1}$ at 0.5 V to 342±18 mg $cm^{-2}$ $h^{-1}$ at 1.3 V/SCE, in accordance with the increase of the current (LV curves) or charge (MPSC curves) passing trough the cell. The dissolution rate constants obtained in 1M $HNO_3$ were higher than in 1M $HClO_4$, even though the voltammograms or MPSC curves were comparable in the range of potential under consideration (insert of Fig. 2). This difference is accounted for a chemical oxidation of UC by $HNO_2$ accumulated in the electrolyte as a result of $NO_3^-$ ions reduction at E < 1.0 V/SCE. This conclusion is proved by the estimates of current efficiency (Table 1).

| Electrolyte | Dissolution rate constant, (mg $cm^{-2}$ $h^{-1}$) | | Current efficiency |
|---|---|---|---|
| | *PCE* | *CE* | (%) |
| 1M $HNO_3$ | 134 | 183 | 137 |
| 1M $HClO_4$ | 106 | 109 | 103 |

Table1: Results of PCE experiments carried out at 1 V/SCE.

The increase of electrolysis time up to 1 hour resulted in the deviation of UC dissolution kinetics from linearity (Fig. 2). Apparently, this decrease of dissolution rate is associated with the growth of the thickness of the pseudo-passive film (products of primary oxidation of UC carbon) at the UC electrode surface. The latter statement is found in good compliance with the current density decrease in time, observed during PCE experiments (Fig. 2).

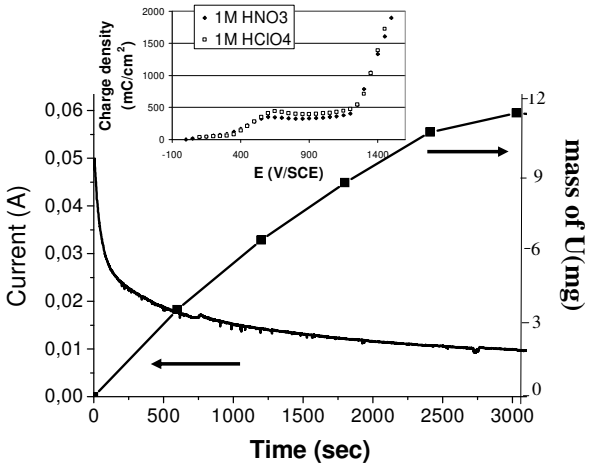


Fig. 2: Long duration (1 hour) electrolysis of a UC microsphere at 1.1 V/SCE in 1M $HClO_4$; Evolution of the current density and of the total mass of dissolved U(VI) in 20 ml of solution.
Insert: examples of MPSC curves or plots of the charge density passed through the UC electrode and integrated over 1 minute as a function of the applied potential

## References

[1] L.M. Ferris, "Head-end processes for graphite based and carbide reactor fuels" in *Progress in Nuclear Energy*. Series III. Process Chemistry, vol. 4. Ed. By E.A. Mason and A.T. Gresky. Pergamon Press, p. 121-170 (1970).

[2] A. Palamalai, S.K.Rajan, A. Chinnusamy, M. Sampath, P.K.Varghese, T.N.Ravi, V.R.Raman, G.B.Balasubranian, et al., *Radiochimica Acta* **55**, 29-35 (1991).

[3] A. Maslennikov, N. Boudanova, B. Fourest, Ph. Moisy, M. Lecomte, Proceedings 5P30 of Actinides 2005, Manchester, July 4-8 (2005).

# P13

## First-principles study of point defects and of helium incorporation in uranium carbide

**Michel Freyss, Julien Durinck**

*Commissariat à l'Energie Atomique (CEA), Centre de Cadarache, DEN/DEC/SESC/LLCC, Bâtiment 130, 13108 Saint-Paul lez Durance, France*
*e-mail: Michel.Freyss@cea.fr*

Mixed uranium and plutonium carbides (U,Pu)C or mixed nitrides (U,Pu)N are investigated as possible nuclear fuels for Generation IV reactors. The level of knowledge on these materials is not yet as high as for the standard $UO_2$ fuel, and basic research is still needed in order to understand their behaviour under irradiation. We focus here on the stability of point defects and of helium in the monocarbide UC, using ab initio electronic structure calculations. This approach enables to study some ground-state properties of UC, such as its magnetic properties, and to get insight into the stability of different kinds of point defects: uranium and carbon vacancies and interstitials, as well as Frenkel pairs and anti-site defects. The localization of helium produced by alpha-decay and its stability in the UC lattice are also investigated (see Fig. 1).

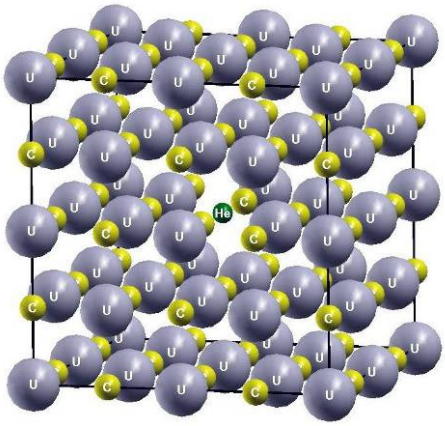


Fig. 1. Helium incorporation in the sodium chloride lattice of UC.

The calculations are performed using the Projector Augmented Wave method in the Generalized Gradient Approximation (GGA) of the Density Functional Theory (DFT), as implemented in the code VASP [1].
The results show that carbon defects are most favorable than uranium defects in UC, in agreement with the fact that carbides accommodate the deviation from stoichiometry by carbon defects [2]. Helium atoms are found to be most stable at a substitution uranium site, with a small incorporation energy of 0.7 eV comparable to the one found for helium incorporation in different actinide dioxides [3].

### References

[1] http://www.cms.mpi.univie.ac.at/vasp
[2] Hj. Matzke, Solid State Ionics **12**, 25 (1984).
[3] M. Freyss *et al.*, *Journal of Nuclear Materials* **352**, 144 (2006).

# P14

## $^{119}$ Sn Mössbauer spectroscopy in UPtSn

**P. Gaczyński,[1] A. Grykałowska,[2] B. Nowak [2] and J.C. Waerenborgh[1]**

[1] *Dept. Quimica, Instituto Tecnológico e Nuclear/CFMC-UL*
*Estrada Nacional 10, 2686–953 Sacavém, Portugal*
[2] *W. Trzebiatowski Institute of Low Temperature and Structure Research,*
*Polish Academy of Sciences, P.O. Box 1410, 50-950 Wrocław 2, Poland*

The specific heat data obtained on the half-Heusler-type compound UPtSn, crystallizing in a cubic MgAgAs-type of structure (space group $F\bar{4}3m$) revealed pronounced λ-like anomaly at $T_0$ = 35 K, suggesting some sort of phase transition [1,2]. The order parameter of this phase transition has not been established up to now. The results of magnetic measurements are controversial and do not provide definitive answer on the nature of the phase transition in UPtSn. Different authors [1-3] have emphasised the difficulty of preparing UPtSn samples that are completely free from any of the parasitic phases, especially from those having ferromagnetic properties at low temperatures, even if their contribution in the sample cannot be detected by other than magnetic methods. At first, this transition was expected to have a magnetic origin [2] similar to that of the isoelectronic and isostructural type-I antiferromagnet UNiSn with $T_N$ = 43 K. However, no magnetic reflections have been observed in neutron diffraction experiment (R. Troć and G. André, unpublished).
From the analysis of $^{119}$Sn and $^{195}$Pt NMR spectra the occurrence of the phase transition suggested by specific heat anomaly at $T_0$ = 35 K has been confirmed [4]. At ambient temperature all elements of UPtSn have the same site symmetry $\bar{4}3m$. Therefore, the observation of anisotropic line shape of both $^{119}$Sn and $^{195}$Pt resonance provided microscopic evidence for the symmetry lowering below $T_0$ in UPtSn although no external lattice distortion (*i.e.* a reduction in the total symmetry *e.g.* from cubic to tetragonal) was observed in the X-ray diffraction (XRD) experiment [4]. Such a behavior has been attributed to the occurrence of long-range uranium 5*f*-orbital ordering. [4].
However, an internal structural distortion below $T_0$ (*i.e.* atomic displacement from regular crystallographic positions) or magnetic ordering with strongly reduced magnetic moment, cannot be excluded.
The aim of the present work was to use the $^{119}$Sn Mössbauer spectroscopy for investigation of microscopic properties of UPtSn. To our knowledge no such data have yet been reported.
The Mössbauer absorber was prepared by packing in a perspex holder a powdered fraction of the same sample of UPtSn used in the previous studies [3,4]. In these reports a detailed description of the sample preparation, x-ray analysis, magnetic susceptibility, $^{119}$Sn and $^{195}$Pt NMR measurements may be found.
The $^{119}$Sn Mössbauer spectra were taken at 10 K and 295 K in transmission geometry using a constant acceleration spectrometer with a 10 mCi $Ca^{119m}SnO_3$ source. The velocity scale was calibrated with a metallic α-Fe foil. Isomer shifts, IS, are given relative to $CaSnO_3$ at 295 K. The spectra were analysed using Lorentzian lines.
The Mössbauer spectra at 295 K and 10 K (fig.1) contain only a single line. Change in IS values is explained by the second – order Doppler shift. The only parameter that changes in an unusual way with temperature is the linewidth (Γ) which increases by approximately 0.15 mm/s.
Two reasons may be suggested for the broadening of the absorption peak: (a) a non-zero quadrupole splitting (QS) or (b) a non-zero transferred hyperfine magnetic field ($B_{transf}$). To distinguish between these two possibilities two models were used in the analysis of the 10 K spectrum: Model 1: a quadrupole doublet; Model 2: a magnetic sextet with QS = 0. In both

models fixed linewidths similar to that found at 295 K were considered. Both refinements lead to IS = 1.86 mm/s and $\chi^2$ = 1.52. For model 1, QS= 0.32 mm/s and for model 2 $B_{transf}$ = 0.3T, were estimated.

The weak broadening of the Mössbauer line at 10K, leading to a negligible $B_{transf}$ value in model 2, seems to rule out magnetic ordering in UPtSn, similar to that observed in UNiSn [5], in agreement with the above referred neutron diffraction data. Slow magnetic relaxation phenomena, however, may not be excluded. On the other hand, since external crystallographic distortion is ruled out by low-temperature XRD, the most probable cause for the line broadening observed at 10 K seems to be the redistribution of electron density around Sn atoms caused by internal crystallographic distortion or by orbital ordering of U – 5f quadrupoles, as suggested in [4]

Further investigations in the region near 35 K to search for signatures of the phase transition indicated by specific-heat [1,2] and NMR [4] experiments are still underway and will be presented at the conference.

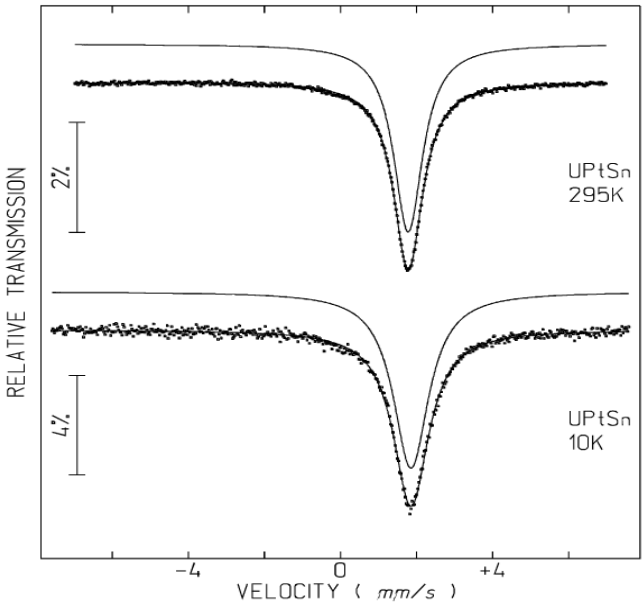


Figure 1. $^{119}$Sn Mössbauer spectra in UPtSn recorded at 10K and 295 K

## References

[1] T.T.M. Palstra, G.J. Nieuwenhuys, R.F.M. Vlastuin, J.A. Mydosh and K.H.J. Buschow, J. Appl. Phys. 63 (1988) 4279-4281

[2] R.Troć, M Strydom, P. de V. du Plessis, V.H. Tran, A.Czopnik and J.K. Cockroff, Philos. Magazine 83 (2003) 1235-1253

[3] A. Grykałowska, B. Nowak, J. Alloys Compd. (2006), doi:10.1016/j.jallcom.2006.11.072

[4] A. Grykałowska, M. Wołcyrz, B. Nowak, Phys. Rev. B 73 (2006) 212404

[5] T. Akazawa, T. Suzuki, F. Nakamura, T. Fujita, T. Takabatake, H. Fujii, J. Phys. Soc. Japan 65 (1996) 3661-3665

# P15

## Two independent magnetic sublattices in $U_{0.6}Fe_6Sn_6$ compound?

**P. Gaczyński*, L.C.J. Pereira, J.C. Waerenborgh**

*Dept. Quimica, Instituto Tecnológico e Nuclear/CFMC-UL, 2686-953 Sacavém, Portugal*

$A_xFe_6Sn_6$ (R = rare earth or U, $x \leq 1$) ternary compounds are derived from the binary CoSn–type (*P6/mmm*) FeSn compound and in the case of U or the smaller rare-earth atoms crystallize in the hexagonal $HfFe_6Ge_6$–type or as defect isotypes of the $SmMn_6Sn_6$ – type structure in the *P6/mmm* space group [1, 2]. Maximal amount of uranium atoms that can be introduced into FeSn sublattice was found to be 0.6 atoms *per f. u*. It increases the magnitude of the magnetic hyperfine field at the Fe sites but does not change the magnetic structure of the Fe sublattice. In both FeSn and $U_{0.6}Fe_6Sn_6$ compounds the Fe magnetic moments, $\mu_{Fe}$, lie on the *ab* – plane [1,3] in the 295-10K temperature range. In $U_{0.6}Fe_6Sn_6$ the Fe sublattice orders above 300 K. No well-defined magnetic transition assigned to U magnetic ordering was found on magnetization measurements [1].

$^{119}$Sn Mössbauer spectra of $U_{0.6}Fe_6Sn_6$ were recorded between 300 and 4 K. At 300 K one third of the Sn atoms in $U_{0.6}Fe_6Sn_6$ compound, those on 2*e* sites, lie on the *ab*-plane, surrounded by ferromagnetically coupled Fe atoms and exhibit a set of three nonzero magnetic hyperfine fields transferred from the neighbouring Fe atoms, $B_{transf}$ [4]. The magnitude of $B_{transf}$ was found to depend on the number of nearest neighbour (NN) and next nearest neighbour (NNN) uranium atoms.

The remaining two thirds of the Sn atoms lie between antiferromagnetically coupled Fe planes. They are expected to have zero $B_{transf}$ and, accordingly, at 300K only quadrupole doublets are assigned for Sn on the 2*c* and 2*d* sites [4]. At 4 K however a broadening of the central absorption peaks of the spectrum may be fitted considering slow relaxation of the direction of non-zero $B_{transf}$ on Sn(2*c*) and Sn(2*d*). The onset of this broadening of the central absorption peaks was now observed to occur between 130 and 150 K and to increase as temperature decreases down to 4 K. It may be explained by the switching on of $B_{transf}$ on the 2*c* and 2*d* sites between 130 and 150 K and by the increase of their magnitude as the temperature lowers. These $B_{transf}$ should not be attributed to the Fe sublattice as Sn atoms are located half-way between antiferromagnetically coupled Fe planes and no change of the magnetic structure of the Fe sublattice has been observed between 300 and 4 K. They may be related to magnetic ordering of the U sublattice.

**Acknowledgement**
This work was supported by SFRH/BPD/17649/2004 postdoctoral grant and POCTI (Portugal) under contract POCTI/CTM/38320/2001.

**References**

[1] J.C. Waerenborgh, L.C.J. Pereira, A.P. Gonçalves, H. Noël, *Intermetallics* 13 (2005) 490
[2] J.M. Cadogan, D.H. Ryan; *J Alloys Compds*. 326 (2001) 166
[3] L. Häggström, T. Ericsson, R. Wäppling, K. Chandra, *Physica Scripta* 11 (1975) 47
[4] P. Gaczyński, L.C.J. Pereira, J.C. Waerenborgh, *J. Alloys Compounds* (*in press*)

# P16

## On the theory of energy spectra of heavy atoms and ions

**Gediminas Gaigalas,[1,2] Zenonas Rokus Rudzikas[1]**

[1] *Vilnius University Institute of Theoretical Physics and Astronomy, A. Gostauto 12, LT-01108, Vilnius, Lithuania, e-mail: gaigalas@itpa.lt*
[2] *Vilnius Pedagogical University, Studentu 39, LT-08106, Vilnius, Lithuania*

The development of efficient methods of theoretical studies of complex many-electron atoms and ions, those having open *f*-shells included, continues to be one of the most important challenges for atomic physicists. Below we shall present the summary of our activities in this field. We do not restrict ourselves only to developing the methods of theoretical description of many-body systems, but also implement them in the set of computer programs, which may be and are used for modelling the structure and spectra of atoms and ions as well as the processes of their interactions with fields or particles.

Accounting for the symmetry properties of many-electron systems allowed us to formulate the efficient general method of calculation of matrix elements of various operators, describing the energy spectra or electronic transitions. Both relativistic and correlation effects may be taken into account while performing the sophisticated large scale calculations of energy levels, wavelengths and probabilities of electric and magnetic multipole transitions.

If relativistic effects are relatively small, then they may be accounted for as corrections in Breit-Pauli approximation, otherwise the relativistic wave functions (Dirac-Hartree-Fock approximation) must be used from the very beginning.

The use of the second-quantization method in coupled tensorial form as well as quasispin approach [1] leads to a general method of finding the algebraic expressions for matrix elements of one- and two-electron operators for an arbitrary number of shells in the atomic configuration, requiring neither coefficients of fractional parentage nor unit tenors [2]. For example, the matrix elements of two-particle operator, non-diagonal with respect to electronic configurations included, may be written in the form [2]:

$$
\begin{aligned}
&(\psi_u(LS)\| G \|\psi_u(L'S')) = \\
&= \sum_{n_i l_i n_j l_j, n_i' l_i', n'_j l'_j} (\psi_u(LS)\| \hat{G}(n_i l_i, n_j l_j, n_i' l_i', n_j' l_j') \|\psi_u(L'S')) \\
&= \sum_{n_i l_i n_j l_j, n_i' l_i', n'_j l'_j} \sum_{k_{12}, \sigma_{12}, k'_{12}, \sigma'_{12}} \sum_{K_l, K_s} (-1)^{\Delta} \Theta'(n_i\lambda_i, n_j\lambda_j, n_i'\lambda_i', n_j'\lambda_j', \Xi) \\
&\times T(n_i\lambda_i, n_j\lambda_j, n_i'\lambda_i', n_j'\lambda_j', \Lambda^{bra}, \Lambda^{ket}, \Xi, \Gamma) R(\lambda_i, \lambda_j, \lambda_i', \lambda_j', \Lambda^{bra}, \Lambda^{ket}, \Gamma), \quad (1)
\end{aligned}
$$

where $\lambda \equiv l, s, \quad \Lambda_l^{bra} \equiv (L_i, L_j, L_i', L_j')^{bra}, \Lambda_s^{bra} \equiv (S_i, S_j, S_i', S_j')^{bra}$ and $\Gamma$ refers to the array of coupling parameters connecting the recoupling matrix $R(\lambda_i, \lambda_j, \lambda_i', \lambda_j', \Lambda^{bra}, \Lambda^{ket}, \Xi, \Gamma)$ to the submatrix element

$T(n_i\lambda_i, n_j\lambda_j, n_i'\lambda_i', n_j'\lambda_j', \Lambda^{bra}, \Lambda^{ket}, \Xi, \Gamma)$. The expression has summation over intermediate ranks $k_{12}, \sigma_{12}, k_{12}', \sigma_{12}', K_l, K_s$ in $T(n_i\lambda_i, n_j\lambda_j, n_i'\lambda_i' n_j'\lambda_j', \Lambda^{bra}, \Lambda^{ket}, \Xi, \Gamma)$.

In this approach the usual coefficients of fractional parentage are replaced by so-called reduced coefficients (subcoefficients) of fractional parentage according to the following expression:

$$(l^N \alpha Q L S \,\|\, l^{N-1}(\alpha_1 Q_1 L_1 S_1)\, l) =$$

$$= (-1)^{N-1} N \left[(2Q+1)(2L+1)(2S+1)\right]^{-1/2} \begin{bmatrix} Q_1 & 1/2 & Q \\ M_{Q_1} & 1/2 & M_Q \end{bmatrix}$$

$$= \left(l \;\; \alpha Q L S \,\middle\|\, a^{(q\,l\,s)} \,\middle\|\, l \;\; \alpha_1 Q_1 L_1 S_1\right), \qquad (2)$$

Here $Q = 1/2\,(2l+1-v),\;\; M_Q = -1/2\,(2l+1-N),$ $\begin{bmatrix} Q_1 & 1/2 & Q \\ M_{Q_1} & 1/2 & M_Q \end{bmatrix}$ stands for Clebsch-Gordan coefficient and $a^{(q\,l\,s)}$ represents the second-quantization operator having ranks $q, l, s$ in quasispin, orbital and spin spaces respectively. Their use simplifies considerably the calculations of matrix elements, particularly in the case of complex electronic configurations, having several open shell, *f*-shells included.

Similar expression is obtained for the case of relativistic wave functions, as well. This methodology is implemented in a number of universal computer codes [3,4]. Preliminary results of the application of the methods developed and computer programs written to the calculations of the energy spectra of $Cm^{+4}$ will be presented. Convergency of the process of the accounting for the electron correlation effects as well as the accuracy of the results obtained have been investigated too.

**References**

[1] Z. Rudzikas, *Theoretical Atomic Spectroscopy*, (Cambridge University Press, Cambridge, 1997).
[2] G. Gaigalas, Z. Rudzikas, C. Froese Fischer, *J. Phys. B,* **30**, 3747 (1997).
[3] C. Froese Fischer, G. Tachiev, G. Gaigalas, M. Godefroid, Computer Physics Communications, (in press).
[4] S. Fritzsche, C. Froese Fischer, G. Gaigalas, Computer Physics Communications, **148**, 103 (2002).

# P17

## FP-LAPW study of the quantum size effects in (001) films of α-uranium

**Li Gan, Tang Tao**

*China Academy of Engineering Physics, P.O.Box 919-71, 621900, Mianyang, Sichuan, P.R.China*
*e-mail: 2002ligan@sina.com*

The all-electron full-potential linear augmented plane wave (FP-LAPW) method have been carried out to study the thickness dependences on properties of ultra-thin (001) films of α-uranium, up to seven layers thick, at the four levels of approximations, namely, NSP-NSO, NSP-SO, NSO-SP, and SO-SP. The incremental energy ($E_{inc}$), surface energy ($E_s$), work function ($W$), local magnetic moment per surface layer atom ($M_s$=$M_{spin}$+$M_{orb}$), spin polarization and spin-orbit energy per atom ($E_{sp}$ and $E_{so}$) are all rapidly convergent with respect to the film thickness (see Fig.1~ Fig.3 and Table 1), suggesting that a 3-layer film can be used to model the (001) surface of α-uranium to a fairly good approximation. The surface energy of the semi-infinite solid and work function for 7-layer film are calculated to be 0.105 eV/Å$^2$ and 3.63 eV, respectively, at SO-SP level, which are in a reasonable agreement with experimental values of 0.094 eV/Å$^2$ and 3.63~3.90 eV, respectively.

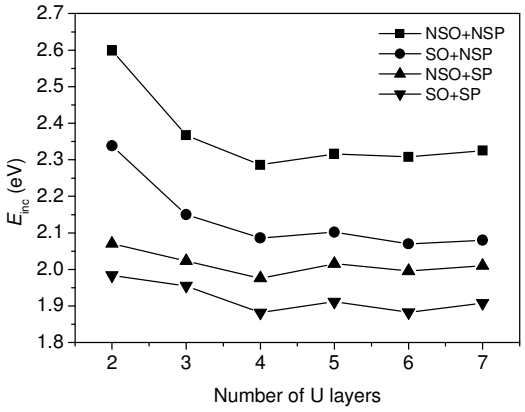


Fig. 1. Incremental energy versus number of U layers

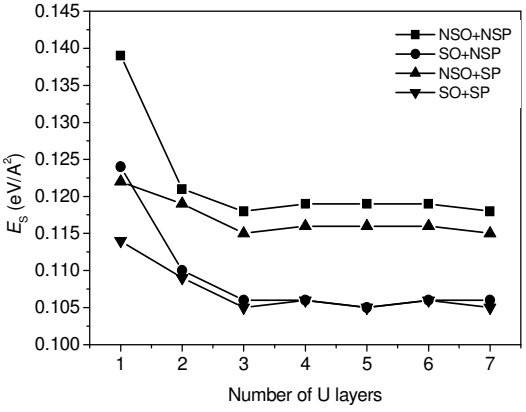


Fig. 2. Surface energy versus number of U layers

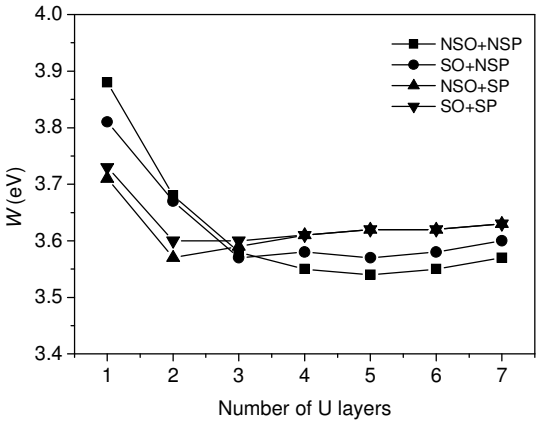


Fig. 3. Work function versus number of U layers

Table 1. Spin-polarization energies per atom $E_{sp}$, spin-orbit coupling energies per atom $E_{so}$ and local magnetic moments per surface layer atom $M_s$ ($M_{spin}$+$M_{orb}$) for α-U (001) $N$ layers ($N$=1-7)

| $N$ | $E_{sp}$ (eV) | | $E_{so}$ (eV) | | $M_s$ (μB) | |
|---|---|---|---|---|---|---|
| | NSO | SO | NSP | SP | NSO | SO |
| 1 | 0.310 | 0.193 | 2.435 | 2.319 | 2.3 | 2.2 |
| 2 | 0.022 | 0.016 | 2.305 | 2.299 | 0.9 | 0.8 |
| 3 | 0.017 | 0.010 | 2.276 | 2.267 | 1.0 | 0.9 |
| 4 | 0.015 | 0.005 | 2.266 | 2.256 | 1.2 | 1.0 |
| 5 | 0.014 | 0.004 | 2.258 | 2.248 | 1.2 | 1.1 |
| 6 | 0.012 | 0.004 | 2.248 | 2.241 | 1.3 | 1.1 |
| 7 | 0.011 | 0.005 | 2.244 | 2.237 | 1.3 | 1.0 |

## References


[1] J.Katz and E.Rabinowitch, The Chemistry of Uranium, (McGraw-Hill, New York, 1951).
[2] E.K.Schulte, Surf. Sci. 55, 427 (1976).
[3] A.K.Ray and J.C.Boettger, Phys. Rev. B 70, 085418 (2004).
[4] X.Wu and A.K.Ray, Phys. Rev. B 72, 045115 (2005).
[5] C.S.Barrett, M.H.Mueller, and R.L.Hitterman, Phys. Rev. 129, 625 (1963).
[6] P.Blaha, K.Schwarz, G.K.H.Madsen, D.Kvasnicka, and J.Luitz, WIEN2k, An Augmented Plane Wave plus Local Orbitals Program for Calculating Crystal Properties (Techn. Universität Wien, Austria, 2001).
[7] J.P.Perdew, K.Burke, andM.Ernzerhof, Phys. Rev. Lett. 77, 3865 (1996).
[8] D.D.Koelling and B.N.Harmon, J. Phys. C **10,** 3107 (1977).
[9] A.H.MacDonnald, W.E.Picket, and D.D.Koelling, J. Phys. C **13,** 2675 (1980).
[10] N.Stojić, J.W.Davenport, M.Komelj, and J.Glimm, Cond-mat. **20**, 0302423 (2003).
[11] J.G.Gay, J.R.Smith, R.Richter, F.J.Arlinghaus, and R.H.Wagoner, J. Vac. Sci. Technol. A **2**, 931 (1984).
[12] J.C.Boettger, Phys. Rev. B **49**, 16798 (1994).
[13] CRC Handbook of Chemistry and Physics, (CRC Press, Boca Raton, 1992)
[14] B.J.Hopkins and A.J.Sargood, Suppl, Nuovo Cimento **5**, 459 (1967).
[15] C.Lea and C.H.B.Mee, J. Appl. Phys. **39**, 5890 (1968).

# P18

## Models for the initiation of hydride attack sites on uranium

**Joseph Glascott**

*AWE, Aldermaston, Reading. UK. RG7 4PR*
*joe.glascott@awe.co.uk*

The attack of uranium by hydrogen generally occurs in a localised manner initially. The induction time to the initiation of the first observable hydride attack site decreases and the rate at which hydride attack sites are initiated after the induction time increases with increase of hydrogen pressure or temperature[1]. On the other hand, common gaseous impurities in the hydrogen atmosphere[2] or the presence of thick surface oxide films[3,4] can reduce the rate of attack of the metal. Furthermore, others have reported that hydride attack can be initiated in the metal beneath, and not at, the metal-oxide interface[5]. Any hydride initiation mechanism must explain all of these observations. Mathematical models of some possible mechanisms of hydride site initiation have been derived and are considered in the light of the above and other recent experimental data[6].

### References

[1] J. Glascott, Discovery – Science & Technology Journal of AWE, Issue 6 (2003)
[2] J. Bloch, D. Brami and A. Kremner, J. Less Common Met., 139, 371 (1988)
[3] L.W. Owen and R.A. Scudamore, Corr. Sci., 6, 461 (1966)
[4] R. Harker, J. Nuc. Mat. in press
[5] J.F. Bingert, R.J. Hanrahan, R.D. Field and P.O. Dickerson, J. Alloys & Compounds, 365, 138 (2004)
[6] T. Scott, G. Allen, I. Findlay and J. Glascott, Phil. Mag.. in press
[7] R. K. Schulze Los Alamos Report LA-UR-04-2672 (2004)
[8] M.W. Mallett and M.J. Trzeciak Trans. A.S.M., 50, 981 (1957)
[9] J. J. Katz and F. Rabinowitch, "The Chemistry of Uranium", Part 1, p 183ff, McGraw Hill (1951)
[10] W.D. Davies AEC Research & Development Report KAPL-1548 (1956)

# P19

## Magnetic Properties of Perovskites $BaUO_3$, $KUO_3$, Ordered Perovskite $Ba_2CoUO_6$, and $CoU_2O_6$

**Yukio Hinatsu,[1] Yoshihiro Doi[1]**

[1] *Division of Chemistry, Graduate School of Science, Hokkaido University, Sapporo 060-0810, Japan*
*e-mail: hinatsu@sci.hokudai.ac.jp*

Several uranium oxides in which uranium atoms are octahedrally coordinated by six oxygen atoms have been prepared. Their magnetic properties have been investigated through magnetic susceptibility, specific heat and neutron diffraction measurements. Both $BaUO_3$ and $KUO_3$ crystallize with cubic perovskite structure and $Ba_2CoUO_6$ is found to form in the ordered perovskite in which Co and U atoms are ordered.

Oxygen stoichiometric $BaUO_3$ shows temperature-independent paramagnetism over the temperature range between 4.2 K and room temperature, which is due to the octahedral oxygen coordination around the $U^{4+}$ ion [1].

$KUO_3$ shows an antiferromagnetic-type of transition at 16.8 K in the magnetic susceptibility vs. temperature curve. Neutron diffraction measurements have been performed on the powdered $KUO_3$ below and above the transition temperature. The neutron diffraction pattern measured at 10 K shows no appreciable difference from that measured at 50 K. A small ordered magnetic moment of $U^{5+}$ ion will make it very difficult to observe magnetic diffractions, even if a magnetic ordering occurs.

The temperature dependence of the reciprocal magnetic susceptibility for $Ba_2CoUO_6$ shows a ferromagnetic ordering below 9.1 K. Measurements of the specific heat also indicate the existence of the second-order transition at the same temperature. The magnetization measurements show that a large field dependence of the susceptibility is present at 5 K. The saturation moment is obtained to be 2.3 $\mu_B$, which is smaller than the saturation moment determined from the number of unpaired electrons, 3 $\mu_B$ [2].

Two compounds $CoU_2O_6$ and $NiU_2O_6$ are crystallized hexagonally in the $Na_2SiF_6$ structure, in which both cobalt (nickel) and uranium ions are in the distorted octahedral crystal field by six oxygen ions. Magnetic susceptibility and specific heat measurements indicate that $CoU_2O_6$ and $NiU_2O_6$ order antiferromagnetically at 32.2 and 35.6 K, respectively [3]. The analysis of the magnetic susceptibility data indicates that the ionic models $Co^{2+}U^{5+}{}_2O^{2-}{}_6$ and $Ni^{2+}U^{5+}{}_2O^{2-}{}_6$ are valid. Neutron diffraction measurements for $CoU_2O_6$ were performed at 10 K. The magnetic structure is a multi-sinusoidal structure with a propagation vector (0, 0, 1/6), in which the magnetic moments of the Co ions are parallel to a (1 1 0) direction. The magnetic moments of the U ions have a component of 0.46 $\mu_B$ along the (1 1 0) direction and a component of 0.25 $\mu_B$ along the (0 0 1) direction.

### References

[1] Y. Hinatsu, *J. Solid State Chem.*, **102**, 566 (1993).
[2] Y. Hinatsu and Y. Doi, *J. Solid State Chem.*, **179**, 3575 (2006).
[3] Y. Hinatsu, *J. Solid State Chem.*, **114**, 595 (1995).

# P20

## Ligand effect on $ThO_2$ dissolution. Leaching behaviour of $Th_{0.87}Pu_{0.13}O_2$.

**Solange Hubert,[1] Guillaume Heisbourg[1], Nicolas Dacheux[1], Philippe Moisy[2]**

[1] *Institut de Physique Nucléaire- Université Paris Sud- UMR8608, 91406 Orsay, France., e-mail: shubert@ipn.in2p3.fr*

[2] *CEA- Marcoule- 30207 Bagnols/Cèze Cedex, France, e-mail: moisy@amandine.cea.fr*

In the French underground repository (Bures), the groundwater is found to be highly charged with anions such as $Cl^-$ ($10^{-1}$ M) and $SO_4^{2-}$ ($10^{-1}$ M). In order to predict the dissolution behaviour of actinide dioxide, it is important to study the influence of such ligands on the chemical durability of actinide dioxide. $ThO_2$ has been considered as a reference material because $Th^{4+}$ is the only oxidation state in solids, and no redox reaction can occur during the dissolution. Moreover, it is well- known that one of the most important molecular oxidants identified in spent fuel dissolution experiments as products of radiolysis of water is hydrogen peroxide. Because $Th^{4+}$ is the most stable valence state, it cannot be oxidized by the hydrogen peroxide in the opposite of $U^{4+}$. However, hydrogen peroxide has a strong complexing affinity with $Th^{4+}$ that can affect the dissolution process.

Therefore, in order to provide the influence of complexing reagents in the leachate on the dissolution process, leaching experiments of $ThO_2$ were carried out in acidic solutions containing ligands such as perchlorate, nitrate, chloride, sulphate, and hydrogen peroxide with several concentrations.

At pH = 1, the release of Th and the dissolution rate of thoria are much greater in sulfate than in nitrate or chloride media. Nevertheless, compared to non complexing perchlorate media, the thorium release in nitrate and chloride is slightly larger as indicated in Fig. 1a.

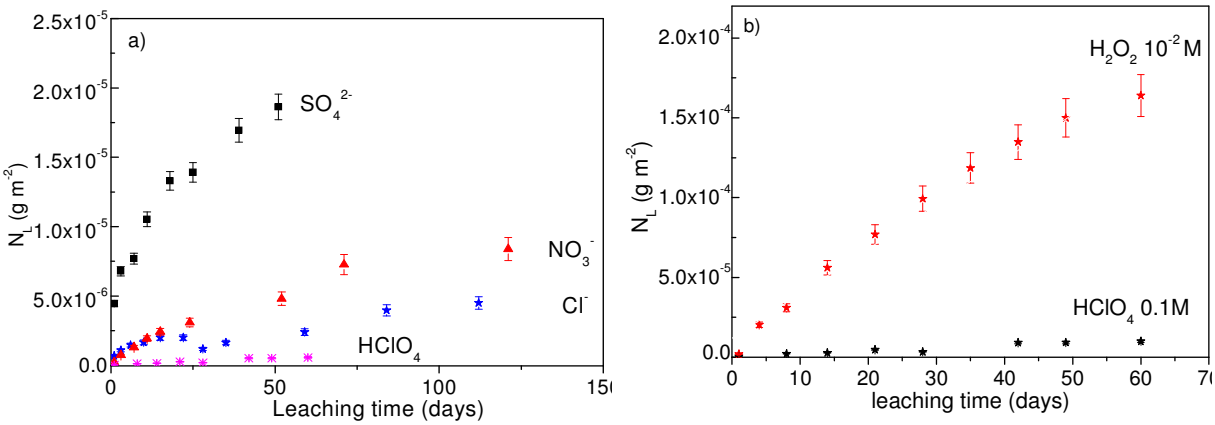


Fig.1. a) *Evolution of $N_L$ in $10^{-1}$ M $HClO_4$ (✳),$10^{-1}$ M HCl (★),$10^{-1}$ M $HNO_3$ (◢),$10^{-1}$ M $H_2SO_4$ (■),* b), *$10^{-2}$ M $H_2O_2$ in $10^{-1}$ M $HClO_4$ versus leaching time (Fig. 1b)*

Since $Th^{4+}$ is stable, it is obvious that complexing anions in the leachate, play an important role in the dissolution process. In addition to the protons, the ligands participate to the formation of more soluble activated surface complexes. Taking into account the equilibrium constant of $Th^{4+}$ with the different ligands [1-2], the release of thorium, as well as the dissolution rate increase with that of the complexation constant β. While nitrate and chloride media which are slightly complexing, $R_L$ has the same order of magnitude compared to perchlorate media, the presence of sulphate and peroxide in the leachate increases the normalized dissolution rate by several orders of magnitude. It is interesting to notice that the

normalized dissolution rate of thoria increases linearly with the equilibrium constant log $\beta_{11}$ of the ligands with thorium. The increase by 2 orders of magnitude of the normalized dissolution rate obtained in perchlorate containing $10^{-2}$ M $H_2O_2$, in comparison with the values obtained in perchlorate media indicates that hydrogen peroxide has stronger affinity with $Th^{4+}$ than sulphate ions.

The evolution of the normalized leaching $N_{L(Th)}$ obtained in $HNO_3$ and HCl for $ThO_2$ and $HNO_3$ for radioactive mixed oxide $Th_{0.87}Pu_{0.13}O_2$ with ligand concentration ranging from 5 M down to $10^{-3}$ M versus leaching time was also measured. From the linear variation of the logarithm of the normalized dissolution rate, $R_L$, with the logarithm of the proton concentration, the parameters describing the kinetics law of the dissolution was determined following the expression:

$$R_H = k'_T(\gamma_{H3O^+}[H_3O^+])^n = k'_{T,I}[H_3O^+]^n \qquad (1)$$

As it is the case for $ThO_2$ in nitrate media, the dissolution curve obtained for $Th_{0.87}Pu_{0.13}O_2$ presents an inflexion after 50 days of leaching. The normalized dissolution rate $R_L$ obtained after 50 days, ranges from about $10^{-6}$ g $m^{-2}d^{-1}$ in 5 M $HNO_3$, and 1.8 $10^{-7}$ g $m^{-2}d^{-1}$ in $10^{-1}$ M $HNO_3$, down to about $10^{-8}$ g $m^{-2}d^{-1}$ in $10^{-3}$ M $HNO_3$. The dissolution curves of $Th_{0.87}Pu_{0.13}O_2$ exhibit the same behaviour as the $ThO_2$ curves. However the normalized dissolution rate is about 4 to 10 times greater in the case of the solid solution compared to $ThO_2$ [3].

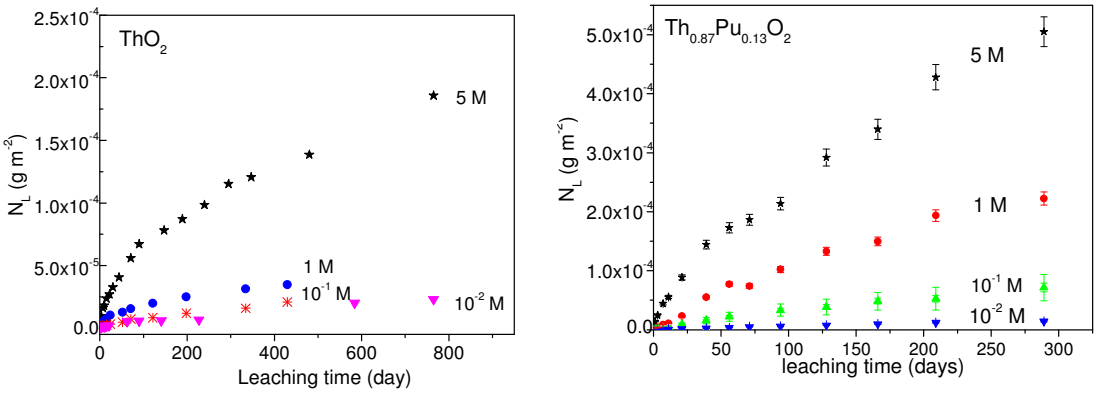


Fig. 2. Leaching of $ThO_2$ and $Th_{0.87}Pu_{0.13}O_2$ in several concentrations of $HNO_3$

Leaching measurements in several complexing media demonstrates that the dissolution rate of thoria is dependent on the ligands present in the leachate all the more as ligand has a strong affinity with $Th^{4+}$. This statement is important since that groundwater from the French repository contains large amount of complexing anions and that radiolysis effect are expected. Moreover, the release of Th/Pu mixed dioxide solid solution is found to be slightly greater than the $ThO_2$ one in the same leaching conditions.

## References

[1] L. Morss, N. Edelstein and J. Fuger *"The Chemistry of the Actinide and Transactinide Elements"* Third Edition Springer (2006).

[2] R. J. Lemire *"Chemical thermodynamic of neptunium and plutonium"* OCDE, Nuclear Energy Agency, Eds. Elsevier (2001).

[3] G. Heisbourg, S. Hubert, N. Dacheux, J. Ritt, *J. Nucl. Mater.* **321,** 141 (2003).

# P21

## Effect of Am doping on the superconductivity of $PuCoGa_5$

**F. Jutier, R. Jardin, E. Colineau, J.-C. Griveau, J. Rebizant, F. Wastin**

*European Commission, Joint Research Centre, Institute for Transuranium Elements, Postfach 2340, Karlsruhe, D-76125, Germany, e-mail: Franck.Wastin@ec.europa.eu*

The discovery of superconductivity at $T_c$ = 18.5 K in $PuCoGa_5$ [1] and $T_c$ = 9.5 K in $PuRhGa_5$ [2] have lead to a substantial impact given the nearly order-of-magnitude larger $T_c$ than any other *f*-electron intermetallic. Not only are these the first Pu-based superconductors, but also several of their features reveal both localized and itinerant *f*-electron behavior suggesting a "dual-nature" of Pu. On the one hand, with nearest *f-f* spacing well beyond the Hill limit and Curie-Weiss-like magnetic susceptibilities, these Pu-based superconductors appear to have localized 5*f* electrons. On the other hand, their enhanced Sommerfeld coefficients, $\gamma \approx 100$ mJ/mol-$K^2$, and BCS-like jump $\Delta C/\gamma T_c$, are consistent with bulk superconductivity developing out of a relatively narrow, correlated band of conduction electrons [2-4]. Although this picture of Pu's 5*f* dual character may still leave open the possibility that superconductivity is conventional, power-laws in specific heat [3] and, most convincingly, in the spin-lattice relaxation rate $1/T_1$ well below $T_c$ of $PuCoGa_5$ [5] and $PuRhGa_5$ [6] argue strongly for a superconducting gap with nodes. The most accepted picture establishes spin-singlet pairing in $PuCoGa_5$, similar to what was evidenced in the isostructural heavy-fermion superconductor $CeCoIn_5$, and the formation of an unconventional superconducting state favored by low-energy antiferromagnetic spin fluctuations [7].

The effects doping on the *f*- or *d*-element sites [8] and of self-irradiation on the superconductor $^{239}PuCoGa_5$, where the deterioration of the critical temperature $T_c$ is weak (~ -0.2 K / month), have been previously presented [9]. Increasing the radiation effects in this superconductor will be then rich in informations about the superconducting nature of this class of compound. One possibility is to "dope" $^{239}PuCoGa_5$ with a more active radioelement. Americium isotopes were chosen (half-life time of $^{241}Am$ and $^{243}Am$ are respectively 433 and 7400 years, to be compared to 24,000 years for $^{239}Pu$). Furthermore, Am doping is also interesting because it is equivalent to incorporate a non-magnetic impurity. Indeed, the Am atoms substituting Pu atoms would have an electronic configuration [Rn] $5f^6$ (oxidation number +III), resulting in a total angular momentum *J* equal to 0. In the present contribution, we report on effects of doping with Am both from the point of view of modifying the overall *5f* electrons count (no isotope effect) and from the ageing (isotope relative) effects by self-irradiation.

First looking from the aspect of doping effect on the *f*-site (neglecting the self-irradiation effect, fresh samples), figure 1 shows a dramatic decrease of the initial values of $T_c$ versus the americium amount. This shows that the *5f* electrons are indeed involved in the superconductivity and agrees with an unconventional superconducting nature of $PuCoGa_5$ because of the non-magnetic nature of the incorporated americium [10]. Looking at the ageing effect and its influence on the critical parameters tuning, it is interesting to note that independently of the intrinsic characteristics, a similar evolution as a function of the c/a ratio is preserved in iso-electronic series. A further discussion of both effects will be presented in our contribution.

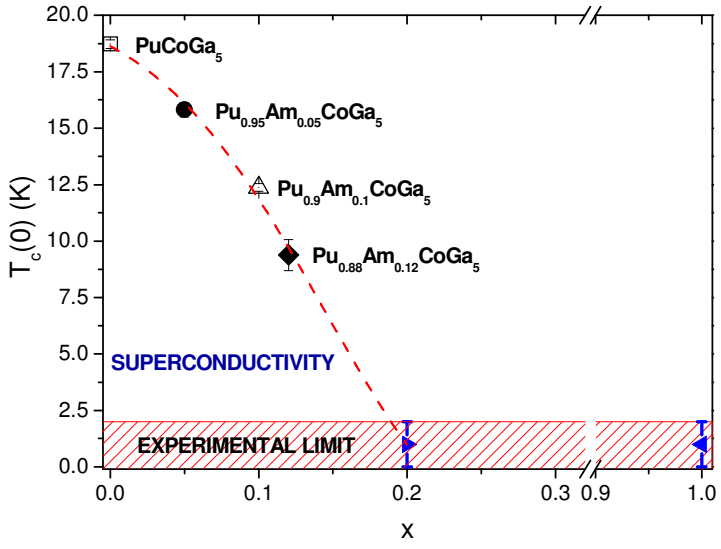


Fig. 1: Superconducting phase diagram of $^{239}Pu_{1-x}Am_xCoGa_5$ compounds, representing the initial critical temperature $T_c(t=0)$ (i.e. with no self-irradiation damage) versus the amount of Am content $x$. The experimental limit corresponds to the minimal temperature of 2K reachable by our measurement apparatus of which the temperature precision at the sample level can also be affected due to self-heating effects mainly coming from the $\alpha$-decay of americium. The dashed curve is a guide for the eye.

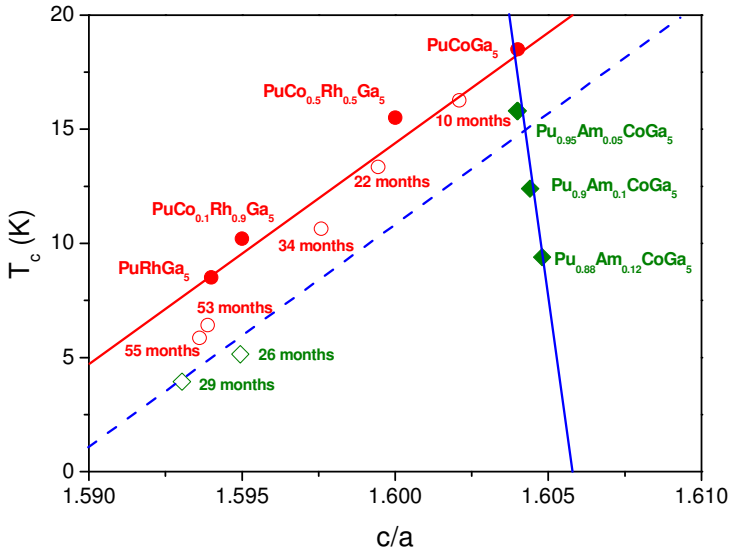


Fig. 2: Superconducting critical temperature *vs* the *c/a* lattice parameters ratio for $Pu(Co_{1-x}Rh_x)Ga_5$ and $(Pu_{1-x}Am_x)CoGa_5$ for "fresh" samples (closed symbol) and aged samples (closed symbols).

## References


[1] J. L. Sarrao *et al.*, Nature 420 (2002) 297
[2]F. Wastin *et al.*., J. Phys. Condens. Mat. 15 (2003) S2279
[3] E. D. Bauer *et al.*, Phys. Rev. Lett. 93 (2004) 147005
[4] A. B. Shick, V. Janis and P. Oppeneer, Phys. Rev. Lett. 94 (2005) 016401
[5] N. J. Curro *et al.*, Nature 434 (2005) 622
[6] H. Sakai *et al.*, J. Phys. Soc. Jpn. 74 (2005) 1710
[7] J.D. Thompson *et al.*, "Superconductivity in Actinide Materials " appeared in Recent Advances in Actinide Science, Eds. I. May, R. Alvares, N. Bryan, RSC Publishing (2006), 680, ISBN 0-85404-678-X
[8] P. Boulet *et al.,* Physical Review B 72 (2005) 104508
[9] F. Jutier *et al.*, J. Phys. Soc. Jpn. **75** (2006) Suppl., 47
[10] R.H. Heffner *et al.*, Comments Cond. Mat. Phys. 17 (1996), 361

# P22

## Superconductivity in the new $Y_3Os_8B_6$ boride

**E.B. Lopes[a], O.L. Sologub[a,b], A. Casaca[a,c], L. Havela[d], J. Sebek[e], E. Santava[e], Z. Janu[e], A.P. Gonçalves[a,*]**

[a] *Departamento de Química, Instituto Tecnológico e Nuclear/CFMC-UL, P-2686-953 Sacavém, Portugal*
[b] *Research Centre of Low Temperature Studies, L'viv National University, Dragomanova str. 50, 79005 L'viv, Ukraine*
[c] *ISEL, Área Científica de Física, P-1949-014 Lisbon, Portugal*
[d] *Charles Univ, Fac Math & Phys, Prague, CZ-12116 Czech Republic*
[e] *ASCR, Inst Phys, Prague, 18221 8 Czech Republic*

A recently discovered $Y_3Os_8B_6$ ternary boride was prepared by arc melting. This compound crystallizes in the $Ca_3Rh_8B_6$ type-structure, which is closely related with the $CeCo_3B_2$-type. Ac-susceptibility, magnetization, electrical resistivity and specific heat measurements show that $Y_3Os_8B_6$ is a new type II superconductor with a transition temperature, $T_C$, of 5.8(3) K and a maximum upper critical field, $B_{c2}(0)$, of ~2 T. $Y_3Os_8B_6$ is the first representative of a possible new family of superconducting borides. The structure and properties of this compound are discussed in relation to other ternary superconducting borides.

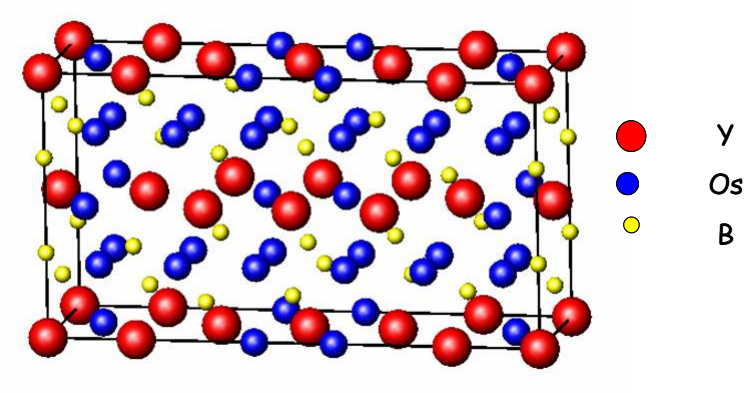

# P23

## Plutonium oxide transformation kinetics and diffusion coefficient measurement

**Peter Morrall[1], Simon Tull[1], Joseph Glascott[1], Paul Roussel[1]**

[1] *AWE, Aldermaston, Reading RG7 4PR UK, e-mail: peter.morrall@awe.co.uk*

When subjected to ultra high vacuum (UHV) conditions, a thin surface dioxide covering on a plutonium metal substrate will undergo a spontaneous, thermodynamically driven, reduction to the trivalent sesqui-oxide, $\alpha$-$Pu_2O_3$. Kinetic information about the surface transformation from $PuO_2$ to $Pu_2O_3$, is gained by following the changing depths of these two oxide layers, using x-ray photoelectron spectroscopy (XPS) as a probe. A mathematical model is proposed to follow this auto-reduction reaction, based on a simple 2D layered structure. The rate of this plutonium oxide inter-conversion is controlled by diffusion of oxygen across the steadily expanding $\alpha$-$Pu_2O_3$ layer. Through investigating the kinetics of this auto-reduction reaction, a value of $1.4 \times 10^{-16}$ $cm^2$ $s^{-1}$ is obtained for the diffusion coefficient of oxygen diffusing through $\alpha$-$Pu_2O_3$ at 30°C.

# P24

## New intermetallic compounds in the U-Ru-Si system

**M. Pasturel[1], O. Tougait[1] M. Potel[1], H. Noël[1], A.V. Zelinskiy[2]**

[1] *Unité Sciences Chimiques de Rennes, Chimie du Solide et Matériaux, Campus de Beaulieu, bât. 10A, 35042 Rennes Cedex, France.*

[2] *Department of Inorganic Chemistry, Ivan Franko L'viv National University, Kyryl & Mefodiy str. 6, 79005 L'viv, Ukraine*

Eight intermetallic phases have been reported so far in the U-Ru-Si system: URuSi [1], $U_2RuSi_3$ [2], $U_2Ru_3Si$ [3], $U_6Ru_{16}Si_7$ [3], $URu_2Si_2$ [4], $U_2Ru_3Si_5$ [5], $U_2Ru_{12}Si_7$ [6] and $URu_3Si_2$ [7]. The determination of this phase diagram is of interest both from theoretical and applied points of view:

- Within the already known phases, $URu_2Si_2$ is a well-known heavy-fermion ($\gamma$ = 180 $mJ.mol^{-1}K^{-2}$) presenting coexistence of an antiferrromagnetic state ($T_N$ = 17.5 K) and superconductivity ($T_c$ = 0.8 K) [4]. $U_2RuSi_3$ crystallizes in an original ordered structure deriving from the hexagonal $AlB_2$-type structure [2] and is a moderate heavy-fermion ($\gamma$ = 90 $mJ.mol^{-1}K^{-2}$) [8].
- Ruthenium is an ultimate fission product of uranium. The interactions in the U-Ru-Si system have to be known in order to evaluate the long-term stability of $U_3Si_2$ fuels that are presently used in research reactors, and to increase knowledge about interactions phases for waste reprocessing. These low $^{235}U$-enriched uranium fuels are substituting the highly enriched $UAl_3$ in order to decrease the proliferation risks.

Thus, the isothermal section at 1073 K of the U-Ru-Si phase diagram has been investigated. At least four new phases have been discovered and are now under analysis.

For example, the new intermetallic compound $URuSi_3$ crystallizes in the $BaNiSn_3$-type structure (space-group I4mm, n° 107) with a = 4.028 Å and c = 9.837 Å. It shows a ferromagnetic transition at $T_c$ = 43(2) K.

The $URu_6Si_3$ phase crystallizes in a quadratic structure (space-group P4/mbm, n° 127) with cell parameters a = 9.406 Å and c = 8.791 Å. The magnetic susceptibility follows a Curie-Weiss law.

The crystal structure and the magnetic properties of these new intermetallics will be presented.

### References

[1] R. Troc et al., *J. Magn. Magn. Mater.* **73**, 389 (1988).
[2] R. Pöttgen et al., *J. Mater. Chem.* **4**, 463 (1994).
[3] P. Lejay et al., *Physica B* **206-207**, 522 (1995).
[4] T.T.M. Palstra et al., *Phys. Rev. Lett.* **55**, 2727 (1985).
[5] E. Hickey et al., *J. Magn. Magn. Mater.* **90-91**, 501 (1990).
[6] A.V. Zelinskiy et al., Abstract of the 8th Conference on Chemistry of Intermetallic Compounds, L'viv, Ukraine (2002).
[7] H. Barz, *Mat. Res. Bull.* **15**, 1489 (1980).
[8] N. Takeda et al., *J. Phys. Chem. Jpn.* **67**, 1062 (1998).

# P25

## Evidence of different stoichiometries for the limiting carbonate complexes of lanthanides(III) by solubility measurements.

**Violaine Philippini[1,1], Thomas Vercouter[1], Pierre Vitorge[1,2], Annie Chaussé[2]**

[1] *Commissariat à l'énergie atomique : DEN/DANS/DPC/SECR/LSRM, 91191 Gif-sur-Yvette, France*
*e-mail: violaine.philippini@cea.fr, thomas.vercouter@cea.fr*
[2] *UMR 8587 (Evry University-CEA- CNRS), Boulevard François Mitterrand, 91025 Evry, France*

After the thorough review on thermochemical data on actinides (An) by the Nuclear Energy Agency, the stoichiometry of the limiting carbonate complexes of An(III) is still discussed. Two stoichiometries for An(III) and their lanthanides(III) (Ln(III)) chemical analogues are proposed: $M(CO_3)_3^{3-}$ and $M(CO_3)_4^{5-}$ (M = An or Ln) [1-11]. We suggest that such differences can be correlated to the metal radii, and/or to interactions between the counter-ion and the highly negatively charged aqueous complexes.
Carbonate complexation data are needed to predict the speciation of radionuclides in natural environments. The Callovo-Oxfordian geological formation is studied in France for a possible radioactive waste repository. It is in anoxic chemical conditions, where Pu, Am and Cm can be stable at the +3 oxidation state. In this study, $Ln(III)/H_2O/HCO_3^-/CO_3^{2-}/OH^-$ aqueous systems were investigated. When extracting thermodynamic formation constants from experimental data, considering erroneous species in the speciation model can affect the numerical values of the stability constants fitted for the other complexes. The aim of this study is to check the stoichiometries of the limiting carbonate complexes.
To elucidate the stoichiometries of the Ln(III) and An(III) limiting complexes, three complementary techniques are used: solubility, coprecipitation and capillary electrophoresis. Only the solubility results are presented here.
The limiting complexes are stable in concentrated $Alk_2CO_3$ aqueous solutions ($Alk^+$=alkaline ions, *i.e.* $Na^+$ in the present study), particularly when they are in equilibrium with the solid $AlkM(CO_3)_2,xH_2O(s)$ [4-6]. We already reported synthesis methods at room temperature for $NaLn(CO_3)_2,xH_2O(s)$ (Ln=La, Nd, Eu, Dy) [12], in chemical conditions close to those used for solubility measurements.
Several batches (containing NaOH, $NaHCO_3$, $Na_2CO_3$, $NaClO_4$, NaCl) were prepared with different $[CO_3^{2-}]$ and $[Na^+]$. A few tens of milligrams of the $NaLn(CO_3)_2,xH_2O(s)$ solid were added to the carbonate solutions, so that they were initially undersaturated. Comparing the Ln concentrations measured after various equilibration periods, a steady state was observed after a few days only.
The experimental solubilities are presented after ionic strength corrections. The experimental results were extrapolated to 3 M $NaClO_4$ by using the specific ion interaction (SIT) formula. The choice of this particular reference state minimizes the calculated corrections by comparison to the usual standard state of zero ionic strength.
Under these conditions, the main dissolution reaction is:

$$NaLn(CO_3)_2,6H_2O(s) + (i-2)CO_3^{2-} \leftrightarrows Na^+ + Ln(CO_3)_i^{3-2i} + 6H_2O$$

A classical log-log plot of the experimental solubilities against the $CO_3^{2-}$ concentration (**fig. 1**) should draw a curve, built from linear straight lines, whose slopes are equal to (i-2). The values 2 and 1 give the best fit in limiting conditions for $NaNd(CO_3)_2,6H_2O(s)$ and $NaEu(CO_3)_2,6H_2O(s)$, respectively, which evidences the $Nd(CO_3)_4^{5-}$ and $Eu(CO_3)_3^{3-}$

[1]Part of PhD thesis

stoichiometries. Similar experiments were performed for La and Dy. The $Ln(CO_3)_4^{5-}$ stoichiometry was evidenced for the lighter (hence bigger) lanthanides (La and Nd), whereas the heavier (Eu and Dy) form $Ln(CO_3)_3^{3-}$ limiting complexes.

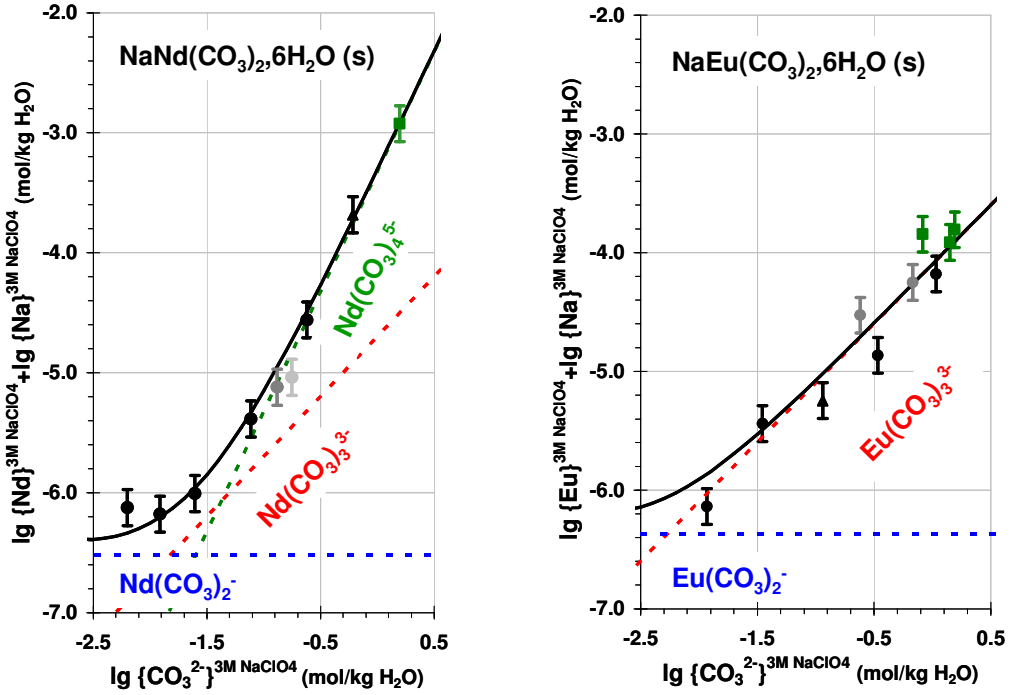


**Fig. 1**: Corrected **Nd and Eu solubilities** measured after 70 to 120-day equilibration periods. (●) $[Na^+]$=3M, (●) $[Na^+]$=1M, (●) $[Na^+]$=0.5M, for different holding electrolytes (▲) NaCl, (●) $NaClO_4$, (■) $Na_2CO_3$ (no holding electrolyte). The concentrations are extrapolated to 3M $NaClO_4$ aqueous conditions to minimize the ionic strength corrections (see text).

To our knowledge, it is the first time that two different stoichiometries are confirmed by the same laboratory, using the same experimental methodology. Further measurements using other techniques are in progress, in order to elucidate the stoichiometry for the whole series of lanthanides(III) (except Pm), Am(III) and Cm(III), in $Na^+$ solutions and with other counter-ions.

## References

[1] Chemical Thermodynamics Series, Volumes 2 and 5, Elsevier B.V. Amsterdam and NEA-OECD (1995, 2003).
[2] P. Robouch., thesis, Louis Pasteur University, Strasbourg, France (1987).
[3] E. Giffaut, thesis, Paris-Sud University, Orsay, France (1994).
[4] T. Vercouter, thesis, Evry University, Evry, France (2005).
[5] W. Runde, J.I. Kim, Technische Universitat Munchen, report RCM 01094 (1994).
[6] L. Rao et al., Radochim. Acta, **75**, 141 (1996).
[7] D. Ferri et al., Acta Chem. Scand. Ser. A, **37**, 359, (1983).
[8] A. Chatt et al., Mat. Res. Soc. Symp. Proc., **127**, 897 (1989).
[9] R. Rao et al., Radiochim. Acta, **54**, 181 (1991).
[10] T. Vercouter et al., New J. Chem., **29**, 544 (2005).
[11] J. Faucherre et al., Rev. Chim. Miner., **3**, 953 (1966).
[12] V. Philippini et al., proceedings 36th JDA (2006).

# P26

## Functionalized calixarenes-an alternative tool for the remediation of the radioactive contaminated mine waters from Romania

**Ioana-Carmen Popescu**[1]

[1] *Research and Development National Institute for Metals and Radioactive Resources, Blvd. Carol I no.70, sector 2 020917, Bucharest Romanial, e-mail: ioana.popescu@icpmrr.ro*

The Romanian uranium industry met its top development, beginning with 1950s, when uranium-bearing ore bodies were found, using radiometric investigations and gamma prospecting, in three main areas, namely Banat, Apuseni Mountains and Eastern Carpathians [1].

Under the complex international context and due to the public concern increasing about the radiological risk and the radioactive contamination threat, the uranium extraction and processing activities were almost closed in Romania, following the European pattern, and the entire scientific interest was shifted towards the environment radioactive decontamination within the areas affected by uranium exploration, exploitation and processing activities [2].

An important interest was granted to the radioactive decontamination of the mine waters resulted from the uranium mining activities and different organic media were tested in this purpose.

Recently, promising results were reported related to the functionalized calix[n]arenes utilization as effective reagents for uranium's removal from mine waters [3]. All the tests were carried out on synthetic solutions having the composition similar to the real mine waters [4]. In this direction similar researches were carried out in Romania as well [5].

The present contribution is a poster presentation and it aims to be only the beginning of a future much more detailed research study.

It shall overview the main procedures used in Romania in order to decontaminate the radioactive mine waters related to the actual international trends beside the progresses registered in the utilization of the calix[n]arenes as radioactive decontaminant reagents.

### References

[1] Information available on the institute's website: www.icpmrr.ro

[2] I.C. Popescu, et al., "Consideration concerning the role played by uranium organo-metallic complexes during the treatment of radioactive waste waters resulted from uranium mining industry", International Symphosium "Environment and Industry", Bucharest, Romania (2005)

[3] K. Schmeide, K. H. Heise, G. Bernhard, D. Keil, K. Jansen, D. Praschak, Uranium(VI) separation from aqueous solution by calix[6]arene modified textiles", Journal of Radioanalytical and Nuclear Chemistry, Vol. 261, No. 1 (2004) 61-67

[4] E. Schollmeyer, K. Jansen, H.-J. Buschmann, and Katja Schmeide, "**Functionalization of Synthetic Polymers by Supramolecular Compounds: Immobilization of Calix[n]arenes on Polyester",** Polymer Surface Modification: Relevance to Adhesion 3 (K.L. Mittal, ed.). VSP, (2004), p. 353-366.

[5] Lucia Mutihac, Hans Jürgen Buschmann, Elena Diacu, "Calixarene derivatives as carriers in liquid membrane transport", Desalination 148 (2002) p. 253–256

# P27

## Raman and infra-red spectroscopy of some inorganic actinide compounds

**C.D.Puxley**

*AWE Aldermaston, Aldermaston, BERKSHIRE RG7 4PR,United Kingdom*

The published data relating to the vibrational spectra of the actinides compounds, particularly those containing transuranium elements, remain very limited. Technological developments in the area of Raman spectroscopy and the production of progressively smaller infra-red spectrometers have made the field of vibrational spectroscopy more practically applicable to the analysis of actinide compounds.

Lasers which lase in the visible region of the spectrum in conjunction with charge-coupled devices have allowed fibre-optic technology to be applied to the field of Raman spectroscopy. Examples of Raman spectra of inorganic plutonium compounds (e.g. plutonium (III) oxalate decahydrate) recorded using this type of equipment will be presented and discussed.

The miniaturisation of infra-red spectrometers has allowed these instruments to be more easily installed within gloveboxes for direct infra-red analyses of plutonium compounds. Infra-red spectra of inorganic plutonium compounds (e.g. plutonium (IV) nitrate pentahydrate) recorded using an attenuated total reflectance FT-infra-red spectrometer will be presented and discussed.


Fig. 1. Glovebox-Housed Raman Probe for Actinide Compound Analysis

# P28

## U-Au-Sb system: phase equilibria at 600 °C and crystal structures of compounds

**Leonid Salamakha[1,2], Antonio P. Gonçalves[2], Henri Noël[3], Thierry Roisnel[3], Stepan Mudryi[1], Ivan Scherba[1], Manuel Almeida[2]**

[1] *Department of Physics of Metals, Faculty of Physics, L'viv National University, Kyryla i Mefodiya str. 8, 79005 L'viv, Ukraine, e-mail:salamakhaleonid@rambler.ru*
[2] *Dept. Química ITN / CFMC-UL, E. N. 10, P-2686-953 Sacavém, Portugal*
[3] *Laboratoire de Chimie du Solide et Materiaux, UMR CNRS 6226, Université de Rennes, 1Avenue du Général Leclerc, 35042 Rennes, France*

The phase equilibria in the ternary system U-Au-Sb at 600 °C have been established in full concentration region employing X-ray diffraction and electron probe microanalysis.
The metals used were uranium ingots (uranium platelets 99.8%, Merck, surface cleaned in diluted $HNO_3$ before use), gold (drops, 99.99%, ÖGUSSA-Wien, Austria) and antimony (ingots, 99.999%, ChemPur, Karlsruhe, Germany). In total 19 samples were prepared by argon arc-melting the elements on a water cooled copper hearth with a tungsten electrode. Zirconium served as a getter. Extra amount of Sb was also added beforehand to compensate possible weight losses caused by vaporization. To ensure good homogeneity the buttons were turned over and re-melted. Weight losses were generally smaller than 0.5 mass%. The arc-melted alloys were wrapped in tantalum foil, sealed in evacuated quarts tubes, annealed at 600 °C for 14 days and finally water quenched. X-ray powder diffraction data were collected at room temperature from the powdered alloys with the Philips X'Pert diffractometer (Cu $K_\alpha$ radiation, 2θ range 10-120 deg). Phase identifications and lattice parameters refinements were accomplished using the Powder Cell, WinPlotr, TREOR and DICVOL programs. Metallographic and quantitative analyses were obtained with the use of a 6400-JSM scanning electron microscope equipped with an Oxford Link Isis spectrometer. The crystal structures of compounds were determined from X-ray powder (FULLPROF98) and single crystal diffraction data (Nonius Kappa CCD, Mo Kα radiation, ω-scan, WinGX 1.70).
The boundary systems U-Sb, U-Au and Au-Sb were accepted from the compilation of binary alloy phase diagrams by Massalski [1]. Crystallographic data of the boundary phases can be found in [2] and are listed in Table 1.

Table 1. Crystallographic data of unary and binary boundary phases of the U-Au-Sb system

| Phase | Space group | Prototype | Lattice parameters (Å) a | b | c | Remarks | Reaction |
|---|---|---|---|---|---|---|---|
| αU | Cmcm | αU | 2.8537 | 5.8695 | 4.9548 | <688 °C | polymorphic |
| Au | Fm-3m | Cu | 4.078 | | | <1064 °C | melting |
| Sb | R-3m | As | 4.3007 | | 11.222 | <630 °C | melting |
| $U_5Sb_4$ | $P6_3/mcm$ | $Ti_5Ga_4$ | 9.237 | | 6.211 | <1800 °C | melting |
| USb | Fm-3m | NaCl | 6.204 | | | <1850 °C | melting |
| $U_3Sb_4$ | I-43d | $Th_3P_4$ | 9.112 | | | <1695 °C | peritectic |
| $USb_2$ | P4/nmm | $UAs_2$ | 4.270 | | 8.746 | <1355 °C | peritectic |
| $UAu_2$ | P6/mmm | $UHg_2$ | 4.756 | | 3.11 | <1390 °C | melting |
| $U_{14}Au_{51}$ | P6/m | $Gd_{14}Ag_{51}$ | 12.648 | | 9.135 | <1340 °C | melting |
| $AuSb_2$ | Pa-3 | $FeS_2$ | 6.658 | | | <460 °C | peritectic |

# P28

Experimental data (powder and single crystal XRD, EPMA) on the phase relations at 600 °C are summarized in Table 2. Accordingly, phase equilibria are characterized by the formation of three ternary phases: ($\tau_1$) ~$U_{25}Au_{25}Sb_{50}$ with a slight homogeneity range, ($\tau_2$) ~$U_{38}Au_{50}Sb_{12}$, ($\tau_3$) ~$U_{45}Au_{15}Sb_{45}$ and two substitutional Au/Sb solid solutions based on $U_{14}Au_{51}$ and $UAu_2$. A low temperature eutectic was observed in the region near the composition ~28U:44Au:28Sb.

Table 2. Crystallographic data of selected ternary alloys U-Au-Sb, annealed at 600 °C

| Nominal composition U - Au - Sb (at.%) | X-ray phase analysis | Space group | Prototype | Lattice parameters (Å) a | b | c |
|---|---|---|---|---|---|---|
| 15 – 70 – 15 | $U_{14}Au_{51}$ | P6/m | $Gd_{14}Ag_{51}$ | 12.68 | | 9.17 |
| | Au | Fm-3m | Cu | 4.09 | | |
| | ($\tau_1$) | tetragonal[a] | | 4.375 | | 9.84 |
| 20 – 40 - 40 | Au | Fm-3m | Cu | 4.09 | | |
| | $AuSb_2$ | Pa-3 | $FeS_2$ | 6.658 | | |
| | ($\tau_1$) | tetragonal[a] | | 4.375 | | 9.840 |
| 20 – 20 - 60 | Sb | R-3m | As | 4.38 | | 11.45 |
| | $AuSb_2$ | Pa-3 | $FeS_2$ | 6.658 | | |
| | ($\tau_1$) | tetragonal[a] | | 4.380 | | 9.840 |
| 30 – 10 – 60 | $USb_2$ | P4/nmm | $UAs_2$ | 4.28 | | 8.75 |
| | ($\tau_1$) | tetragonal[a] | | 4.361 | | 9.732 |
| 30 – 30 - 40 | $U_{14}Au_{51}$ | P6/m | $Gd_{14}Ag_{51}$ | 12.68 | | 9.15 |
| | $U_3Sb_4$ | I-43d | $Th_3P_4$ | 9.112 | | |
| | ($\tau_1$) | tetragonal[a] | | 4.365 | | 9.791 |
| 33.3 – 51.6 - 15 | $U_{14}Au_{51}$ | P6/m | $Gd_{14}Ag_{51}$ | 12.67 | | 9.15 |
| | $U_3Sb_4$ | I-43d | $Th_3P_4$ | 9.112 | | |
| | $U(Au,Sb)_2$ | P6/mmm | $UHg_2$ | 4.77 | | 3.17 |
| 40 – 40 - 20 | $U(Au,Sb)_2$ | P6/mmm | $UHg_2$ | 4.76 | | 3.17 |
| | ($\tau_2$) | unknown | | | | |
| | ($\tau_3$) | rhombohedral[a] | | 9.26 | | 18.47 |
| 40 – 20 - 40 | $U_3Sb_4$ | I-43d | $Th_3P_4$ | 9.112 | | |
| | ($\tau_3$) | rhombohedral[a] | | 9.26 | | 18.47 |
| | $U(Au,Sb)_2$ | P6/mmm | $UHg_2$ | | | 3.12 |
| 62.5 – 25.0 - 12.5 | U | Cmcm | αU | 2.85 | 5.87 | 4.95 |
| | $U_5Sb_4$ | $P6_3/mcm$ | $Ti_5Ga_4$ | 9.23 | | 6.20 |
| | $UAu_2$ | P6/mmm | $UHg_2$ | 4.76 | | 3.11 |

[a] single crystal X-ray diffraction data

## References


[1]. T.B. Massalski, in: Binary Alloy Phase Diagrams, second ed., ASM International, Materials Park, OH, 1990.

[2]. P. Villars and L.D. Calvert, Pearson's Handbook of Crystallographic Data for Intermetallic Phases (2nd ed.), ASM International, Materials Park, OH (1991).

# P29

## New XPS and Band Structure Characteristics of UN

**Małgorzata Samsel-Czekała[1], Robert Troć[1], Ewa Talik[2]**

[1] *Institute of Low Temperature and Structure Research, Polish Academy of Sciences, P.O. Box 1410, 50-950 Wrocław 2, Poland, e-mail: m.samsel@int.pan.wroc.pl*
[2] *Institute of Physics, University of Silesia, Uniwersytecka 4, 40-007 Katowice, Poland*

In previous years a very great number of experimental studies have been reported on the electronic structure, magnetic, thermal and electrical properties of uranium mononitride (UN) [1], nevertheless UN still remains very puzzled antiferromagnet and many riddles of its unusual behavior require further explanation.
UN has a fcc crystal structure of the NaCl type in its paramagnetic region and orders below $T_N$ = 53 K in a type I antiferromagnetic (AFI) structure with a single-**k** magnetic moment alignment along the [001] axis. A large difference exists between magnitudes of the ordered moment ($\mu_0$ =0.75 $\mu_B$) and the effective one ($\mu_{eff}$ = 2.66 $\mu_B$). The electronic heat capacity coefficient $\gamma(0)$ = 50 mJ/K$^2$ mol.
A recent high-resolution angle-resolved photoemission study of UN reveals the dual (itinerant and localized nature) of 5f electron bands near the Fermi level ($E_F$) [2]. Hence, some localized character seems to remain in UN and it is really observed, e.g. by a high value of $\mu_{eff}$.
A photoelectron spectroscopy investigation of UN films confirms the 5f-electronic states at $E_F$ in this compound showing a high density of states (DOS) at the $E_F$ [3]. There is a general good agreement between the measured position of the N 2p band with the values of self-consistent LMTO band structure calculations [4]. However the most interesting fact is that in binding energy (BE) of 3 –6 eV the photoemission graph contains also the 5f states having a broad local maximum there at 4 eV. One can than conclude that the 5f electrons preserve band character, but it is revealed as well that the majority of the 5f states are shifted from $E_F$ towards higher BE [3]. Indeed the localization is predicted on the basis of the 4f core hole, although the previous XPS and 4f spectra have not been of a good quality [5].
In present studies of UN, the band structure calculations for the paramagnetic state have been performed by the full relativistic version of the full-potential local-orbital (FPLO) minimum-basis code [6]. In this computation method the 4-component Kohn-Sham-Dirac equation, containing implicitly spin-orbit coupling up to all orders, is solved self-consistently. The Perdew-Wang parametrization [7] of the exchange-correlation potential in the local spin-density approximation (LSDA) was applied. UN crystallizes in the popular rocksalt structure (Fm3m) and for the calculations an experimental value of the lattice parameter $a$ = 4.890 Å [8] was assumed. The following basis sets were used: for U the 5d5f;6s6p6d;7s7p and for N the 2s2p;3d states were treated as valence states. The high-lying 5d,6s and 6p semicore uranium states that might hybridize with the 6d and 5f valence states were included in the basis. The maximum size of the *k*-point mesh in the Brillouin zone was 25×25×25.
The theoretical band energies $E_n(\mathbf{k})$, total and partial DOS were computed. The latter for each atomic site as well as for all the atomic states in the unit cell. In order to compare these calculations with the experimental X-ray photoemission spectrum (XPS), the theoretical valence band XPS was calculated by the standard procedure. Namely, the partial DOS for the constituent atoms were multiplied by the respective weight factors proportional to atomic subshell photoionization cross sections [9]. The outputs were summed and convoluted with a Gaussian to simulate the instrumental energy resolution of the analyzer used in the experiment.
The theoretical XPS was further compared with the experimental XPS obtained with monochromatised Al $K_\alpha$ (1486.6 eV) radiation at room temperature on the monocrystalline

sample. The emitted electrons were detected and analyzed with an energy resolution of 0.3 eV.

The calculated DOS predict a very broad and multi peak contribution from the U 5f states ranging from 6 eV below $E_F$ and up to 6 eV above $E_F$. Due to the spin-orbit splitting there are two main U 5f peaks shifted from each other at about 1 eV and a pseudogap occurs between them at 0.7 eV above $E_F$. The first peak cuts the Fermi level yielding relatively high DOS at $E_F$. There are also two broad peaks of the U 5f electrons, one between 2 and 6 eV below $E_F$ and another one for 2.5-6 eV above $E_F$. In the same energy range where the U 5f states occur there is also a pronounced contribution from the U 6d states hybridizing with the former. In the vicinity of $E_F$ and between 1.5 and 5 eV below $E_F$ there are very small contributions from the U 6p states as well. In the region of 1.5-6 eV below $E_F$ there is also a broad peak from the N 2p states. However, in the calculated valence band XPS, displayed in the figure, the large contribution from the U 5f states completely dominates not only near $E_F$ but also in the range 2-6 eV BE because the contributions from both the U 6d and N 2p states are cancelled by the photoemission weight factors and therefore are invisible in the graph. In addition, a small contribution from the U 6p is slightly visible between 1.5 and 5 eV BE. In general, all this is in good agreement with the experimental XPS.

In our opinion the obtained results extend much more the knowledge of the electronic structure of UN.

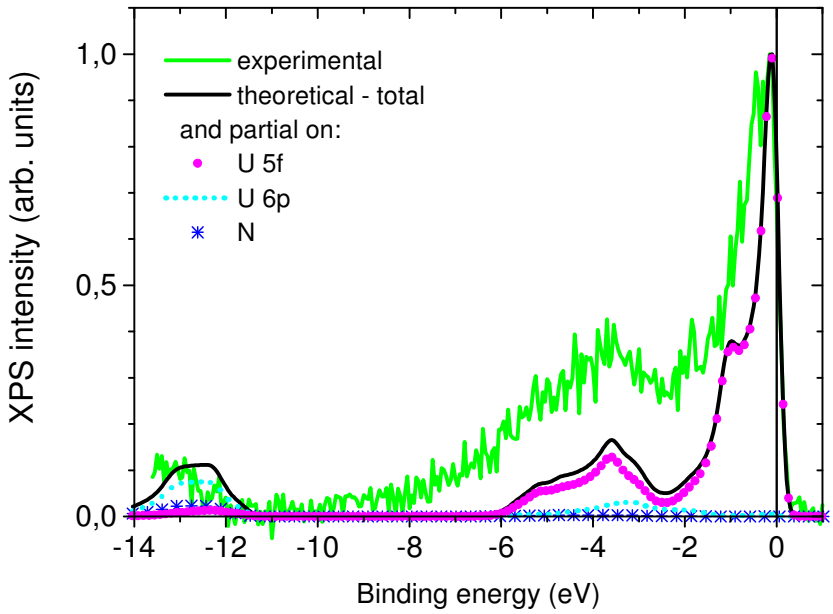


Fig.1. Theoretical and experimental XPS for UN.

## References

[1] Landolt-Bornstein: New Series III/27B6α.
[2] T. Ito et. al., *J. Magn. Magn. Mat.* **226-230**, 68 (2001).
[3] L. Black et al., *J. Alloys Compd.* **315**, 36 (2001).
[4] M.S.S. Brooks, *J. Phys. F: Met. Phys.* **14**, 639 (1984).
[5] P.R. Norton et al., *Phys. Rev. B* **21**, 2572 (1980).
[6] FPLO-5.00-18 [improved version of the original FPLO code by K. Koepernik and H. Eschrig, *Phys. Rev. B* **59**, 1743 (1999)]; http://www.FPLO.de.
[7] J.P. Perdew and Y. Wang, *Phys. Rev. B* **45**, 13244 (1992).
[8] H.W. Knott et al., *Phys. Rev. B* **21**, 4159 (1980).
[9] J.J. Yeh and I. Lindau, *At. Data Nucl. Data Tables* **32**, 1 (1985).

# P30

## Magnetic short range order in $DyFe_xAl_{12-x}$ intermetallics

**S. Sério[1], L. C. J. Pereira[1], M. Godinho[2], J. C. Waerenborgh[1]**

[1] *Dept Química/CFMC-UL, Instituto Tecnológico e Nuclear, 2685-953 Sacavém, Portugal*, *e-mail: susana.serio@itn.pt*
[2] *Dept. Física/CFMC-UL, FCUL, Campo Grande ed.C8, P-1749-016 Lisboa, Portugal.*

The magnetic properties of $AFe_xAl_{12-x}$ (A = *f* element, $4 \leq x \leq 6$) ternary intermetallics with the $ThMn_{12}$-type structure continue to attract much interest mainly because isostructural intermetallics such as $DyFe_{11.5}Ta_{0.5}$ or $SmFe_{10}Si_2$ have high Curie temperatures and relatively high uniaxial magnetic anisotropies [1]. Furthermore $AFe_xAl_{12-x}$ intermetallics have evidenced complex and unusual magnetic properties, even in the simplest cases such as $AFe_4Al_8$ (A=Y, Lu), where the iron atoms are located in only one crystallographic position (8f) and the f-element is non-magnetic. In order to contribute to the investigation of the magnetism of the $AFe_xAl_{12-x}$ compounds the study of the $DyFe_xAl_{12-x}$ system was undertaken. Samples with $DyFe_xAl_{12-x}$ (x = 4, 4.2, 4.5, 4.7 and 5) nominal compositions were prepared by induction melting and found to crystallize in the $ThMn_{12}$-type structure. The magnetic properties were studied by magnetization, AC susceptibility measurements and Mössbauer spectroscopy.

The analysis of the iron content influence on the magnetic properties allows evaluating the contribution of the different magnetic sublattices. The present study showed the decrease of the ordering temperature ($T_c$) from 180 to 160 K, in the composition range $4 \leq x < 4.7$, as a result of the magnetic frustration originated from the competition between the antiferromagnetic coupling of the R and Fe sublattices and the ferromagnetic exchange within those sublattices. For compounds with $x > 4.7$ the ordering temperatures increase gradually, due to the prevalence of ferromagnetic interactions arising from the occupation of *8j* sites by iron atoms.

Although for all compositions the thermal dependence of magnetization evidences a magnetic transition at app. 280 K, which disappears with the increase of the measurement field, Mössbauer and AC susceptibility revealed that this transition is not related to long range order. This particular behavior can be attributed to the existence of iron-rich clusters with short-range ferro or ferrimagnetic order, similar to those observed for the isostructural compounds $YFe_xAl_{12-x}$ ($4.4 \leq x \leq 5.8$) [2, 3]. Long-range magnetic order only takes place below the transition temperature values, $T_c$, detected by magnetization and Mössbauer data.

### References

[1] K. H. J. Buschow, "*Novel permanent magnetic materials*" in: Long GJ, Grandjean F, editors. Supermagnets, hard magnetic materials. Dordrecht: Kluwer; 1991. p.41.
[2] S. Sério, J. C. Waerenborgh, M. Almeida, M. Godinho, *J. Magn. Magn. Mat*. 265 (2003) 33.
[3] S. Sério, L.C. J. Pereira, M. M. Cruz, M. Godinho, J. C. Waerenborgh, *J. Alloys Comp.* (available on line since 17 December 2006).

# P31

## Isothermal section of U-Pt-Sb system at 600 °C (0 - 70 at.% Pt)

**Oksana Sologub[1], Leonid Salamakha[2], Antonio P. Gonçalves[1], Henri Noël[3], Thierry Roisnel[3], Manuel Almeida[1]**

*[1] Dept. Química ITN / CFMC-UL, E. N. 10, P-2686-953 Sacavém, Portugal, e-mail:sologub@itn.pt*
*[2] Department of Physics of Metals, Faculty of Physics, L'viv National University, Kyryla i Mefodiya 8, 79005 L'viv, Ukraine*
*[3] Laboratoire de Chimie du Solide et Materiaux, UMR CNRS 6226, Université de Rennes, 1Avenue du Général Leclerc, 35042 Rennes, France*

The phase equilibria in the ternary system U-Pt-Sb at 600 °C have been established in the concentration region 0 – 70 at. % Pt employing X-ray diffraction and electron probe microanalysis.

The metals used were uranium ingots (uranium platelets 99.8%, Merck, surface cleaned in diluted $HNO_3$ before use), platinum (powder, 99.99%, ÖGUSSA-Wien, Austria) and antimony (ingots, 99.999%, ChemPur, Karlsruhe, Germany). In total 18 samples were prepared by argon arc-melting the elements on a water cooled copper hearth with a tungsten electrode. Extra amount of Sb was added beforehand to compensate possible weight losses caused by vaporization. To ensure good homogeneity the buttons were turned over and re-melted. Weight losses were generally smaller than 0.5 mass%. The arc-melted alloys were wrapped in tantalum foil, sealed in evacuated quarts tubes, annealed at 600 °C for 14 days and finally water quenched. X-ray powder diffraction data were collected at room temperature from the powdered alloys with the Philips X'Pert diffractometer (Cu $K_\alpha$ radiation, 2θ range 10-120 deg). Phase identifications and lattice parameters refinements were accomplished using the Powder Cell, WinPlotr and DICVOL programs. Metallographic and quantitative analyses were obtained with the use of a 6400-JSM scanning electron microscope. The boundary systems U-Sb, U-Pt and Pt-Sb were accepted from the compilation of binary alloy phase diagrams by Massalski [1]. Crystallographic data of the boundary phases can be found in [2].

Experimental data (PXRD, EPMA) on the phase relations at 600 °C are summarized in Table 1. EDS images of selected alloys are shown in Fig. 1. Accordingly, phase equilibria are characterized by the formation of four ternary phases: $U_3Pt_3Sb_4$, ($\tau_1$) ~$U_{36}Pt_{49}Sb_{15}$, ($\tau_2$) ~$U_{46}Pt_{47}Sb_7$ and ($\tau_3$) ~$U_{46}Pt_{41}Sb_{13}$.

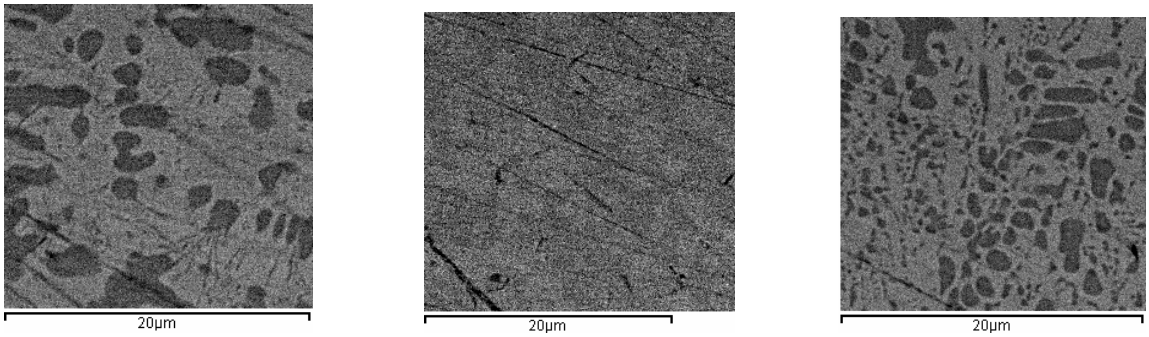


a b c

Fig. 1. EDS images of 35U:45Pt:20Sb (a), 45U:45Pt:10Sb (b) and 33U:57Pt:10Sb (c) alloys

# P31

Table 1. Crystallographic data of selected ternary alloys U-Pt-Sb, annealed at 600 °C

| Nominal composition U-Pt-Sb(at%) | X-ray phase analysis | Space group | Prototype | Lattice parameters (Å) a | b | c | Comments |
|---|---|---|---|---|---|---|---|
| 25 – 50 – 25 | $UPt_3$ | $P6_3/mmc$ | $CdMg_3$ | 9.753 | | 4.910 | powder XRD |
| | $PtSb_2$ | Pa-3 | $FeS_2$ | 6.442 | | | powder XRD |
| | $U_3Pt_3Sb_4$ | I-43d | $Y_3Au_3Sb_4$ | 9.690 | | | powder XRD |
| 25 – 25 - 50 | $PtSb_2$ | Pa-3 | $FeS_2$ | 6.442 | | | powder XRD |
| | $U_3Pt_3Sb_4$ | I-43d | $Y_3Au_3Sb_4$ | 9.690 | | | powder XRD |
| | $USb_2$ | P4/nmm | $UAs_2$ | 4.278 | | 8.745 | powder XRD |
| 37 – 25 – 38 | USb | Fm-3m | NaCl | 6.192 | | | powder XRD |
| | $U_3Pt_3Sb_4$ | I-43d | $Y_3Au_3Sb_4$ | 9.595 | | | powder XRD |
| | ($\tau_3$) | tetrag., I | | 10.95 | | 7.426 | SC XRD |
| 33 – 33 – 34 | $U_3Pt_3Sb_4$ | I-43d | $Y_3Au_3Sb_4$ | 9.678 | | | powder XRD |
| | ($\tau_2$) | unknown | | | | | powder XRD |
| 35 – 45 - 20 | $U_3Pt_3Sb_4$ | I-43d | $Y_3Au_3Sb_4$ | 9.678 | | | EPMA,PXRD |
| | ($\tau_1$) | tetrag., P | | 7.61 | | 3.87 | SC XRD |
| 33 – 57 - 10 | $U_3Pt_3Sb_4$ | I-43d | $Y_3Au_3Sb_4$ | 9.697 | | | EPMA,PXRD |
| | $U(Pt,Sb)_2$ | Cmcm | $UPt_2$ | 4.202 | 9.763 | 5.650 | EPMA,PXRD |
| | ($\tau_1$) | tetrag., P | | 7.61 | | 3.87 | SC XRD |
| 45 – 45 – 10 | ($\tau_2$) | unknown | | | | | EPMA,PXRD |
| | ($\tau_3$) | tetrag., I | | 10.95 | | 7.426 | SC XRD |
| 49 – 24 – 27 | USb | Fm-3m | NaCl | 6.192 | | | powder XRD |
| | $U_5Sb_4$ | $P6_3/mcm$ | $Ti_5Ga_4$ | 9.203 | | 6.200 | powder XRD |
| | ($\tau_3$) | tetrag., I | | 10.95 | | 7.426 | SC XRD |
| 57 – 11 – 33 | $U_5Sb_4$ | $P6_3/mcm$ | $Ti_5Ga_4$ | 9.206 | | 6.198 | powder XRD |
| | UPt | $P2_1$ | UIr | 5.73 | 10.78 | 5.75 | powder XRD |
| | | | | | β=99° | | |
| | U | Cmcm | αU | 2.857 | 5.871 | 4.953 | powder XRD |

**Acknowledgement.** The work of O.S. at the Institute of Nuclear Technology, Sacavém, Portugal was supported by the FCT grant (project SFRH/BPD/18810/2004). This work was partially supported by Portuguese French Exchange Program PESSOA.

## References

[1]. T.B. Massalski, in: Binary Alloy Phase Diagrams, second ed., ASM International, Materials Park, OH, 1990.

[2]. P. Villars and L.D. Calvert, Pearson's Handbook of Crystallographic Data for Intermetallic Phases (2nd ed.), ASM International, Materials Park, OH (1991).

# P32

## Speciation of uranium(VI) in presence of chloride ions in ionic liquids

**M.-O. Sornein[1], C. Cannes[1], C. Le Naour[1], G. Lagarde[1], E. Simoni[1], J.-C. Berthet[2]**

*[1] Institut de Physique Nucléaire, 15 rue Georges Clémenceau, 91406 Orsay cedex, France, e-mail: sornein@ipno.in2p3.fr*
*[2] CEA Saclay, CEA-SCM, bât. 125, 91191 Gif-sur-Yvette, France*

Room Temperature ionic liquids (RTILs) have currently gained interest in many chemical processes. Their remarkable properties make these new solvents good candidates to replace usual organic solvents in the field of "green chemistry". Recently, electrochemical and spectroscopic studies of actinides in RTILs have shown their potentiality in nuclear industry. However, fundamental knowledge on the behaviour of actinides in these media is necessary to perform nuclear fuel reprocessing by extraction or electrodeposition.
In this context, we have studied uranium(VI) speciation in presence of choride ions in the following ionic liquids: 1-butyl-3-methylimidazolium ($Bumim^+$) and n-tributylmethylammonium ($MeBu_3N^+$), both associated to bis-triflimide anion $(CF_3SO_2)_2N^-$ ($Tf_2N^-$). For this study, samples containing the uranyl salt $UO_2(OTf)_2$ ($OTf^- = CF_3SO_3^-$) alone or in presence of choride salts BumimCl and $MeBu_3NCl$ were prepared respectively in $BumimTf_2N$ and $MeBu_3NTf_2N$, with a care to control the water content (~ 100 ppm).
The studies we performed by UV-visible spectroscopy, time resolved laser spectrofluorometry and electrochemistry clearly put in evidence the formation of at least three chloro-complexes, supposed to be $UO_2Cl_2$, $UO_2Cl_3^-$ et $UO_2Cl_4^{2-}$, in the investigated range of choride ions concentrations. If more than 4 equivalents of chloride ions are added to uranyl, it has been put in evidence with the three techniques that the tetrachloro complex is the only one in solution. In agreement with literature, we observed a remarkable fine structure with bands splitting of the absorption and emission spectra of this species (Fig. 1). The possibility to isolate $UO_2Cl_4^{2-}$ in solution allowed us to study its redox properties in both ionic liquids. The mechanism we proposed for this species is a monoelectronic reduction followed by a chemical reaction.[1]

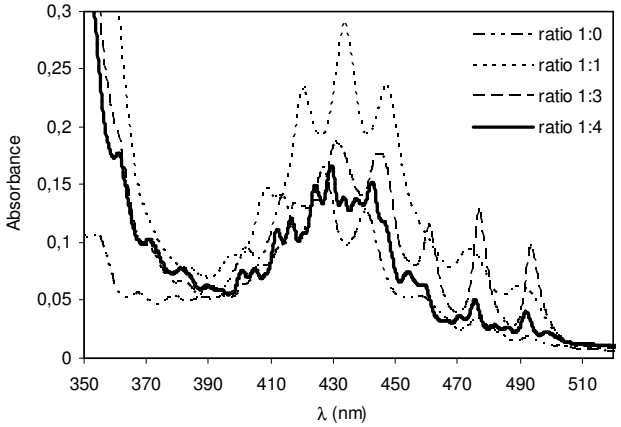


Fig. 1. Absorption spectra of uranyl (0.01 M) in presence of chloride ions for different uranyl-to-chloride ratios in $MeBu_3NTf_2N$ at 60°C.

### References

[1] M.-O. Sornein et al., *Inorganic Chemistry* **45**, 10419 (2006) and references therein.

# P33

## Thorium partitioning in Murataite-based ceramic produced by inductive melting in cold crucible

**Sergey Stefanovsky,[1] Alexander Ptashkin,[1] Oleg Knyazev,[1] Sergey Yudintsev,[2] Boris Nikonov[2]**

[1] *SIA Radon, 7th Rostovskii lane 2/14, Moscow 119121 Russia, profstef@mtu-net.ru*
[2] *Institute of Geology of Ore Deposits RAS, Staromonetny lane 35, Moscow 119017 Russia, syud@igem.ru*

Murataite (three-fold fluorite unit cell) and related phases (with eight- and five-fold fluorite unit cell) are promising hosts for actinides and corrosion products of high-level waste [1]. One of the advantages of these phases is their congruent melting that makes possible to produce them using melting routes such as an inductive cold crucible melting (ICCM) [2,3]. Murataite-based ceramics contained 10 wt.% of actinide oxides ($UO_2$, $NpO_2$, $PuO_2$) were produced by melting and examined in details [4-7]. Thorium is convenient element for investigation of structure and properties of ceramics because it is always tetravalent and, moreover, a study of its behavior in ceramics may be of importance in future at processing of waste of advanced thorium fuel cycle. Previous test on ICCM of the Th-loaded murataite ceramic yielded non-uniform product with significant amount of extra phases - especially crichtonite and zirconolite due to incomplete melting and homogenization [3]. In the next experiment we have applied an improved technique including melter start-up and initial melt formation using a graphite rod rather then SiC rod as in our previous test. Thus the Th-bearing ceramic with target chemical composition (wt.%): 5 $Al_2O_3$, 10 CaO, 55 $TiO_2$, 10 MnO, 5 $Fe_2O_3$, 5 $ZrO_2$, 10 $ThO_2$ has been produced in the cold crucible under steady-state conditions.

The block of solidified material in the cold crucible is non-uniform (Fig. 1a) that is due to specific melting conditions and occurrence of "skull" on inner surface of cold pipes originating the cold crucible. Upper part of the block contains large-sized pores due to captured gas bubbles, which were unable to be released after fast solidification of the melt rim. The centre of the block is composed of dense ceramic (Fig. 1b) consisting of major murataite (85-90 % of total bulk) and minor crichtonite (~10%) as well as traces of rutile, perovskite, zirconolite, and glass (Figs 1 and 2). As follows from SEM data (Fig. 1) the ceramic is more uniform and has much lower content of extra phases as compared with the sample obtained in our previous test [3]. Computer simulation of major murataite reflection suggests that the 8C polytype is predominant (60-65% of total) but the 5C and 3C polytypes are also present in approximately equal amounts (15-20% each) (Fig. 2).

Grain size in the side and bottom parts of the ingot is much smaller but these parts are composed of the same phases. In spite of $ThO_2$ content in perovskite type phase and zirconolite was found to be much higher than in the murataite polytypes (Table 1) the phases containing murataite modules, especially the 5C polytype, are major hosts for both thorium and zirconium because total amount of perovskite and zirconolite does not exceed ~5 vol.%. Interstitial glass formed due to melt contamination with $SiO_2$ and $Al_2O_3$ from protective putty of the cold crucible contains only traces of thorium.

The murataite grains in Th-bearing ceramics produced in the cold crucible are characterized by high homogeneity and more uniform elemental distribution as compared with U-bearing ceramics [2] and the Th-bearing ceramics produced by different methods [4-7]. Melting / solidification of Th- and U-bearing oxide mixtures in small crucibles in resistive furnace and U-bearing oxide mixture in cold crucible results in gradual crystallization of polytypes with increasing of fraction of murataite modules in their structure from core to rim of the grain. In the Th-bearing ceramics produced in the cold crucible one of the polytypes seemed to be

predominant (5C or 8C) and content of the other polytypes was negligible. This fact requires further investigation.

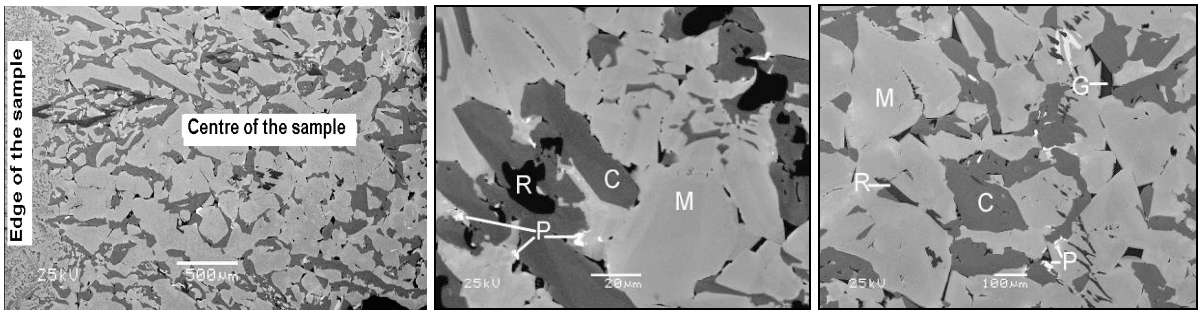


Fig. 1. SEM images of the ceramic (left), and its edge zone (middle) and central (right) parts. C/L – crichtonite/loveringite, G – glass, M – murataite polytypes, P –perovskite, R – rutile.

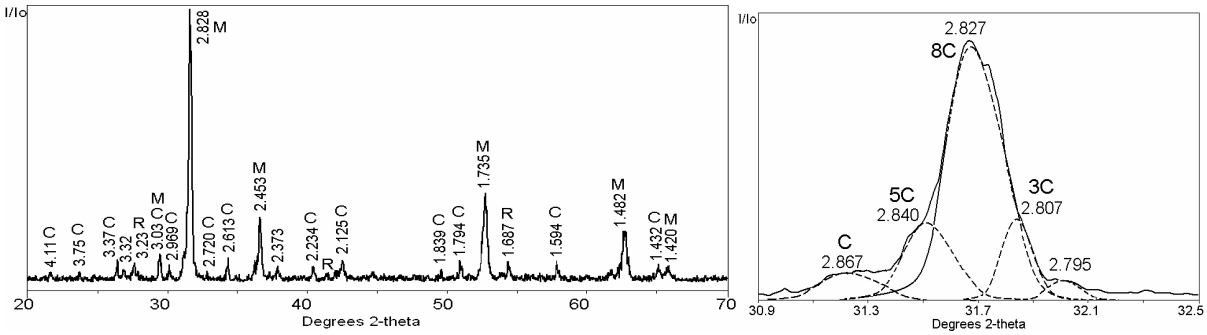


Fig. 2. XRD pattern of murataite-based ceramic produced by ICCM (left) and computer simulation of major reflection on XRD pattern (right). C – crichtonite, 5C, 8C, 3C – murataite polytypes with five-, eight- and three-fold fluorite unit cell, respectively, R – rutile.

Table 1. Chemical composition (wt.%) of the phases in the murataite ceramic.

| Oxides | 5C | 8C | 3C | C/L | R | P-1 | P-2 | Z | G |
|---|---|---|---|---|---|---|---|---|---|
| $Al_2O_3$ | 2.23 | 3.33 | 6.21 | 5.13 | - | - | - | 1.24 | 15.62 |
| $SiO_2$ | - | - | - | - | - | - | - | - | 30.56 |
| CaO | 8.75 | 9.08 | 8.92 | 4.55 | - | 9.06 | 6.51 | 7.81 | 21.60 |
| $TiO_2$ | 49.67 | 52.25 | 51.82 | 65.92 | 94.57 | 41.40 | 36.09 | 47.00 | 12.08 |
| MnO* | 10.67 | 12.27 | 14.87 | 11.39 | - | 6.38 | 7.16 | 6.74 | 16.17 |
| $Fe_2O_3$ | 4.21 | 5.47 | 8.08 | 8.22 | - | 1.19 | 1.36 | 3.36 | 2.83 |
| $ZrO_2$ | 10.25 | 5.52 | 0.45 | 1.98 | - | 4.99 | 3.29 | 15.08 | - |
| $ThO_2$ | 10.72 | 9.65 | 8.92 | 3.46 | 4.68 | 32.67 | 36.59 | 15.99 | 1.15 |
| Total | 96.50 | 97.57 | 99.27 | 100.65 | 99.25 | 95.69 | 91.00 | 97.22 | 100.00 |

The work was supported by the Russian Agency for Science and Innovation.

## References

[1] S.V. Yudintsev et al. Structural Chemistry of Inorganic Actinide Compounds, Elsevier B.V. (2007) 457-490.
[2] S.V. Stefanovsky et al. Proc. Waste Management '01 Conf. Tucson, AZ (2001) CD-ROM. ID 324.
[3] S.V. Stefanovsky et al. 36iemes Journees des Actinides, Oxford, UK (2006) CD-ROM. ID P-36.
[4] S.V. Yudintsev et al. *Mat. Res. Soc. Symp. Proc.* **663**, 357-366 (2001).
[5] S.V. Stefanovsky et al. *Mat. Res. Soc. Symp. Proc.* **893**, 429-434 (2006).
[6] S.A. Perevalov et al. *Radiochim Acta*, **94**, 509-514 (2006).
[7] S.V. Yudintsev et al. *Journ. Alloys Comp.* 2006, doi: 10-1016/j.jallcom.2006.10.129.

# P34

## The $UCu_2T_3Al_7$ alloys in high magnetic fields and their specific heat.

**W. Suski[a,b], A.Hackemer[a], K.Wochowski[a], A.Gilewski[b] T.Mydlarz[b]**

[a] *Polish Academy of Sciences, W.Trzebiatowski Institute of Low Temperature and Structure Research, P.O.Box 1410, 50-950 Wrocław 2, Poland*

[b] *International Laboratory of High Magnetic Fields and Low Temperatures, P.O.Box 4714, 50-985 Wrocław 47, Poland*

The investigations of the $U(Cu,T)_{4+x}Al_{8-x}$ derivatives have been carried out in our laboratories for long time. Particularly interesing problem is the reason for the enhanced coefficient of the electronic specific heat $\gamma$: the strongly correlated electrons or crystallographic disorder. The observation of $\gamma$ amounting to value between 100 and 200 $mJmol^{-1}K^{-2}$ independently on the composition seems to favourize the first concept. Therefore, in turn we decided to investgate the $UCu_2T_3Al_7$ alloys where T = Cr, Mn and Fe. The examination of the magnetic properties in low magnetic field and electrical resistivity measurement have shown that the Cr based alloy is paramagnetic. The Mn containing compound is ferrimagnetic whereas the Fe alloy is ferromagnetic. All three compounds follow a modified Curie – Weiss law at higher temperatures and the temperature dependence of the electrical resistivity of all materials shows metallic character [1].

The magnetization has been measured at T = 4.2 K and 77 K in the magnetic field up to 140 kOe using capacity magnetometer with superconducting solenoid whereas the specific heat has been examined in the temperature range 1.2 – 70 K in magnetic field H = 0 and 7 T using a homemade and fully automatic calorimeter.

Fig.1 shows the magnetization of the investigated alloys. The results are in fair agreement with the previous measurements. For the Fe compound the saturation is not reached even in the highest field and amounts to 4.1 $\mu_B$. This value is obviously higher than that in Ref.1 (3.3 $\mu_B$ ). However, it seems to confirm earlier conclusion that the iron participate in magnetic ordering as well. Also the histeresis is rather low. In the contrary to the Ref.1 for the Mn alloy the saturation is obtained quite easily with the saturation moment equals to ~ 2 $\mu_B$ and this value is considerably higher than that obtained previously. The magnetization of the Cr compound is low and weakly, and linearly depends on magnetic field. Generally, one can claim that the magnetic field as high as 140 kOe does not change the magnetic structure of examined materials.

In Fig.2 the heat capacity $C_p$ versus T for the Mn compound measured in 0 and 7 T magnetic field is presented. One can see that at low temperature there are the diffuse anomalies which could be related to the magnetic transitions (spin-reorientation transition SRT). Carefull inspection can discerne the anomalies at T = 5 and 9 K, however, the low temperature anomaly did not find any confirmation in magnetic measurements whereas that at 9 K is supported by the anomaly in the $\delta M/\delta T$ vs.T plot [1]. The magnetic field suppresses these anomalies. Inset presents $C_p/T$ vs.$T^2$ plot and extrapolated $\gamma$ amounts to almost 0.6 $J/(molK^2)$, the huge value which was not observed previously in these systems (see e.g.[2]).

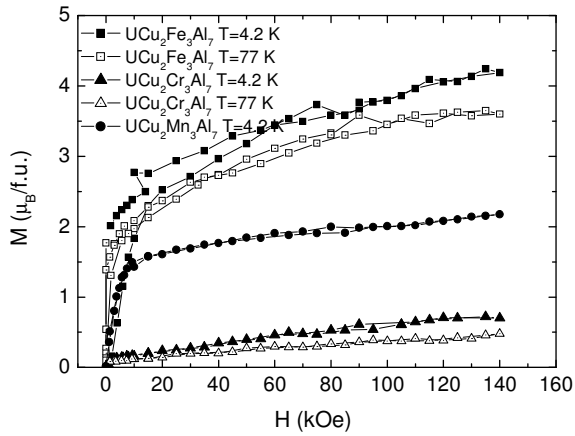


Fig. 1

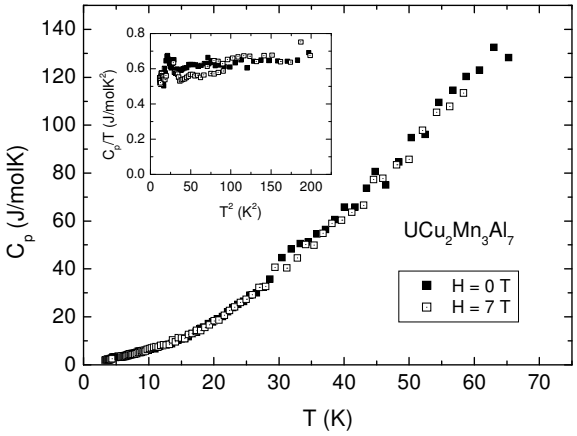


Fig. 2

## References

[1] W.Suski, K.Wochowski : *J.Alloys Comp.* in press.
[2] W.Suski, K.Gofryk, A.Hackemer, K.Wochowski : *J.Alloys Comp.* **423** (2006) 37

# P35

## Ferromagnetic properties of single-crystalline $U_2NiSi_3$

**Maria Szlawska and Dariusz Kaczorowski**

*Institute of Low Temperature and Structure Research, Polish Academy of Sciences,*
*P Nr 1410, 50–950 Wrocław 2, Poland, e-mail: M.Szlawska@int.pan.wroc.pl*

Most of the ternary intermetallic phases $U_2TSi_3$ ($T$ = 3d-, 4d- or 5d-electron transition metal) crystallize in a hexagonal structure of the $AlB_2$–type or its disordered derivatives [1,2]. Recently, they attracted much attention because of their unusual magnetic properties related to atomic disorder and/or topological frustration in the uranium sublattice [3,4]. The compound $U_2NiSi_3$ has previously been studied on polycrystalline samples and characterized as a cluster-glass system with the spin-freezing temperature $T_f$ = 22 K [3,5]. On the contrary, the neutron diffraction experiment performed on a single crystal has revealed a long-range ferromagnetic ordering below $T_C$ = 30 K with sizeable uranium magnetic moments of 0.6 $\mu_B$ oriented perpendicular to the hexagonal $c$ axis [6]. This indispensable discrepancy motivated us to undertake a reinvestigation of the bulk properties of $U_2NiSi_3$ on single-crystalline specimens.

Single crystal of $U_2NiSi_3$ was grown by the Czochralski pulling method in a tetra–arc furnace under argon atmosphere. Magnetic measurements were performed in the temperature range 1.72–400 K and in magnetic fields up to 5 T using a Quantum Design SQUID magnetometer. The electrical resistivity was measured from 5 to 300 K by a conventional four–point dc technique. The heat capacity was studied within the temperature interval 2–100 K employing a Quantum Design PPMS platform.

Fig. 1 shows the low-temperature dependencies of the magnetization measured in zero-field-cooled (ZFC) and field-cooled (FC) regimes in a magnetic field applied parallel ($\sigma_\parallel$) and perpendicular ($\sigma_\perp$) to the $c$ axis. The general shape of these curves as well as the magnitude of $\sigma_\perp$ obtained in the FC mode unambiguously indicate strongly anisotropic ferromagnetism with pronounced domain effect. The Curie temperature, defined as the inflection point on the $\sigma_\perp(T)$ variation, amounts to 26 K. The magnetic moments are confined to the basal hexagonal plane.

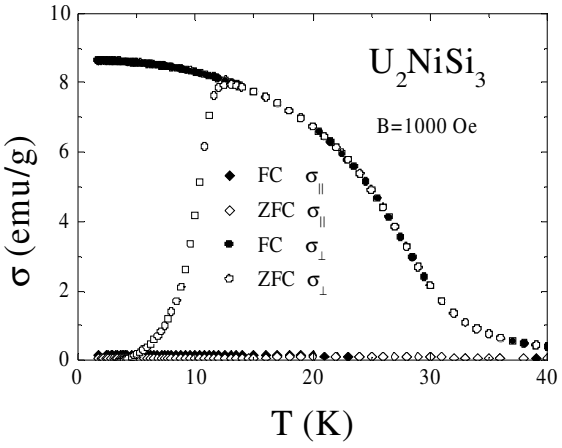


Figure 1

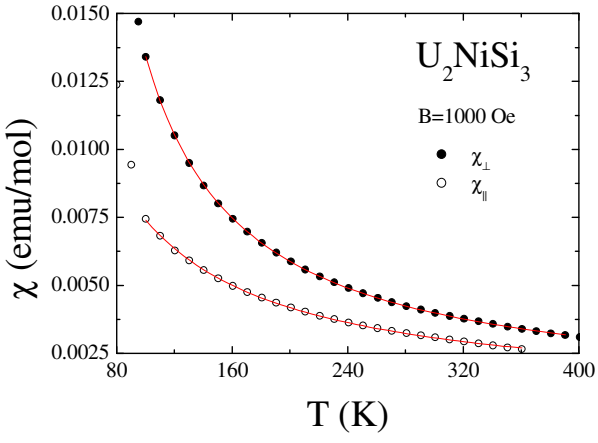


Figure 2

As shown in Fig. 2, strong magnetocrystalline anisotropy is observed also in the paramagnetic state: the magnetic susceptibility measured along the *c* axis ($\chi_{\parallel}$) is much smaller than the component taken within the *a*–*b* plane ($\chi_{\perp}$). Above about 100 K the $\chi_{\parallel}(T)$ and $\chi_{\perp}(T)$ variations can be described by a modified Curie–Weiss law with following parameters: $\chi_0^{\parallel} = 6 \times 10^{-4}$ emu/mol, $\mu_{eff}^{\parallel} = 2.47\ \mu_B$, $\theta_p^{\parallel} = -14$ K and $\chi_0^{\perp} = 8 \times 10^{-4}$ emu/mol, $\mu_{eff}^{\perp} = 2.64$ and $\theta_p^{\perp} = 31$ K.

The ferromagnetic ordering in single-crystalline $U_2NiSi_3$, being much evident in the magnetic characteristics, manifests only faintly in the heat capacity and electrical transport data. Fig. 1 displays the temperature dependence of the specific heat of $U_2NiSi_3$. The magnetic phase transition at $T_C$ manifests itself just as a small kink on the $C(T)$ curve. Similarly, the electrical resistivity, measured with the current flowing along ($\rho_{\parallel}$) and perpendicular ($\rho_{\perp}$) to the *c* axis, shows only tiny anomalies at $T_C$ (see Fig. 4). Above ca. 60 K, the two resistivity components change with the temperature in a metallic manner, yet at lower temperatures some anomalous features are seen. Both curves exhibit shallow minima near 50 K, and in the ordered state the resistivities slightly increase with decreasing temperature. Worth noting is also that the overall changes in the values of $\rho_{\parallel}$ and $\rho_{\perp}$ over the entire temperature range are very small. The observed behavior likely results from the presence of atomic disorder in the unit cell of the compound studied.

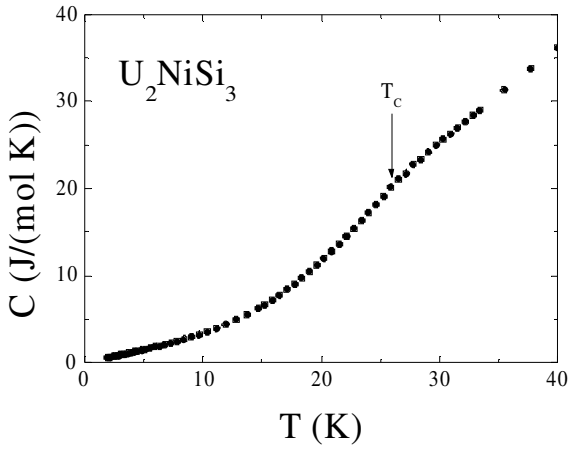


Figure 3

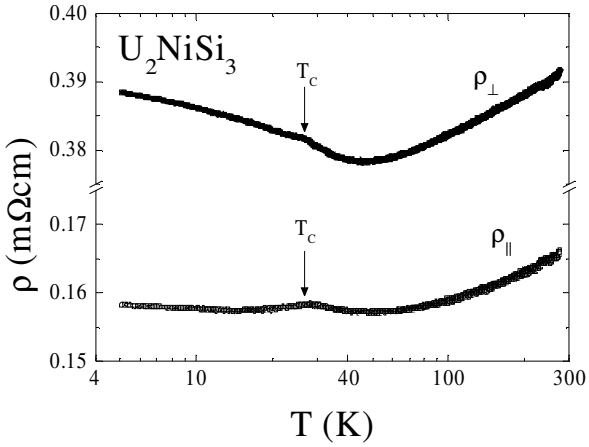


Figure 4

The new results obtained for the single crystal of $U_2NiSi_3$ reveal the long-range ferromagnetic ordering that sets in at low temperatures, in agreement with the neutron diffraction data [6]. The Curie temperature of 26 K is however quite different from the value given in Ref. 6. Most likely the investigated system is very sensitive to the level of atom disorder or/and possible deviations from the ideal stoichiometry. In each particular case $T_C$ may differ considerably, or even ferromagnetism may be replaced by spin-freezing as established for the polycrystalline samples of $U_2NiSi_3$ studied in Refs. 3 and 5.

[1] R. Pöttgen and D. Kaczorowski, *J. Alloys Compd.* **201**, 157 (1993).
[2] B. Chevalier et al., *J. Alloys Compd.* **233**, 150 (1996).
[3] D. Kaczorowski et al., *J. Phys.: Condens. Matter* **5**, 9185 (1993).
[4] D. X. Li et al., *Phys. Rev. B* **57**, 7434 (1998).
[5] D. X. Li et al., *J. Phys.: Condens. Matter* **11**, 8263 (1999).
[6] A. Schröder et al., *J. Magn. Magn. Matter.* **140-144**, 1407 (1995).

# P36

## Magnetic features and electronic structure of uranium quaternary $U_2ScB_6C_3$

**V. H. Tran[1], P. Rogl[2], T. Mori[3], H. Ripplinger[4], K.H. Schwarz[4] and W. Miiller[1]**

*[1] W. Trzebiatowski Institute of Low Temperature and Structure Research, Polish Academy of Sciences, P.O. Box 1410, 50-950 Wrocław, Poland, V.H.Tran@int.pan.wroc.pl*
*[2] Institut für Physikalische Chemie, Universität Wien, Währingerstr. 42, A-1090 Wien, Austria*
*[3] National Institute for Materials Science, Namiki 1-1, Tsukuba, 305-044, Japan*
*[4] Physikalische Chemie und Theoretische Chemie, TU-Wien, Getreidemarkt 9/156, A-1060 Wien, Austria*

The dual nature of the 5*f*-electrons in intermetallic uranium compounds such as $UPt_3$, $UPd_2Al_3$ [1], $UGe_2$ [2], URhGe [3] and UIr [4], responsible for both magnetism and superconductivity, has attracted considerable attention. A particularly interesting feature is the fact that in all ferromagnetic compounds [2-4] the Curie temperature $T_C$ was found to be higher than the superconducting critical temperature $T_{SC}$. In this context we have recently reported on fundamental physical properties of itinerant ferromagnet β-$UB_2C$ ($T_C$ = 74.5 K, $\gamma$ = 35 mJ/molK$^2$, $T^*$ = 37 K) [5] resembling very much to the ferromagnetic superconductors. β-$UB_2C$ is a high-temperature modification adopting the rhombohedral $ThB_2C$-type structure containing three puckered metal layers per unit cell sandwiched between planar layers of BC-nonmetal layers (space group $\bar{R}$3m) [6]. Some time ago, Rogl et al [7] have reported on hexagonal and truly quaternary boron carbides, $(Th,U)_2ScB_6C_3$, as an ordered variant of the rhombohedral $ThB_2C$-type structure. In view of the interesting physico-chemical behaviour of β-$UB_2C$ and with respect to its close structural relationship to $U_2ScB_6C_3$, it deemed fruitful to investigate the fundamental properties of $U_2ScB_6C_3$. In this work, we present details on an X-ray single crystal study, as well as on low-temperature physical properties obtained from the measurements of the magnetization, specific heat, electrical resistivity, magnetoresistance and thermopower on polycrystalline material. The ground state of the studied compound is supported by the electronic band structure calculations, carried by the full potential linearized augmented plane plus local orbitals [7].

The crystal structure of $U_2ScB_6C_3$ was derived from room temperature X-ray single crystal counter data supported by neutron powder diffractometry. $U_2ScB_6C_3$ crystallises with a unique structure type (P6/mmm). The unit cell dimensions are: a = 0.65096(2), c = 0.34265(2) nm, c/a = 0.5264. The structure of $Th_2ScB_6C_3$, which has been first described from X-ray powder data [7] is isotypic (a = 0.660296(7), c = 0.358421(4) nm, c/a = 0.5406). The crystal structures of $(U,Th)_2Sc_6B_3$ are typical non-metal layer metal boron carbide compounds $M_2BC$. Metal atoms in z = 0 form a planar hexagonal net of uranium atoms centered by the smaller scandium atoms. Non-metal atoms are found in planar Kagomé nets 6B.$(6B+3C)^2$ in z = 1/2. The two-dimensional non-metal network corresponds to the one in $ThB_2C$ and forms a link to the simple structure of $AlB_2$-type.

Measurements of the magnetic susceptibility, magnetization, electrical resistivity, magnetoresistance, specific heat and thermoelectric power on a polycrystalline sample of $U_2ScB_6C_3$ indicate itinerant ferromagnetism with ordering at $T_C$ = 61(0.5) K and a characteristic transition temperature $T^* \approx$ 45 K, below which the magnetization shows up an upturn (Fig. 1). The investigated compound is characterized by an enhanced Sommerfeld coefficient at low temperatures (40 mJ/mol.UK$^2$ at 2 K) and a broad maximum in $C_p(T)/T$-curve (Fig. 2). The magnetic specific heat data (see inset of Fig. 2) can be fitted by the relation for ferromagnetic system with an energy gap Δ: $C_{5f} = \gamma T + CT^{3/2}\exp(-\Delta/T)$ with $\Delta$ = 18 K. The magnetic entropy gain at $T_C$ reaches 86% of Rln2.

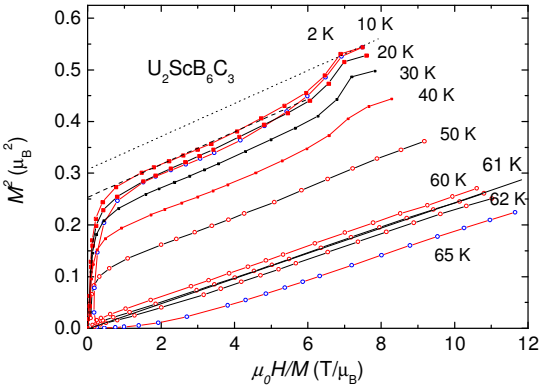


Fig. 1 Arrott plot for $U_2ScB_6C_3$.

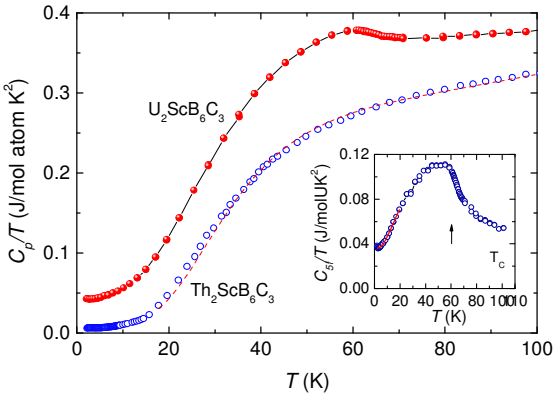


Fig. 2 *C/T* vs *T* for $(U,Th)_2ScB_6C_3$.

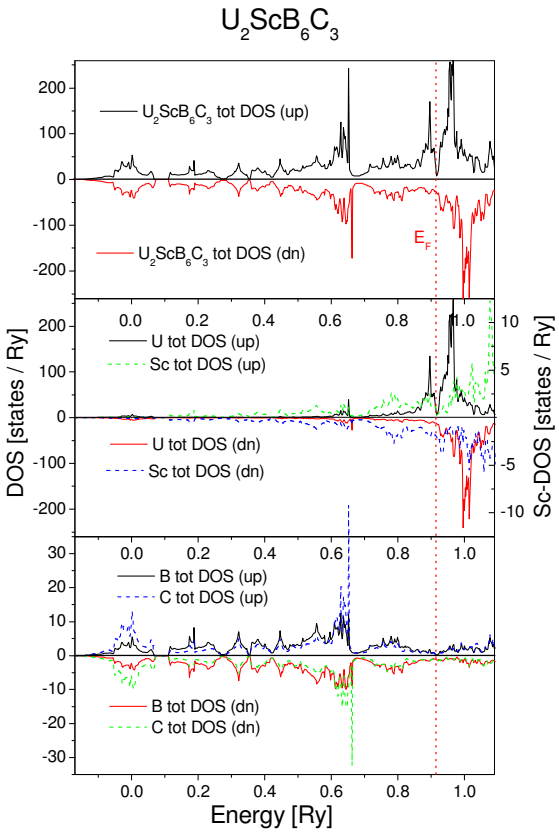


Fig. 3 Spin projected local densities of states calculated by LAPW+LO for $U_2ScB_6C_3$.

The electronic transport measurements (electrical resistivity ρ, thermoelectric power *TEP*, and Hall coefficient $R_H$) point to metallic character of the compound. Up to 20 K the $\rho(T)$ data can be fitted satisfactorily by $AT^2$ law with $A = 0.05$ μΩcm/K$^2$.

Based on the theoretical calculations data (Fig. 3), one concludes that significant contribution to the density of states originates from the 5f-orbitals. The calculations predict a ferromagnetic ground state with a spin moment of 1.3 $\mu_B$.

In conclusion, the substitution of U by Sc in $UB_2C$, which decreases the magnetic ion concentration, obviously leads to a decrease of the ordering temperature. However, anomalous features observed in the magnetization and specific heat in $U_2ScB_6C_3$ may be argued for the simple effect of substitution, which not only enhances the Sommerfeld ratio but also results in an additional transition at 45 K. Unfortunately, at the moment it is not clear what is the nature behind this phenomenon.

## References

[1] G. Zwicknagl et al., Phys. Rev. B **65**, R81103 (2002).
[2] S. S. Saxena et al., Nature (London) **406**, 587 (2000).
[3] D. Aoki et al., Nature (London) **413**, 613 (2001).
[4] N. Tateiwa et al., J. Phys.: Condens. Matter **13**, L17 (2001).
[5] V. H. Tran et al., J. Phys.: Cond. Mat **18** 703 (2006).
[6] P. Rogl and P. Fischer J. Solid State Chem. **78**, 294 (1989).
[7] P. Blaha et al., Program for calculating crystal properties, Wien2k (2001), ISBN 3-9501031-1-2.
[8] P. Rogl et. al., "*Structure and Properties of Quaternary $Th_2ScB_6C_3$*", paper presented at the 16th IUPAC Conference on Thermodynamics, Dalhousie University, Halifax, Canada, August 6-11, 2000.

# P37

## Uranium processing in supercritical carbon dioxide

**Yang Weicai, Luo Wenhua, Zhang Guangfeng**

*China Academy of Engineering Physics, P.O.Box 919-71, Mianyang* 621900*, Sichuan, P.R.China*
*e-mail: YWC712@YAHOO.COM.CN*

Cleaning the residual contaminations from uranium specimens with normal and ultrasonic strengthening supercritical carbon dioxide ($SCCO_2$) was studied. And plating Ni film on uranium surface by decomposing $Ni(CO)_4$ in $SCCO_2$ was performed as well. The characters of uranium surface were verified by auger electron energy spectrum and X-ray diffraction. The results reveal that at 60°C and 10 MPa, machine oil and water are dissoluble in $SCCO_2$, while triethanolamine is hardly dissoluble. When the powerfull ultrasonic is introduced into $SCCO_2$, the cleaning effects can be improved dramatically attributing to the sonochemistry effects. It is proved by further corrosion experiments that the uranium specimens treated by $SCCO_2$ shown better corrosion resistance than those untreated. During the cleaning period, $CO_2$ decomposed as C and O atoms, and then the products deposited on the surface layer of uranium specimens, which is indicated by auger electron energy spectrum. It is remarkable in the X-ray diffraction pattern of the cleaned uranium surface that the major products of the chemical reactions between uranium and $SCCO_2$ during cleaning period are $UO_2$, $UC_2$, and $U_2C_3$.

$Ni(CO)_4$ can be decomposed at lower temperature range as 70~135°C in ultrasonic strengthening $SCCO_2$, and the active nickel atoms deposited on surface of uranium specimens to form a continuous nickel film. It is suggested by the corrosion reaction kinetics experiments that corrosion reaction of nickel-plating uranium in moist atmosphere follows a three-dimensional diffusing model, and the corrosion barrier energy is 126 kJ/mol, which is 12 kJ/mol more than that of the specimen cleaned with $SCCO_2$.

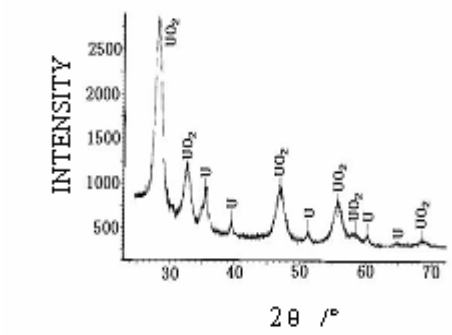


Fig. 1. XRD pattern of the cleaned U surface layer

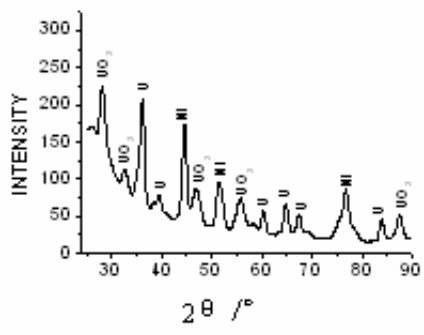


Fig. 2. XRD pattern of the plated U surface layer

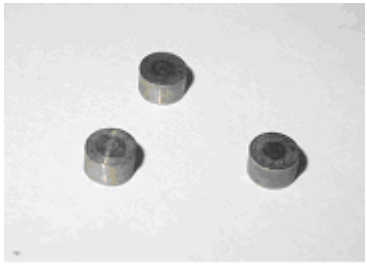

Fig. 3. The photograph of the plated specimens

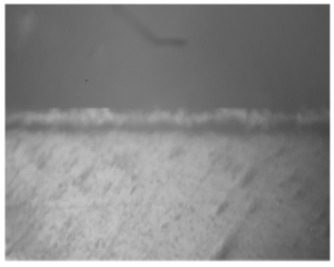

Fig. 4. The micrograph of the plated specimens

## References

[1] Graig M. V. Taylor, et al., Supercritical fluids carbon dioxide (SCCO2) cleaning of nuclear weapon components. LA-UR-97-4420.
[2] Stephanie J. Hale. Supercritical fluids carbon dioxide cleaning of plutonium parts. RFP-4530 or LA-UR-93-3103.
[3] P. Diodati, G. Giannini, L. Mirri, et al., Sonochemical production of non-crystalline phase of palladium. Ultrasonics Sonochemistry, 1996, 3: S135~S139.
[4] W. Dale Spall, et al., Precision cleaning with supercritical carbon dioxide for the elimination of hazardous waste. LA-UR-94-3136.
[5] Rbert F. Salermo, et al., High pressure supercritical carbon dioxide efficiency in removing hydracarbon machine coolants from metal componts and components parts. MLM-3744(OP). DE92-014129.

# P38

## Chemical, structural, spectroscopic and electrical studies of three new anhydrous rubidium and cesium uranyl phosphates.

**S. Yagoubi[1,2], R. Caciuffo[2], S. Obbade[1], M. Benseghir[1], C. Renard[1], F. Abraham[1]**

*[1]UCCS UMR CNRS 8181, ENSCL-USTL, BP 90108, 59652 Villeneuve d'Ascq Cedex, France*
*Said.yagoubi@ec.europa.eu*
*[2]European Commission, Joint Research Centre-Institute for Transuranium Elements, Postfach 2340, D-76125 Karlsruhe, Germany*

During these last decades, the uranyl compounds have received a great and particular attention in solid state chemistry owing to their very important environmental aspect and the possibility of their applications in different domains ; medicine, nuclear industry and material science where uranium compounds have possible applications as ion exchangers, ionic conductors, selective oxidation catalysts or storage materials for radionuclides. Thus, the association of uranyl ion with transition metals (V, Nb, Mo, W...) oxoanions, carbonate, nitrate, phosphate, sulfate... allowed the synthesis of several compounds with complex and varied crystal structures that often lead to interesting properties such as cationic exchange or mobility (1-5).

In this presentation we report synthesis, crystal structure, electrical and spectroscopic properties of one cesium and two rubidium anhydrous uranyl phosphates, with general formula $Cs_3U_2PO_{10}$, $Rb_6U_5P_4O_{28}$ and $Rb_6U_5P_2O_{23}$ can be named thereafter CsUPO, RbUPO1 and RbUPO2, respectively.

Single crystals of all compounds were prepared by high temperature solid state reaction of a new uranyl phosphate precursor in a large excess of molten Alkaline salts. For each preparation, molten mixture was slowly cooled (5°C/h) to room temperature and washed with water to dissolve the excess of alkaline salt, giving orange-yellow single crystals. In the three compounds, phosphorus atoms adopt their usual environment, with a tetrahedral coordination. For CsUPO and RbUPO1 materials, uranium atoms adopt a square and pentagonal bipyramids coordination, respectively. However, in the last compound RbUPO2, the crystal structure contains two coordination types of uranium atoms, square and pentagonal bipyramids.

Thus, RbUPO1 crystallizes in the monoclinic system and the crystal structure is characterized by corrugated uranyl phosphate layers parallel to (100) of which the cohesion is assured by interlayer $Rb^+$ ions. Uranyl tetragonal bipyramids $(UO_2)O_4$ are linked by corners to form infinite chains $^1_\infty[UO_5]$ parallel to the $\vec{c}$ axis. These chains are linked together by symmetrical diphosphate units $P_2O_7$ sharing two corners with each chain $(UO_5)_\infty$ to form an infinite uranyl phosphate layer. The second rubidium compound RbUPO2, crystallize in triclinic symmetry with bidimensional structure, where the $(UO_2)_5O_{16}$ uranyl pentamer entities share edges to built infinite ribbons $^2_\infty[U_5O_{24}]$ connected together by phosphorus tetrahedra $PO_4$ sharing corners and edges to form parallel uranyl phosphate layers. For the cesium compound CsUPO with a monoclinic system, the crystal structure is built by two independent uranium atoms in square bipyramid coordination, connected by two opposite corners to form an infinite sheet $^1_\infty[UO_5]$ and by one phosphorus atom in a tetrahedral environment $PO_4$. The two last entities $^1_\infty[UO_5]$ and $PO_4$ are linked by sharing corners to form a three-dimensional structure presenting different types of channels occupied by alkaline cations $Cs^+$.

The conductivity measurements, $\boldsymbol{log\sigma}$ vs $\boldsymbol{10^3/T}$, between 280 and 800 °C, show an Arrhenius law evolution, figure 1, with low conductivity and high activation energy values compared to other alkaline uranyl compounds.

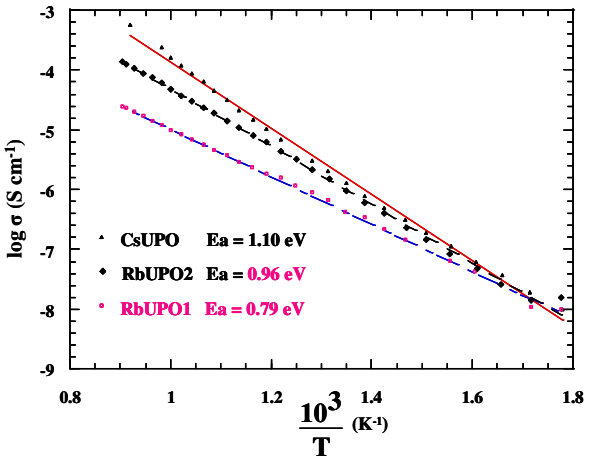


**Figure 1**: Arrhenius plots and comparison of electrical conductivities of CsUPO, RbUPO1 and RbUPO2 compounds

For all compounds, the infrared spectrum recorded at room temperature in the frequency range 400-4000 $cm^{-1}$, using the KBr dispersion technique (1 mg of sample in 125 mg KBr) with a Bruker Vector 22 Fourier Transform Infrared Spectrometer, has been used to characterize different vibration modes of uranyl ions in different coordinations and of $PO_4$ tetrahedra.

## References

[1] – S. Obbade , C. Dion, E. Bekaert, S. Yagoubi, M. Saadi and F. Abraham *Journal of Solid State Chemistry* ***172****, (2003) 305-318.*

[2] - S. Obbade, S. Yagoubi, C. Dion, M. Saadi and F. Abraham. *Journal of Solid State Chemistry,* ***174****, (2003) 19-31.*

[3] - S. Obbade , C. Dion, M. Saadi and F. Abraham. *Journal of Solid State Chemistry,* ***177****, (2004) 1567-1574.*

[4] - S. Obbade, S. Yagoubi, C. Dion, M. Saadi and F. Abraham. Journal of Solid State Chemistry, **177**, (2004) 1681-1694.

[5] - S. Surblé, S. Obbade**,** S. Saad, S. Yagoubi, C. Dion and F. Abraham *Journal of Solid State Chemistry*, ***179****,* (*2006*) *3238.*

# P39

## Functional and structural chemistry of uranium(III) amide complexes

**Tomoo Yamamura, Dexin Li, Kenji Shirasaki, Yutaka Yoshida, Suguru Ohta, Isamu Satoh, Yoshinobu Shiokawa**

[1] *Institute for Materials Research, Tohoku University, 2-1-1 Katahira, Aoba, Sendai, Miyagi 980-8577, Japan, e-mail: yamamura@imr.tohoku.ac.jp*

Light actinides (An) including uranium has two very unique characteristics; (i) four oxidation states in solutions and (ii) reversible or quasi-reversible electrode reaction in two couples of isostructural ions ($AnO_2^{2+}/AnO_2^{+}$, $An^{4+}/An^{3+}$). These characteristics are exactly what are required for high efficiency of redox-flow battery. The existing battery using vanadium satisfies the above condition (i), but its electrode reaction is non-reversible due to association and dissociation of oxygen at electrode reaction in positive electrolyte ($VO^{2+}/VO_2^{+}$). Based on the characteristics of the light actinides, we have proposed the uranium redox-flow battery using uranium complex as an active material for the purpose of leveling of natural-energy output[1, 2]. The proposal is in accordance with potential uses of depleted uranium, abundantly derived from nuclear power generation, which has been pursued owing to cessation of plan of fast breeder reactor (FBR) [3]. Result of charge and discharge experiments carried out by using β-diketone-derived complex of uranium suggest instability of U(III) complex. As far as our knowledge, few literature mentioned of stability of U(III) complex with organic ligands in solution [4]. Drastic improvement in stability of U(III) in solution was found to be essential.

The abundant examples of organometallic (non-Werener-type) complexes of U(III) are indicative of that U(III) ion functions as soft acid [5]. Since hardness/softness depends on oxidation states of the active material as varying from hard U(VI) to soft U(III), a single kind of ligand is required to form Werener-type complex with these metal ions. One of the candidates may be diamides which coordinate to actinides at various valences including Am(III) and thus is used as extraction agents in a nuclear fuel reprocessing, *i.e.* DIAMEX method [6]. However, only one literature was found for U(III) complex with a diamide [4]. Therefore, this study is to study magnetism, spectroscopy and electrochemistry of amides complex of U(III) to elucidate coordination, stability and functionality of the U(III) complexes.

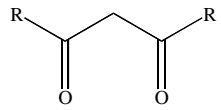


**β-diketones** (acetylacetone for R=$CH_3$)

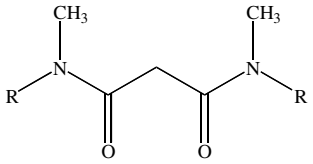


**diamides** (*N,N*'-dimethylmalonamide for R=H; *N,N,N',N*'-tetramethylmalonamide for R= $CH_3$)

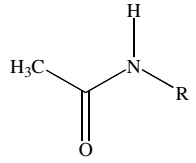


**amides** (acetamide for R=H; N-methylacetamide for R=$CH_3$; acetoanilide for R= $C_6H_5$)

Fig. 1. Classification of structures of β-diketones, diamides and monoamides.

For preliminary study, various amides are checked in terms of coexistence with U(III), *i.e.* no reduction of ligand by U(III) and no oxidation of U(III) by ligand. Two kinds of monoamides; acetamide and *N*-methylacetamide, and three kinds of diamides; acetanilide, *N,N,N',N'*-tetramethylmalonamide (Htmma), *N,N'*-dimethylmalonamide (Hdmma) were found to coexist with U(III) in solutions. In this study, complexes with tmma and dmma were prepared, as $U(tmma)_4(BPh)_3$ [7] and $U(dmma)_4Cl_3$.

The magnetic susceptibility data obtained for these U(III) samples are fitted to a modified Curie-Weiss law [$\chi = \chi_0 + C/(T - \theta_p)$], which give an effective moment ($\mu_{eff}$) of *ca.*

2 bohr magnetons per atom of U ($\mu_B$(atomU)$^{-1}$), an antiferromagnetic Curie-Weiss $\theta_p$ of -20 ~ -30 K, and a small temperature-independent $\chi_0$ of the order of $10^{-6}$ $\mu_B$(atomU)$^{-1}$ (Table 1). In both complexes of U(III), effective moment ($\mu_{eff}$) is quite smaller than theoretical values based on LS coupling for $U^{3+}$ free ion (3.62 $\mu_B$(atomU)$^{-1}$). We will analyze these results by discussing (i) strong coordination interaction between U(III) and amide ligands and (ii) itinerant nature of 5f electrons in these complexes.

Absorption spectra of U(III) in THF solutions were also measured in this work. Small shift to lower energy are observed in both complexes compared with perchlorate salt due to nephelauxetic effect. Intensity of $^4F_{7/2}$ band of U(dmma)$_4$Cl$_3$ decreases by following exponential decay with half-life of 19.8 hours, it is longer than that of 11.0 hours of U(tmma)$_4$(BPh)$_3$. These results of itinerant nature of 5f electrons in solid and small nephelauxetic effect in solution seem to be contradictory because the former and the latter suggests the strong and the weak coordination between U(III) and ligands, respectively. Structural investigation may provide further insight on the characteristics of the U(III) complexes.

Table 1. Effective moment, Curie-Weiss temperature and temperature-independent term determined for U(III) and U(IV) complexes

| | $\mu_{eff}$ /$\mu_B$(atomU)$^{-1}$ | $\Theta_p$ /K | $\chi_0$ /$\mu_B$ (atomU)$^{-1}$ |
|---|---|---|---|
| U(tmma)$_4$(BPh$_4$)$_3$ | 1.95 | -29 | 5.05 x $10^{-6}$ |
| U(dmma)$_4$Cl$_3$ | 2.07 | -23 | 3.03 x $10^{-6}$ |
| U(tmma)$_4$(PF$_6$)$_4$ | 3.24 | -149 | 2.97 x $10^{-6}$ |

## References


[1] Y. Shiokawa, H. Yamana, H. Moriyama, J. Nucl. Sci. Tech., **37**, 253 (2000).
[2] T. Yamamura, Y. Shiokawa, H. Yamana, H. Moriyama, Electrochim. Acta, **48**, 43 (2002).
[3] OECD/NEA, IAEA, Management of Depleted Uranium: a joint report, Nuclear Energy Agency, Organisation for Economic Co-operation and Development, Paris, 2001.
[4] J. I. Bullock, A. E. Storey, P. Thompson, J. Chem. Soc., Dalton Trans., 1040 (1979).
[5] R. G. Pearson, J. Am. Chem. Soc., **85**, 3533 (1963).
[6] O. Courson, M. Lebrun, R. Malmbeck, G. Pagliosa, K. Römer, B. Sätmark, J.-P. Glatz, Radiochim. Acta, **88**, 857 (2000).
[7] T. Yamamura, K. Shirasaki, D. X. Li, Y. Shiokawa, J. Alloys Compds., **418**, 139 (2006).

# P40

## The $A^+$ monovalent cation mobility and crystal structure in $AUV_3O_{11}$.

**S. Obbade, C. Renard, F. Abraham**

*Unité de Catalyse et de Chimie du Solide - UMR CNRS 8181*
*ENSCL – Bât. C7 – BP 90108 - 59652 Villeneuve d'Ascq Cedex - France*

For the metal ratio U/V = 1/3, reduced binary oxide $UV_3O_{10}$ has been prepared by reaction between $UO_3$ or $U_3O_8$ and $V_2O_5$ at 650°C under vacuum or by reduction of $UV_2O_8$ under vacuum or from mixtures of $V_2O_3$, $V_2O_5$ and $\alpha$-$U_3O_8$ in stoechiometric proportions heated in sealed, evacuated silica tubes at 550°C. The three-dimensional crystal structure of $UV_3O_{10}$ can be described from layers with sheet anion topology formed of hexagons, squares and triangles. The squares are occupied by V, the hexagons by U and the triangles are empties. There are two independent V atoms, V(1) and V(2) with charges +4 and +5, respectively that implies the correct electronic formulation $U^{VI}V^{IV}V^{V}{}_2O_{10}$.

Compounds with U/V = 1/3 are also known to exist with a general formula $MUO_2(XO_3)_3$ where X can be P or V and M is commonly a monovalent cation : $H_3O^+$, $Na^+$,$Cs^+$, $NH_4^+$. For X = P, uranyl-polyphosphate acid $HUO_2(PO_3)_3$ and monovalent cations salts, $Na^+$ and $Cs^+$ have been isolated and their structures established. Uranyl-phosphate layers linked into a three-dimensional framework by polyphosphate chains are distinguished in the structure of H or Na compounds. In contrast, the structure of $CsUO_2(PO_3)_3$ involves cyclohexaphosphate rings $(P_6O_{18})^{6-}$ (with proper symmetry $\bar{1}$) which constitute the basis of the structure, together with the $UO_2^{2+}$ and $Cs^+$ ions. Uranyl-phosphate layers linked in a three dimensional skeleton through – P – O – P – bridges can also be distinguished. In the three compounds, the uranyl group has a pseudo symmetric, linear structure, with five other oxygen atoms at greater distance in the equatorial plane to constitute a U seven-vertex polyhedron.

For X = V, a natural variety $U_2V_6O_{21}{\cdot}15H_2O$, called uvanite, exists and different derived salts belonging to the class of compounds of general formula $M^{n+}{}_{1/n}UO_2(VO_3)_3.xH_2O$ with M = $H_3O^+$, $Na^+$, $NH_4^+$, $Mg^{2+}$ are suspected to have a layered structure on the basis of their exchange properties. The cations, found between the $[UO_2V_3O_9]^-$ layers can be exchanged for inorganic and organic cations and some water molecules can be replaced by other solvent molecules. The crystal structures of the anhydrous compounds $M(UO_2)(VO_3)_3$ have been determined for M = K and Cs.

$KUV_3O_{11}$ and $CsUV_3O_{11}$ are layered compounds built on the same type of sheets as $UV_3O_{10}$ but containing only $V^{5+}$ ions, so the V(1) polyhedron is rather a square pyramid with displacement of V(1) atom out of the plane to form a short V(1) = O vanadyl bond and an opposite longer V - - - O bond. In $CsUV_3O_{11}$, starting from the layer described in $UV_3O_{10}$, V(1) displacements to form bonds are on the same side of the layer (down for example), so around an $UO_2$ ion, there are four $VO_5$ square pyramids pointing down and two up to form the *4down-2up* $^2_\infty[UV_3O_{10}]^-$ isomer layer. There is no formal chemical bond between two consecutive layers at $z = \pm 0.18$, the closest contacts fall along the [104] direction and are of two types, U = O(1) - - - V(1) = O(3) and V(3) = O(5) - - - V(2) = O(4) for which the "long" bonds are 2.98 and 2.66 Å, respectively, their corresponding contributions to the bond valence sums about vanadium are only 0.08 and 0.13. So double layer sheets are form with $Cs^+$ ions in the interspace between consecutive double layer sheets. As a matter of fact, $CsUV_3O_{11}$ is composed of neutral sandwiches of oppositely charged infinite layers $\{(UV_3O_{11})^- - (Cs)_2^{2+} - (UV_3O_{11})^-\}$ stacked one above another along [104], with any "bonds" between the neutral sandwiches being very weak (as is the case in the "talc" silicate minerals). In $KUV_3O_{11}$ two types of $^2_\infty[UV_3O_{10}]^-$ layers coexist, *4down-2up* and *6down* (or *6up*), , triple layers (*6down /*

*4down-2up / 6up*) sheets are formed, $K^+$ ions occupy the interspace between consecutive triple layers sheets, thus they are sandwiched by a *6up* and a *6down* layer.

Excepted for the oxygen atoms of the uranyl and vanadyl groups all other oxygen atoms are shared by $VO_5$ pyramids and $UO_8$ bipyramids, thus, the formula could be written as $AUO_2(VO_3)_3$, which is in agreement with the use of the "metavanadate" name often given for this series, but which does not represent the crystal structure; in fact, the (001) layers are well described as extended covalent solids.

The monoclinic base cell (a, b) of $CsUV_3O_{11}$ (table 1) corresponds to the C-centered orthorhombic multiple cell of the hexagonal primitive one (Fig. 1) and the cell parameters are linked by the relation $a_{mono} = \sqrt{3}\, a_{hex}$, with $b_{mono} = b_{hex}$; actually, the $a_{mono}$ / $b_{mono}$ ratio is 1.743. However, the *4down-2up* layer itself lacks hexagonal symmetry.

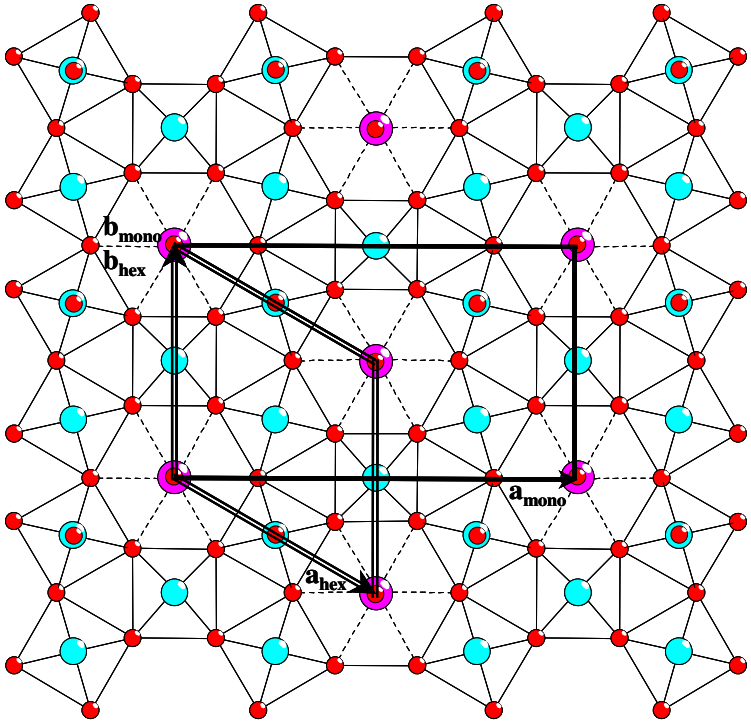


**Fig. 1:** Relationship between orthorhombic and hexagonal pseudo cells in the (001) plan of the $AUV_3O_{11}$ (A = K, Cs) structures.

| Compound | a | b | c | β | S. G. |
|---|---|---|---|---|---|
| $UV_3O_{11}$ | 12.0554(3) | 6.9426(2) | 16.2228(3) | | Fddd |
| $CsUV_3O_{11}$ | 11.904(2) | 6.8321(6) | 12.095(2) | 106.989(5) | $P2_1/a$ |
| $KUV_3O_{11}$ | 11.905 | 6.869 | 34.051 | | F222 |

**Table 1.** Uranyl vanadates based on 2-D network of $VO_5$ square pyramids and isolated $UO_8$ bipyramids.

The Arrhenius plots of conductivity vs. $10^3$/T for several uranyl vanadates, evidenced that the 3-D compounds $A(UO_2)_4(VO_4)_3$ with partial occupation of the monovalent cationic sites in perpendicular channels exhibit high conductivity with low activation energy (0.17 0.27ev for Na and Li compounds, respectively). The case of $CsUV_3O_{11}$ is particularly interesting, the conductivity is very high for a so large cation as $Cs^+$ with a low activation energy. Further studies on this class of materials with 2-D structure but containing small ions such as $Na^+$ or $Ag^+$ would be of interest for potential applications in various electrochemical systems.

# LIST OF PARTICIPANTS

| Name | First Name | Country of Affiliation | E-mail |
|---|---|---|---|
| Afonin | Mikhail | Russia | afonin1@lti-gti.ru |
| Ahuja | Rajeev | Sweden | rajeev.ahuja@fysik.uu.se |
| Allen | Geoff | United Kingdom | g.c.allen@bristol.ac.uk |
| Almeida | Manuel | Portugal | malmeida@itn.pt |
| Andreev | Alexander | Czech Republic | a.andreev@seznam.cz |
| Aupiais | Jean | France | jean.aupiais@cea.fr |
| Batuk | Olga | Russia | batuk@radio.chem.msu.ru |
| Berthebaud | David | France | david.berthebaud@univ-rennes1.fr |
| Brevet | Aude | France | aude.brevet@cea.fr |
| Butorin | Sergei | Sweden | sergei.butorin@fysik.uu.se |
| Caciuffo | Roberto | Germany | roberto.caciuffo@ec.europa.eu |
| Chevalier | Bernard | France | chevalie@icmcb-bordeaux.cnrs.fr |
| Clavier | Nicolas | France | patrick.jermidi@cea.fr |
| Colineau | Eric | Germany | eric.colineau@ec.europa.eu |
| Coqblin | Bernard | France | coqblin@lps.u-psud.fr |
| Costa | M. Margarida | Portugal | guida@pollux.fis.uc.pt |
| Dacheux | Nicolas | France | dacheux@ipno.in2p3.fr |
| Dawes | Marina | United Kingdom | marina.dawes@awe.co.uk |
| Detlefs | Blanka | Germany | blanka.detlefs@esrf.fr |
| Di Giandomenico | Maria Vita | France | digiando@ipno.in2p3.fr |
| Dias | Marta | Portugal | marta.dias@itn.pt |
| Domanov | Vladimir | Russia | domanov@nrmail.jinr.ru |
| du Fou de Kerdaniel | Erwan | France | dufoudek@ipno.in2p3.fr |
| Dupont | Michel | France | toto_dupont@hotmail.com |
| Duvieubourg-Garela | Laurence | France | said.obbade@ensc-lille.fr |
| Fanghaenel | Thomas | Germany | thomas.fanghaenel@ec.europa.eu |
| Fourest | Blandine | France | fourest@ipno.in2p3.fr |
| Freyss | Michel | France | michel.freyss@cea.fr |
| Gaczyński | Piotr | Portugal | piotr@itn.pt |
| Gaigalas | Gediminas | Lithuania | gaigalas@itpa.lt |
| Gal | Joseph | Israel | jgal@bgu.ac.il |
| Geeson | David | United Kingdom | david.geeson@awe.co.uk |
| Giovannini | Mauro | Italy | giovam@chimica.unige.it |
| Glascott | Joseph | United Kingdom | joe.glascott@awe.co.uk |
| Gofryk | Krzysztof | Germany | krzysztof.gofryk@ec.europa.eu |

| | | | |
|---|---|---|---|
| Guet | Claude | France | claude.guet@cea.fr |
| Haire | Richard | U.S.A. | hairerg@ornl.gov |
| Havela | Ladislav | Czech Republic | havela@mag.mff.cuni.cz |
| Hinatsu | Yukio | Japan | hinatsu@sci.hokudai.ac.jp |
| Hingant | Nina | France | hingantn@ipno.in2p3.fr |
| Hubert | Solange | France | shubert@ipno.in2p3.fr |
| Ibers | James | U.S.A. | ibers@chem.northwestern.edu |
| Izosimov | Igor | Russia | izig@mail.ru |
| Kaczorowski | Dariusz | Poland | d.kaczorowski@int.pan.wroc.pl |
| Kopyrin | Alexey | Russia | kopyrin@lti-gti.ru |
| Lander | Gerard | Germany | lander@ill.fr |
| Li | Gan | China | 2002ligan@sina.com |
| Livneh | Tsachi | Israel | tsaliv@netvision.net.il |
| Lopes | Elsa | Portugal | eblopes@itn.pt |
| Luo | Wenhua | China | luowenhua712@yahoo.com.cn |
| Magnani | Nicola | Germany | nicola.magnani@ec.europa.eu |
| McEwen | Keith | United Kingdom | k.mcewen@ucl.ac.uk |
| Miiller | Wojciech | Poland | w.miiller@int.pan.wroc.pl |
| Mokhtari | Hamid | France | hamid.mokhtari@cea.fr |
| Moore | Kevin | U.S.A. | moore78@llnl.gov |
| Morrall | Peter | United Kingdom | peter.morrall@awe.co.uk |
| Moura | Miguel | Portugal | mmoura@itn.pt |
| Noël | Henri | France | henri.noel@univ-rennes1.fr |
| Obbade | Said | France | obbade@ensc-lille.fr |
| Ochkin | Alexander | Russia | ochkin@rctu.ru |
| Paixão | José António | Portugal | jap@pollux.fis.uc.pt |
| Pasturel | Mathieu | France | mathieu.pasturel@univ-rennes1.fr |
| Pereira | Laura | Portugal | lpereira@itn.pt |
| Pereira Gonçalves | António | Portugal | apg@itn.pt |
| Perron | Hadrien | France | perron@ipno.in2p3.fr |
| Philippini | Violaine | France | violaine.philippini@cea.fr |
| Picart | Sebastien | France | sebastien.picart@cea.fr |
| Pikul | Adam | Poland | a.pikul@int.pan.wroc.pl |
| Popescu | Ioana-Carmen | Romania | ioana.popescu@icpmrr.ro |
| Puxley | Christopher | United Kingdom | chris.puxley@awe.co.uk |
| Reiffers | Marian | Slovakia | reiffers@saske.sk |
| Reitz | Thomas | Germany | thomas.reitz@fzd.de |

| | | | |
|---|---|---|---|
| Renard | Catherine | France | catherine.renard@ensc-lille.fr |
| Rivenet | Murielle | France | murielle.rivenet@ensc-lille.fr |
| Rogl | Peter Franz | Austria | peter.franz.rogl@univie.ac.at |
| Rusz | Jan | Sweden | rusz@mag.mff.cuni.cz |
| Saad | Siham | France | sihamsaad1@yahoo.fr |
| Salamakha | Leonid | Ukraine | salamakhaleonid@rambler.ru |
| Samsel-Czekala | Malgorzata | Poland | m.samsel@int.pan.wroc.pl |
| Schoenes | Joachim | Germany | j.schoenes@tu-bs.de |
| Scott | Tom | United Kingdom | t.b.scott@bris.ac.uk |
| Sério | Susana | Portugal | susana.serio@itn.pt |
| Shamir | Noah | Israel | noah.shamir@gmail.com |
| Shick | Alexander | Czech Republic | shick@fzu.cz |
| Shiryaev | Andrei | Russia | shiryaev@ns.crys.ras.ru |
| Sologub | Oksana | Portugal | sologub@itn.pt |
| Sornein | Marie-Olga | France | sornein@ipno.in2p3.fr |
| Spalek | Jozef | Poland | ufspalek@if.uj.edu.pl |
| Springell | Ross | France | ross.springell@esrf.fr |
| Stefanovsky | Sergey | Russia | profstef@mtu-net.ru |
| Stora | Thierry | Switzerland | thierry.stora@cern.ch |
| Suski | Wojciech | Poland | w.suski@int.pan.wroc.pl |
| Szlawska | Maria | Poland | m.szlawska@int.pan.wroc.pl |
| Tobin | James | U.S.A. | tobin1@llnl.gov |
| Tougait | Olivier | France | tougait@univ-rennes1.fr |
| Tran | Vinh Hung | Poland | v.h.tran@int.pan.wroc.pl |
| Treimany | Catherine | France | catherine.treimany@cea.fr |
| Vigier | Nicolas | France | nicolas.vigier@cea.fr |
| Vogt | Oscar | Switzerland | vogt@solid.phys.ethz.ch |
| Wachter | Peter | Switzerland | wachter@solid.phys.ethz.ch |
| Waerenborgh | João Carlos | Portugal | jcarlos@itn.pt |
| Wastin | Franck | Germany | franck.wastin@ec.europa.eu |
| Wochowski | Konrad | Poland | K.wochowski@int.pan.wroc.pl |
| Yagoubi | Said | Germany | said.yagoubi@ec.europa.eu |
| Yamamura | Tomoo | Japan | yamamura@imr.tohoku.ac.jp |
| Yang | Weicai | China | ywc712@yahoo.com.cn |
| Zlatic | Veljko | Croatia | zlatic@ifs.hr |